MICROTUBULES: THE

RHYTHM

OF ASSEMBLY AND THE EVOLUTION OF

FORM

by

Deborah Kuchnir Fygenson

A DISSERTATION PRESENTED TO THE FACULTY OF

PRINCETON UNIVERSITY

IN CANIDACY FOR THE DEGREE OF

DOCTOR OF PHILOSOPHY

RECOMMENDED FOR ACCEPTANCE

BY THE DEPARTMENT OF

PHYSICS

June, 1995

ABSTRACT

The subject of this thesis is an unusual protein polymer, essential to life in all eukaryotic (nucleus-bearing) cells, known as a *microtubule.* Microtubules are especially interesting because they exhibit *dynamic instability,* a process in which chemical energy (GTP-hydrolysis) is converted into macroscopic length fluctuations.

Tubulin, the constituent protein of microtubules, was purified from cow brain. Its assembly into microtubules was observed in real time under the light microscope using video-enhanced DIC microscopy. The chemical condition of the aqueous environment and the temperature were varied.

This thesis presents the phase diagram of microtubule self-assembly and length dynamics over a wide range of temperatures (10-40°C) and tubulin concentrations (6-60μM). Both heterogeneous and homogeneous nucleation are investigated and a qualitative transition in the length dynamics, from bounded to unbounded growth, is documented. In addition, the stabilizing effect of glycerol is explored. Of the many observations, the effect of temperature on the frequency of fluctuations between assembly and disassembly is particularly noteworthy since it is not explicable by current models for dynamic instability. A new model is called for in which destabilization of the microtubule is uncoupled from the growth rate at low temperatures and strongly coupled to it at high temperatures. The intermittent "zippering" of a tubulin sheet into a microtubule is suggested as a possible destabilizing mechanism.

The experimental control over microtubules given by the phase diagram permits the use of microtubules far from their native environment. In the second part of this thesis, microtubules are used to create a simple model system for studying biological morphogenesis and force generation.

Tubulin is encapsulated within phospholipid vesicles at low temperatures. Microtubules assemble when the temperature is raised and the vesicles are observed under the light microscope. The microtubules deform near-spherical membranes through a specific, reversible and unusual sequence of shapes. Their polymerization exerts a force of several picoNewtons on the membrane which, in turn, often results in the buckling of the microtubules themselves. The possibility of a thermal ratchet mechanism for force generation is discussed.

Advisor: Professor Albert Libchaber

ACKNOWLEDGEMENTS

the theory of thermal ratchets and membranes with me; and Denis Chrétien and Eric Karsenti for some inspiring results from far away. Along with Michael Elbaum and John Marko, Nihal Altan, Didier Chatenay, Ivan Cohen, Peter Kaplan, G.V. Shivashankar and Jun Zhang have given me plenty to look forward to as the thesis ends.

Being the work of many years, there have been many indirect contributions which I should like to acknowledge as well. Working side by side with Andrew Belmonte and Luc Faucheux, my "comrades in arms" in the lab at Princeton, I have enjoyed uncommonly easy and enriching interactions. Laurent Bourdieu, Peter Kaplan and Gregoire Bonnet shared their enthusiasm in the textbook phase of learning biology. Sarah Keller was always a friend I could count on, and my best thanks comes from offering the same. The Princeton Physics Department is unusually rich in physicists interested in biological phenomena. Besides Stan and Sol, I was pleasantly influenced by Bob Austin, Ray Goldstein, V. Adrian Parsegian (usually at the NIH) and E. Shyamsunder.

My graduate career really began during my thrid year in college, at M.I.T. I will never forget Prof. John Negele for encouaging me in my lowest moment. My undergradute thesis advisor, Prof. David Pritchard, took me seriously and gave me the opportunity to get my feet wet in his lab. Eric Cornell made the experience pleasant and fruitful, and the net result was critically encouraging. My sincere thanks to all three.

I am grateful to Princeton for funding my first two years of graduate school and to the NSF for picking up the next three.

I would like to thank Aaron Lemonick for the opportunity to help him teach. He is a gifted and inspiring teacher with a wonderful and kind character. I am also happy to thank the people at Princeton who made the ins

and outs of grad school clear, simple, and pleasant: Laurel Lerner, Claude Champagne, John Washington, and Ted Griffith.

Then there are the friends that have kept me sane and stoked my optimism. Kevin Cunningham and Macalene, brother and sister at heart, have been a true inspiration for daring. Linda Kim, my sister of choice, has always come forward in a loving and calm manner, to put wind in my sails. To both of you, more thanks than words will hold.

Underneath it all has flowed true and deep, the love of my best friend, and husband, Mendy. I am at once proud and humbled by his steadfast support and sincere faith in me. Even if I could have done it on my own, I could never have done it as well alone. I am happy to have a lifetime to return the favor.

At the end of my student life, I look back and behind it all, I see my family: Mom and Dad and Louis. They gave me the values that I use to define myself and the opportunity and courage to act on them. On the solid foundation of their love and concern, I have built my character and pursued my dreams. Thanks will never be enough.

Finally, to Augusta, the wisest person I know, beacuse she always knew I could and, though I haven't told her much, it made all the difference: "God bless you."

LIST OF FIGURES

xiii

CHAPTER I

INTRODUCTION

The microtubule is a material unlike any other. It combines features of both crystals and polymers. It consumes chemical energy. And, in an otherwise constant environment, it alternates unpredictably between assembly and dissolution. Such a remarkable material naturally arouses curiosity and prompts investigation. Even more, though, because it is a biological material with a fundamental role in the life, reproduction, and organization of every eukaryotic cell.

This thesis is a study of the microtubule as a fascinating, biological material with an emphasis on its material aspects, rather than its biological ones. A brief review of the history of microtubules is given at the end of this chapter and an introduction to the biology which concerns them is given in the next. Chapter II also introduces details of their structure, their dramatic assembly/disassembly dynamics, and the current models of this behavior.

Understandably, experiments on microtubules have been carried out primarily by biologists. Simply obtaining the material has presented a considerable obstacle to scientists from other disciplines. This situation, however, is ripe for change. The relevant experimental techniques have become truly simple and accessible. Details of the methods used for obtaining, controlling and observing microtubules are discussed in Chapter III, with a step-by-step checklist for purification provided in Appendix A and recipes for the buffer solutions listed in Appendix B. Written with a clear recollection of the trepidation of a non-biologist, it is hoped that the guidelines in this chapter will encourage other non-biologists interested in experimenting with microtubules – there is a lot to be learned from this unique material outside of its biological context.

1

The main result of this thesis is a thorough characterization of microtubules as a material, presented in Chapter IV. A phase diagram is mapped in the temperature-concentration plane. Homogeneous and heterogeneous nucleation are described. These familiar physical phenomena are understandably altered by the unique structure and assembly dynamics of microtubules. Heterogeneous nucleation (section IV.1) is limited by the assembly dynamics and reveals a transition between two qualitatively different dynamical regimes: bounded and unbounded growth (section IV.2). Homogeneous nucleation (section IV.3) depends critically on the microtubule structure, the limiting step being the curling of a sheet into a tube.

In the relevant portion of the phase diagram, between heterogeneous and homogeneous nucleation, the assembly and disassembly of individual microtubules are studied in detail (section IV.2). Both are found to be entropically driven reactions which go faster at higher temperatures. Transitions from assembly to disassembly generally become less frequent as assembly accelerates and the opposite transitions, from disassembly to assembly, become increasingly likely. Eventually, when the former transition happens less than once in every 11 minutes, the latter transition is certain to follow, independent of the assembly rate: unbounded growth sets in.

An important exception to this general behavior is observed at the highest temperatures. The frequency of the transitions becomes essentially independent of the temperature even though the assembly reaction continues to increase in speed. Evidently at high temperatures the process destabilizing the microtubule becomes strongly coupled to the assembly reaction. Drawing heavily from a recent electron microscopy study for inspiration (Chrétien and Karsenti, 1995), a new model for the mechanism underlying dynamic instability is suggested.

2

Having documented how high temperatures promote assembly and stabilize the microtubules, it is shown that the chemical stabilizer, glycerol, works in a fundamentally different way (section IV.4). Glycerol has no net effect on the assembly reaction but slows disassembly and reduces the frequency of transitions from assembly to disassembly. Despite their differences, the stabilizing effects of temperature and glycerol can both be explained in terms of changes in the *potential entropy* of surrounding water molecules.

Chapter IV concludes with a general picture of microtubule behavior (section IV.5). Changes in shape/form are the underlying theme. A conformational change of the individual protein molecules within the microtubule leads to the fundamental instability of the structure. A structural change in the assembly as a whole, as a sheet-like aggregate curls into a tube, magnifies the instability to macroscopic proportions.

Besides yielding new insight into microtubule behavior, the investigations in Chapter IV lead to the experimental control necessary to use microtubules to perform simple physical experiments at the microscopic level. Chapter V presents an example. Microtubules are encapsulated in lipid vesicles, creating a simple system which is topologically similar to a cell. Inside the vesicle, assembling microtubules eventually span the finite volume and interact with the membrane, generating a mechanical force that dramatically deforms the vesicle and eventually causes the microtubules themselves to buckle. Thus, chemical energy is transformed into mechanical work on the microscopic/molecular level. An attempt is made to understand the observed deformations in terms of the membrane curvature energy and to understand the generation of mechanical force with a thermal ratchet mechanism.

3

In the end, perhaps, the results presented here will have some relevance to biology. It must be emphasized, however, that biological relevance is neither the motivation nor the justification for this work. Instead, it is hoped that it will serve as an example of how new and unimaginable aspects of nature, living or merely animate, can be uncovered and understood by a "physics" approach to biological systems.

Historical perspective

Based of the references and discussion given in Schliwa (1986).

At the end of last century, the first indications of the fibrous nature of cellular structures were revealed by the light microscope. In 1849, Remak noted 'fibrils' in neurons. In 1875, Ranvier described fiber bundles in the cytoplasm of nucleated red blood cells (Figure 1.1). Soon after, in 1879, fibrillar structures of the mitotic spindle were described by Flemming; and as early as 1888 Ballowitz observed that cilia and flagella frayed into several fine filaments (Figure 1.1). These findings suggested that mechanical properties of cells, and even cell shapes, are mediated by a sort of skeleton. Definitive proof was lacking however, until the mid-1950's and the introduction of electron microscopy (EM) as a biological tool. Electron micrographs of a tremendous variety of cells (e.g. neurons, plant cells, protozoans) revealed arrangements of approximately 25 nm diameter tubules, which came to be known as microtubules (Slautterback, 1963). For a review of early EM observations see Porter (1980).

Microtubules were soon associated with the mitotic spindle (Taylor, 1965), so actually their properties were first studied in terms of the effects of drugs and physical variables (e.g. temperature, pressure) on the mitotic apparatus (Pease, 1941; Inoué, 1959). In 1968, the temperature sensitivity and

4
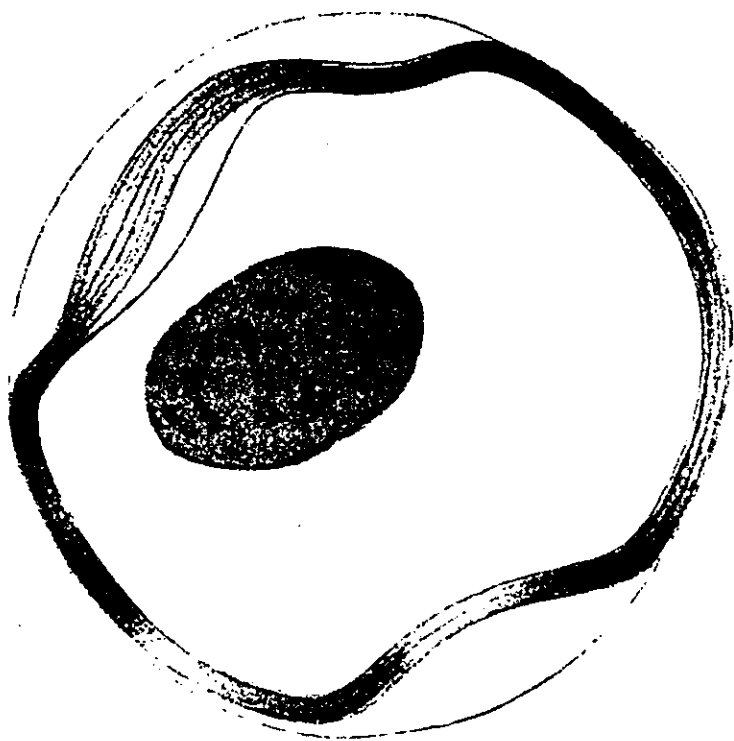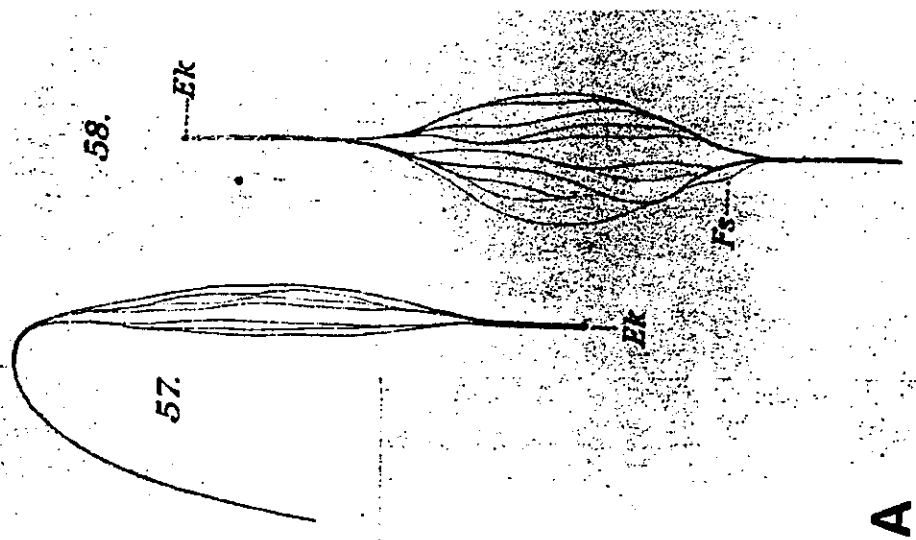
Fig. 1.1 A) Macerated sperm tails stained with genetian violet as noted by Ballowitz. B) Ring of fibers in an amphibian red blood cell stained with genetian violet, as drawn by Meves. Both images from (Schliwa, 1990).

drug binding properties of the mitotic spindle were used to develop a method for purifying microtubules (Shelanski and Taylor, 1967). This method isolated tubulin, the constituent protein of microtubules, along with microtubule-associated proteins, or MAPs (Sloboda, et al., 1975). Once a protocol for removing MAPs was adopted (Weingarten, et al., 1975), studies of the assembly and enzymatic activity of pure microtubules began.

For the first decade after their purification, microtubule assembly kinetics and enzymatic activity were inferred primarily from bulk measurements: sedimentation coefficients, solution turbidity and radioactivity (Dustin, 1984), and the results were understood in a equilibrium thermodynamic framework (Oosawa and Asakura, 1975). The static intricacies of microtubule structure were and are to this day studied by electron microscopy and X-ray fiber diffraction (Amos and Amos, 1991).

In 1984, in a pair of pivotal papers, Mitchison and Kirschner surprised the field with the discovery "that microtubules coexist in growing and shrinking populations which interconvert rather infrequently" (Mitchison and Kirschner, 1984b; Mitchison and Kirschner, 1984a). They labeled this phenomenon *dynamic instability* and not long after it was observed directly under the light microscope using the dark-field technique (Horio and Hotani, 1986).

The challenge of visualizing individual tubes 250Å in diameter with the light microscope is obvious. The past decade has seen the development of video-enhanced DIC microscopy (Allen, et al., 1981; Inoué, 1986), which has made the observation of single microtubules and their dynamic instability practically routine. It is currently the technique of choice as research focuses on elucidating of the mechanism underlying dynamic instability — to which cause this thesis hopes to contribute.

CHAPTER II

MICROTUBULES

This chapter is a brief introduction to microtubules: where they come from, what they are made of, how they behave and current guesses as to why. Thorough coverage of their biological context is given in any standard cell biology text book, such as *The Molecular Biology of the Cell*, (Alberts, et al., 1994). Good review articles include (Kirschner and Mitchison, 1986; Caplow and Shanks, 1990; Mandelkow and Mandelkow, 1990; Mandelkow, et al., 1991; Caplow, 1992; Erickson and O'Brien, 1992; Cassimeris, 1993).

2.1 Biology

If stability against evolution is any criterion, microtubules are fundamental in biology. They are found in every eukaryotic cell, from the primitive yeast to the human neuron. The distinction between eukaryotic and prokaryotic cells is among the first in the evolutionary tree. Prokaryotes are the simplest cells (e.g. bacteria and algae). Their cytoplasm is one large soup without internal partitions. Eukaryotes are distinguished by the existence of a nucleus, a distinct volume for the storage and transcription of the genetic material. Along with the nucleus, eukaryotes have many other internal compartments, called organelles, and a skeleton which organizes and connects them. Microtubules are a major component of the cytoskeleton.

Microtubules have several roles in the cell. First, they are like bones, supporting the shape of the cell. They radiate from near the nucleus, beginning at a structure called the centrosome, to the periphery of the cell, concentrating somewhat in protrusions; see Figure 2.1. Cells with complex shapes (e.g. neurons), or hair-like structures (e.g. villi, flagella) are especially rich in microtubules.

7
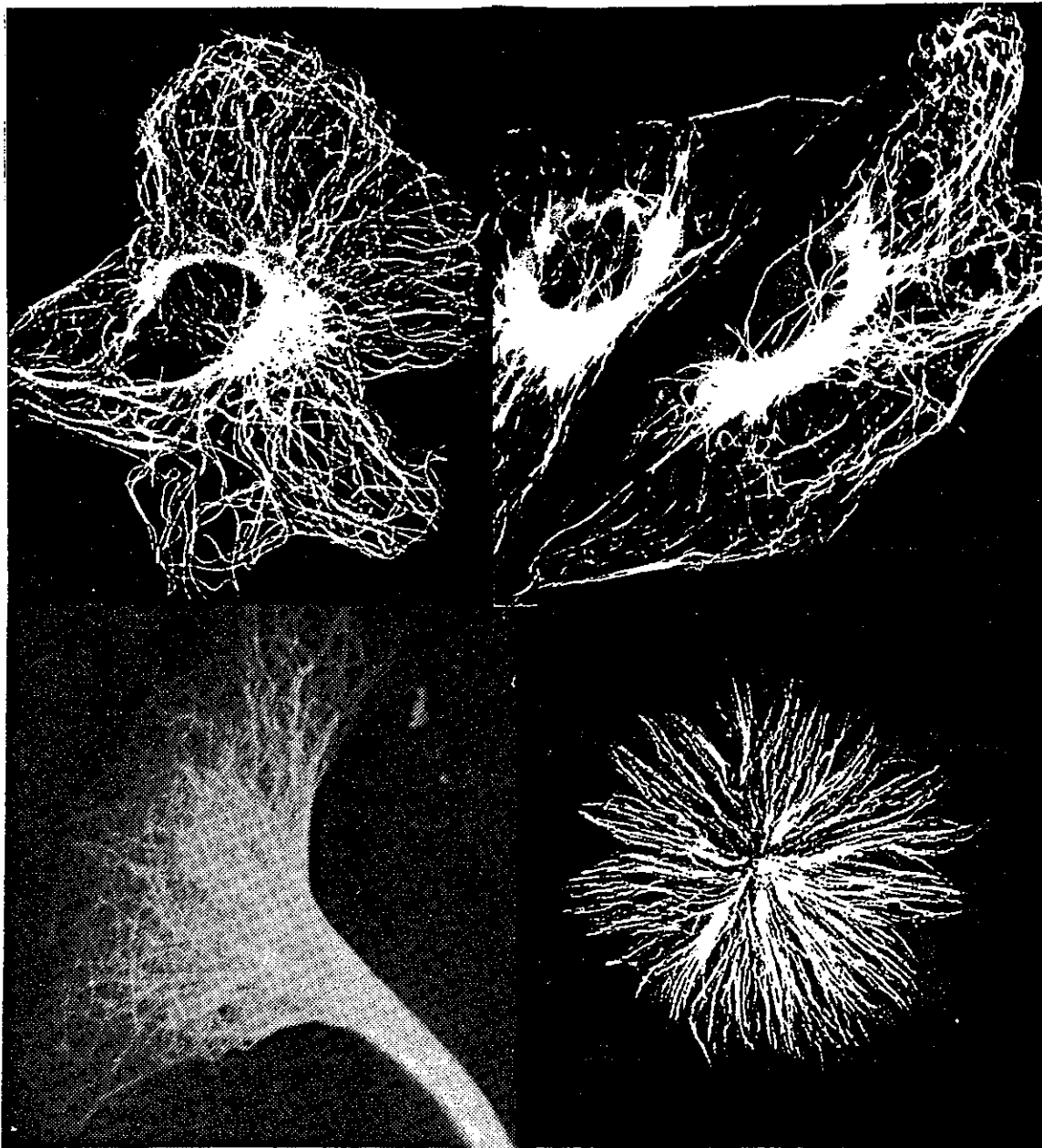
Fig. 2.1. The distribution of microtubules in some cells, imaged by immunofluorescence microscopy. Taken from (Schliwa, 1986) and (Weber and Osborn, 1981). Upper left: chick embryo; Upper right: mouse 3T3 cells; Lower left: 'growth cone' of neuroblastoma; Lower right: angelfish melanophore.

8

Microtubules also act as a circulatory system, connecting and nourishing distant regions of the cell. They are paths along which nutrients, wastes, proteins, etc. are transported in packages, called vesicles, by specific "motor" proteins (e.g. kinesin) (Warner and MacIntosh, 1989; Vale, 1990).

From these analogies, it might be expected that microtubules are long, strong and permanent. Indeed, they easily span most cells (1-10 μm) in a fraction of their persistence length (~ 5 mm) (Gittes, et al., 1993), so they are long and strong by most standards. But microtubules are not permanent.

Microtubules switch mysteriously between growing and shrinking and back again. This behavior is known as *dynamic instability*. The biological relevance of dynamic instability is most obvious during cell division (mitosis); see Figure 2.2. When a cell begins to divide, astonishing changes take place. The microtubule network reorganizes, the centrosome replicates and the two copies, called "daughters," move to opposite sides of the cell. Microtubules radiate from the centrosomes in all directions, assembling and disassembling quite rapidly. They effectively search for, capture and align the chromosomes in a plane. The process takes about 1 hour. Once every chromosome is in place, the microtubules disassemble in concert and guide one of the sister chromatids towards each centrosome to form the nuclei of the daughter cells. Thus, microtubules are the mitotic spindle.

Much of the current research on microtubules is done in the context of cell division. Major questions include: how does the cellular timing mechanism interact with microtubules (Verde, et al., 1992), how do chromosomes move along microtubules (Cassimeris and Salmon, 1991; Coue, et al., 1991; MacIntosh and Hering, 1991), how are microtubules involved in establishing the precise alignments of the chromosomes, and what triggers their coordinated retraction (Hyams and Brinkley, 1989)

1 PROPHASE

cytoplasm
plasma membrane
dispersing nucleolus
centromere with attached kinetochores
intact nuclear envelope
condensing chromosome with two sister chromatids held together at centromere

separating centrosomes will form the spindle poles

NUCLEAR ENVELOPE BREAKS DOWN

2 PROMETAPHASE

plasma membrane
polar microtubule
kinetochores
kinetochore microtubules
astral microtubule
spindle pole
randomly placed chromosome in active motion
nuclear envelope vesicles
spindle pole

CHROMOSOMES MOVE TO METAPHASE PLATE

3 METAPHASE

chromosomes aligned at metaphase plate halfway between the poles
spindle pole
spindle pole
nuclear envelope vesicles
kinetochore microtubule
polar microtubule

SUDDEN SEPARATION OF SISTER KINETOCHORES BEGINS ANAPHASE

4 ANAPHASE

kinetochore microtubules shorten as the chromatid (chromosome) is pulled toward the pole
elongating polar microtubule
shortening kinetochore microtubule
astral microtubule
increasing separation of the spindle poles

NUCLEAR ENVELOPE RE-FORMS

5 TELOPHASE

decondensing chromosomes without kinetochore microtubules
polar microtubules
nuclear envelope re-forming around individual chromosomes

CLEAVAGE FURROW SPLITS CELL IN TWO

6 CYTOKINESIS

reappearing nucleolus
midbody: region of microtubule overlap
constricted remains of polar spindle microtubules
re-formation of interphase array of microtubules nucleated by the centrosome
completed nuclear envelope surrounding decondensing chromosomes
contractile ring creating cleavage furrow
centriole pair marks location of centrosome

Fig. 2.2. Microtubules and mitosis. Schematic of the various stages of mitosis with annotations highlighting the specific role of microtubules. Taken from (Alberts, et al., 1994).

10

Besides curiosity, a common motivation for this research comes from its implications for cancer treatment. Cancer is characterized by a breakdown in the regulation of cell division. Healthy cells typically allow at least a day between divisions. Cancerous cells take half that time or less. Many treatments for cancer are based on selectively killing cells in the process of division, the logic being that, at any given time, there are more cancerous cells than healthy cells in the process of dividing. More than one cancer fighting drug targets cell division by either destroying microtubules (e.g. colchicine) or stabilizing them (e.g. taxol, vinblastine) (Clarkson, et al., 1986).

Drugs are not the only modifiers of microtubules. Some proteins naturally alter microtubule behavior *in vivo*. These are called microtubule-associated proteins, or MAPs. The best characterized MAPs, known as MAP2 and tau, come from mature neurons, which have very stable microtubule networks since they never undergo mitosis. Not surprisingly, these MAPs promote microtubule assembly and slow disassembly. Proteins have been found which specifically inhibit spontaneous nucleation of microtubules or even sever them. Probably many MAPs exist, each enhancing or suppressing different aspects of dynamic instability. For a review on MAPs, see Matus (1990) or Cassimeris (1993). With all the possibilities for interactions between proteins in biological systems, perhaps the most surprising fact is that the amazing dynamic instability of microtubules is due to only one, tubulin itself.

2.2 Structure

The constituent protein of microtubules is called *tubulin*. It is a dimer of two very similar globular proteins, called α-tubulin and β-tubulin (MW ~ 55 kiloDaltons ~ 55,000 g/mole) (Krauhs, et al., 1981; Postingl, et al., 1981). The dimer is ~ 40Å in diameter and ~ 80Å long. It has not yet been

crystallized, but its structure has been resolved to a resolution of ~ 20Å by electron microscopy. Structural information is compiled in Amos and Amos, (1991). The dimer does not dissociate unless subjected to severe chemical or thermal stress.

A microtubule is a polymer of the protein tubulin. A protein polymer is an ordered aggregate of identical proteins. They can be linear, like microtubules, flagella or actin filaments, or of a closed geometry, like the coats of viruses and vesicles. Note the word 'aggregate'. Unlike conventional chemical polymers, the subunits of protein polymers are linked by Van der Walls, hydrophobic and other relatively weak interactions, not covalent bonds. What is meant by "polymerize" in this context is equivalent to "aggregate". "Depolymerize" can similarly be replaced by "dissolve". For microtubules, the only sense which is preserved is the sequential nature of the process: the last subunit added must be the first to come off. Throughout this thesis the terms "assemble/disassemble", "polymerize/depolymerize", "grow/shorten" and "aggregate/dissolve" are used interchangeably.

True to its name, a microtubule is a hollow tube. It has an outer diameter of ~ 250Å and an inner diameter of ~ 170Å; see Figure 2.3. The walls of the tube are made of dimers aligned head-to-tail (α-to-β) in long parallel lines called protofilaments. Neighboring protofilaments are offset by a fraction of a dimer ~10Å, so that the surface lattice looks like a stack of three helices, each with a pitch a dimer-and-a-half high. As a consequence, the helices "change flavor" (i.e. from α to β, or β to α) every turn and there is a sort of seam that runs the length of the tube. The tube has polarity, not just from the sense of the helices, but also because one end exposes only α-tubulin and the other only β-tubulin (Mandelkow, et al., 1986).
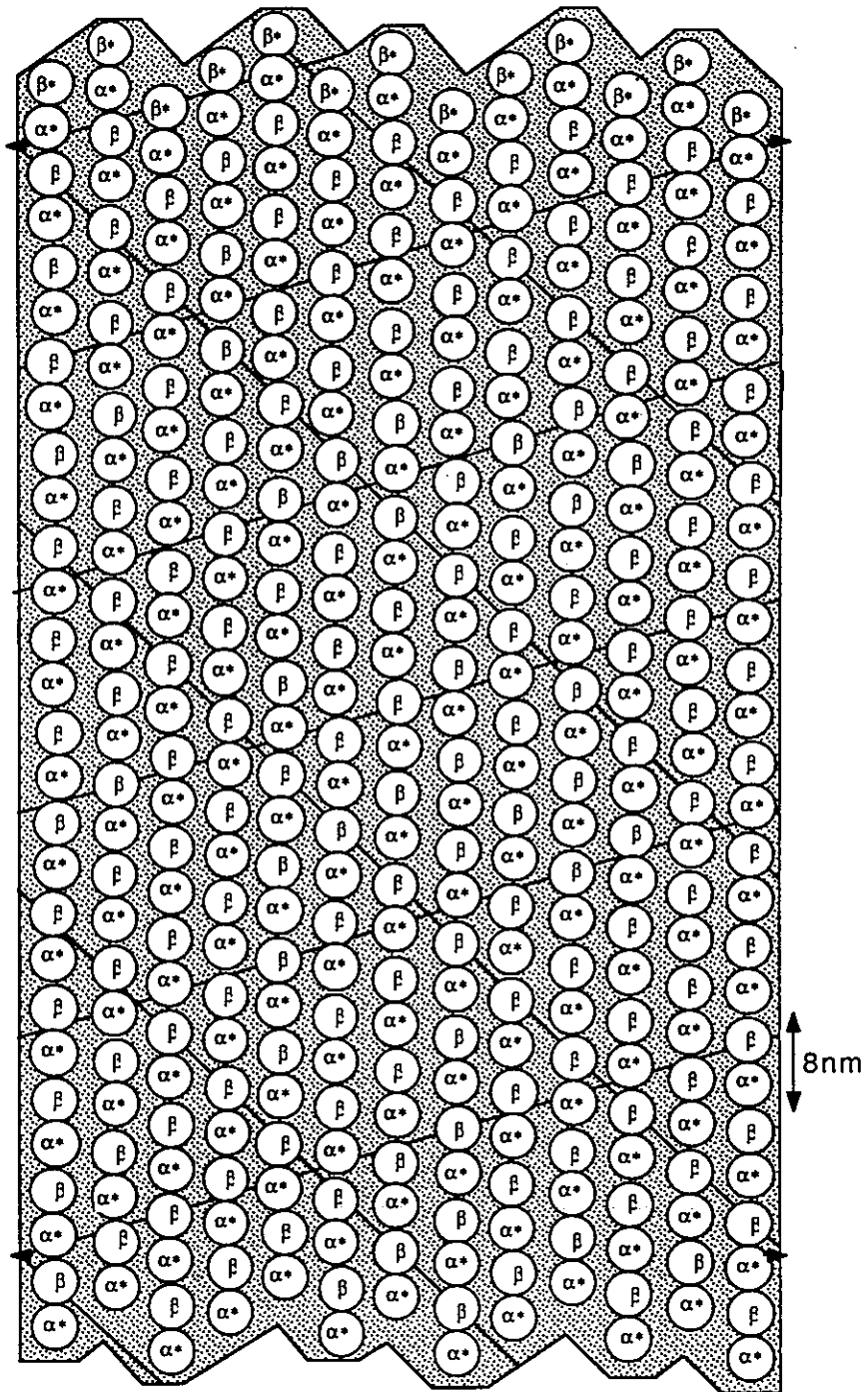
Fig 2.3. A schematic of the lattice structure of the microtubule wall. The '*' represents a monomer which has bound a molecule of GTP (section 2.3). "Photocopy this page (enlarging it, if possible) and cut around the boundary, leaving a white strip along one side for gluing. When joining the two sides to make a cylinder, the arrows at the sides should line up." Reprinted from (Amos and Amos, 1991), p.120. (Note: the seam is not properly depicted.)

13

The number of protofilaments (n_{pf}) in a microtubule can be distinguished under the electron microscope. In living systems, they usually number 13 and are aligned with the tube axis. In purified systems, protofilament numbers ranging from 10 to 17, have been observed. In microtubules with $n_{pf} \neq 13$, a super-twist about the microtubule axis is needed to accommodate the offset between neighboring protofilaments (Chrétien and Wade, 1991). The distribution of n_{pf} in a population of microtubules is sensitive to surrounding chemical conditions (Ray, et al., 1993).

2.3 Chemistry

Microtubules assemble from tubulin dimers, either spontaneously or on nucleating sites, in a buffer at near-neutral pH (6.3 < pH < 7.0), provided the temperature is right (10°C<T<40°C) and excess amounts of guanosine-tri-phosphate (GTP) and Mg^{++} are available. α-tubulin and β-tubulin each bind one molecule of GTP (represented by an asterisk '*' in Figure 2.3) and, during assembly, the dimer also binds a Mg^{++} ion.

GTP is a common source of chemical energy in living systems. It is a nucleotide (the same one that is used in the genetic code, RNA) with three 'high-energy' phosphate di-ester bonds. When one of these bonds is broken, or *hydrolyzed*, the reaction produces GDP (guanosine-di-phosphate), inorganic phosphate and about 10 kT of free energy (Lehninger, 1970).

Mg^{++} is essential for microtubule assembly and tubulin stability. It increases the affinity of tubulin for binding GTP. In its absence, tubulin preferentially binds GDP (Correia, et al., 1987). Tubulin is remarkably sensitive to the difference between Mg^{++} and Ca^{++}. The standard explanation is based on the difference in the co-ordination numbers of the two cations: Mg^{++}: 6 and Ca^{++}: 8 (Fraústo da Silva and Williams, 1991). In fact, tubulin has

14

a much stronger affinity for Ca^{++} than for Mg^{++}. When Ca^{++} is available, tubulin cannot assemble into microtubules. To observe microtubule assembly *in vitro*, EGTA is added to the buffer. EGTA binds Ca^{++} with great affinity, effectively removing it from solution.

The GTP bound to α-tubulin never hydrolyzes and never exchanges with GTP in solution. The GTP bound to β-tubulin can exchange with GTP in solution and does hydrolyze, but only after its dimer is part of a microtubule. After hydrolysis, the β-tubulin GDP is no longer exchangeable and remains bound as long as the dimer remains part of the microtubule (Weisenberg, et al., 1976). Thus, GTP hydrolysis is catalyzed by microtubule assembly. However, it is not necessary for assembly. This is demonstrated by experiments with non-hydrolyzable analogs of GTP (e.g. GMPPCP) bound to tubulin: microtubules nucleate and grow, but do not disassemble. So, GTP-hydrolysis is essential for dynamic instability (Hyman, et al., 1992).

2.4 Dynamic Instability

If a single microtubule is monitored for ten or fifteen minutes, its length will be seen to fluctuate macroscopically and erratically. This extraordinary behavior is called dynamic instability. Figure 2.4 shows a typical plot of a microtubule's length vs. time. Note the steady polymerization at a rate of a few microns (1 μm ~ 1625 dimers) per minute. Occasionally, abrupt changes in the rate of growth are seen (Gildersleeve, et al., 1992). Even more dramatic are the sudden switches to shortening at a rate about ten times faster than growth. This abrupt transition is called a "catastrophe." Catastrophes are sometimes followed by their equally dramatic counterparts, "rescues," in which the microtubule suddenly stops depolymerizing and begins polymerizing once again.

15
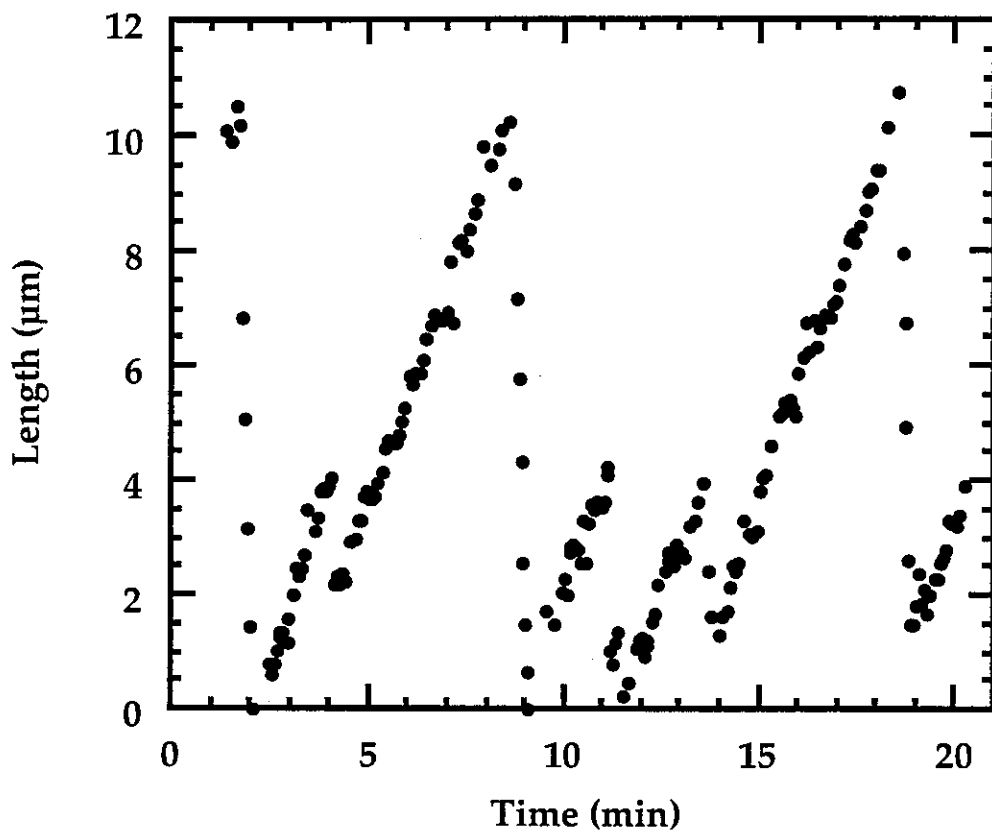
Fig 2.4. Length vs. time of a single microtubule. An example of dynamic instability. Data taken from the plus end, C = 14 μM, T = 25°C.

Dynamic instability can be observed in real time under the light microscope (see section III.3). Most observations are made on microtubules which grow from fixed nucleating sites. Anchored in this way, a microtubule does not leave the plane of focus and the dynamics of each end can be distinguished. The end of the microtubule that exposes only β-tubulin has been identified as the faster-growing, more dynamic "plus" end (Mitchison, 1993). The α-tubulin end grows more slowly, has catastrophes less frequently and rescues with a higher probability. It is called the "minus" end. The distinction can actually be rather subtle. When the growth rates of populations of plus and minus ended microtubules are compared, considerable overlap is found. The most noticeable difference is in the frequency of rescue, which is higher for the minus ends (Kowalski and Williams, 1993).

Immediately the question arises, are catastrophes and rescues independent events? do they occur at random? or, are they correlated? and, do they happen at regular intervals? Ideally the answers would be found in Fourier transforms of the length vs. time of individual microtubules over times long enough to cover hundreds of events. Unfortunately, time series of individual microtubules that contain even as many as ten events are very difficult to obtain. One obstacle is the occurrence of "complete catastrophes," in which a microtubule is not rescued and disassembles all the way back to the nucleating site. Even under conditions where complete catastrophes are rare, the gradual denaturation of tubulin limits the observation time to only ~ 10 times the average period of growth (see section III.1.4). The best experimental evidence for the stochastic nature of the transitions between growth and shortening comes from the exponential nature of the distribution of microtubule lengths in a population (see section IV.2.2).

17

2.5 GTP cap models

What can be said about the underlying cause of dynamic instability? The only thing that is absolutely clear is that it requires the hydrolysis of GTP. Several models have been developed based on this fact. Reviews are given in Caplow (1992) and Erickson and O'Brien (1992). All models follow the same general reasoning, which goes as follows:

Tubulin with GTP bound to its β-monomer (GTP-tubulin) assembles into microtubules. Presumably, therefore GTP-tubulin is stable within the microtubule. When GTP is hydrolyzed and GTP-tubulin becomes GDP-tubulin, some of the energy released by the hydrolysis excites the associated dimer into a different state (i.e. conformation). In this new state, it is energetically more favorable for GDP-tubulin to be in solution rather than in the microtubule and, given the chance, GDP-tubulin will leave the microtubule. However, if before hydrolysis the dimer was buried in the microtubule by the addition of other dimers, it will not be able to escape. Thus, the microtubule is usually depicted as a fundamentally unstable structure made of GDP-tubulin, held together by a stable "cap" of GTP-tubulin at its end which has not yet hydrolyzed. The conclusion is that loss of this cap exposes GDP-tubulin at the microtubule end, allowing it to return to solution, and resulting in disassembly of the microtubule. In other words, loss of the cap causes catastrophe. (These model formally considers rescue.)

Models differ in their proposed mechanisms for hydrolysis, as shown in Figure 2.5. Some treat it as a stochastic process, independent of the growth rate (Figure 2.5a) (Carlier and Pantaloni, 1981; Mitchison and Kirschner, 1984). Others assume it is catalyzed by the presence of a neighboring GDP-tubulin dimer, and therefore propagates as a front (Figure 2.5b) (Carlier, et al., 1987;
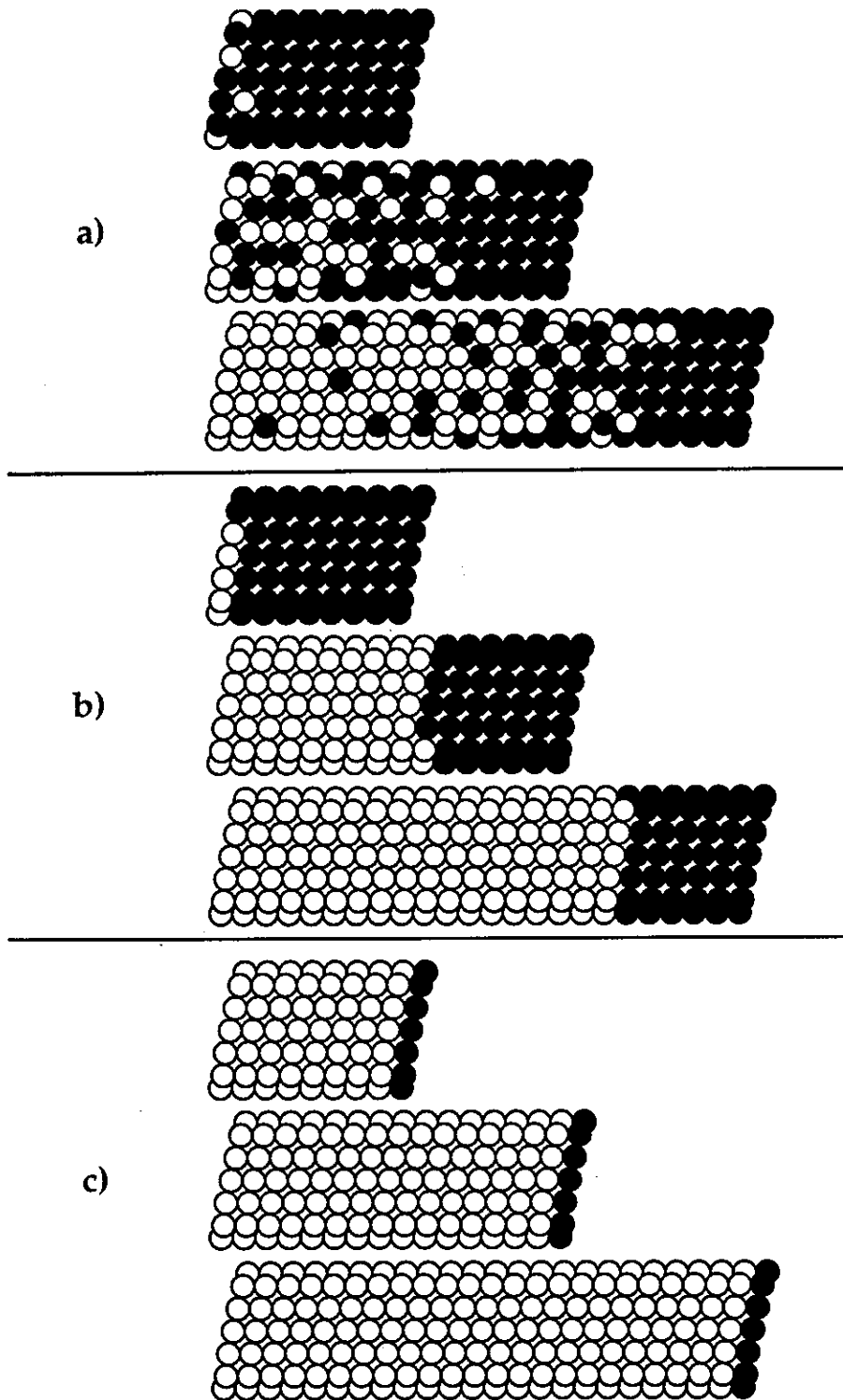
Fig 2.5. Schematics of the GTP-cap models. White dots represent GDP-tubulin dimers and black dots represent GTP-tubulin dimers. a) Stochastic hydrolysis b) Front propagation of hydrolysis c) Immediate hydrolysis. Images adapted from Figure 7 of (Stewart, et al., 1990).

19

Melki, et al., 1990). A third class of models proposes that hydrolysis is catalyzed simply by the addition of the very next dimer, creating a cap only one dimer deep (Figure 2.5c) (Bayley, et al., 1990).

These models all fail to match observations of how the frequency of catastrophe depends on the rate of microtubule assembly (Caplow, 1992; Erickson and O'Brien, 1992). The main problem is that they set a time scale which is independent of the growth rate. They therefore all find the frequency of catastrophe is extremely sensitive to the difference between that time scale and the time for addition of new dimers.

This problem has been solved in a more recent model. It is a sort of combination of two of the previous models. In this model, hydrolysis is both a stochastic process, nucleating at random along the microtubule, and a front, propagating from the site of initial hydrolysis towards either end of the microtubule. A key feature is that the front is presumed to be fluctuating, or diffusing. That is, the front does not propagate smoothly, but rather in spurts or hops. The size of the hop has an exponential distribution with a characteristic size (in units of dimers) fit to the data. This model has had success where the others have failed (Flyvbjerg, et al., 1994).

We use a variation on this model to interpret the observations in this thesis (section IV.6). It shifts the emphasis from GTP-hydrolysis to microtubule structure. The model is based on cryo-electron microscopy observations of growing microtubules (Chrétien and Karsenti, 1995). Micrographs show microtubules that are "unzipped" beyond some point and open into sheets at their ends, as illustrated in Figure 2.6. In the model, the sheet portion acts as a stabilizing cap, while the tubular portion is unstable to disassembly. To make correspondence with the previous model, the sheet grows smoothly, but the zipper both fluctuates (moves forward in spurts) and
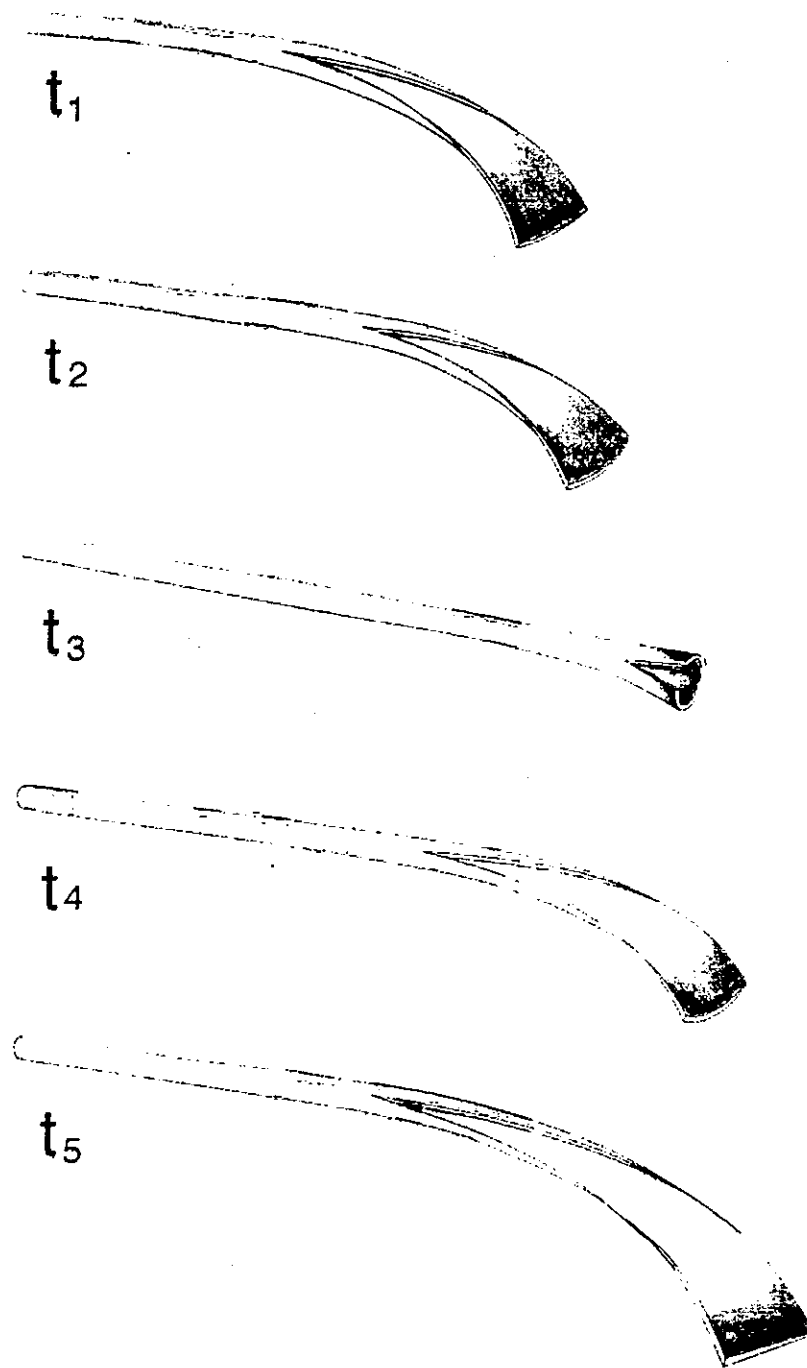
Fig 2.6.   Artist's conception of a zippering microtubule.   Reproduced from (Chrétien and Karsenti, 1995).

and nucleates (when a portion of sheet independently wraps into a tube). When the zippered region consumes the sheet and a blunt end is created (Chrétien, et al., 1995), the destabilizing effects of hydrolysis that have been accumulating within the microtubules become effective and catastrophe occurs.

Thus, the zipper model should have mathematical aspects in common with the most successful GTP-cap model. In addition, it creates a mechanical imagery which can be a powerful tool for developing intuition and inspiring further models. For example, this model immediately suggests a natural mechanism for rescue: If a sheet portion becomes very long (outstrips the zipper) it may curl into a tube on its own, and begin a new zippering front. There is a chance, then, that this process will trap a dislocation or defect between the two zippering fronts. Thus, a rapidly growing microtubule will be littered with defects along its seam which may force it to pause as it disassembles, creating an opportunity for assembly to begin again (i.e. rescue).

It should be noted that attempts to measure the size of a GTP-cap have generally failed. Radioactive labeling experiments find the amount of GTP-tubulin in assembling microtubules is undetectably small (O'Brien, et al., 1987; Stewart, et al., 1990). Rapid dilution experiments, which abruptly stop growth and measure the time elapsed before catastrophe, have placed an upper bound of about 1.5 μm (~ 200 dimers head-to-tail) on the cap size and failed to detect any dependence on the assembly rate (Voter, et al., 1991; Walker, et al., 1991). Finally, cutting the microtubules at various distances from growing ends has been shown to result in catastrophe of the plus end and rescue of the minus end, yielding no measure of cap size for either (Walker, et al., 1989). The consensus is that a GTP-cap, if it exists, must lie below the resolution of all of these experiments, < 200 dimers deep.

CHAPTER III

METHODS

This chapter is dedicated to those interested in conducting experiments on microtubules but who, like the author, come to the subject without any experience in biological techniques. Thinking back, I can recall my initial skepticism: the techniques seemed like a combination of cooking and black magic. This attitude can make for an agonizing beginning. To gain experience and confidence quickly and pleasantly, my first piece of advice is, suspend disbelief.

My other pearl of wisdom is, introduce yourself to the working world of biology. Biologists are perpetually acquiring, developing and sharing new techniques. They will often take the time to introduce a humble novice to a procedure. There is no better way to learn proper technique than by this kind of apprenticeship. If tutors are not readily available but the methods that interest you are outlined in a paper, consider requesting a copy of the detailed protocol from the authoring lab. Home protocols will often contain helpful steps or notes too minor for publication. Finally, remember to reference the library and bio-tech supply companies. There is a wealth of journals, books, laboratory manuals and ready-to-use kits with step-by-step protocols all devoted to communicating technique and procedures.

The body of this chapter is divided into four parts. The first is a series of tidbits, essential for control over the experiment, which should become second nature. The second tells how to purify, characterize and maintain a stock of pure tubulin. The third details the sample preparation for observation under the microscope. The fourth describes the microscope, apparatus, data acquisition and analysis. A list of the manufacturers and suppliers is given after the references at the end of the thesis.

0. Fundamentals

Keep Clean. Cleanliness is control – control over solution composition and control over bacterial contamination. Disposable labware is the easiest answer. When disposables are too expensive, a careful wash with clean-rinsing soap (e.g. Micro®, International Products) and tap water, a final rinse with pure (distilled or deionized) water, and oven drying usually suffice. Clean glassware should be stored with its openings covered (e.g. with aluminum foil) to prevent dust from accumulating inside.

Wear Gloves. Not only do they keep hands clean, they keep the enzymes, grease and germs that live on hands out of the experiment, which is actually more important. They should fit well and be discarded and replaced with fresh ones regularly. For sample preparation, use powder-free gloves.

Watch the Pipette Tip. Pipetting is to biology what soldering is to electrical engineering. We used Rainin® pipettors and tips. For good results it is essential to keep an eye on the pipette tip. Make sure it is clean and dry. Make sure it seals tightly to the body of the pipettor. Try not to plunge it deep into the liquid being aspirated to avoid get drops of liquid on the outside. During aspiration, check the speed. There should be no splashing and no air bubbles entering the tip. In transfer, don't let anything touch the tip or knock a drop out. If you need to use two hands (say, to open a bottle) before dispensing, consider putting down the pipette. Use a gentle motion and lay the pipette at an angle that keeps the liquid in the tip. Again, make sure the tip doesn't touch anything (like yourself). When dispensing, touch the tip to the side of the container or hover it above the liquid surface to let the last drop wet its way off of the tip. Check to be sure that the entire volume was delivered. Never reuse pipette tips. Never use a pipettor without a tip.

For the best accuracy, pipettors should be used near their full capacity. Viscous liquids must be pipetted slowly, if at all. Usually, better results are obtained by weighing a viscous liquid and referencing its density. Precision, gas-tight syringes (e.g. series 1700, Hamilton) should be used for volatile liquids or liquids that might dissolve the plastic of normal pipette tips (e.g. chloroform).

1. Tubulin Purification

The purification of tubulin is a good exercise for the experimental physicist interested in approaching biological systems. It involves only very basic biological techniques and it yields a gratifyingly large quantity of pure protein – typically several milligrams. The logic is simple. First, separate the microtubules from the rest of the tissue. Then, separate pure tubulin from microtubule-associated proteins (MAPs, section II.1). Finally, determine the concentration and purity of the tubulin solution.

Microtubules are separated from tissue by repeated cycles of centrifugation at alternately high and low temperatures. Since they tend to assemble at high temperatures and disassemble at low temperatures, they are isolated by saving the lighter fluid (supernatant) after the cold spins and the heavier sediment (pellet) after the warm spins. To separate tubulin from MAPs, the solution is washed over a column of cation-exchange resin (e.g. phosphocellulose). At pH<7, tubulin is negatively charged and MAPs are positively charged, so MAPs stick to the resin while tubulin passes through the column unretarded. Finally, the concentration of the pure tubulin solution is adjusted with another cycle of centrifugation and measured from its absorption of ultra-violet light. The level of contaminating protein is determined, or at least bounded, by gel electrophoresis.

The rest of this section discusses these procedures *in detail*. These comments are intended to supplement the purification checklist included in Appendix A. The checklist includes every step, from securing fresh tissue to storing the purified solution, and prompts the user for essential notes and calculations. It was designed to be taped into the laboratory notebook and annotated during the procedure.

The purification of tubulin was taught to me, with generosity and patience, in Ted Salmon's lab at the University of North Carolina, Chapel Hill. It is based on the original by Shelanski and Taylor (1967). A similar protocol is published in (Williams, et al., 1982). In fact, volume **85** of the journal *Methods in Enzymology* contains many useful tubulin-related protocols.

1.0 Making Buffers

Every biological experiment or procedure begins with making buffer. It is a lot like cooking: an essential task, a chore, a mystery to the novice, but a lot easier. (I am not a very good cook.) Still, a few hints may be helpful:

The goal is to put a known weight of dry material into a known volume of liquid (e.g. water) at a desired pH. Make all the calculations (i.e. figure the desired amount of dry weight) before starting. Put an empty weighing dish on the balance and add dry material, being careful not to spill onto the balance pan outside the weigh-dish. If you overshoot the target, discard some of the material from the weigh-dish, but do not return it to the container (to avoid contaminating the stock). Put about 3/4 of the final volume of water into a beaker. Transfer the dry weight into the water by adding a little water to the weigh-dish, suspending the contents, and pouring them into the beaker. Check to make sure the weigh-dish is completely

empty. If not, add a little more water to the dish, swish, and return it to the beaker. After adding all the buffer components to the beaker, stir until they are completely dissolved. Use a pH meter to measure the pH of the solution while stirring with a magnetic stirrer. Adjust the pH to its proper value by adding drops of concentrated acid or base (e.g. 10 M NaOH or HCl). Note that some buffer salts (e.g. PIPES) do not go into solution if the pH is too high/low. If salts do not dissolve, check the pH with pH paper and adjust it coarsely while stirring. Finally, bring the solution to its final volume with water.

To avoid bacterial contamination, sterilize the buffer (e.g. by forcing it through a 0.2 μm filter) and store it sealed, at 4°C (in a refrigerator). When working with buffer that has been in storage for a long time, sterilize it once again before use (a syringe and syringe filter is suitable for quantities ~ 1 to 10 ml). If the buffer is consumed steadily, consider keeping concentrated liquid stocks of the components so they can be combined and diluted as new buffer is needed. The recipes for the buffers used in this thesis are given in Appendix B.

1.1 Isolating Tubulin

We begin with a brain. Brain tissue is particularly suited for purifying tubulin since neurons are full of microtubules which support their axons and many dendrites. Brain *protein* (i.e. excluding water, sugar, etc.) is about 30% tubulin by weight, but don't expect a yield anywhere near that figure. We typically extracted about 60 mg of tubulin from about 300 g of brain. We used cow brain (~ 250 g each). It is reasonable to assume that the tubulin from pig, also commonly used in the literature, behaves comparably. However, tubulin from animals that live in extremely different conditions (e.g, Arctic fish) can be expected to differ (Himes, 1989).

The freshness of the brain is paramount. Death releases enzymes which digest proteins like tubulin. As little as two hours after the kill, there is not enough viable tubulin left in a room-temperature brain to bother purifying. It is essential to cultivate good relations with the people at your favorite slaughterhouse (e.g. Trenton Packing). The FDA inspector must be persuaded to inspect the head as soon as its removed, and the slaughtermen must be willing to saw open the skull and remove the brain immediately thereafter. It should be possible to immerse the brain in ice-cold buffer and bury it in crushed ice before half an hour has passed since the time of death. On ice, the digestive processes are much slower and the brain(s) can be taken to the lab without much loss. Still, the faster, the better.

The number of brains used is usually constrained by the volume that can be centrifuged at one time. Such calculations should be made well in advance, so that sufficient quantities of chemicals and buffers can be prepared and the proper centrifuge(s) and rotor(s) can be reserved.

In the lab, with the brain(s), everything should be on hand to begin the first spin (centrifugation) as soon as possible. The goal is to keep the tissue cold through all the manipulations (often at the expense of your own comfort). A cold room makes this easier, but we have managed with a lot of crushed ice and a refrigerator.

First, the meninges, the tough, bloody membrane that surrounds the brain, must be removed and the cerebellum, the white mushy lump at the base of the brain, must be discarded. Unfortunately, I have never found a convincing reason for these steps. I assume the goal is to begin with a homogeneous product. Removal of the meninges is easiest if the brain is nice and cold. Wear gloves and use Kimwipes® (Kimberly-Clark) to get a good grip on the membrane.

Once clean, the brain is snipped into chunks and put in a blender with buffer, ATP and PMSF (see Appendix B). PMSF inhibits the enzymes that digest proteins (proteases). It isn't very soluble in water, so don't worry if it doesn't seem to mix in well, blending will do the trick.

The resulting homogenate (brain shake) is transferred into chilled centrifuge tubes, placed in a chilled rotor and spun at 4°C. Centrifuge tubes should be filled to just below (not touching) the cap and balanced in pairs. It is better to balance leftover solution with a tube of water/glycerol rather than split it between two tubes and leave each less than half full. This is because the separation between heavy and light is better defined over larger distances. The theory and practice of centrifugation are reviewed in Rickwood (1984).

The first cold spin separates the material into a red liquid supernatant (containing tubulin) and a flesh colored, mushy pellet. The pellet typically occupies about half the volume of a tube. The supernatant is poured into a chilled graduated cylinder, on ice. When pouring, pay attention to minimize mixing at the pellet/liquid interface. When the pellet is mushy, as it is at this stage, the liquid should be poured off slowly, holding the tube with the pellet side down. If the pellet is firm, as it will be later on, it is better to minimize the contact between the fluid and the pellet by pouring with the pellet side up.

A 100 µl sample of the supernatant should be removed and saved in a freezer (~-20°C). This is repeated at every stage in order to create a record of the purification. The samples should be labeled according to the temperature of the centrifugation: H(ot) or C(old), the round of centrifugation: 1(st), 2(nd), etc., and whether it comes from the P(ellet) or S(upernatant). For example, this sample is labeled C1S. After the purification is complete, and especially if it is not successful, these samples can be run on an electrophoresis gel to see which steps were most efficient and which were wasteful.

The rest of the supernatant is prepared for the next spin by adding ATP, GTP and glycerol. Here ATP is used to remove motor proteins (see section II.1) which bind strongly to microtubules in the absence of ATP (the rigor state). GTP is essential for microtubule polymerization (see section II.3), and glycerol enhances polymerization (see section IV.4).

The enhanced supernatant, which has been kept cold until now, is then distributed into warm centrifuge tubes. The tubes are balanced in pairs and incubated in a water bath at 35°C to promote microtubule polymerization. Actually, 37°C (cow body-temperature) is the recommended temperature, but 40°C can damage the tubulin, so we tend to err towards cooler temperatures.

During the incubation period, preparations are made for the warm spin to come. Both the centrifuge and rotor must be warmed. As soon as a cold spin is over, the centrifuge should be set to a warm temperature. If it isn't able to exceed ambient, at least the refrigeration should be turned off. The rotor is about 10 kg of solid titanium and won't warm quickly enough if simply left in a warm environment. We warmed a chilled rotor by running hot tap water over it for 5 to 10 minutes. It is very important to dry the rotor thoroughly to prevent 1) contamination of the centrifuge vacuum system and 2) corrosion and pitting in the rotor cavities. For the same reasons, after incubating, the centrifuge tubes are wiped dry before being loaded into the rotor.

If time remains before the warm spin, dispose of the mushy pellets. (They become *very* foul *very* quickly.) Dump them into a zip-lock bag, seal the bag, and take it directly to an outside dumpster. Rinse the tubes well and let them soak in soapy water until there is time to clean them properly.

After the warm spin, the centrifuge is set for 4°C and the rotor is immersed in a tub of crushed ice or ice water. The supernatant, still red, is decanted (pellet up) into a graduated cylinder and the centrifuge tubes, with thick, yellow, jelly-like pellets (containing microtubules) in them, are stuck in crushed ice. The volume of the supernatant is recorded and ~100μl (labeled H1S) is removed and saved for later. The rest of the supernatant is discarded.

The pellets are resuspended in cold buffer + GTP, without glycerol. The volume of buffer used is proportional to the total volume of the pellets. A small amount of buffer is added to each centrifuge tube and the pellets are swished and scraped with a clean glass rod until they can be poured out of the tube into a chilled dounce-type homogenizer. The remaining buffer is added to the tubes to rinse out any leftover pellet material, and then added to the homogenizer.

The homogenizer is a large glass tube that comes with a close fitting teflon pestle mounted on a stainless steel rod. The rod is held in the chuck of a drill head (stirrer) in a cold room or refrigerator and the tube is moved up and down over the pestle as it turns (30 - 50 rpm). Fluid is forced through the tight gap between the pestle and the glass, breaking up large particles.

Several important tips for successful homogenization: First, do not exceed the stated capacity of the homogenizer. Second, keep the system cold: hold the tube with a thumb and two fingers near its opening (do *not* grab it in the palm of your hand); also, guide the tube gingerly to minimize the heat generated by friction between pestle and glass. Third, don't create air bubbles! Oxygen in solution denatures protein. The key to avoiding a froth is to make sure the liquid level never falls below the top of the pestle.

After homogenizing, the tube is left to incubate, covered, on ice in the fridge, so that the microtubules depolymerize. The solution is not distributed

31

into centrifuge tubes until *after* incubation. In general, to minimize losses, the solution is transferred as little as possible and only when cold, when the microtubules are depolymerized and the solution is less viscous. This is why warm incubations take place in the centrifuge tubes and cold ones do not. After the cold incubation, another 100μl (labeled H1P) is saved in the freezer.

The cycle of cold and warm centrifugation and incubation is repeated two more times. The details remain the same but the solutions become colorless and the volumes decrease. At the end of the third cycle there may be only two centrifuge tubes (~ 50 ml). From the slaughterhouse to this point takes no less than 12 hours. Therefore, the purification is performed over two days. This is a good stopping point. To stop, cover the pellets with a small, known amount of buffer and freeze them rapidly, in their centrifuge tubes, by submersion in liquid nitrogen. Store the tubes closed, overnight in a -70°C freezer.

The main part of the second day involves washing the protein solution over a phosphocellulose (PC) column. The column can be set up and equilibrated a few days beforehand. Set-up includes 'cleaning' the phosphocellulose and pouring the column. PC is purchased as a dry powder (type P11, Whatman). It must be washed several times in solutions of pure NaOH and pure HCl to replace all the counter ions with Na^+ and Cl^-. Those counter ions are then replaced with the ones in the tubulin buffer and the overall pH is adjusted to 6.7. The protocol is given in Appendix A.

The column is a glass tube with an insert for adjusting its volume and special plumbing for introducing and eluting the solution (cat no. 44x250, Amicon). Clean PC is poured into the column and allowed to settle. It must settle uniformly, without any cracks or furrows to channel the flow. It should be allowed to pack for ten minutes or so under a flow of buffer at the rate that

will be used to pump the protein solution through. The buffer flow rate is controlled by a peristaltic pump (Rabbit-Plus, Rainin). The cross-section of the column, the volume of PC and the flow rate are optimized by experience. General practice is discussed in Scopes (1987) and Harris and Angal (1989).

When the column is ready, the pellets that were frozen overnight can be thawed. They should be thawed quickly in a warm water bath (~ 34°C), and then stuck in ice. Once more, they are resuspended, homogenized, and incubated in the cold (~4°C). 100μl (labeled H3P) is saved, and the rest is centrifuged cold to get rid of anything that denatured overnight. The supernatant is decanted, measured and kept cold. 100μl is saved (labeled C4S) and the rest is washed over the PC column. Flow from the column is collected in 3-5 ml fractions with a fraction collector (model 2110, Bio-Rad) and 10μl from each fraction is rapidly tested for the presence of protein using the Bradford Test (cat. no. 500-0002, Bio-Rad, includes protocol).

The fractions containing tubulin are pooled together, polymerized (incubated warm) and centrifuged one last time. In the meanwhile, 100μl is used in a more precise Bradford Test to estimate the amount of the tubulin in the centrifuge. Based on this estimate, the pellet will be resuspended to the desired concentration for the stock solution. Since the final volume is usually too small (~ 10 ml) to homogenize, the pellets are resuspended by hand (e.g. scraping and stirring with a flame-sealed Pasteur pipette) and allowed to dissolve on ice for a couple hours. To avoid further cycles of centrifugation (and the associated losses), the concentration of the tubulin stock should be greater than the highest working concentration expected, typically 60 or 100μM. The actual concentration of the stock is determined as described in the next section.

The resulting tubulin stock solution tubulin is stored as 500μl 'aliquots' in a liquid nitrogen dewar (model 10XT, Taylor-Wharton). The volume of the aliquots is chosen to 1) reduce the number of times an aliquot is thawed and re-frozen and 2) minimize the surface area per unit volume exposed to air (small volumes can evaporate completely into the very cold dry air). At the beginning of a series of experiments, one aliquot may be further divided and re-stored, so that those volumes are thawed only once more before use.

1.2 Measuring Concentration

Methods for determining the concentration of a protein in solution are generally unable to distinguish between different kinds of protein. It is therefore essential to work with a solution of pure protein in order to accurately determine its concentration. (see section III.1.3). The only absolute measurement of concentration comes from weighing the dry material that remains when a known volume of solution is evaporated. All other methods must be standardized against a solution calibrated in this manner. For a review of methods for determining protein concentration, see Harris and Angal (1989).

The most common techniques are dye-binding (i.e. Bradford, Lowry) and UV-absorption. I found it very difficult to get reproducible results with the dye-binding techniques. UV-absorption has the advantage of being rapid, non-destructive, and robust, plus it does not have the systematic errors of a dye which varies from batch to batch and over time. It requires only a quartz cuvette (cat. no. 8419-W35, Thomas), a cuvette washer (cat. no. 58020-014, VWR) and a UV-spectrophotometer (model DU-45, Beckman).

The one complication with measuring the concentration of *tubulin* by UV-absorption is that GTP also absorbs in the UV. Fortunately, the absorption of protein has a very different spectrum from that of GTP. (Between 240 - 300 nm, the former is largely due to the aromatic amino acids, tyrosine and tryptophan, while the latter is due to the rings of the guanosine nucleotide.) Thus it is possible to extract the relative contributions of each when they are present together.

1.2.1 GTP

At pH 7 GTP has its peak absorbance at a wavelength of 253 nm with an optical density of 13.7 ($O.D. = \log(I_o/I)$) for every 1 cm of path length through a solution of 1 mg/ml concentration (Dawson, et al., 1986). The standard notation is $A_\lambda = \varepsilon_\lambda (^{ml}/_{mg \cdot cm}) C (^{mg}/_{ml}) \ell (cm)$, where $^{GTP}\varepsilon_{253} = 13.7$ mg/(ml·cm) is the extinction coefficient, C is the concentration of protein in mg/ml, and ℓ is the optical path length through the solution. The UV-absorption spectrum of GTP is shown in Figure 3.1 (in our buffer, pH 6.9). Notice that $A_{253}/A_{260} = 1.13$ and $A_{280}/A_{260} = 0.66$.

1.2.2 Tubulin

The extinction coefficient of tubulin has been measured taking into account the contribution from the two molecules of bound GTP, $^{Tubulin}\varepsilon_{280} = 1.15$ (Eipper, 1974). (The measurement was made on rat brain tubulin, which has essentially the same percentage of UV-absorbing amino acids (tryptophan and tyrosine) as cow brain tubulin. Pig brain is significantly different (Lee, et al., 1973).) The UV absorption of tubulin in GTP-free buffer is shown in Figure 3.2. Notice the circled points which indicate that for tubulin $A_{280}/A_{260} = 1.32$.
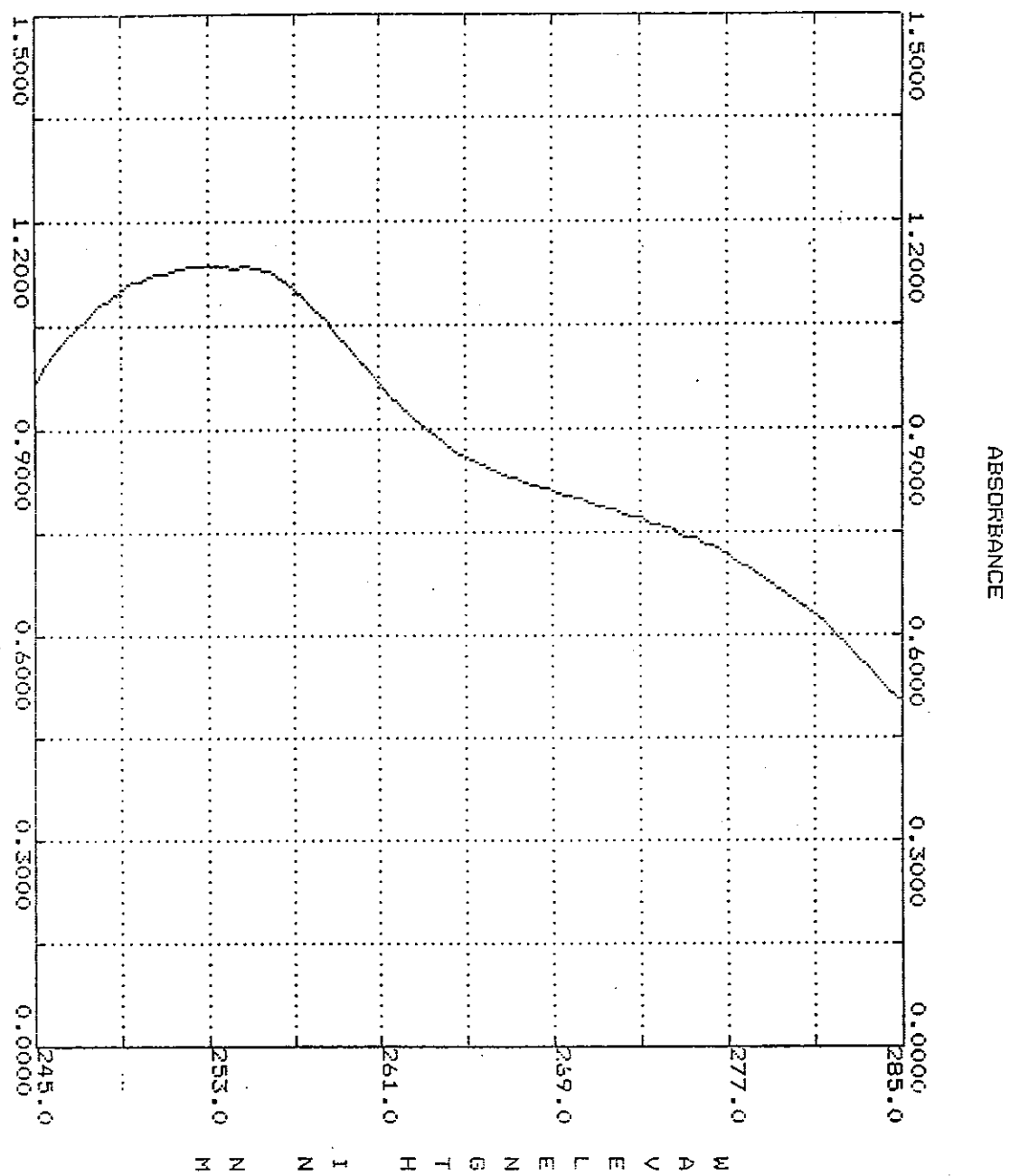
Fig. 3.1. The UV-absorption spectrum of GTP. GTP-sodium salt is dissolved in the standard buffer (see section III.2.2).
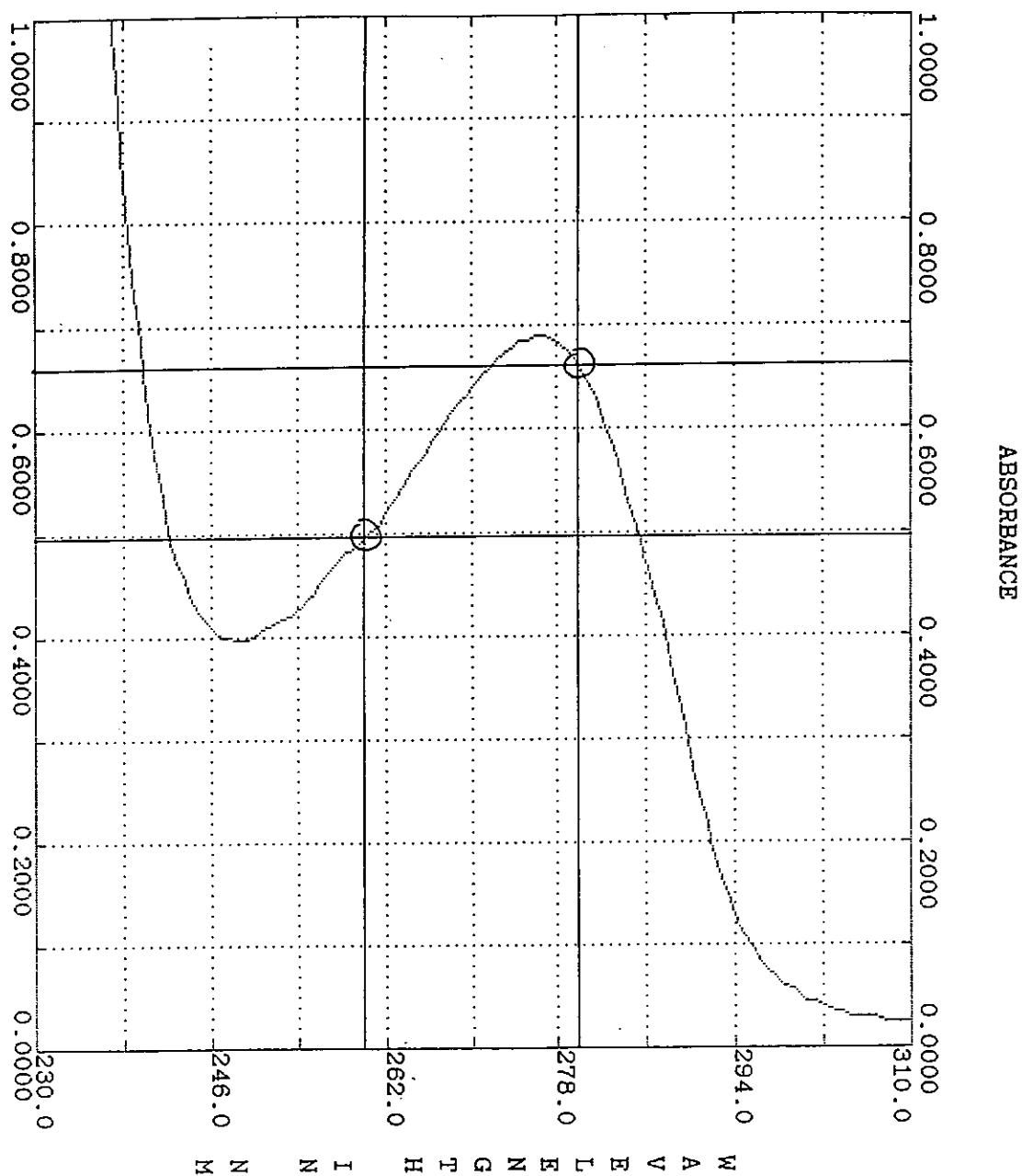
Fig. 3.2. The UV-absorption spectrum of pure tubulin. 0.5 ml of pure tubulin stock was dialyzed overnight at 4°C against 500 ml of standard buffer (see section III.2.2 – no GTP). Though the protein denatures, its absorption is based on the presence of certain amino acids and so is not noticeably affected. The circles emphasize $A_{260} = 0.495$ and $A_{280} = 0.655$.

1.2.3 Tubulin + GTP

For proper perspective, the extinction coefficients can be rescaled by the molecular weight to reflect absorption per molecule. The molecular weight of tubulin (~ 110,000 g) is about 200 times that of GTP (~ 530 g). Thus, GTP molecules absorb 20 times less at their peak wavelength than tubulin dimers at their peak wavelength. Since the stock contains GTP (~1 mM) at 10 to 20 times the concentration of tubulin (~ 50-100 μM), we expect the two peak absorptions to be similar in magnitude. In order not to saturate the spectrophotometer, the stock must be diluted by about 1:20. Figure 3.3 shows the UV-absorption spectrum of the purified tubulin stock solution, diluted by a factor of 1:20 and 1:50 in GTP-free buffer. Note that $A_{280}/A_{260} = 1.10$.

1.2.4 The Calculation

Given the parameters listed above, it is not hard to calculate the concentrations of tubulin and GTP from the absorption spectrum of the tubulin stock. Since this approach was new to the biologists I initially referred to for advice, I will describe the calculation in detail:

From the UV-absorption spectrum of 1:20 diluted stock (Figure 3.3), $A_{280} = 0.740$, $A_{260} = 0.675$, and $A_{253} = 0.640$. Since absorbances add,

$$A_{280} = A_{280}^{GTP} + A_{280}^{Tubulin} \quad \text{and} \quad A_{260} = A_{260}^{GTP} + A_{260}^{Tubulin}. \tag{III.1}$$

Defining $R = A_{280}/A_{260}$, $R^{GTP} = A_{280}^{GTP}/A_{260}^{GTP}$, $R^{Tubulin} = A_{280}^{Tubulin}/A_{260}^{Tubulin}$, equations (III.1) imply

$$R = \frac{A_{280}^{GTP} + A_{280}^{Tubulin}}{A_{260}^{GTP} + A_{260}^{Tubulin}} = \frac{R^{GTP} + R^{Tubulin}\left(A_{260}^{Tubulin}/A_{260}^{GTP}\right)}{1 + \left(A_{260}^{Tubulin}/A_{260}^{GTP}\right)}. \tag{III.2}$$

Since $R^{GTP} = 0.66$ and $R^{Tubulin} = 1.32$ are known (see sections III.1.2.1 and III.1.2.2, above) and $R = 1.10$ is measured (section III.1.2.3), equation III.2 can be solved for $\left(A_{260}^{Tubulin}/A_{260}^{GTP}\right) = 2$. Combined with the right-hand equation of (III.1), this result yields $A_{260}^{Tubulin} = 0.450$ and $A_{260}^{GTP} = 0.225$.
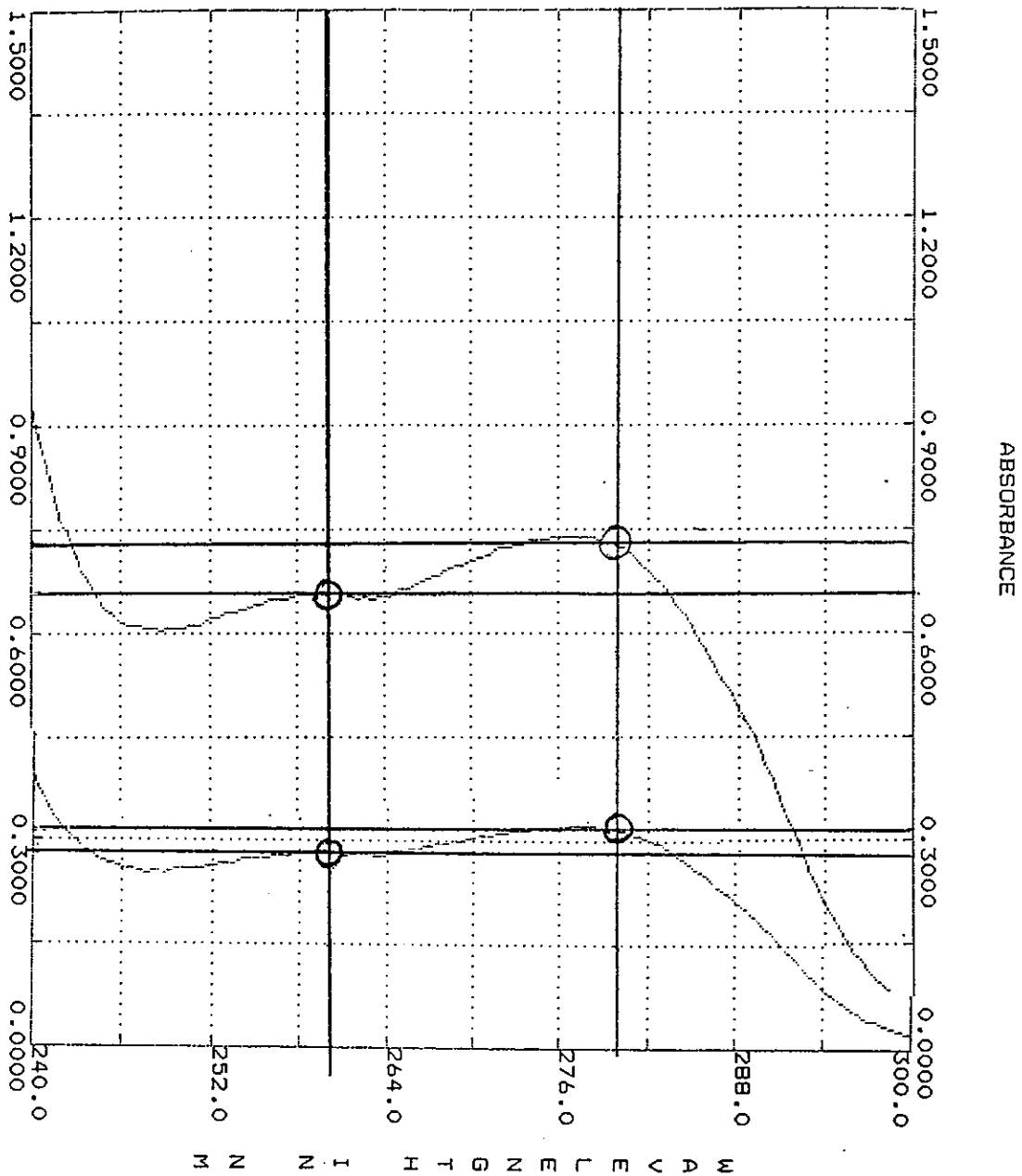
Fig. 3.3. The UV-absorption spectrum of tubulin stock solution. To accommodate the range of the spectrophotometer, the solution has been diluted in buffer (without GTP) by a factor of 1:20 (upper curve) and 1:50 (lower curve). Note the circled points in the upper and lower curves which represent $A_{280} = 0.730$ and $A_{260} = 0.660$, and $A_{280} = 0.315$ and $A_{260} = 0.285$, respectively.

Combined with the ratios from the standard UV-absorption spectra given above, we find

$$A_{280}^{Tubulin} = 0.595 \rightarrow [Tu] = 0.517 \text{mg} / \text{ml} = 4.7 \mu M$$

$$A_{253}^{GTP} = 0.254 \rightarrow [GTP] = 0.019 \text{mg} / \text{ml} = 35 \mu M$$

Since we used the 1:20 dilution of stock, we can conclude that the stock contains 0.7 mM GTP and 94 μM tubulin. The error in this measurement is ±10%, the limit of our ability to dilute accurately (determined by performing several independent dilutions) (see section III.0). As mentioned in the beginning, we must assume that tubulin is the only protein in the solution, which brings us to the next section.

1.3 Determining Purity

To check for contaminating proteins in the purified tubulin solution, gel electrophoresis is used. Electrophoresis separates proteins according to their mobility in a gel matrix. The proteins are completely denatured so their mobility is directly related to their polymer chain length (length ∝ number of amino acids ≈ molecular weight). The technique is standard and detailed protocols come with the necessary equipment. We used the Mini-Protean and Silver Staining Kits and protocols (cat. nos. 165-2940 and 161-0449, Bio-Rad). For a detailed discussion of electrophoresis techniques see Hames and Rickwood (1990).

We loaded three of the five wells of a 12% polyacrylimide gel with excessive amounts of the stock solution and looked for any bands outside of the two characteristic of tubulin (~ 55,000 Daltons). Silver staining reveals bands of proteins with as little as ~ 1 ng in a band. Knowing the total amount of protein loaded into the column which has a barely detectable band, we can estimate the percent (by weight) of the contaminating protein.

40

Figure 3.4 is an example of such a gel (12% polyacrylamide). MAPs are typically higher molecular weight than tubulin (see section II.1), and therefore travel less of a distance in the gel. Contamination is barely visible even at the maximum protein load of 20μg (center column). We conclude that there is <0.005% (w/w) contaminating protein in the stock.

Figure 3.5 is an example of a gel (12% polyacrylamide) of samples saved during the purification procedure. It reveals at which stages unusually large amounts of tubulin were lost. Note the sharp contrast between the samples C4S and PC, which demonstrates the removal of MAPs by the PC column.

1.4 The Lifetime of Tubulin

It is only appropriate that we end the discussion of how to obtain and characterize tubulin with comments about how long the product will last. Tubulin stock can be stored in liquid nitrogen for at least a year without noticeable degradation. At the temperatures needed for experiments (15-40°C), however, tubulin does not last nearly so long. We made all measurements within the first two hours after a sample was brought from storage to room temperature. We originally based this time limit on observations of a microtubule over eight hours at 35°C. Figure 3.6 shows how, after four hours, the length dynamics are noticeably changed.

Recently, our measurements of the rate of spontaneous nucleation of microtubules (which is very sensitive to the tubulin concentration) have yielded an estimate of the lifetime of tubulin $\tau \sim 7.3$ hours at a temperature of 30°C. (Defined as $C(t = \tau)/C(t = 0) = e^{-1} \approx 0.36$, see section IV.1.3). Though the temperature dependence of this lifetime remains to be characterized, it seems our original time limit was probably quite adequate.

41
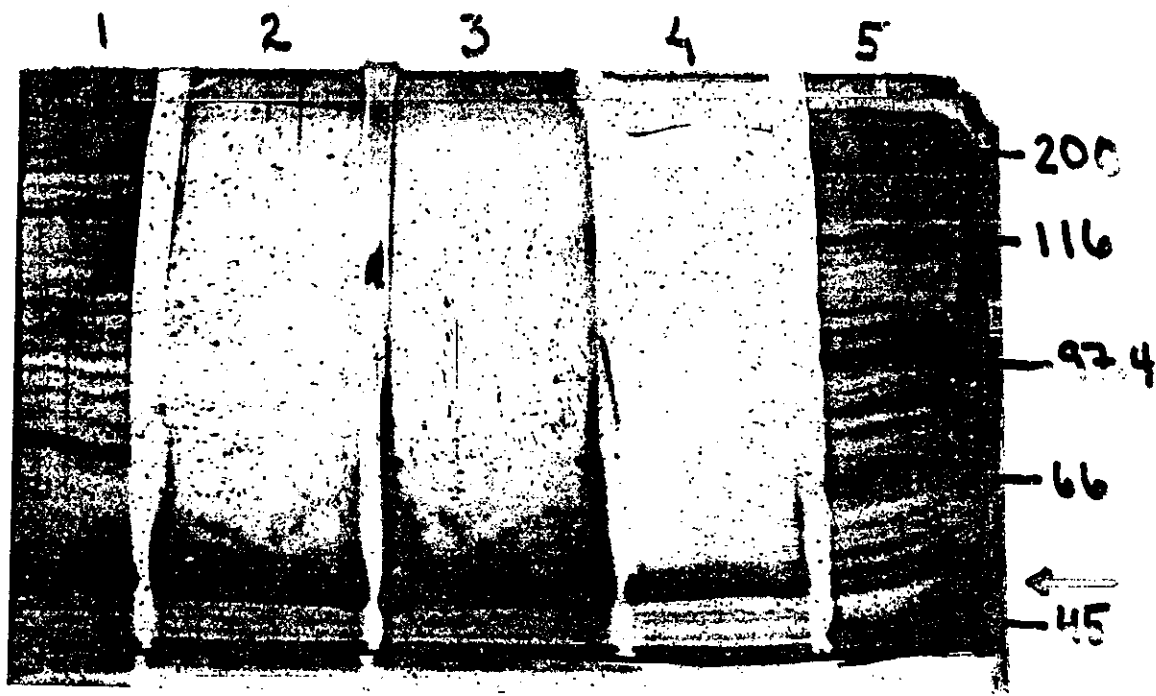
Fig. 3.4. An electrophoresis gel of tubulin stock for determining purity. Reading from left to right, the columns are:

1) 20 μl of sample C4S (before the removal of MAPs);
2) 50 μl of tubulin stock diluted 1:50 (~10 μg protein);
3) 100 μl of tubulin stock diluted 1:50 (~20 μg protein);
4) 10 μl of tubulin stock diluted 1:50 (~ 2 μg protein);
5) 20 μl of molecular weight standards (from top to bottom):
      200kD, 116kD, 97.4kD, 66kD, 45kD. (cat no. 161-0315, Bio-Rad).

The photocopier brings out the faintest of bands in columns 2 and 3 (undetectable by eye). It is generous to presume these represent ~1 ng of high molecular weight impurities, implying that there is <.005% (w/w) MAPs in the tubulin stock. The bulging bands near the bottom are tubulin.
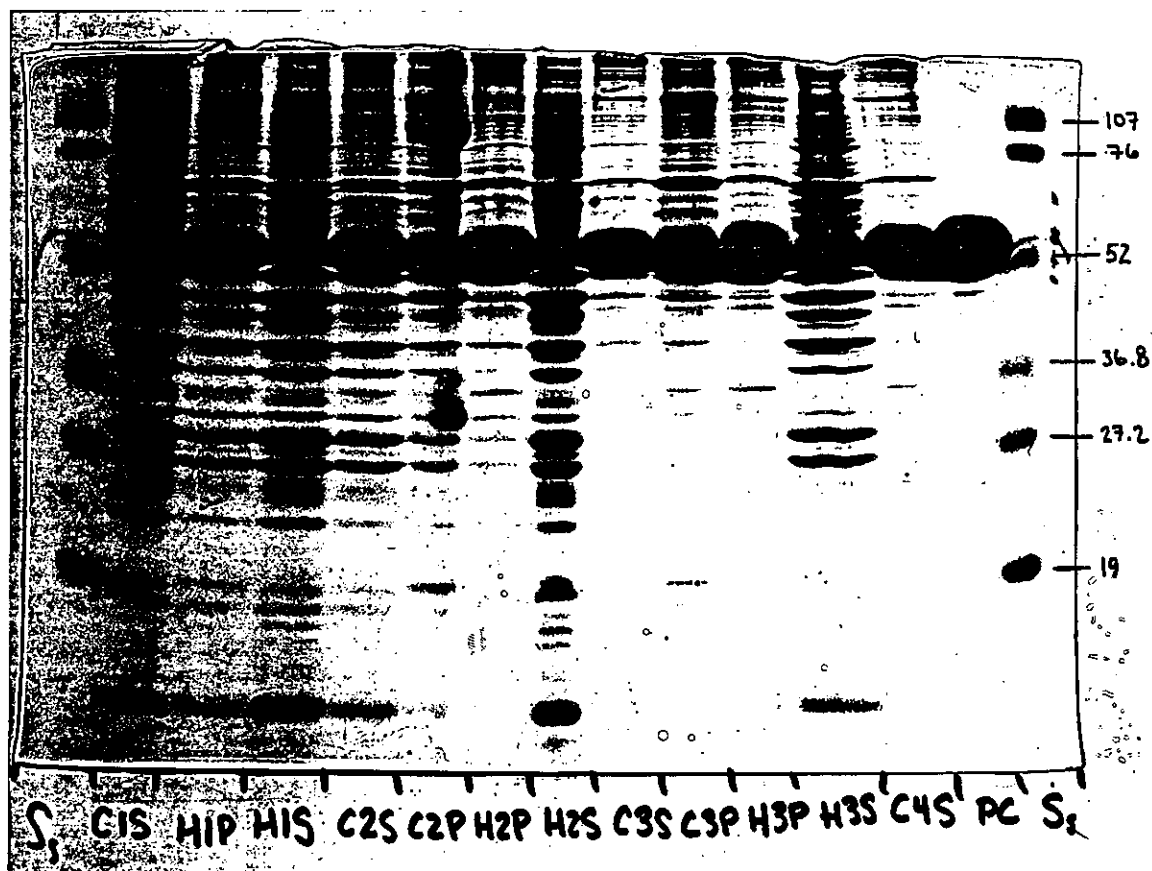
Fig. 3.5. An electrophoresis gel record of the tubulin purification. The columns are labeled according to the temperature (Hot or Cold) and cycle ($1^{st}, 2^{nd}, 3^{rd}, 4^{th}$) of the centrifugation and according to whether the sample came from the Pellet or the Supernatant. The column labeled PC is a sample of the stock after washing through phosphocellulose. Notice the disappearance of high molecular weight protein (MAPs) between columns C4S and PC. The outermost columns, labeled S, are molecular weight standards: (from top to bottom) 107kD, 76kD, 52kD, 36.8kD, 27.2kD, 19kD. (cat no. 161-0304,Bio-Rad).

43
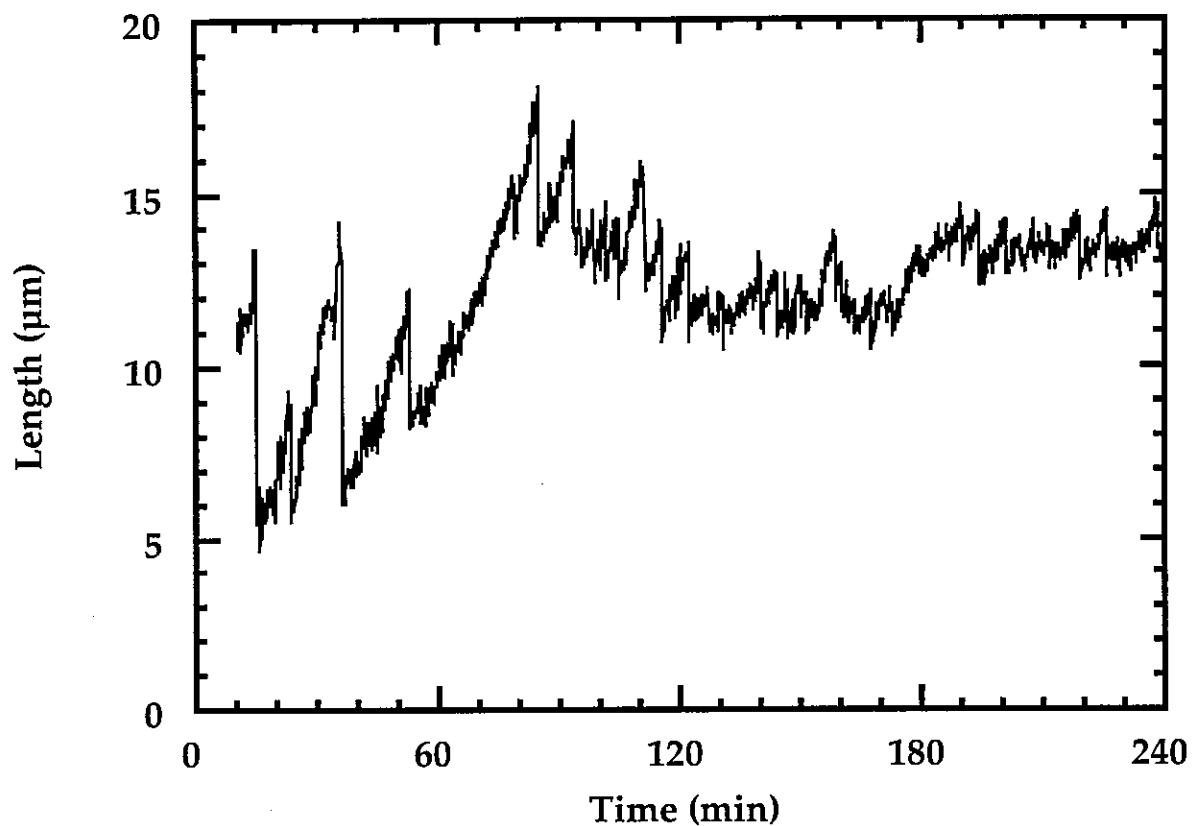
Fig. 3.6. Evidence for the decay of pure tubulin *in situ*. Length versus time of a microtubule from just after warming until four hours have passed. Notice the marked difference in the dynamics that sets in after about 3 hours. C = 14μM, T = 37°C.

2. Sample Preparation

All of the experiments described in this thesis are based on observing tubulin in solution assemble into microtubules under the light microscope. The solution is placed between a glass slide and coverslip which are held apart by wire spacers. The chemical composition (e.g. pH, salt concentration) of the solution is kept constant while the temperature and tubulin concentration are varied. Often, microtubule nucleating sites are included.

2.1 Construction of the Sample

2.1.1 *The Glass*

Each sample was built immediately prior to a measurement from a 75x50 mm (1 mm) microscope slide (no. 2947, Corning) and a 24x30 mm no. 1 coverslip (cat. no. 12-518-105C, Fisher). The slides and coverslips were cleaned by soaking for at least 45 minutes in deionized, sterilized water (PicoPure®, Hydro) (hereafter referred to as pure water) with about 1% detergent (Micro®, International Products) while being heated (~60°C) and "scrubbed" in an ultrasonic cleaner. (The coverslips are conveniently handled with a teflon carrier (cat. nos. A14-01S-0215 and A041-0215, Fluoroware). The slides are conveniently washed in a stainless steel rack (cat. no. 25463-009, VWR). Then they were rinsed for several minutes under flowing tap water, rinsed again in at least three covering volumes of pure water, and stored in 95% pure ethanol. Just before use, a slide was removed from storage with forceps, rinsed in 100% pure ethanol and dried with an ionizing air-gun (TopGun, Simco). The same procedure was repeated for a coverslip. The final rinse is critical. If omitted, the solution may not completely wet the glass as the sample fills, presumably due to deposits of organic residues.

To minimize dust, sample cells were assembled in a laminar-flow hood immediately prior to use. The thickness of the sample is set by a pair of 50μm diameter tungsten wires (California Fine Wire) which run the entire length of the coverslip (see Figure 3.7a). A small brass jig is used to press the coverslip down onto the wires on top of the slide (see Figure 3.7b). In the jig, the slide and coverslip are sealed along the two sides and at the wires with five-minute epoxy (Devcon), as shown in Figure 3.7. The sample thickness can be measured under the microscope by adjusting the focus. Samples built this way are routinely between 1.0 and 1.1 times the wire thickness. Fluctuations across the sample are less than 5 μm.

Before a measurement, the sample cell is filled by capillary action. The open sides are wiped dry with a Kimwipe® (Kimberly-Clark) and sealed with candle wax from a warm Pasteur pipette. The sample is then placed under the microscope for observation. From ice to observation, takes ~ 3 minutes.

2.1.2   The Sample Thickness

Sample thickness is an important parameter in controlling the tubulin concentration. Like most proteins, tubulin sticks to glass (Scopes, 1987). Therefore some fraction of tubulin in the solution is lost to the surfaces of the sample cell. The relative loss decreases as the ratio of volume to surface area increases – that is, as the sample becomes thicker.

Rather than quantify the amount of tubulin lost, we measured the effect of sample thickness on a parameter sensitive to concentration, the proportion of occupied sites, P_{occ} (see section IV.1.1). The results, shown in Figure 3.8, indicate that in samples > 25 μm thick, the effect of the glass surfaces is negligible. Based on this result, our samples were usually spaced with 50 μm wire. Thicker samples were inconvenient because of the limited working distance of the microscope objective.
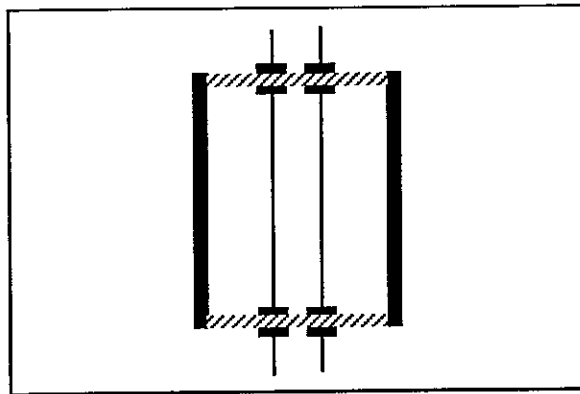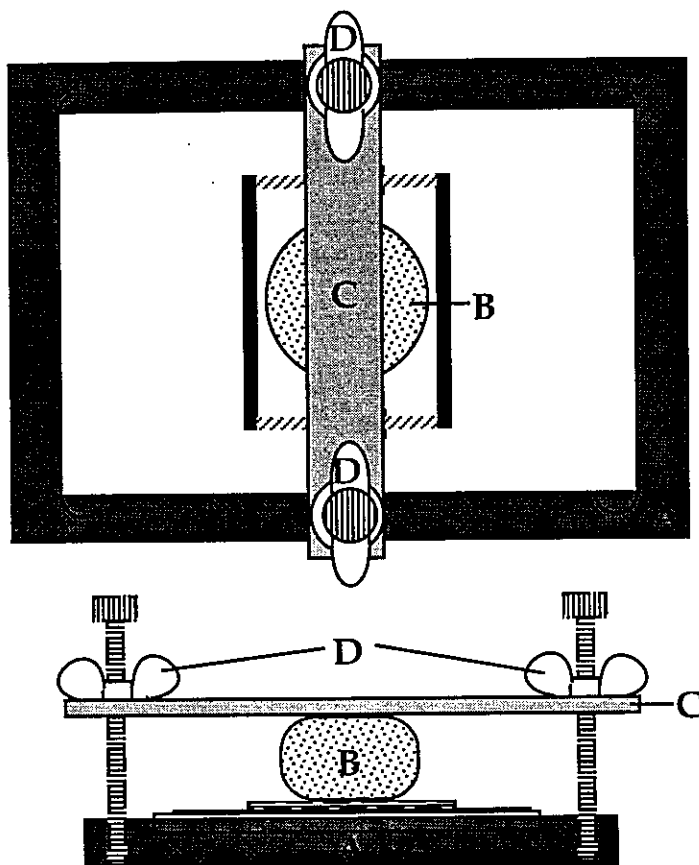
Fig. 3.7. Schematic of a sample cell and the jig used to build it. a) The sample cell, drawn to scale. The black regions are sealed with 5-minute epoxy. The hatched regions are sealed with paraffin (from a candle) after the sample is filled. b) The sample jig. The sample sits in an etched groove in a brass plate (A). The coverslip is pressed onto the wires by a teflon plug (B) when a bar (C), resting on top of the plug, is forced down by tightening a pair of wing-nuts (D).
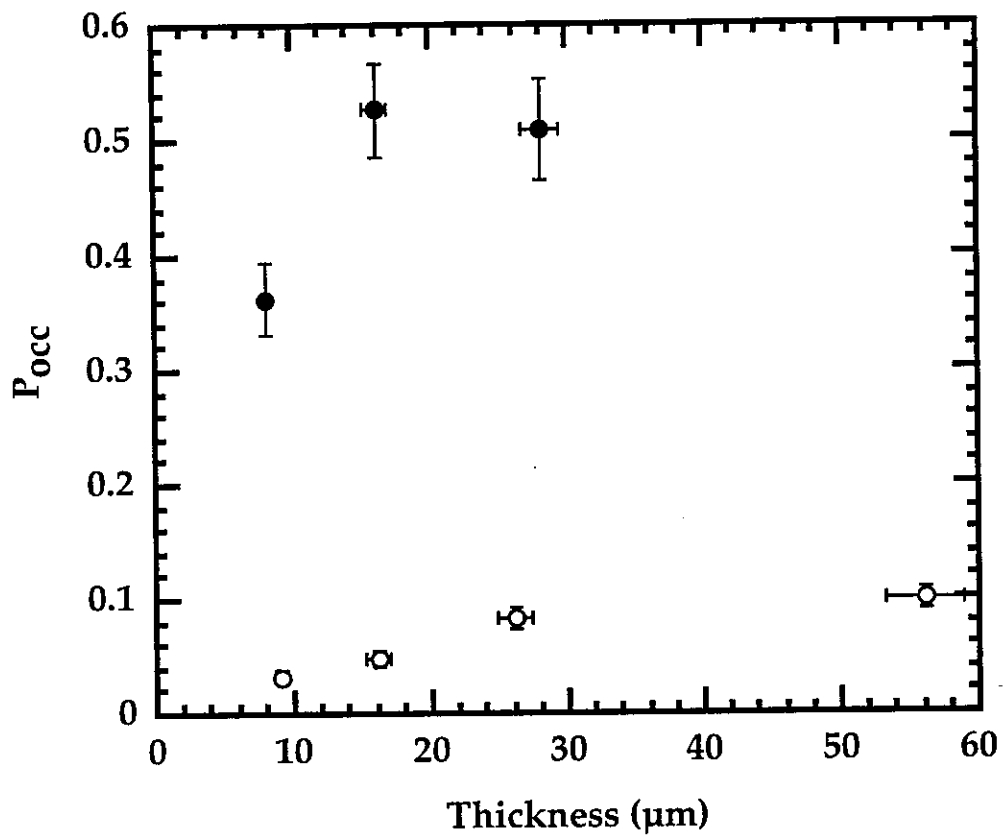
Fig. 3.8. The effect of sample thickness on the proportion of occupied nucleation sites. Black dots: T = 34°C, open dots: T = 25°C; C = 14 μM.

2.2 Solution Composition

2.2.1 The Buffer

The concentration of tubulin in samples is varied between 6 and $54\mu M$ by diluting from the a stock solution ($60\mu M$). To assure homogeneity between samples of the same concentration, and for increased accuracy in dilution, relatively large volumes (several hundreds of microliters) are manipulated and then split into 6-10 aliquots of $45\mu l$ each and stored in liquid nitrogen until immediately prior to use.

The dilution buffer is identical to the stock buffer (see Appendix B). It was chosen for consistency with previous experiments on microtubules (Walker, et al., 1988). The buffer contains 1 mM GTP, 2 mM $MgSO_4$, 2 mM EGTA and 100 mM Pipes, at pH 6.9. Pipes is a standard buffer that works well near this pH. EGTA is a chemical that binds Ca^{++} ions, which otherwise inhibit microtubule assembly (see section II.3). $MgSO_4$ is a source of Mg^{++} which, along with GTP, is needed for microtubule polymerization (see section II.3). These chemical conditions are constant in all the measurements.

The concentrations of GTP and Mg^{++} are chosen to be well in excess of that of tubulin, with Mg^{++} at a higher concentration to compensate for its strong association with GTP (Lehninger, 1970). Since GTP is the only component consumed in the system, its concentration is limiting. The following calculation gives a feeling for the effect: every time a micron of microtubule forms, $\sim 10^3$ GTP molecules are consumed ($1\mu m = 1625$ tubulin). At 1 mM concentration, there are about 10^{10} molecules of GTP per field of view, enough for 10^7 microns of microtubules.

49

It would seem that 1 mM GTP should suffice for the duration of our observations (~2 hours). However, during the short period of warming that takes place as the sample is being filled and placed under the microscope, high concentrations of tubulin (> 60 μM) polymerize almost completely. Under the microscope, the microtubules appear as an extremely dense mesh: one field of view easily contains several thousand microtubules, each at least 30μm long. Thus, a significant amount of GTP is consumed. In particular, we have had trouble reproducing results from samples with tubulin concentrations near 100μM. Rather than changing the composition of the buffer, which has been shown to have independent effects on microtubule dynamics (Simon, et al., 1992), we limited the tubulin concentration <60μM.

2.2.2 The Nucleating Sites

If nucleating sites are desired, they are introduced in the diluting buffer. Many natural microtubule organizing centers exist (e.g. centrosomes, see section II.1). We used axonemes from the flagella of sea urchin sperm prepared as described in Walker, et al., (1988) (a generous gift of E.D. Salmon). Axonemes are bundles of 11 microtubules, held together by other proteins in a beautiful and precise array, see Figure 3.9. A single axoneme is ~250 nm in diameter and very refractive, so it is easily distinguished from the individual microtubules that grow from its ends (see Figure 3.10). Plus and minus ended microtubules grow on opposite ends of the axoneme. In practice, they are distinguished by growth rate (plus ended microtubules grow faster).

The special geometry of axoneme nucleating sites raises several issues. First, 9 of the 11 microtubules in the bundle are doublets. This means they have an extra semi-circle of protofilaments in their cross-section. We do not know whether these nucleate simple microtubules or doublet structures. We assume our measurements are not sensitive to the difference.

50
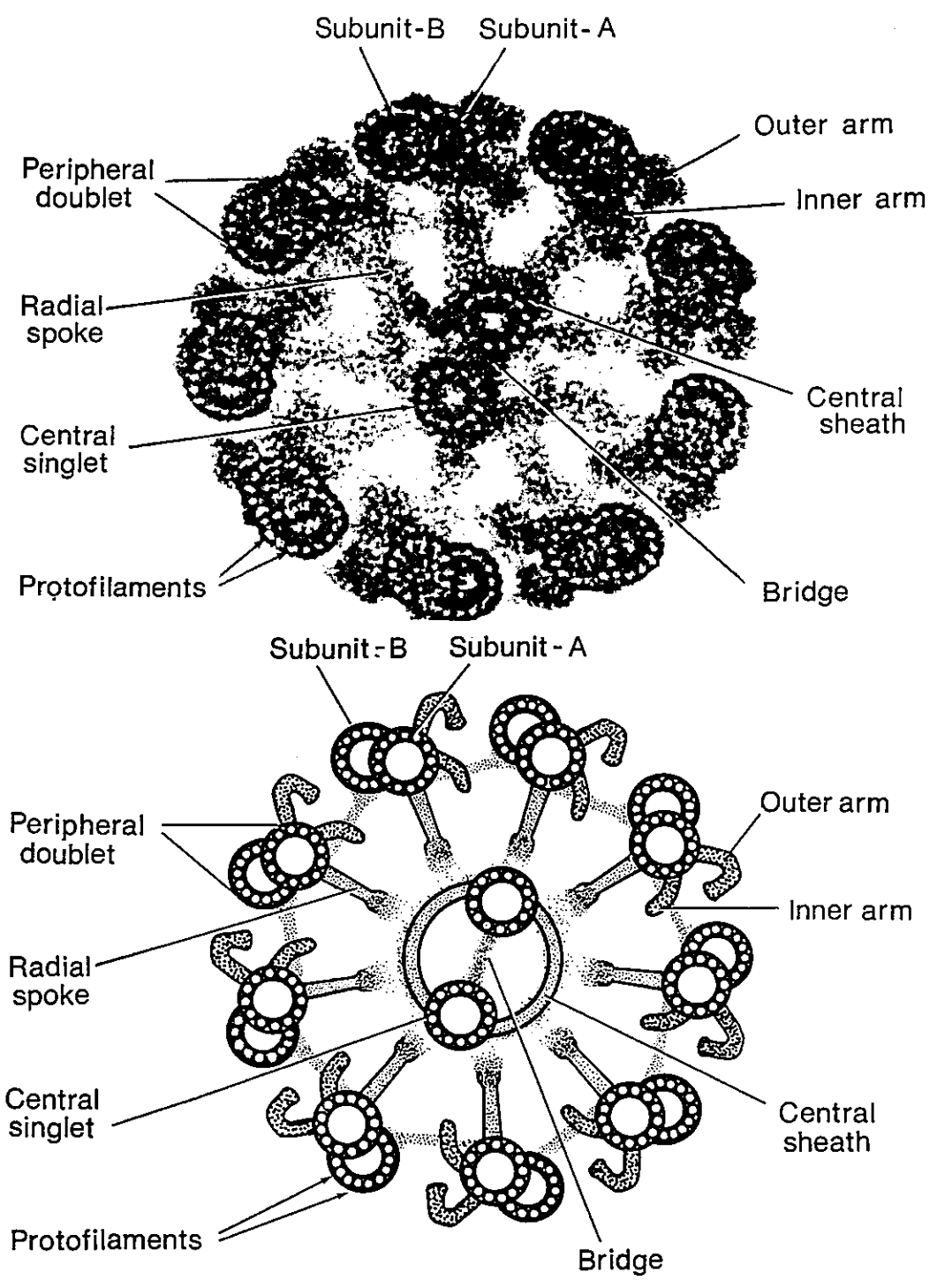
Fig. 3.9. Geometry of the nucleation sites. Above: an electron micrograph of the cross-section of an axoneme. Below: a diagram of the axoneme structure. From Fawcett (1981).
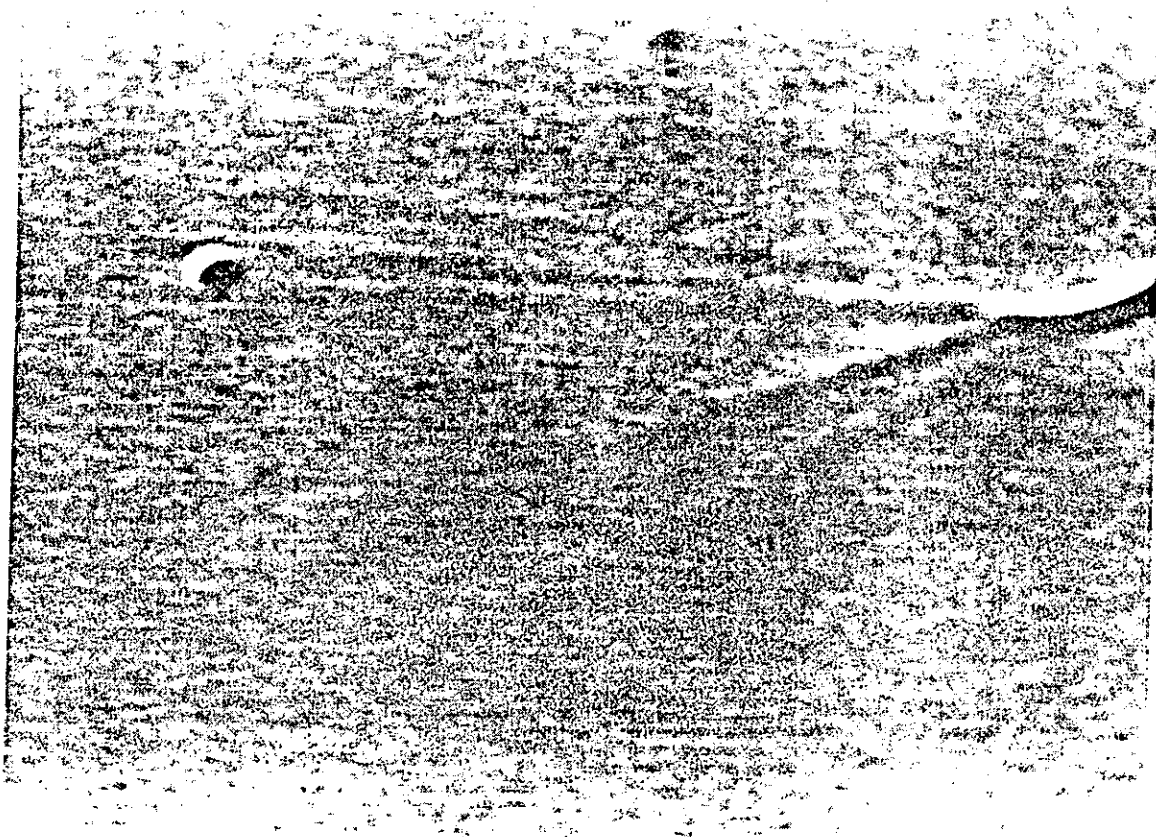
Fig. 3.10. Nucleating site with microtubules as observed by the differential interference contrast (DIC) microscopy. The high contrast object in the upper right is an axoneme. The long, thin, low contrast lines emanating from the axoneme are microtubules. The image is 30 μm from left to right.

Another key feature of the axoneme geometry is that it presents many nucleating sites very close together. Could competition for tubulin between the sites be important? The characteristic size of the depleted region around a growing tip is $\ell_D = \omega/DC$, where ω is the rate of consumption, D is the diffusion constant for a tubulin molecule, and C is the bulk tubulin concentration. For typical values of C and ω, estimated from microtubule growth rates, $\ell_D \sim 10\text{Å}$. This is one order of magnitude less than the distance between sites on an axoneme (see section IV.2.1).

The proximity of nucleating sites does present a limitation in another way, however. When more than three long microtubules are growing from one axoneme end, short microtubules growing from the same end are likely to be hidden among the stalks of the longer ones. This places an upper bound on the extent of nucleation we can measure accurately (see section IV.1.1).

2.3 Initial Conditions

In the process of filling, the sample of tubulin solution reaches room temperature. Depending on the concentration of tubulin and the presence of nucleating sites, considerable polymerization can take place in this time. To insure that all measurements begin with the same initial conditions, the samples under the microscope are first cooled to 4°C for ~ 20 minutes and then warmed to the desired temperature (~ 10 min) before observations began (see section III.3.2).

This procedure introduces only one complication. While cooling, condensation may appear inside of the objective, greatly reducing the image quality. We kept the ambient humidity low with a dehumidifier. A steady stream of dry nitrogen into the microscope was equally effective.

3. Apparatus

3.1 Microscopy

We observed microtubules with an optical microscope (Axioskop FS, Zeiss) using video-enhanced differential interference contrast (DIC). That it is possible to see individual microtubules, whose cross-section is 20 times smaller than the wavelength of visible light, is astonishing. The essential technique, which extracts the spatial gradient in the refractive index of an object, was developed in the 1950's by Nomarski (Allen, et al., 1969). However, the introduction of video-enhancement in the 1980's proved to be key (Allen, et al., 1981). Basically, the high resolution needed to detect microtubules is acquired at the expense of contrast. The analog processing available with the video camera can extract a signal from the bright background which appears featureless to the eye. The application of this technique to microtubules is discussed in Inoué (1986) and Schnapp (1986)

The technique is by no means trivial, but it is becoming standard. A schematic of the light path is sketched in Figure 3.11. Our light source is a 100W halogen lamp (cat. no. 64458AX, Osram), with a concave mirror behind and a heat filter in front. The light passes through a collector lens, two irises, a polarizer, a birefringent prism and a condenser lens before reaching the sample. The goal is to illuminate the sample as brightly and as uniformly as possible. This usually means positioning the image of the lamp filament in a plane *complementary* to the sample plane (i.e. the filament is completely out of focus when the sample is in focus and *vice versa*). The two irises mark the complementary planes: one is imaged onto the sample, the other to the lamp.

IMAGE/CAMERA   — ➤   ▭   ◄ —

TUBE LENS   ⬭

ANALYZER   ▨

WOLLASTON PRISM   ▱

BACK FOCAL PLANE   — ➤   ⬚   ➤ —

OBJECTIVE   ⬭

SAMPLE   — ➤   ▬   ◄ —

CONDENSER   ⬭

CONDENSER IRIS   ➡   ⬚   ⬅

WOLLASTON PRISM   ▱

POLARIZER   ▨

HEAT
REFLECTOR   FILTER   FIELD IRIS   ➡   ▭   ⬅

MIRROR

LAMP   COLLECTOR
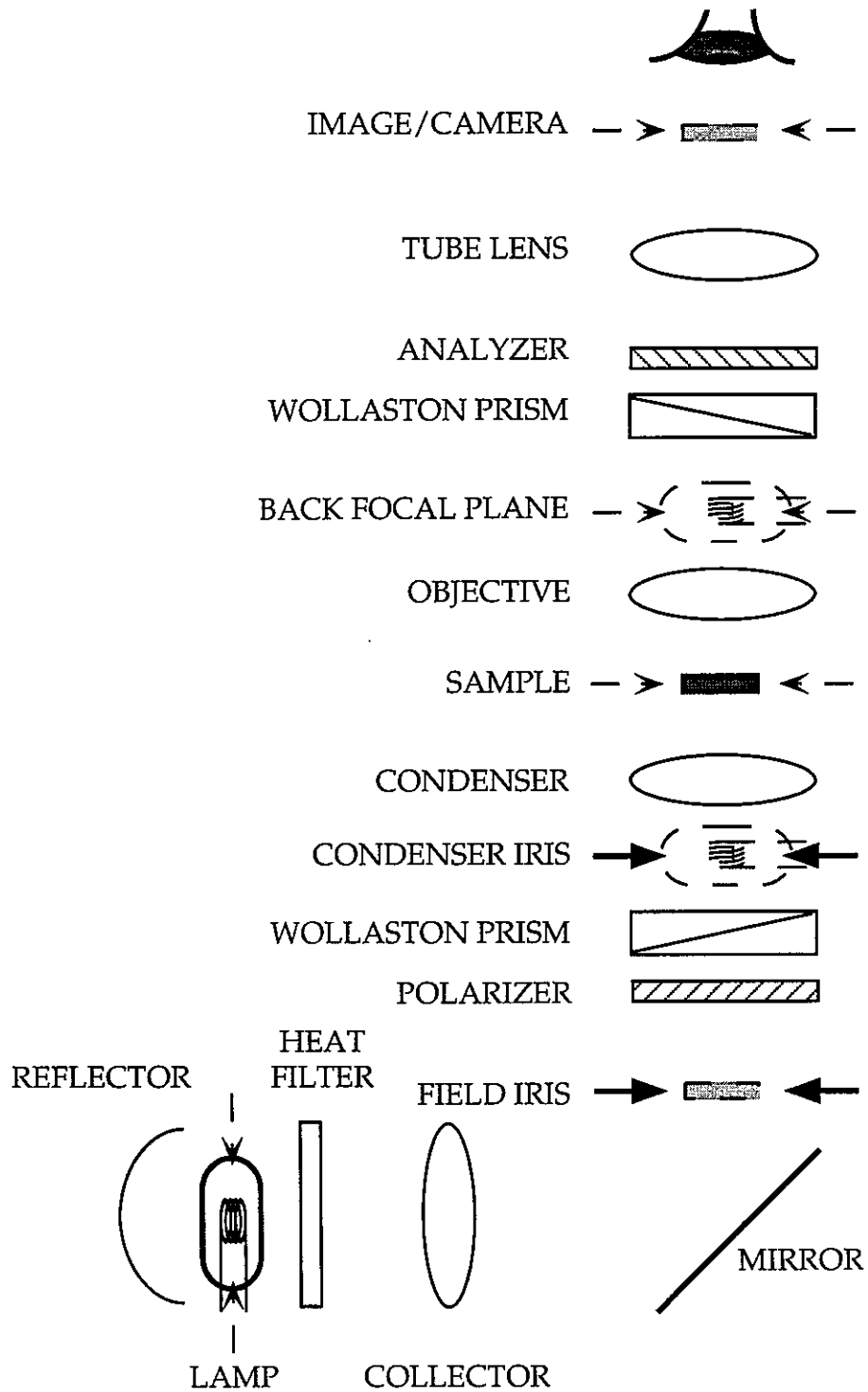
Fig. 3.11. A schematic of the light path in DIC microscopy. Solid arrows represent irises, broken arrows represent images of the irises. The field iris is imaged onto the sample and the condenser iris is imaged onto the lamp. There are two image planes *conjugate* to the object (where the an image of the object appears) and two planes conjugate to the lamp. These are sets of *complementary* planes (when the lamp is in focus the object is completely out of focus, and vice versa). Adapted from Schnapp (1986).

The idea behind DIC is to create two images of the sample, separated by the resolution limit, and force them to subtract, so as to extract an image of the refractive gradient. To this end, the polarizer is oriented at 45° to the axes of the prism. The prism imposes a phase difference between its primary and secondary polarizations and also gives them a slight lateral separation, called the shear. After passing through the sample, the light goes through essentially the reverse sequence of optics before reaching the camera: a lens (the objective), a birefringent prism, a polarizer and another lens. The second prism decreases the lateral separation between the two polarizations and adds to their phase shift. The second polarizer (the analyzer) is oriented perpendicular to the first and forces the two polarizations to add.

The result is an image of the sample which appears shadowed. That is, changes in the index of refraction in a particular direction (the direction of the shear, usually upper left to lower right) are highlighted. The phase shifts imposed by the two prisms can be adjusted to increase the intensity of the shadows at the expense of the overall intensity of the image. To get familiar with the imaging, a good test specimen is the diatom test plate (cat. no. B25D, Carolina Biological Supply). Diatoms are the silica shells of single cell, plant-like creatures. Some have textures with a periodicity of about $0.2\,\mu m$, the resolution limit of this technique.

We chose the objective with the largest possible numerical aperture: an oil-immersed 63x with 1.4 NA (cat. no. 440762, Zeiss) in order to optimize the image resolution. In the end, however, we sacrificed resolution in order to simplify the temperature control (see section III.3.2) by using a dry (no-oil) condenser, 0.9 NA (cat. no. 465266, Zeiss). In retrospect, the 100x objective (cat. no. 440483, Zeiss) (1.3 NA) might be a better choice since it is free of birefringence, while the 63x (despite advertisement to the contrary) is not.

The rest of the experimental set-up is depicted in Figure 3.12. Video-enhancement was provided by a Newvicon tube camera (model C2400, Hamamatsu) with built-in gain and offset control. We had poor results substituting a CCD camera (model TI-24A, NEC) and an external analog enhancement circuit (model 605, Colorado Video) for the Newvicon. The additional magnification of the CCD and its lower horizontal resolution seemed to combine to deteriorate the image quality significantly.

The total magnification to the video monitor was 7056x, acquired in four stages: a 63x objective, a 1.6x lens, a 4x lens before the camera, and, finally, the camera itself introduced a factor of 17.5x. Thus, a diffraction limited spot, 0.2 μm in diameter, occupied almost 2 mm on the screen. Further magnification would reveal no additional information.

It is possible to distinguish individual microtubules without further image treatment, but detection, especially of the microtubule ends, is greatly enhanced by subtracting a background image, rescaling the gray levels and averaging over 2 – 4 video frames. These functions were all performed in real time by a dedicated video-processing module (Omnex®, Imagen). We recorded our images on video tape in S-VHS format.

Our images were forever light-limited. The best images were obtained in Köhler illumination (see Lacey (1989)) with the condenser aperture wide open, the field aperture fully closed and the adjustable prism positioned so as to barely provide enough light to the camera. The camera gain was set to maximum and the offset adjusted to taste. We plan to replace the halogen lamp with a fiber-optic coupled xenon arc lamp (Technical Video). This will allow greater extinction between the Wollaston prisms, and increase the contrast of microtubules in the image. Introducing an interference filter and replacing the film polarizers with a pair of prisms should also help.
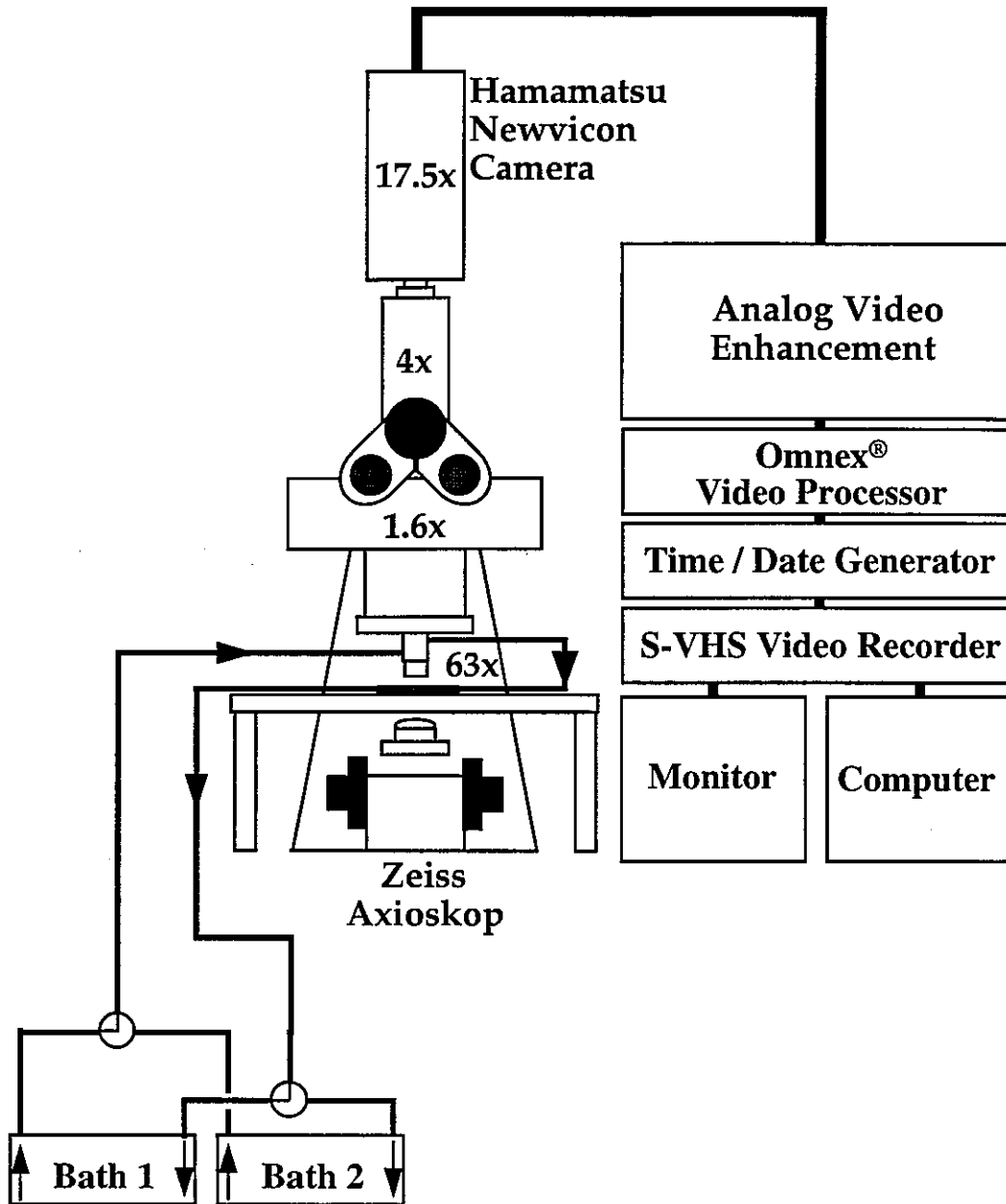
Fig. 3.12. The experimental set-up.

In closing this discussion about microscopy, let me add a few words about the other applicable microscopy techniques, dark-field and fluorescence. The most significant problem with these other two techniques is background. In dark-field, background comes from strong scatterers outside of the focal plane. In fluorescence, it comes from labeled molecules (e.g. tubulin dimers) in solution. In both cases, it is controlled by working in either very thin or very dilute samples. The problem is that thin samples can significantly alter the concentration of tubulin inside (see section II.2.4) and dilute ones are simply inappropriate. If there is a disadvantage to DIC, it has to be the comparatively low contrast of the final images, which makes automated image analysis very difficult.

3.2 Temperature Control

Under the microscope, the sample temperature is determined by the objective, which hovers ~ 70 µm above the thin glass coverslip in a puddle of oil. To control the sample temperature, we built a collar for the objective, and a holder for the sample, both with flow passages for fluid from a temperature controlled bath, as shown in Figure 3.13. The holder insulates the sample from air currents, preventing large thermal gradients. We used a dry (no oil) condenser so that its temperature did not need to be controlled as well.

The temperature was calibrated by constructing a dummy cell with a thermocouple (cat. no. CHCO-0005, Omega) inside and comparing it to another in ice water (0°C). The voltage was recorded by a chart recorder (Yokogawa) and correspondence was made with the temperature of an RTD (cat. no. F3105, Omega) in the slide holder. The resistance of the RTD was measured by a multimeter (model 195, Keithley) whose analog voltage output was recorded on another channel of the chart recorder. See Figure 3.14.
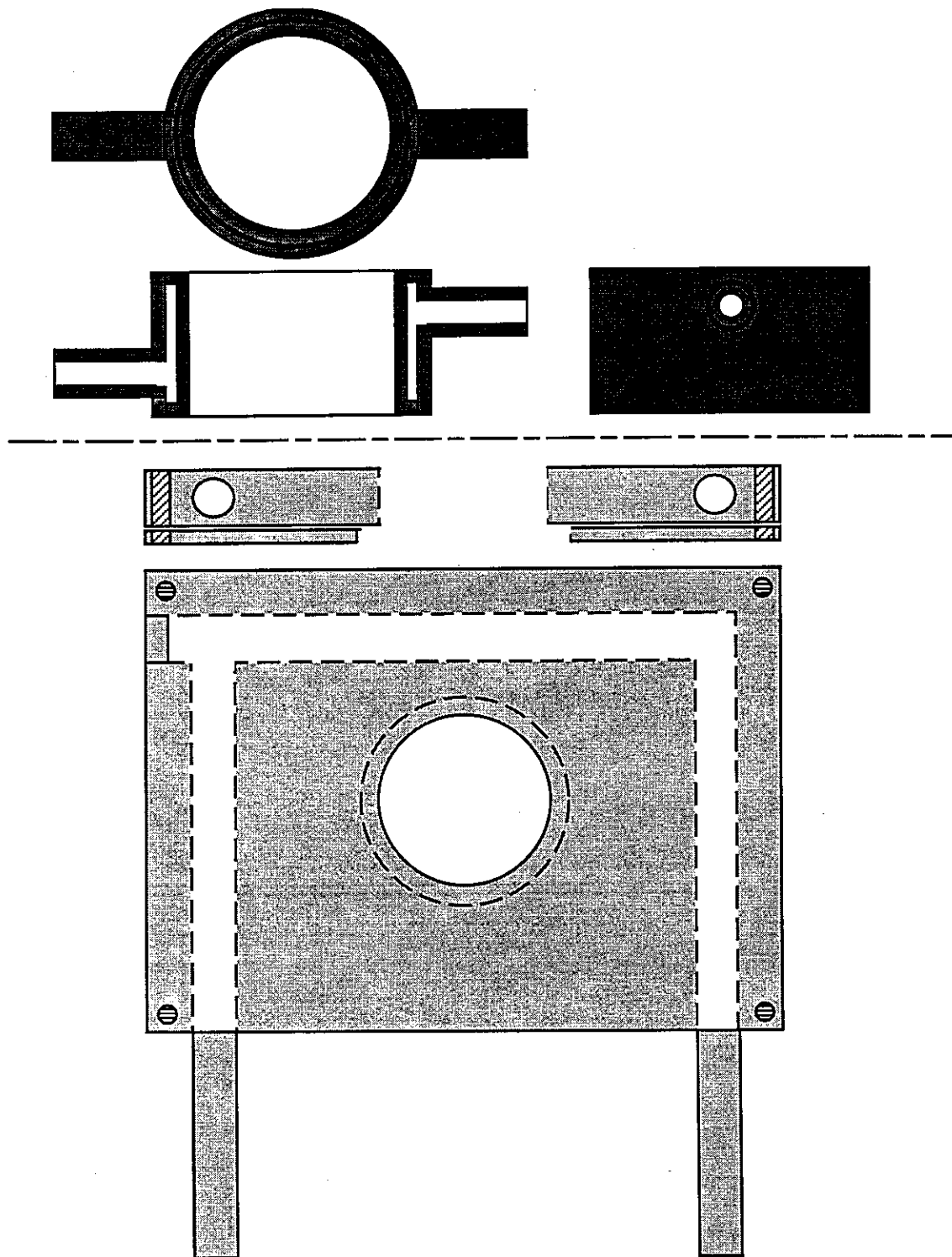
Fig. 3.13. Objective collar and temperature-controlled stage. Both pictures are drawn to scale. The sleeve was made of brass and the stage was made of copper. The top of the stage had a 75x50x1mm groove to accommodate the sample. The hole for the condenser (below) had to be a little larger than the one for the objective.
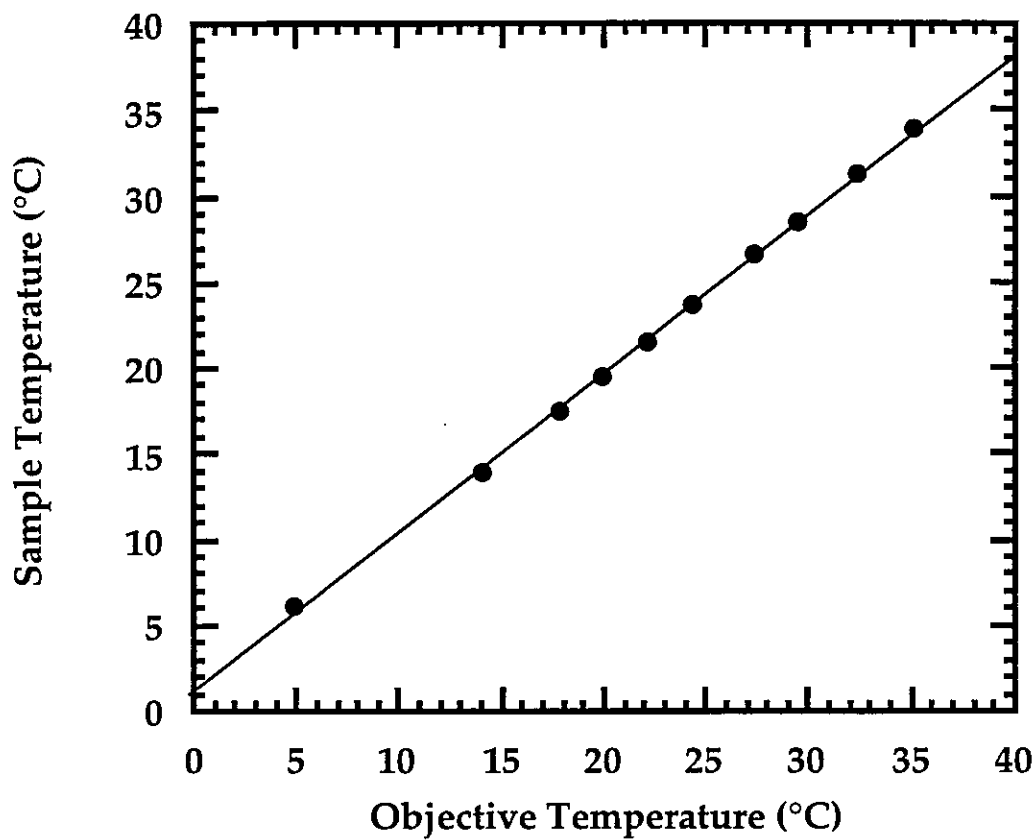
Fig. 3.14. Temperature calibration of the sample. Notice that the sample follows the objective temperature very closely. The line is a least-squares fit: $y = 1.3 + 0.93x$.

The temperature calibration is accurate to at least ±0.25°C and the sample temperature is stable over at least two hours. To change the sample temperature rapidly, we introduced a second water bath into the flow circuit. The baths were connected as shown in Figure 3.12. One bath was set to give a sample temperature of about 4°C and the other was adjusted to the temperature of interest. The sample temperature jumped to within a degree of its final value in the first two minutes after switching baths. It took another five minutes to achieve the final temperature (see Figure 3.15.)

3.3 Data Acquisition

Measurements of microtubule length as a function of time were made by hand, with the help of a Macintosh computer (model IIfx, Apple). The video signal, live or from tape, was fed into the computer via an image grabber board (Pixel Pipeline, Perceptics) and displayed on the monitor using a customized version of the image processing software NIH Image VDM (due to A. Tilgner).

While looking at the video, the observer uses the mouse to locate the free end of a microtubule. When the observer clicks the mouse button, the computer grabs a frame (the tape continues to play) and records the time and the location of the cursor. The observer then moves the cursor to another point in the still image (e.g. the other end of the microtubule) and clicks again. The computer records the location of the second point and returns to live display. The final result is a plot like the one shown in Figure 2.5.

The quality of the images combined with the accuracy of the observer limited the spatial resolution to ±0.5μm. The temporal resolution, left to the observer, was ±6 seconds. Better temporal resolution, using frame by frame analysis, was possible but generally uncalled for.
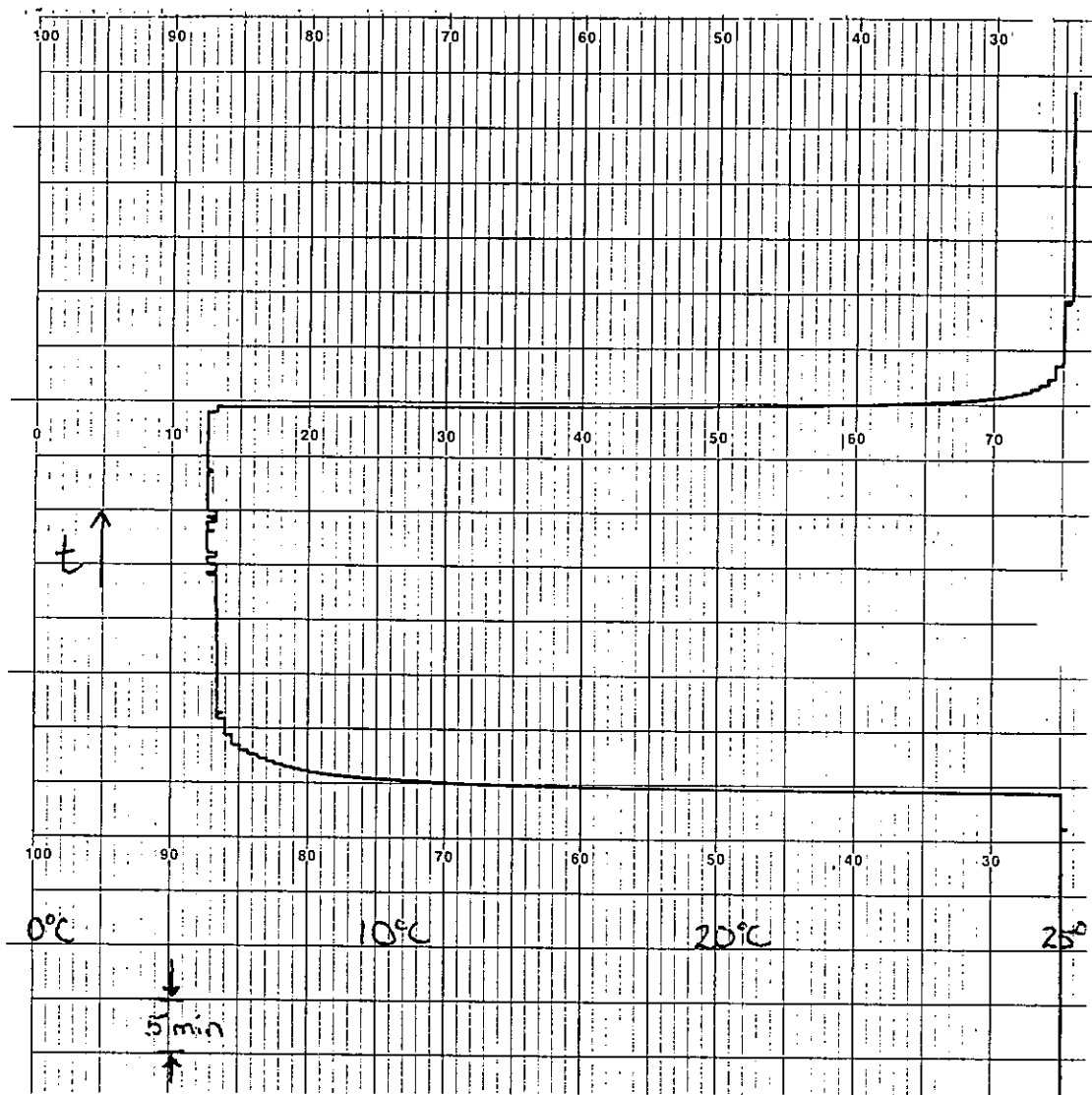
Fig. 3.15. Temporal response of the sample temperature upon cooling and heating. Temperature is plotted horizontally, increasing from left to right, and time is plotted vertically, increasing from bottom to top.

CHAPTER IV

THE ORGANIZATION OF MICROTUBULE BEHAVIOR

The main work of this thesis is to present an organization of the behavior of microtubules, pure and simple. On one level, this achievement is narrow and pedantic: By isolating microtubules and exploring conditions of no biological relevance (e.g. low temperatures), we lose the complex dance of 'real life,' with its chemical choreography of microtubule behavior, and look, instead, to understand the rhythm inherent to microtubules alone. On another level, it is a study of a natural phenomenon of fundamental importance to biology: the conformational change of a protein.

Biology is rooted in the workings of proteins as molecular machines. These share a common routine: protein A in conformation 1, has or lacks an interaction with X (e.g. another protein, a sugar, oxygen, etc.). Upon the injection of free energy (usually from the hydrolysis of a nucleotide-tri-phosphate), protein A switches to conformation 2 (an excited state, if you will) and alters the strength of its interaction with X, thereby executing its function. Afterwards, protein A relaxes (decays) back into conformation 1 and the cycle begins again.

Microtubules are a particularly interesting system in which to study the phenomenon of conformational change because they amplify its effect from molecular to macroscopic length scales. By studying the macroscopic length fluctuations of microtubules, we can hope to gain insight into the underlying nature of conformational change.

0. Overview

This chapter begins with an exploration of the phase diagram of microtubules (Figure 4.1), expanding upon results that have been published elsewhere (Fygenson, et al., 1994; Fygenson, et al., 1995). Varying the temperature and tubulin concentration, we observe both heterogeneous (site) and homogeneous (bulk) nucleation of microtubules. These phenomena, familiar in physics and materials science, are modified by the unique features of microtubules. Site nucleation is perturbed by dynamic instability, which destroys microtubules as fast as they nucleate. Bulk nucleation is governed by the special structure of the microtubule, which constrains the geometry of nuclei and limits the growth to one dimension.

In the regime between the onset of site nucleation and the onset of bulk nucleation, we document the evolution of dynamic instability itself. Near the onset of site nucleation, catastrophes are frequent and rescues are rare. As either temperature or tubulin concentration increases, catastrophes become less frequent and rescues become more likely. Eventually, rescues become certain and microtubules grow unbounded.

We find it is not necessary to consider changes in the rates of microtubule assembly and disassembly to understand the qualitative change in dynamic instability (from bounded to unbounded growth). Assembly and disassembly may change in concert or independently as dynamic instability evolves from bounded to unbounded growth. Concentration enhances assembly without affecting disassembly, as is well known (Walker, et al., 1988). Temperature enhances both assembly and disassembly, and in a similar manner, indicating a common underlying mechanism. Finally, glycerol inhibits disassembly while it has no net affect on assembly.
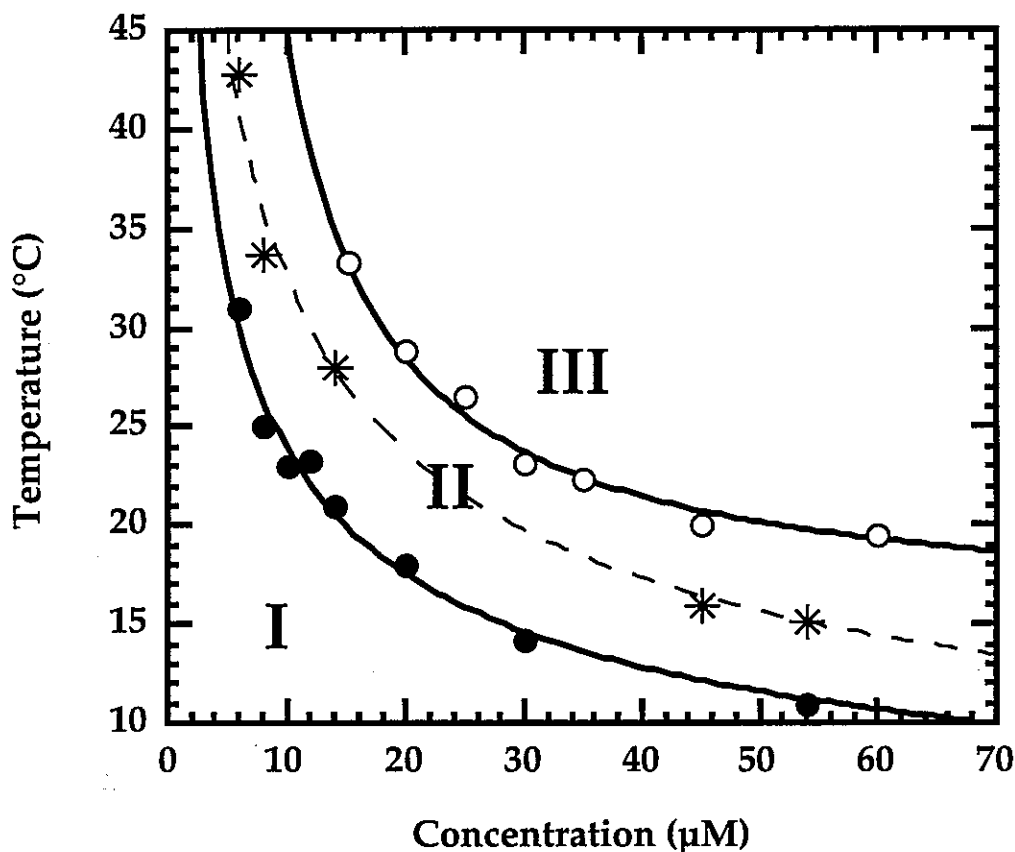
Fig. 4.1. The phase diagram. I: region of no growth. II: region of growth from nucleation sites. III: region of spontaneous nucleation. Filled circles: onset of site nucleation, $P_{occ} = 1/100$ (section IV.1); Stars: transition from bounded growth (below) to unbounded growth (above) (section IV.2); Open circles: onset of bulk nucleation, $r \sim 10^5 \text{cm}^{-3}\text{sec}^{-1}$ (section IV.3). Lines are least-squares fits to the following: $T \sim C^{-0.45}$ (filled circles), $T \sim C^{-0.45}$ (stars), $(T - T_c) \sim (C - C_c)^{-1}$ with $T_c = (15 \pm 1)°C$ and $C_c = (2 \pm 2)$ μM (open circles).

The introduction of glycerol, a simple chemical modifier of microtubule behavior, follows the description of the phase diagram and contributes to our interpretation of the mechanism underlying microtubule behavior. Increasing glycerol moves microtubules through the phase diagram in a manner unlike either temperature or tubulin concentration. It enhances bulk nucleation, suppresses site nucleation, enhances rescue and suppresses catastrophes.

A central theme of the chapter is the attempt to link dynamics to form. We interpret the assembly and disassembly reactions as being driven by the release of water ordered around the tubulin molecule. The hydrolysis of GTP, which intervenes between the two reactions and presumably changes the conformation of tubulin, appears to effectively reorder water within and around the microtubule. We interpret catstrophe and rescue events as consequences of changes in the overall structure of the microtubule, building on the recent work of Chrétien and Karsenti (1995). The presence of a sheet-like structure at the end of the microtubule seems to stabilize against catastrophe and gaps or defects trapped in the structure as the sheet 'zippers' into a tube prompt rescue.

The structure of this chapter sweeps through the phase diagram from lower left to upper right. The first section describes site nucleation. The next focuses on the approach to unbounded growth, in terms of both the microtubule population and the dynamics of individual microtubules. The third describes bulk nucleation. The fourth presents the effects of glycerol. And, finally, in the fifth section, we attempt to place our findings in the general context of rhythm and conformational change presented in the introduction to this chapter.

1. Nucleation on Sites: the onset of bounded growth

In samples containing nucleation sites, the proportion of sites occupied by microtubules is often less than 1 and constant in time. This is very different from the heterogeneous nucleation of most materials which, once energetically allowed, proceed to saturate their nucleation sites over time. The fractional occupation of nucleation sites by microtubules is an important signature of dynamic instability. From studying its behavior, it is possible to estimate the size of the energetic barrier opposing site nucleation and to infer a qualitative transition in the nature of dynamic instability.

1.1 Steady state fractional occupation of sites

P_{occ}, defined as the number of microtubules divided by the number of sites, was measured at various temperatures and four different tubulin concentrations. The results are shown in Figure 4.2.

The measurements were made on samples containing axoneme nucleation sites (section III.2.2.2). Each point is an average over at least 1000 sites (assuming 11 sites per axoneme end). No distinction was made between sites for plus and minus ends. The measurements become unreliable at values of $P_{occ} > 0.1$ because short microtubules often go undetected when several long ones are present on the same axoneme end. We took care to count only well-defined, apparently undamaged sites. Damaged sites unknowingly included in the count would bias the measurement towards lower values. We believe this error is negligible because qualitatively P_{occ} approaches 1 at high temperatures.

The system unambiguously achieves steady-state. When the temperature is changed abruptly, P_{occ} changes rapidly (< 15 min) and then remains constant at its new value (observation time ~ 1 hour).
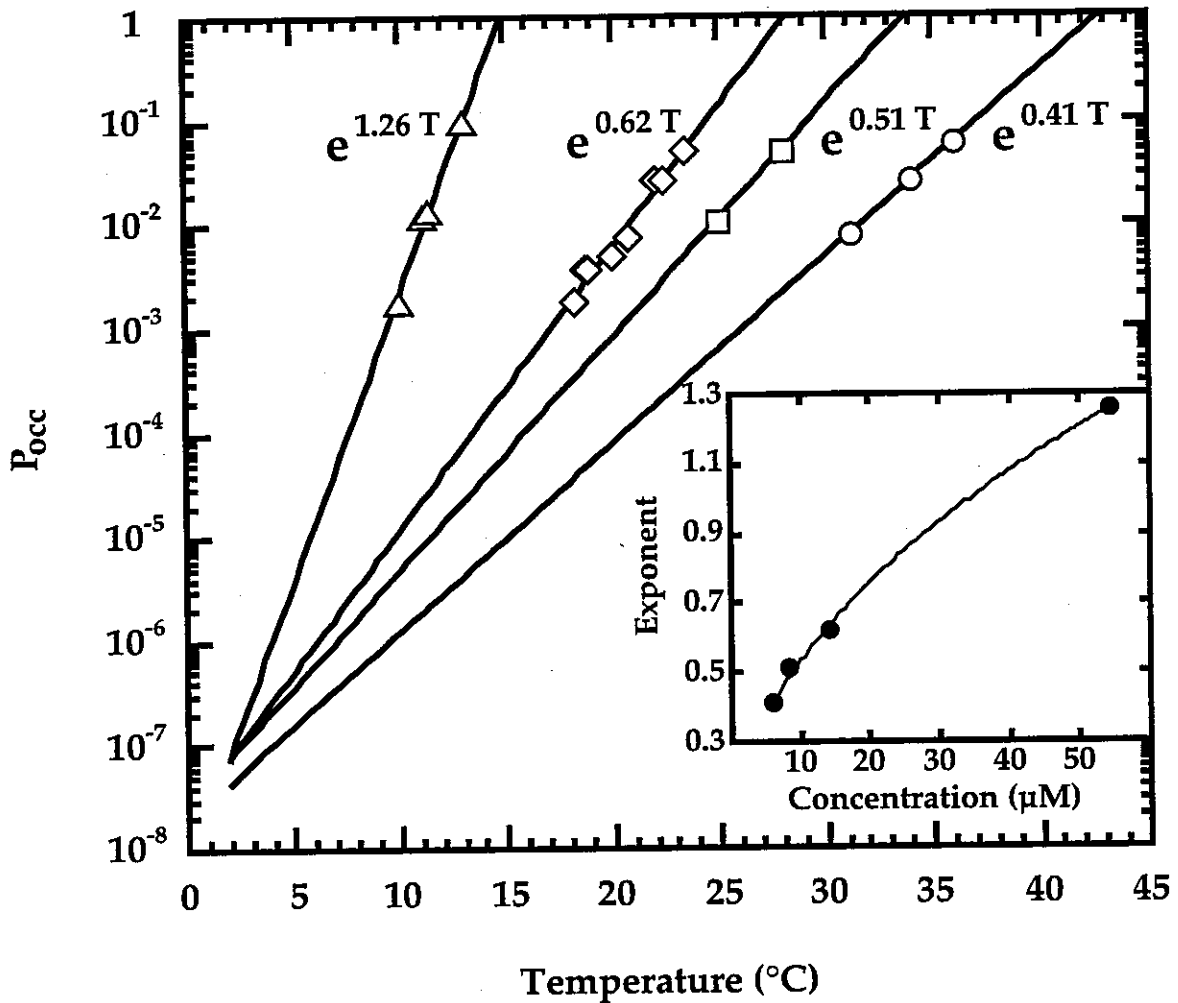
Fig. 4.2. Proportion of occupied sites vs. temperature. Measurements were made at four different tubulin concentrations: 6 μM (circles); 8 μM (squares); 14 μM (diamonds); 54 μM (triangles). Lines are least-squares fits yielding the labeled exponents. The inset is a plot of the exponent vs. concentration and a fit to the form: exponent $\sim C^{1/2}$. See text for comments about the extrapolation to low values of P_{occ}.

The steady-state, fractional occupation of nucleating sites is a signature of dynamic instability. At any given time, a site may lose its microtubule to a catastrophe that is not followed by rescue (i.e., a complete catastrophe). If this occurs at the same rate as nucleation of new microtubules on empty sites, the overall proportion of occupied sites P_{occ} will be constant in time. Of course, the particular sites with microtubules will change.

Mathematically, the steady-state condition can be expressed as

$$R_{nuc}(1 - P_{occ}) = R_{CC}P_{occ} \tag{IV.1}$$

where R_{nuc} is the nucleation rate and R_{CC} is the rate of complete catastrophe. The same equation can be derived by assuming that P_{occ} measures the proportion of time any one site is occupied by a microtubule. This is equivalent to assuming that the statistics of a population of microtubules are reflected in the dynamics of a single microtubule. P_{occ} is then expressed in terms of two time scales: the lifetime of a microtubule, $\tau_{MT} = 1/R_{CC}$, and the lifetime of an empty site, $\tau_{site} = 1/R_{nuc}$ as

$$P_{occ} = \frac{\tau_{MT}}{\tau_{site} + \tau_{MT}} = \frac{1/R_{CC}}{1/R_{nuc} + 1/R_{CC}} = \left(\frac{R_{CC}}{R_{nuc}} + 1\right)^{-1},$$

which is equivalent to equation (IV.1).

1.2 The energetic barrier to site nucleation

Since axonemes are pieces of stabilized microtubules, one might expect them to mimic the ends of growing microtubules. If this were the case, a microtubule which disassembles completely would be, in effect, "rescued" at the nucleation site and begin growing again immediately. So every site would actually be occupied and the observation that $P_{occ} < 1$ would be merely an artifact of overlooking microtubules that are below the resolution limit.

But the small proportion of occupied sites typically observed, $10^{-3} < P_{occ} < 10^{-1}$, cannot be explained in this manner. To reach such low

values of P_{occ} requires that R_{CC} be ten to a thousand times larger than R_{nuc}, which, if approximated by the rate of microtubule assembly, would be about 10 sec^{-1} (section IV.2.2) Furthermore, the majority of observed microtubules would be only slightly longer than the detection limit ($\sim 0.5\ \mu m$). Neither of these is true. For example, when the tubulin concentration is 14 μM and the temperature is 23°C, $P_{occ} \sim 10^{-2}$, microtubules typically grow for several minutes and are on average several microns long (section IV.2.).

Thus, there must be an energetic barrier to site nucleation for microtubules (at least for the particular sites we used). Upon reflection, this is altogether reasonable. A growing microtubule end is made of GTP-tubulin (section II.5) while a stabilized microtubule end has probably undergone hydrolysis, so it should be made of GDP-tubulin instead. The process of attaching fresh GTP-tubulin to a stabilized GDP-tubulin site is likely to be opposed by an energetic barrier. In this sense, nucleation on stabilized ends may bear some resemblance to rescue (we return to this point in section IV.5).

To estimate the size of the barrier, suppose the nucleation rate obeys

$$R_{nuc} = R_0 e^{-(E_n/kT)}, \tag{IV.2}$$

where R_0 is the rate of nucleation attempts and E_n is the height of the barrier to nucleation. Eliminating R_{nuc} from (IV.1) and (IV.2) and solving for E_n,

$$E_n = kT \ln\left(\frac{(1-P_{occ})}{P_{occ}} \times \frac{R_0}{R_{CC}}\right). \tag{IV.3}$$

R_0 is essentially the rate at which tubulin dimers encounter a nucleation site and can be calculated based on diffusion-limited transport. The calculation involves integrating $n(r)$, the number of dimers a distance r from the nucleating site, divided by $t(r)$, the time it takes a dimer to diffuse that distance, times $p(r)$, the probability that a dimer diffuses towards the site:

$$R_0 = \tfrac{1}{2}\int_a^\infty \frac{n(r)}{t(r)} p(r) dr = \tfrac{1}{2}\int_a^\infty \frac{4\pi r^2 C}{r^2/D} \frac{\pi b^2}{4\pi r^2} dr = \frac{\pi b^2 DC}{2a} \tag{IV.4}$$

71

where $a \sim 3 \cdot 10^{-7}$ cm is the radius of a dimer, $b \sim 1.2 \cdot 10^{-6}$ cm is the radius of a site (a microtubule end), $D = kT/6\pi\eta a = 7 \cdot 10^{-7}$ cm^2/sec is the diffusion constant and $C \sim 10^{16}$ dimers/cm^3 is the concentration of dimers. The factor of $\frac{1}{2}$ accounts for the fact that the site can only be accessed from one side. With these numerical values, we estimate a rate $R_0 \sim 5 \cdot 10^4$ attempts/sec.

Note that R_0 is quite insensitive to changes in temperature. This point will come up again later, so we emphasize it here. The temperature dependence of R_0 comes from the diffusion constant $D \propto T/\eta(T)$, which changes less than 10% between $10 - 40°C$.

When the tubulin concentration is 14 µM and the temperature is 23°C, $P_{occ} \sim 10^{-2}$ and $R_{CC} \sim 5 \cdot 10^{-3}$ sec^{-1} (section IV.2.3). Using these numbers and our estimate of R_0, we can solve equation (IV.3) to estimate $E_n \sim 21kT$, and then equation (IV.2) to estimate $R_{nuc} \sim 5 \cdot 10^{-5}$ successes/sec (about a million times less likely than the addition of a dimer to the end of a growing microtubule (section IV.2.2)).

E_n is actually quite insensitive to changes in P_{occ} since as $P_{occ} \to 1$, $R_{CC} \to 0$, according to equation (IV.1) and when P_{occ} decreases at lower temperatures, R_{CC} increases (section IV.2.3). At present, we cannot extract a clear temperature behavior for R_{CC} from the data. Eventually, it would be interesting to contrast the temperature dependence of E_n with that of the energy barrier for microtubule polymerization E_p (section IV.2.2). Further understanding of the nature of the barrier to site nucleation might also come from investigating the concentration dependence of R_{nuc} and comparing it with that of spontaneous nucleation (section IV.3).

1.3 P_{occ} (T,C)

What can be said from the behavior of P_{occ} alone? In Figure 4.2, we see first of all that P_{occ} increases exponentially with temperature. This has the consequence that no sharp onset for site nucleation exists. For practical purposes, we define onset as $P_{occ} = 1/100$ and plot it on the phase diagram (Figure 4.1). The data is fit by a power law $T \sim C^{-0.45}$, suggesting an equation of state of the form $P_{occ} = f(CT^2)$.

Theoretically, the temperature dependence of P_{occ} could be fit equally well by either $P_{occ} = P_o e^{-E/kT}$ or $P_{occ} = e^{A(T-T_o)}$. The first expression saturates as T approaches infinity, but the intuitive appeal of this feature is lost because the data cannot be fit with $P_o < 1$. Since both expressions produce unphysical values of $P_{occ} (> 1)$ above some temperature, we favor the second expression because it makes the "critical" temperature T_o, at which $P_{occ} = 1$, explicit. The inset of Figure 4.2 shows that the exponent $A \sim C^{1/2}$. This implies that $T_o \sim C^{-1/2}$, in agreement with the equation of state found above.

A final remark concerning the long extrapolation of the exponential fits in Figure 4.2: Though they are not very reliable (extending over 5 decades or so), they do converge rather provocatively. If the reader will allow a little wild speculation, we might suggest that somewhere near 0°C, the convergence of these lines indicates a temperature fundamental to this system; a temperature with an effect independent of the concentration of tubulin. Perhaps it is a critical temperature below which polymerization is energetically prohibited. It may be worth considering how to shift the system so that the significance of this low temperature can be tested (e.g. using non-hydrolyzable analogs of GTP, or even glycerol).

1.4 Conclusions

Microtubules put a new twist on the familiar phenomenon of site nucleation. Catastrophes, rescues, (i.e. dynamic instability) and an unusual energetic barrier to nucleation combine to create a system which nucleates only partially, with a consequently ill-defined onset. The level of nucleation is a state function of the system which is easily and quickly measured, making it a useful *in situ* check for sample consistency. Previous references to incomplete site nucleation in the literature (Walker, et al., 1988) can now be placed in the broader context of the phase diagram.

Finally, there is a well-defined transition in the level of site nucleation defined by $T = T_o$ and $P_{occ} = 1$. Above the transition, the lifetime of a microtubule $\tau_{MT} = 1/R_{CC}$ becomes infinite. The existence of a kind of dynamic instability in which microtubules grow on average (unbounded growth) has been suggested (Verde, et al., 1992). In the next section, we show that $P_{occ} = 1$ actually represents the onset of unbounded growth. With a touch of hindsight, then, we regard the regime below this transition as "bounded growth" and the onset of site nucleation as the onset of bounded growth.

2. Overcoming Catastrophe: the transition to unbounded growth

As the proportion of occupied nucleation sites reaches one, the average length of the microtubules diverges. Together, these two results confirm the existence of a phase of unbounded growth. Their simultaneous occurrence indicates that plus and minus ended microtubules make the transition together, implying that 'treadmilling' (a persistent state in which one end grows as the other shortens) is not natural to pure microtubules.

The onset of unbounded growth is also manifested in the dynamic instability of individual microtubules. As the temperature is raised, the rates of assembly and disassembly increase similarly. This result means that the onset of unbounded growth relies on relative changes in the frequency of catastrophe and rescue as a function of temperature. And, indeed, catastrophes become less frequent and rescues become more likely as temperature rises. However, this behavior disappears for certain combinations of high temperatures and low tubulin concentrations. Under such conditions, the frequency of catastrophe is high and independent of temperature and the likelihood of rescue is low and similarly steady.

The necessary elements of a model that might explain these results are discussed. Recent work suggesting that microtubule assembly involves the 'zippering' of tubulin sheets seem very relevant (Chrétien and Karsenti, 1995).

Along with the presentation of the above results, this section contains two digressions. The first presents the length scales for diffusion relevant to microtubule growth and tubulin depletion. The second proposes that the temperature dependence of microtubule assembly and disassembly is primarily due to a changing interaction between tubulin dimers and their surrounding water molecules.

2.1 Divergence in the length distributions

Dynamic instability is readily characterized in terms of four parameters: a velocity of growth V_g, a velocity of shortening V_s, a frequency of catastrophe f_c, and a frequency of rescue f_r. It has been pointed out that for different combinations of these parameters, two types of dynamic instability will be found (Verde, et al., 1992). When $V_g f_r < V_s f_c$, microtubules will be in a steady state, with a well-defined length distribution. This is called the state of "bounded" growth because microtubules remain within a characteristic distance from a nucleating site. When $V_g f_r > V_s f_c$, microtubules grow over time, despite periods of shortening. This is the state of "unbounded" growth.

It is not obvious that unbounded growth should exist. The dynamical states were identified theoretically from a model which ignores any underlying mechanism of dynamic instability. It is formally possible that, due to some intrinsic coupling between the parameters, microtubules never actually grow unbounded. There is some indirect evidence for unbounded growth (Carlier, 1988), but direct measurement of the dynamical parameters are subject to certain large errors (especially in f_r) which prevent the conclusive confirmation of unbounded growth (Verde, et al., 1992). Bounded growth, on the other hand, has been well documented (Walker, et al., 1988; Dreschel, et al., 1992; Verde, et al., 1992).

In the previous section, we suggest that $P_{occ} = 1$ is a signature of unbounded growth. We argue that when only a fraction of nucleation sites support microtubules, it is because dynamic instability occasionally causes microtubules to shorten all the way back to the nucleation site. It stands to reason that when sites are saturated, it is because complete shortening no longer occurs — in other words, microtubules grow on average.

To test this interpretation of $P_{occ} = 1$, we looked at distributions of microtubule lengths. Histograms of the lengths of site nucleated microtubules in samples of 45μM tubulin at five different temperatures are shown in Figures 4.3 and 4.5. Observations were made during two hours. At the four lowest temperatures, the length distributions were constant in time. This was determined by comparing the histograms of the first and second hours. Data from both hours are combined in the histograms of Figure 4.3.

The solid curves drawn on top of the histograms are least-squares fits to the exponential $P(\ell) \sim e^{-\ell/\ell_o}$. At the two warmer temperatures in Figure 4.3, the lowest bin was not included in the fits because $P_{occ} > 0.1$, creating a bias against detecting short microtubules (see section IV.1).

The transition becomes obvious when the characteristic lengths ℓ_o are plotted as a function of temperature, as in Figure 4.4. The points fit the form

$$\ell_o \sim \left(1 - \frac{T}{T_o}\right)^{-1},$$

indicating that the characteristic length diverges at $T_o = (16.0 \pm 0.2)°C$. Above this onset (T = 16.4°C), the length distribution is time-dependent, as is evident in the average and extreme lengths and the overall shapes of the first and second hour histograms (Figure 4.5).

A diverging length scale and a time-dependent length distribution are definitive signs of approach and entry into the state of unbounded growth. The transition can therefore be plotted on the phase diagram (dashed curve, Figure 4.1). The point at 45μM comes from measurements of the length distributions, all the other points are based on $P_{occ} = 1$ (section IV.1). The agreement between them justifies our interpretation of $P_{occ} = 1$.
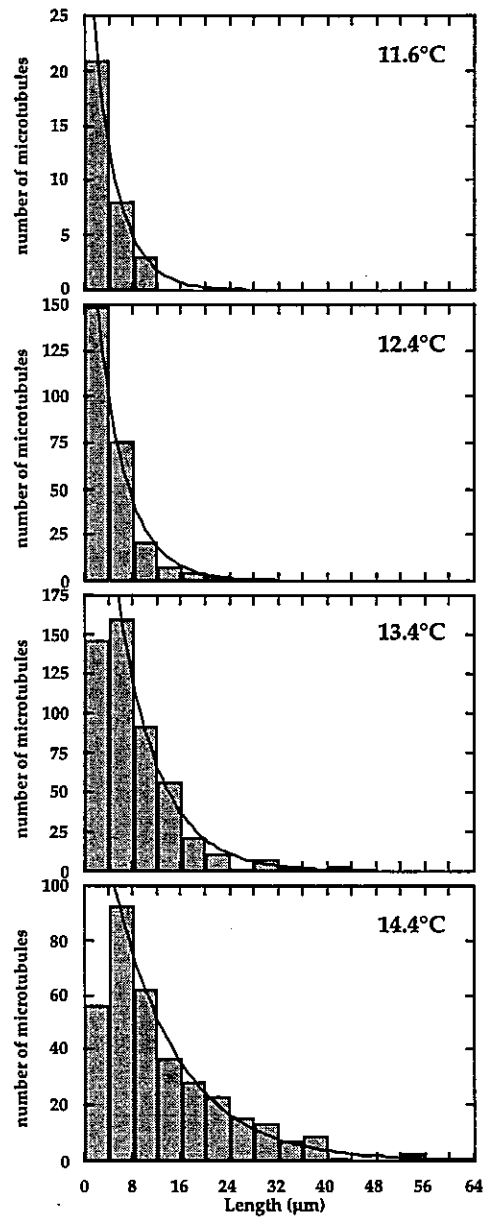
Fig. 4.3. Histograms of microtubule lengths: bounded growth.
C = 45 μM. The lines are least-squares fits to the form $P(\ell) = Ae^{-\ell/\ell_o}$.
11.6°C: $\ell_o = (4.1 \pm 0.2)$ μm; 12.4°C: $\ell_o = (4.8 \pm 0.5)$ μm;
13.4°C: $\ell_o = (6.7 \pm 0.3)$ μm; 14.4°C: $\ell_o = (10.5 \pm 0.5)$ μm.
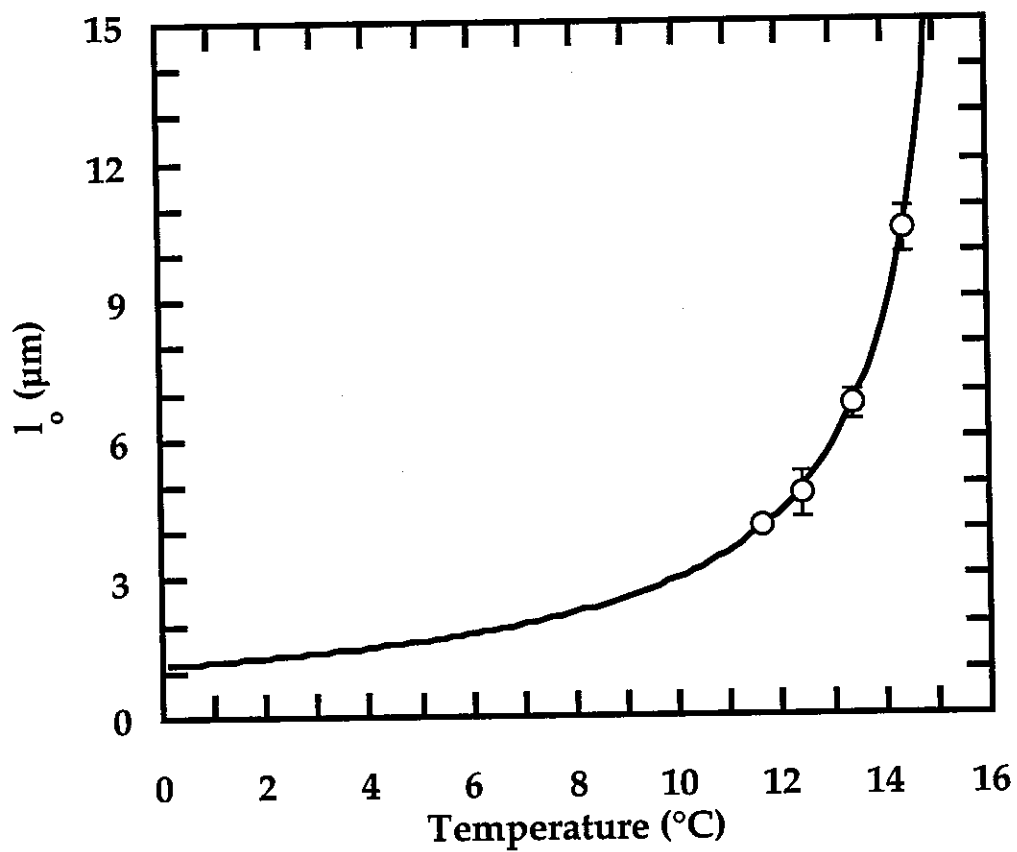
Fig. 4.4. Characteristic length ℓ_o vs. temperature. The line is a least-squares fit to the form: $P(\ell_o) \sim (1 - T/T_o)^{-1}$, where $T_o = (16.0 \pm 0.2)°C$. $C = 45\,\mu M$.
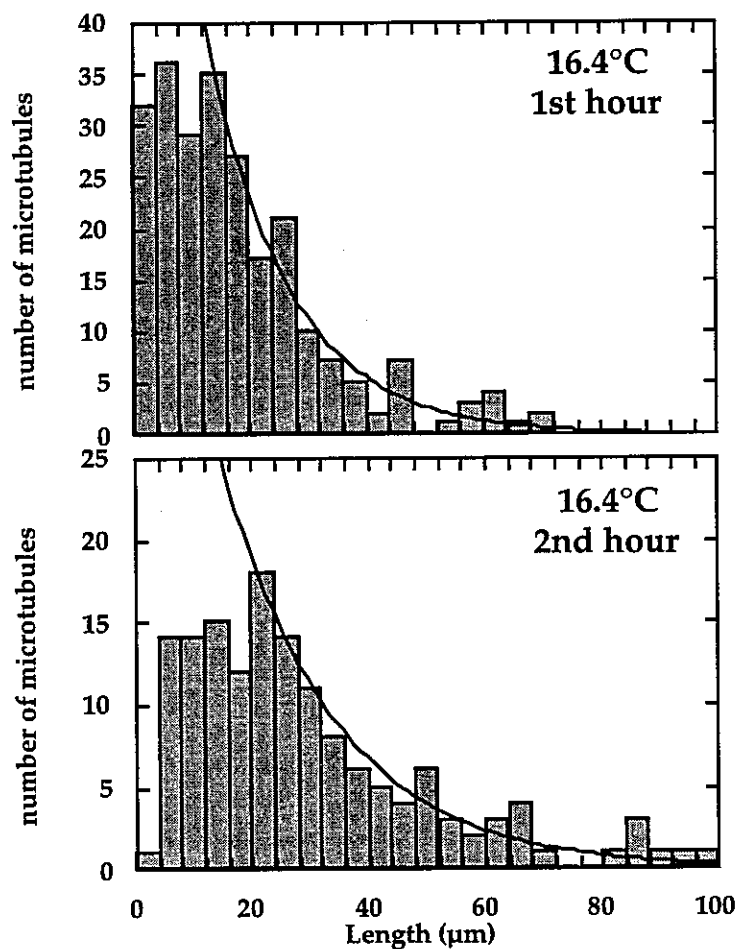
Fig 4.5. Histograms of microtubule lengths: unbounded growth. $C = 45$ μM. The lines are least squares-fits to the tails of the distributions with the form $P(\ell) = Ae^{-\ell/\ell_o}$, as in Figure 4.3: 1st hour: $\ell_o = (14.0 \pm 1.5)$ μm; 2nd hour: $\ell_o = (19.3 \pm 1.7)$ μm. The distribution of lengths below 12 μm clearly deviates from the exponential form. This deviation cannot be ignored (as was done in Figure 4.3) because such long microtubules are not likely to be overlooked. In fact, it is an expected consequence of unbounded growth (see text).

Since neither measurement distinguishes between plus and minus ended microtubules, and since both measurements determine that the transition occurs under the same conditions, we conclude that the transition is the same for plus and minus ends. This conclusion is based on the following reasoning. Saturation of the nucleation sites can happen only if both plus and minus sites support unbounded microtubules. On the other hand, the characteristic length of the microtubule population will diverge as soon as one type of microtubule grows unbounded.

As a consequence we can conclude that "treadmilling" is not natural to pure microtubules. Treadmilling is the name given to the dynamic in which one end of a polymer grows while the other shortens. It was originally proposed as the main function of hydrolysis in microtubule polymerization (Margolis and Wilson, 1978). Since the discovery of dynamic instability it has received less attention, but remained a formal possibility (Carlier, 1989). Now, as there appears to be no region on the phase diagram where one end grows unbounded while the other remains bounded, we must conclude that, in the absence of other proteins or chemical modifiers, treadmilling is only a rare and fleeting occurrence in the life of a primarily growing or shortening microtubule.

Finally, a comment on the shapes of the length distributions. In the bounded regime, the exponential character of the distributions supports the prevailing hypothesis that dynamic instability is generated by a stochastic process. Near onset, where the majority of catastrophes do not rescue, this might simply result from the random times between nucleating events. But at higher temperatures (e.g. 14°C in this case), microtubules experience several catastrophes before returning to the nucleation site, and a correlation between them would be reflected in the length distributions.

In the unbounded regime, the distribution clearly deviates from the exponential. This is an expected consequence of unbounded growth. If each microtubule executes a one dimensional random walk as it grows and shortens, then, in the regime of unbounded growth, this random walk drifts to longer lengths with the characteristic speed $\left(V_g f_r - V_s f_c\right)/(f_r + f_c)$. Nucleation imposes an initial asymmetry on the length distribution which, over time, transforms into a Gaussian shape that travels to longer mean lengths (Verde, et al., 1992).

Digression: On Diffusion and Depletion

There are several length scales related to diffusion that are relevant to a growing microtubule. One, proportional to the diffusion constant over the velocity of growth $\ell_V \sim D/V_g \sim 100$ µm, represents the size of the correlated volume seen by the microtubule end as it advances. Another, given by the square root of the diffusion constant over the rate at which dimers are consumed $\ell_\omega \sim \sqrt{D/\omega} \sim 1$ µm, represents the size of the volume from which the microtubule can pump dimers. A third, $\ell_c \sim \omega/DC \sim 1$ nm, where C is the dimer concentration, represents the distance over which the concentration is perturbed by the microtubule's consumption. The size of a dimer $(4 - 8$ nm$)$ places a lower bound on the relevant length scales.

Since growing microtubules with ends within a diffusion length of one another compete for dimers, depletion effects may give rise to a subpopulation of bounded microtubules among unbounded ones, if nucleated in a dense, parallel alignment (Dogterom and Leibler, 1993). ℓ_ω is the longest length scale over which depletion can occur, but it is only significant on the scale of ℓ_c. For reference, nucleating sites on an axoneme end are about ~ 10 nm apart (section III.2.2.2).   *End of Digression*

2.2. Compensation between the velocities

Having established the transition to unbounded growth in terms of the microtubule population, we now ask: how does unbounded growth emerge in the dynamics of individual microtubules? In particular, is dynamic instability the same everywhere along the transition?

At three tubulin concentrations (6, 14 and 45 µM), and over a different range of temperatures for each, we recorded the lengths of individual microtubules for up to 30 minutes (section III.3.3.3). We focus on the faster growing, plus end microtubules for simplicity (section III.2.2.2). The discussion can be extended to include minus ended microtubules, which behave in a qualitatively similar fashion (section IV.2.4).

We measured V_g and V_s from the weighted averages of positive and negative slopes in the time series of the lengths of individual (plus end) microtubules, as determined by least-squares linear fits. The weighting was proportional to the duration of each slope. Error in the measurement is ±0.1µm/min for V_g and ±10% for V_s.

The data are plotted in Figures 4.6 and 4.7. Since V_g is proportional to the tubulin concentration (Walker, et al., 1988; Dreschel, et al., 1992), the measurements collapse onto a single curve after being divided by the concentration (Figure 4.6). Measurements of V_s, being independent of the tubulin concentration, fall together at once (Figure 4.7) (Walker, et al., 1988).

Fitting an empirical function to the data, lines of constant velocity can be computed and superimposed on the phase diagram (Figure 4.8). Constant V_s defines a family of horizontal lines while constant V_g defines a series of convex curves. The latter are significantly different from the bold convex curves in the diagram, which depict transitions.

83
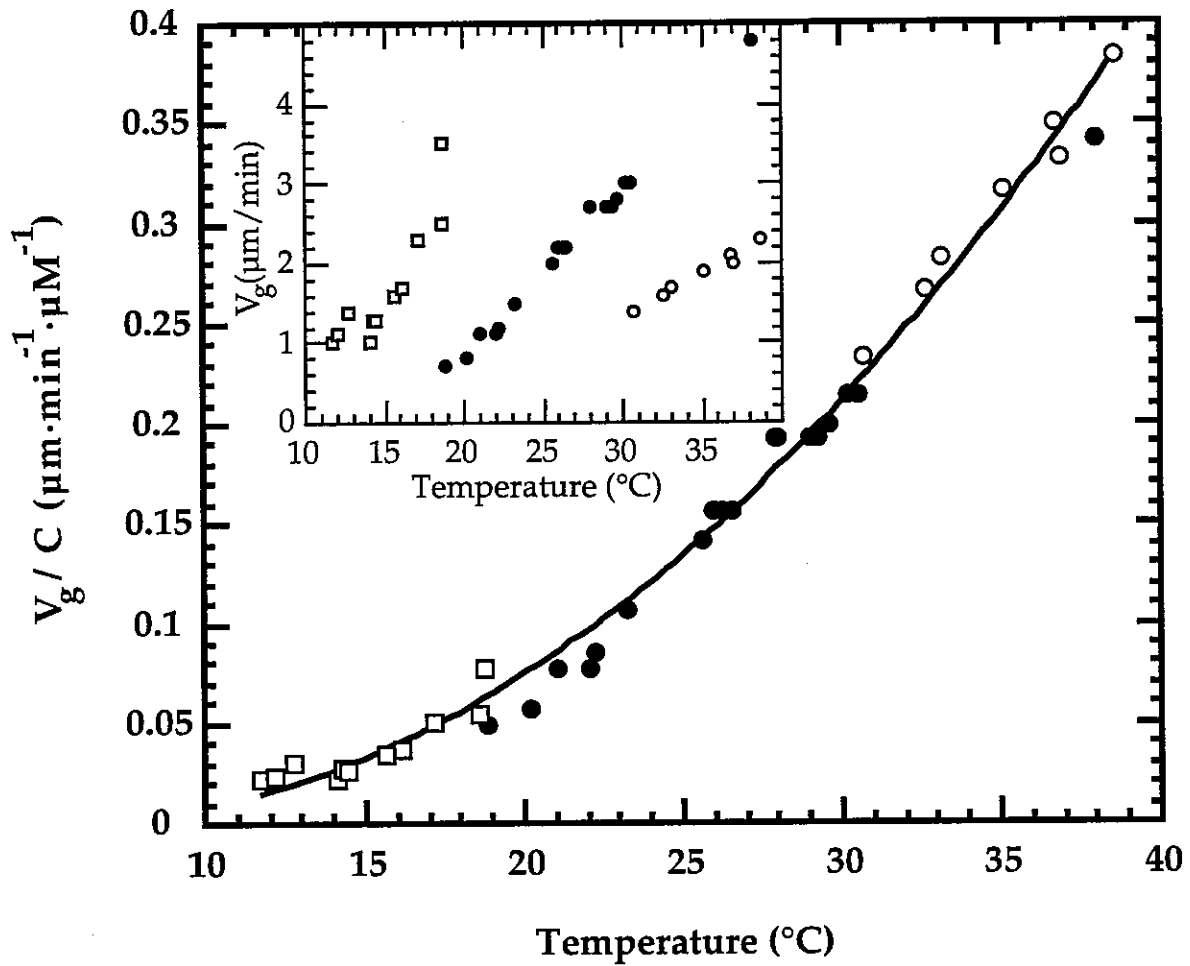
Fig 4.6. Velocity of growth vs. temperature. (Plus ends only.) Re-scaled with respect to tubulin concentration. The line is a least-squares fit to the quadratic polynomial: $V_g = C(0.012 - 0.0038T + 0.00035T^2)$ Inset: same data not re-scaled. C = 6μM (open circles); C = 14μM (filled circles); C = 45μM (open squares);
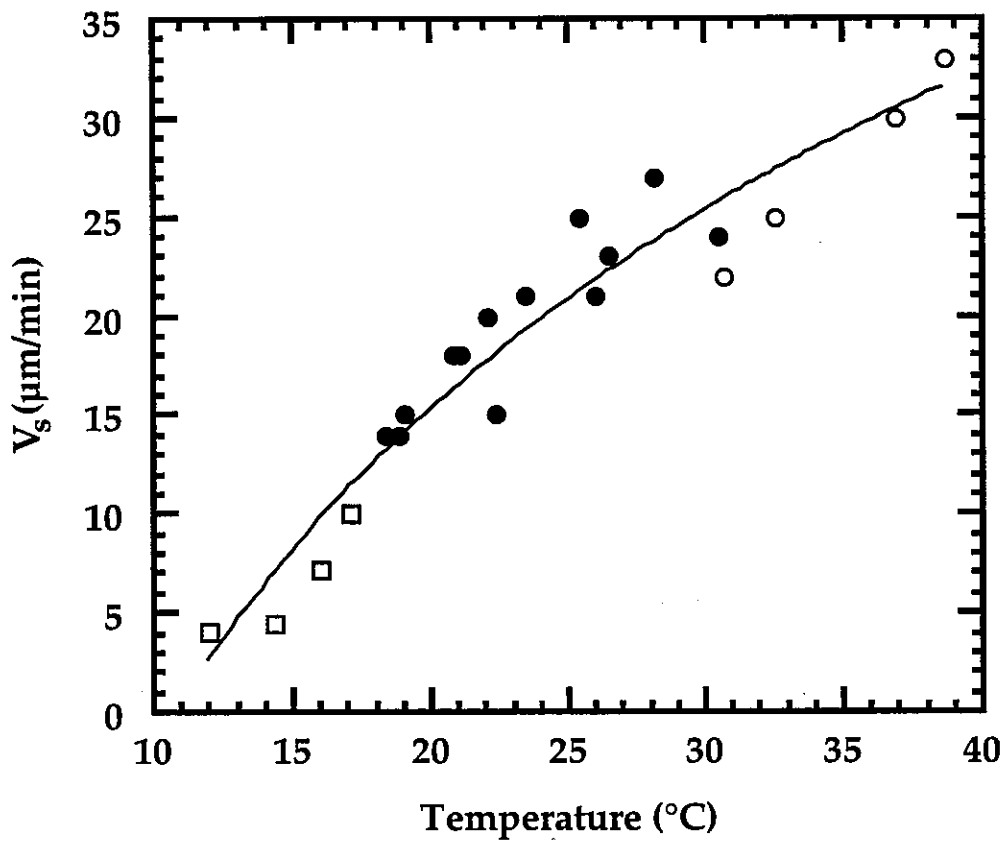
Fig. 4.7. Velocity of shortening vs. temperature. (Plus ends only.)
The line is a least-squares fit to a logarithmic form: $V_s = -59 + 57\ln(T)$
C = 6μM (open dots); C = 14μM (black dots); C = 45μM (open squares).
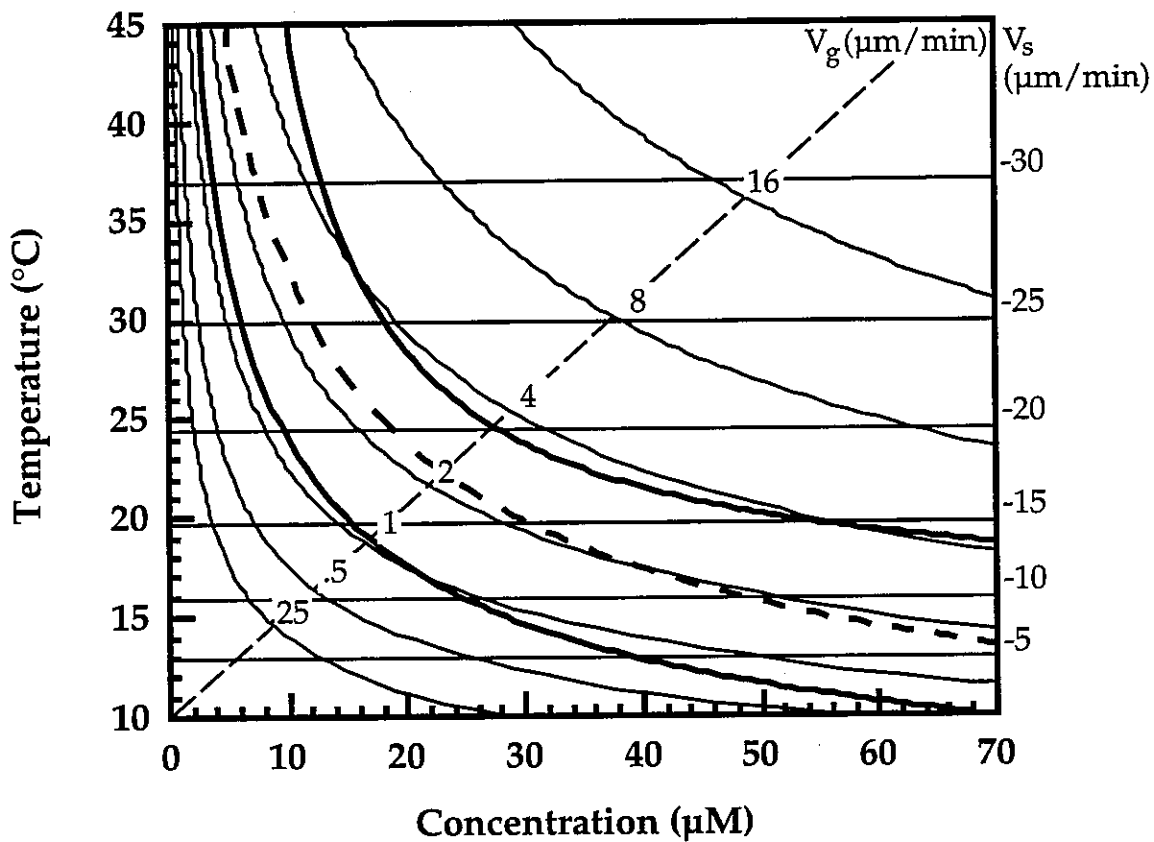
Fig. 4.8. Lines of constant velocity superimposed on the phase diagram. The thick lines represent the three onsets: bounded growth (i.e. site nucleation), unbounded growth (dashed line), and bulk nucleation (see Figure 4.1).

From Figure 4.8 it can be seen that the onset of unbounded growth does not represent a unique set of velocities throughout the phase diagram. (Indeed, neither does the onset of site or bulk nucleation.) Depending on the particular temperature and concentration at which onset is observed, microtubules exhibit different velocities of growth and shortening. Microtubules which begin to grow unbounded at low temperatures are less dramatic (growing and shortening slower) than their counterparts at high temperatures.

The overall effect of temperature on V_g and V_s is essentially the same: an increase of a factor of 8 over 30°C. This is remarkable for three reasons. First, assembly and disassembly seem like opposite reactions, and yet they do not have opposite responses to temperature. Actually, the reactions are not opposites. The intervening reaction of GTP-hydrolysis creates a species of tubulin (GDP-tubulin) which is chemically distinct from the tubulin which assembles onto the microtubule (GTP-tubulin).

Second, it means that the temperature dependence of the velocities can be effectively factored out of the difference $V_g f_r - V_s f_c$. Thus, the transition to unbounded growth, when approached by increasing temperature at a fixed concentration (i.e. along a vertical line in the phase diagram), must be due to changing the relative frequencies of catastrophe and rescue. This is explored further in the next subsection (IV.2.3).

Finally, basic thermodynamics teaches us that higher temperatures must favor less order (higher entropy), but microtubules, which are surely more ordered than tubulin dimers in solution, assemble faster at high temperatures! An increase in assembly at higher temperatures can be explained in terms of interactions between tubulin dimers and surrounding water molecules, as is developed in the digression which follows.

Digression: On the origin of the temperature dependence of the velocities

In which it is argued that neither diffusion nor competing chemical reactions explain the observed temperature dependence of the assembly and disassembly of microtubules. It is proposed that interactions which remove degrees of freedom of nearby water molecules drive both processes. Rough estimates of the number of water molecules involved are made.

The velocity of microtubule growth is not limited by the diffusion of tubulin dimers. It is slower and much more sensitive to temperature. Collisions between diffusing dimers and the end of a microtubule occur with a frequency of $R_o = \pi b^2 DC/2a \sim 5 \times 10^4 / \text{sec}$ (section IV.1.2) while the assembly reaction proceeds at a trickling pace, $\sim 50/\text{sec}$ ($V_g \sim 2\mu\text{m}/\text{min}$). *Only one in every thousand collisions results in incremental growth of a microtubule.* Not surprisingly, the effect of temperature on diffusion ($D = kT/6\pi\eta(T)a$, where $\eta(T)$ is the viscosity of water) has little impact on microtubule growth. A plot of V_g divided by $R_o(T)$, makes it clear that some other, more substantial temperature dependence governs assembly (Figure 4.9).

It has been suggested that the slow growth rate might reflect a reduction in the concentration of available tubulin dimers (Kirschner, et al., 1974; Dreschel, et al., 1992). It is proposed that there may exist a chemically distinct species of tubulin which competes with microtubules for dimers. It would behave as a sort of dimer-sink, reducing the concentration of tubulin available for microtubule assembly. Changes in temperature could shift its chemical equilibrium, altering the dimer concentration and causing the observed temperature dependence of the growth rate. Support for this hypothesis comes from the existence of ring-like oligomers of tubulin which are more stable at lower temperatures (Mandelkow, et al., 1984; Melki, et al., 1989).

However, we find it highly implausible that a competing state should account for all of the observed temperature dependence. Even if such a state were completely unpopulated near 38°C, when C = 6μM and $V_g = 2$ μm/min, this would mean that with C = 45μM near 10°C, where $V_g = 1$ μm/min, only be 3μM of tubulin could be in dimer form. The competing state would have to account for the other 42μM, >90% of all the tubulin. Of course, the formal possibility cannot be completely ruled out without direct observation under the electron microscope but, meanwhile, we propose and develop an alternate explanation.

It is more likely that the microtubule growth rate is limited by a free energy barrier that opposes the tubulin-microtubule binding reaction. Recognizing V_g as the reaction rate, we can consider it in terms of an Arrhenius equation, $V_g = R_o e^{-E_a/kT}$, where E_a is the height of the energy barrier and R_o, the frequency of collisions (Atkins, 1990; Levine, 1995). $V_g/R_o = e^{-E_a/kT}$ is then the probability that a collision will have enough energy to overcome the barrier. Taking the temperature dependence of R_o into account (section IV.1.2), we should be able to estimate E_a from the slope of a van't Hoff plot, $\ln(V_g/R_o)$ vs. $1/T$ (Figure 4.10).

The plot, however, is non-linear and must be fit by the expansion $\ln P = a + b(1/T) + c\ln T$. This common modification of the Arrhenius form accounts for entropic contributions to the barrier, making the effective energy barrier temperature-dependent $E_{eff} \propto (cT - b)$ (Hulett, 1964; Perlmutter-Hayman, 1976). From the fit (see Figure 4.10, caption), we find:

$$\left(\frac{E_{eff}}{kT}\right)_{growth} = (c - b/T) = \frac{(1.1 \pm 0.2) \times 10^5}{T} - (330 \pm 60).$$

V_s can be analyzed in a similar manner, with similar results (Figure 4.11):

$$\left(\frac{E_{eff}}{kT}\right)_{shortening} = \frac{(2.3 \pm 0.4) \times 10^5}{T} - (740 \pm 120).$$

89
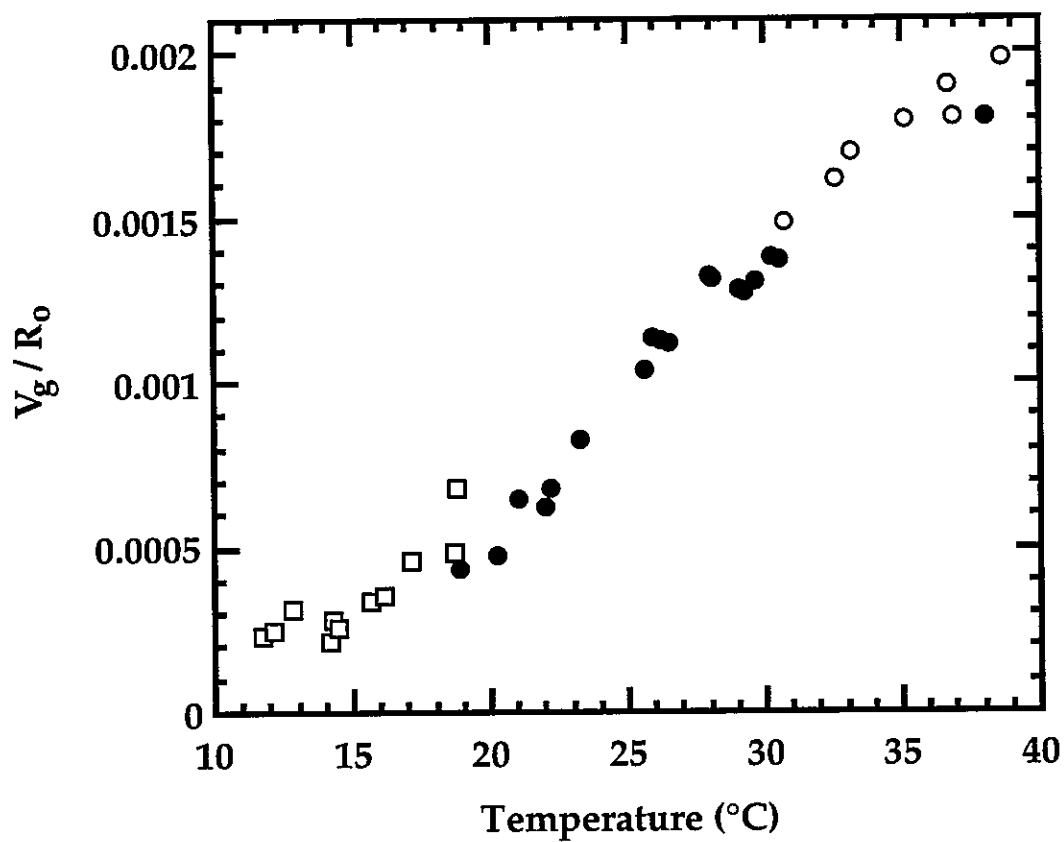
Fig. 4.9. Residual temperature dependence of the velocity of growth. Obtained by dividing V_g by $R_o(T)$ as calculated in section IV.1.1.2. C = 6µM (open dots); C = 14µM (black dots); C = 45µM (open squares).
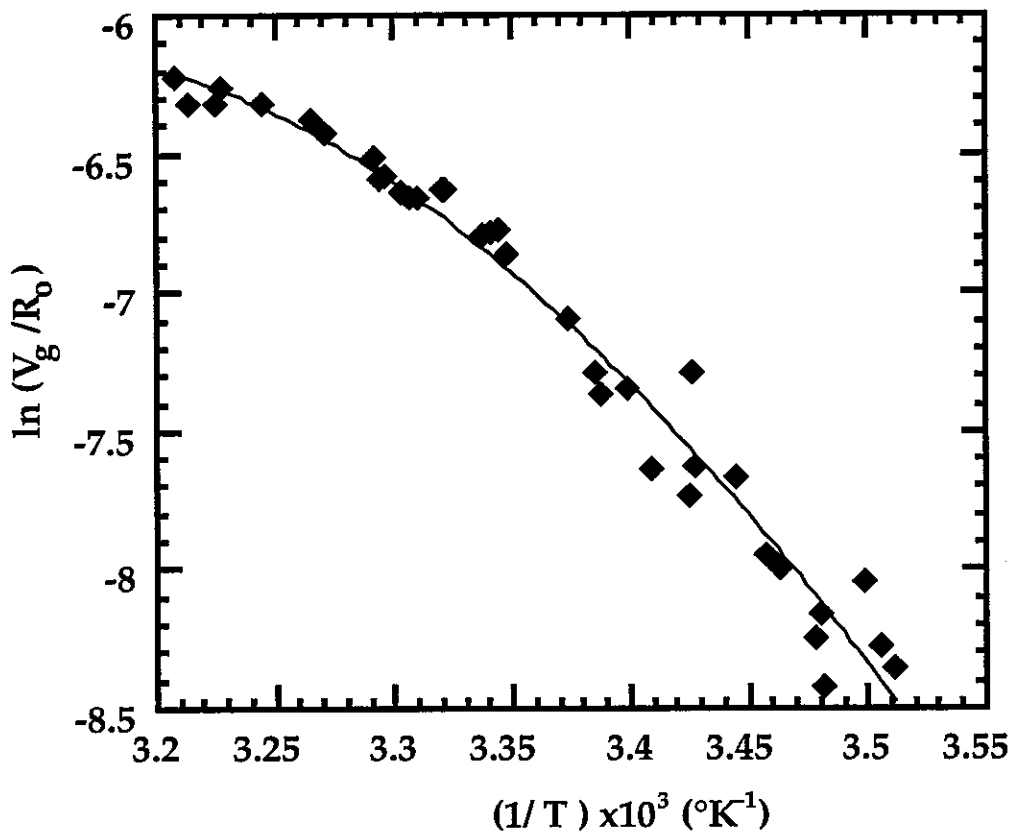
Fig. 4.10. Van't Hoff plot of tubulin assembly. Same data as in Figure 4.9. The curve is a least-square fit to the form $\ln P = a + b(1/T) + c \ln T$ with fitting parameters: $a = (2.2 \pm 0.4)10^3$, $b = -(1.1 \pm 0.2)10^5$, and $c = -330 \pm 60$.
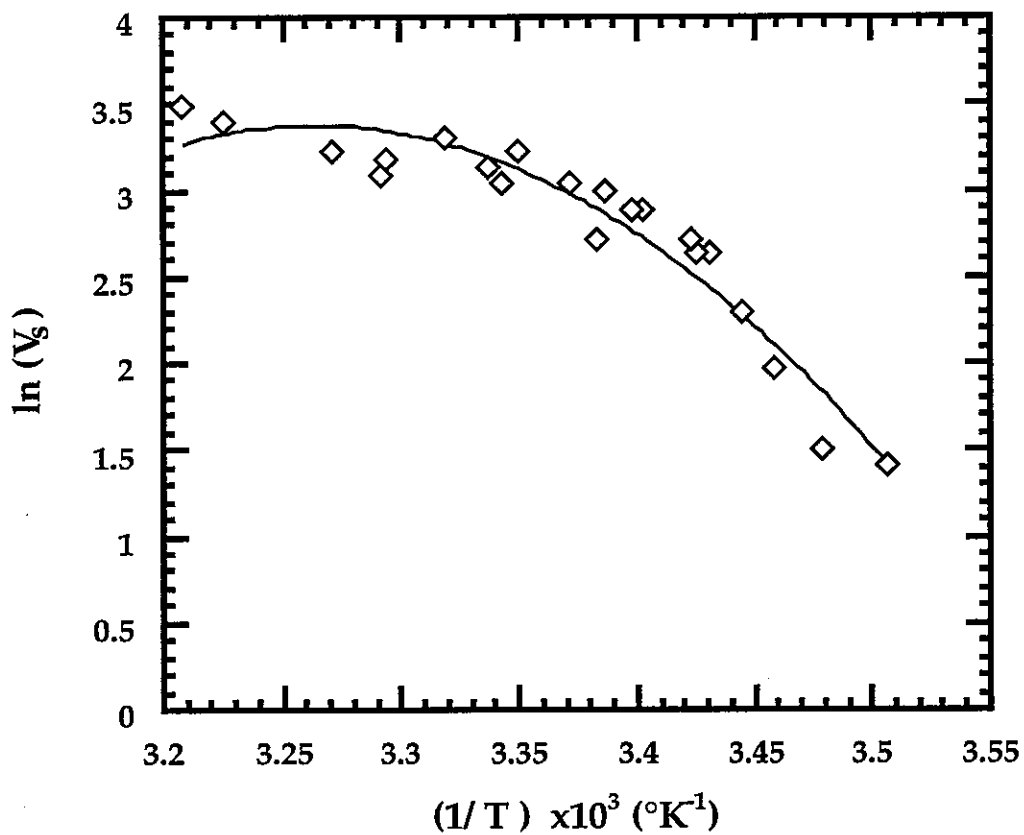
Fig. 4.11. Van't Hoff plot for tubulin disassembly. Same data as in Figure 4.7. The curve is a least-square fit to the form $\ln P = a + b(1/T) + c \ln T$ with fitting parameters: $a = (5.0 \pm 0.8)10^3$, $b = -(2.3 \pm 0.4)10^5$, and $c = -740 \pm 120$.

Although the errors in the parameters are magnified by taking their difference, the values are in good agreement with another study in which the effect of temperature on the apparent equilibrium constant for microtubule assembly was determined from measurements of the turbidity of microtubule solutions $(b = 2.1 \times 10^5; c = 750 \pm 250)$ (Lee and Timasheff, 1977).

Intuitively, it makes sense that a reaction which increases entropy should be favored at higher temperatures but, at first, it might seem that entropy considerations should have the opposite effect in the case of microtubule assembly. Tubulin dimers must *lose* entropy when they leave the solution to become locked in the crystal-like structure of a microtubule. We must conclude that another source of entropy exists in the system. Furthermore, what applies to assembly must apply equally well to disassembly in order to explain the striking similarity between the two.

A commonly overlooked source of entropy common to both reactions is water (Colombo, et al., 1992; Leikin, et al., 1993). Solutes which are either highly non-polar (hydrophobic) or highly polar restrict the orientations of surrounding water by limiting the configurations available for hydrogen bonding (Israelachvili, 1993). The surrounding water is sometimes described as "frozen" and its release, upon aggregation of the offending molecules, can generate a net increase in the entropy of the system. The number of water molecules released in a reaction can be estimated from the apparent change in heat capacity during the reaction, ΔC_p, divided by the difference in the heat capacities of ice and water, ~ 9 cal/mol deg (Hulett, 1964; Perlmutter-Hayman, 1976).

This mechanism is plausible enough in the case of microtubule assembly: GTP-tubulin dimers may have hydrophobic regions on their surfaces which are hidden when they aggregate to form the microtubule. It is

more difficult to imagine in the case of disassembly: surface area is exposed rather than hidden when tubulin leaves the microtubule. The geometry of the microtubule itself is probably important in driving disassembly. (Electron micrographs of disassembling microtubules reveal protofilaments peeling away from the center of the tube (Mandelkow, et al., 1991)). Nevertheless, it seems altogether plausible that hydrolysis changes the conformation of tubulin, reorganizing hydrophobic and charged patches on its surface so that water around and within the microtubule is more ordered than before.

We can estimate the number of water molecules involved, from the apparent change in heat capacity of the reactions $\Delta C_p = \mathbf{R}c$, where $\mathbf{R}$ is the ideal gas constant and c is the parameter in the expanded Arrhenius equation. $\Delta C_p = -660 \pm 120$ cal/mol deg implies $\sim 75 \pm 15$ water molecules are released in the assembly reaction and $\Delta C_p = -1500 \pm 250$ cal/mol deg implies $\sim 170 \pm 30$ water molecules released in the disassembly reaction. Of course, the decision to reference the difference in heat capacity between water and ice is rather arbitrary, so these values can only be looked to as "order of magnitude" estimates. It is useful to note that similar figure was found in a similarly-minded experiment in which it was rigorously determined that about 60 water molecules bind to hemoglobin during its transition from a fully deoxygenated to a fully oxygenated state (Colombo, et al., 1992).

End of Digression

A reminder as we return to the question of dynamic instability and the approach to unbounded growth. We have shown that growth and shortening *velocities* increase similarly with temperature, thereby compensating one another and not contributing to the onset of unbounded growth. Unbounded growth must therefore depend upon changes in the relative *frequencies* of catastrophe and rescue.

2.3 Competition between the time scales

Let us consider the frequencies of catastrophes and rescues in terms of their inverses: the lifetime of the growing state $T_g = f_c^{-1}$ and the lifetime of the shortening state $T_s = f_r^{-1}$. T_g is calculated from the total time spent in the growing state divided by the total number of catastrophes observed, in accordance with the convention in the literature (Walker, et al., 1988). Periods of growth which begin prior to observation or do not have a catastrophe during observation are included, the assumption being that catastrophes occur at random (section IV.2.1). The error is estimated by $\pm T_g/\sqrt{N}$ where N is the number of catastrophes observed.

T_s is more difficult to measure since microtubules often shorten very quickly and rescues are always rare (either because shortening events are truncated by the nucleating site or because catastrophes are infrequent). Instead, reliable measurements can be made of the probability of rescue P_r, the number of rescues divided by the number of catastrophes observed. P_r is particularly useful, for example, in calculating the rate of complete catastrophe $R_{cc} = (1 - P_r)/T_g$, referred to in the earlier discussion of site nucleation (section IV.1). Like T_g, the error in P_r is presumed proportional to $1/\sqrt{N}$, where N is number of catastrophes observed.

T_g and P_r are plotted versus temperature in Figures 4.12 and 4.13. For each concentration used, an unshaded region indicates the regime of bounded growth. A pair of horizontal lines suggests universal criteria for the two onsets which bound this regime. A solid horizontal line indicates the onset of bounded growth, which corresponds to $T_g \sim 120$ sec and $P_r = 0$. A dotted horizontal line indicates the onset of unbounded growth, which begins when $P_r = 1$ (by definition), and is also determined by $T_g \sim 660$ sec = 11 min.

95
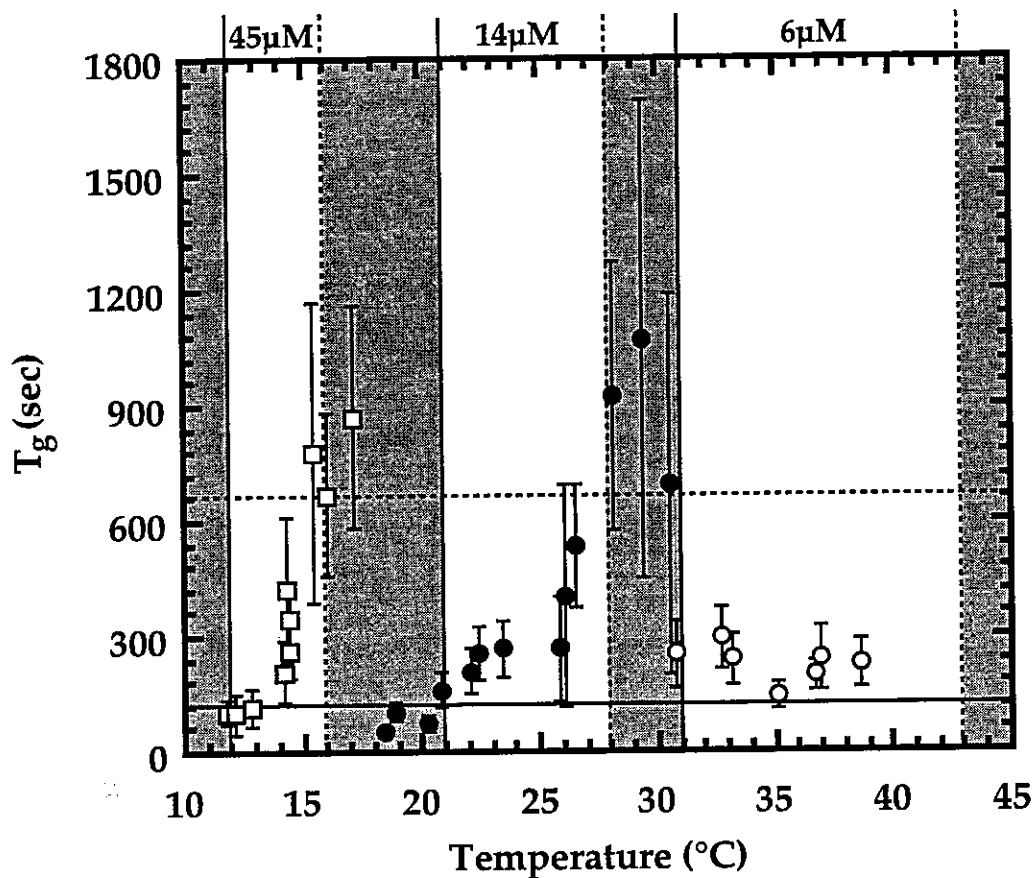
Fig. 4.12. Lifetime of the growing state vs. temperature. (Plus ends only.) The unshaded regions highlight the regime of bounded growth for each of the concentrations used. They are bounded by lines indicating the temperatures of onset of bounded (solid lines) and unbounded (dotted lines) growth. Horizontal lines extract features of the two onsets: $T_g \sim 120$ sec for onset of bounded growth (solid); $T_g \sim 660$ sec for onset of unbounded growth (dotted). $C = 6\mu M$ (open dots); $C = 14\mu M$ (black dots); $C = 45\mu M$ (open squares).
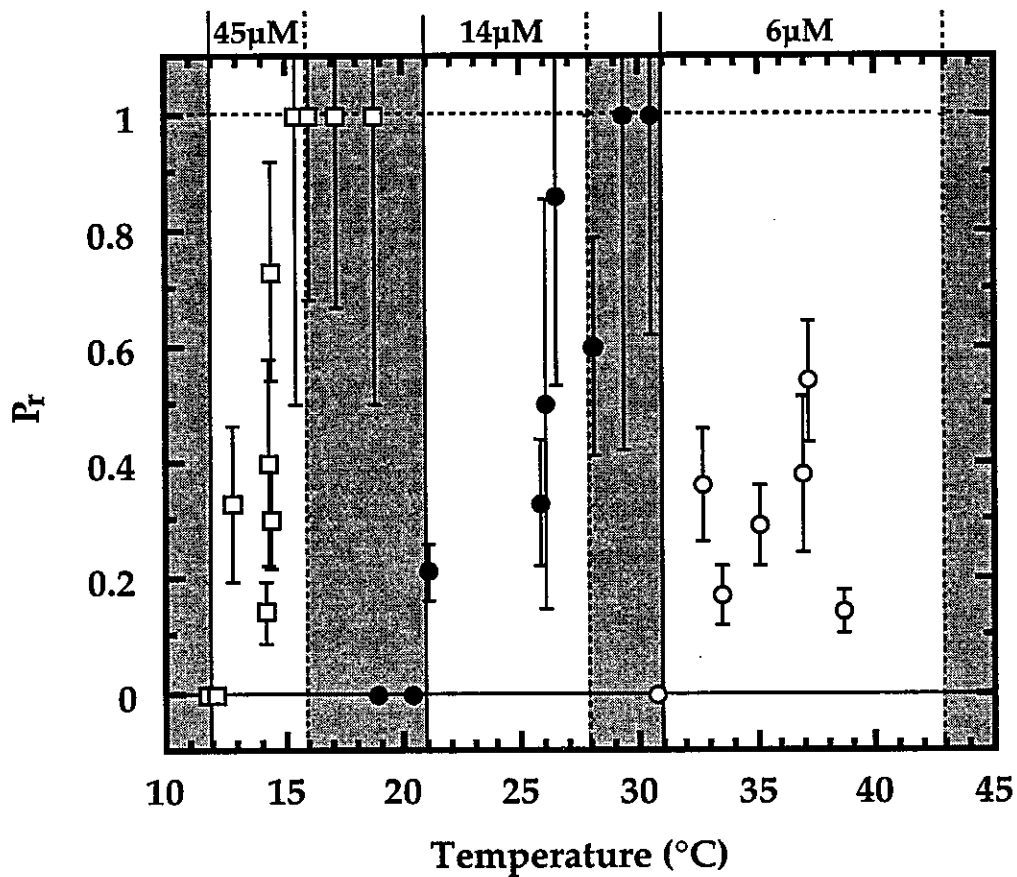
Fig. 4.13. Probability of rescue vs temperature. (Plus ends only.) Unshaded regions highlight regimes of bounded growth for each of the temperatures used (as in Figure 4.12). Horizontal lines extract unifying features of onsets: $P_r = 0$ bounded growth (solid); $P_r = 1$ at onset of unbounded growth (dotted). $C = 6\mu M$ (open dots); $C = 14\mu M$ (black dots); $C = 45\mu M$ (open squares).

There are two opposing trends in the lifetime of a growing microtubule. At a given concentration, T_g increases as the temperature rises (Figure 4.12), but the *rate of increase* decreases at higher temperatures (lower concentrations) until, at the lowest concentration, T_g is steady, independent of temperature. This behavior is even more marked in a plot of T_g versus V_g, (Figure 4.14), which shows that for a fixed V_g, T_g is shorter at higher temperatures (i.e. lower concentrations).

These opposing tendencies reflect the fact that catastrophe results from a competition between the process of assembly and a mechanism which destabilizes the microtubule. At low temperatures (high concentrations) the destabilizing mechanism must be slow and uncoupled from the assembly process. The local increase in T_g with temperature indicates that assembly accelerates faster with temperature than does destabilization. At high temperatures (low concentrations), destabilization accelerates faster but is somehow limited by assembly, causing saturation in T_g.

What model can incorporate these observations? The challenge is to understand the destabilizing mechanism. It is known that destabilization requires the hydrolysis of GTP. However, the GTP-cap models that are currently available (section II.5) cannot be reconciled with our data. In particular, a frequency of catastrophe which is independent of the velocity of growth is generally unexpected. The only model which allows saturation of the catastrophe frequency would require implausible fine-tuning to explain it under the conditions we observe (Flyvbjerg, et al., 1994).

We now indulge in a bit of speculation over a distinct destabilizing mechanism — the zippering of the microtubule. This exercise brings out the key elements needed in any model as well as some intriguing possibilities concerning for rescue.
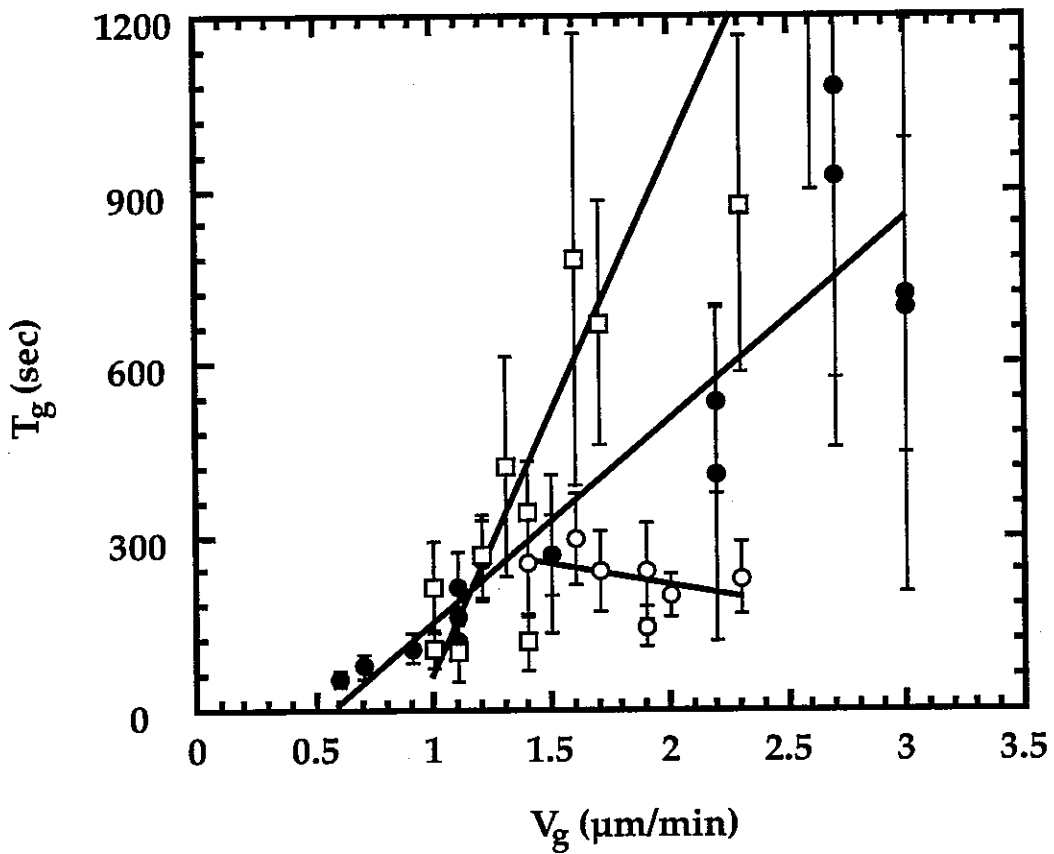
Fig. 4.14. Lifetime of the growing state vs. velocity of growth. (Plus ends only.) The two diagonal lines are least-squares linear fits to the data from 45 μM and 14 μM. The nearly horizontal line is consistent with the data from 6 μM. C = 6μM (open dots); C = 14μM (black dots); C = 45μM (open squares).

Electron micrographs reveal that growing microtubules have two structurally distinct regions (Figure 4.15). Over most of its length, a microtubule is a tube but near the end it has a sheet-like region (Figure 4.16). Apparently, the sheet curls up ('zippers') to form the body of the microtubule. Most likely, curling is a rare thermal fluctuation in the tubulin sheet that is stabilized by the lateral interaction between the two terminal protofilaments.

It has been suggested that curling may be a pre-requisite for the transition from assembly to disassembly. That is, it may be that the microtubule cannot have a catastrophe unless it is completely zippered (Chrétien and Karsenti, 1995; Chrétien, et al., 1995). If true, zippering may be the rate limiting "destabilizing" mechanism and hydrolysis may be secondary.

The key features that make this mechanism suitable for modeling our observations are twofold. First, zippering is likely to be a *fluctuating* process which advances in fits and stops. Thus, even when assembly outruns zippering on average, there is always a means, a chance fluctuation, whereby zippering may overtake the assembly front. Second, zippering has *mechanical* constraints which can couple it to assembly when assembly proceeds comparatively slowly. For example, to zipper may require a certain length of sheet to be energetically favorable. If fluctuations are large (i.e. high temperature) but growth is slow (i.e. low concentration), the zipper may be hindered because the interaction between lateral filaments is not strong enough to seal the tube until a certain length of sheet is available.

This discussion highlights the two features that should be at the core of any model of our data: 1) the destabilizing process must be faster at higher temperatures and 2) the destabilizing process must be rate limited by the assembly process at the highest temperatures.
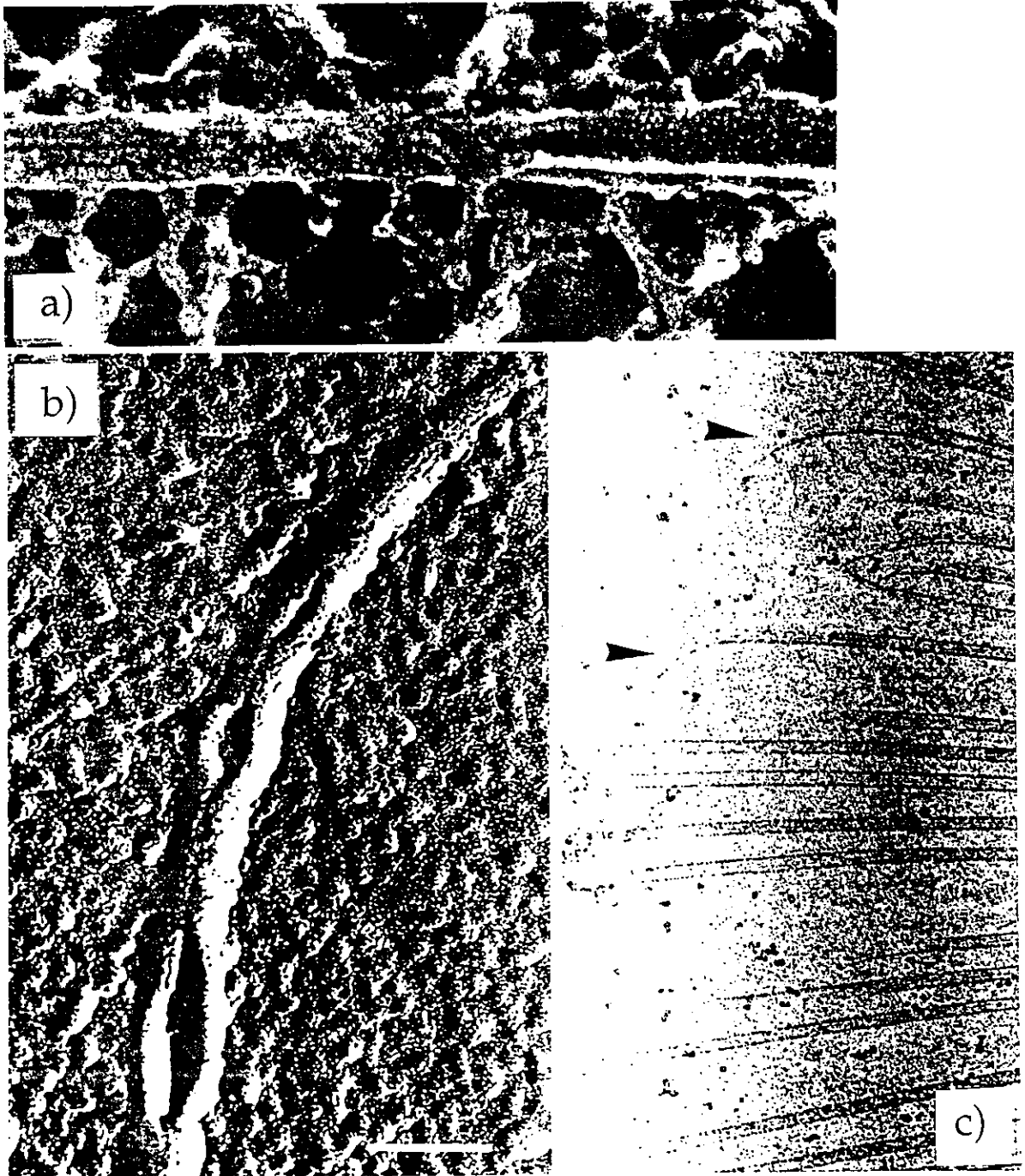
Fig. 4.15. Electron micrographs depicting zippering microtubules. a) From (Schliwa, 1986); b) from (Mandelkow, et al., 1986); c) from (Chrétien and Karsenti, 1995). The older micrographs (a and b) were obtained without correlation to the dynamic state of the microtubules (growing vs, shortening). The most recent ones are known to represent growing microtubules.
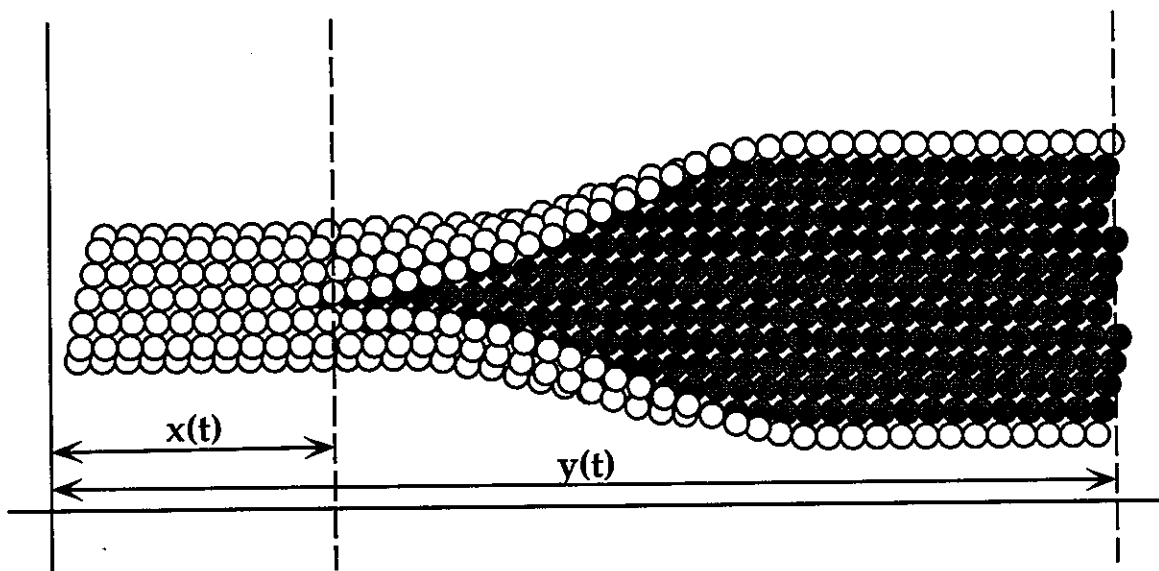
Fig. 4.16. Schematic of a microtubule 'zippering' from a sheet into a tube. The position of the tube front and the sheet front are labeled separately as functions of time to suggest modeling their growth separately.

Consider the illustration in Figure 4.17. The thin curves represent the rate of assembly at several different tubulin concentrations. The higher the concentration, the more rapidly the rate of assembly increases with temperature $(V_g \propto CT)$. The unshaded regions each select a particular curve whose concentration is appropriate for observation in that range of temperatures. The thick curve represents a plausible (exponential) temperature dependence to the typical rate advance of a destabilizing front.

In the leftmost unshaded region (the lowest temperatures and highest concentration), destabilization (e.g. zippering) can only overtake the assembling front if it has a rather large (and consequently rare) fluctuation. The rate of assembly increases faster than the zippering fluctuations at such low temperatures, explaining why the lifetime of a growing microtubule becomes long rather quickly. In the central unshaded region, destabilization overtakes the assembling front more regularly and so the microtubule can not grow for quite as much time. Still, the typical fluctuation is too small to overtake the assembling sheet and catastrophe depends upon a large and rare fluctuation (though not as large nor as rare as before.) Finally, in the rightmost unshaded region, the thick and thin curves have crossed one another, which means that the average destabilizing fluctuation is limited by the rate of assembling the sheet. Consequently, the typical frequency of catastrophe is no longer be sensitive to the fact that the fluctuations are increasing. The lifetime of a growing microtubule saturates.

We emphasize that this reasoning is independent of the zippering model but rather well suited to it. We return to the zippering model for some final comments.
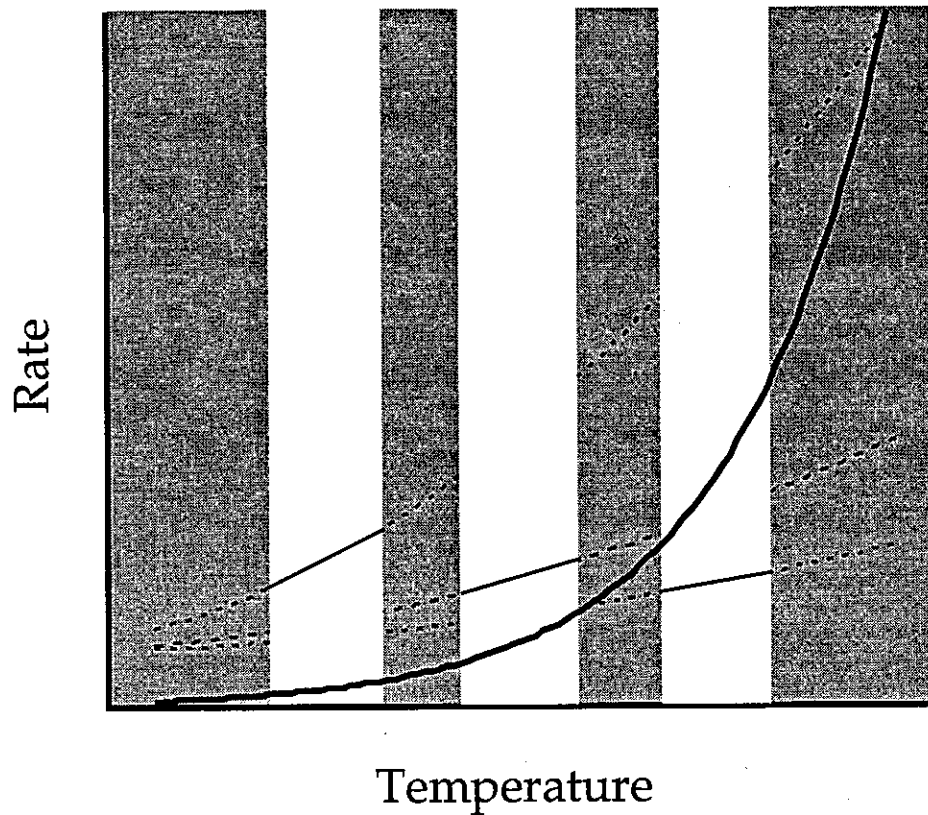
Fig. 4.17. Illustration of our interpretation of the catastrophe data. The rate of assembly is drawn as a function of temperature for three different tubulin concentrations C, 2C, and 6C (thin curves), based on the data plotted in Figure 4.6. The unshaded regions highlight the relevant range of temperatures for each concentration: the highest concentration exhibits bounded growth at the lowest temperatures, the intermediate concentration at intermediate temperatures and the lowest concentration at the highest temperatures. An exponential temperature dependence (thick curve) represents the presumed temperature dependence of the zippering fluctuations. See the text for a thorough discussion.

Zippering microtubules is an intuitive imagery which is both appealing and fertile. The microtubule as a whole can be considered as undergoing a conformational change from a partly open to a fully closed state. The transition is driven by thermal fluctuations and stabilized by a free-energy of binding, similar to the model of conformational change in protein molecules. This naturally suggests a mechanism for rescue – the return to the open state. Namely, gaps or defects left behind when the tubulin sheet spontaneously zippers into a tube, may eventually disrupt the disassembly process and stimulate rescue. We might predict then that the creation of a defect requires a certain length of sheet on the end of a microtubule, and so the probability of rescue will grow with the average length of the sheet. The average length of sheet, however, also determines the time required for catastrophe. Thus we predict that catastrophe and rescue are strongly coupled.

There is some indication in our observations for such a coupling between catastrophe and rescue. Notice that the region of bounded growth spans the same range of T_g for the two higher concentrations (Figure 4.12). This suggests that the onsets of bounded and unbounded growth correspond to lines of constant T_g in the phase diagram. However, these onsets are actually defined in terms of rescue (i.e. unbounded growth: $P_r = 1$; bounded growth: $R_N \cdot T_g = 1 - P_r$). Furthermore, when catastrophe saturates at high temperatures, rescue is similarly steady.

One interesting test of the nature of rescue would be to grow long microtubules at high temperatures and then induce catastrophe by cooling abruptly to the onset of bounded growth. One could then check to see if rescue is a function of the conditions under which the microtubule grew or the conditions under which is shortens.

2.4 Conclusions

The logic underlying microtubule behavior is emerging. Assembly and disassembly share a common mechanism based on the structure of individual tubulin dimers and how they constrain the water molecules around them. GTP hydrolysis is essential for the reorganization of water molecules which drives disassembly but it is not necessarily the instigator of catastrophe. Instead, catastrophe and rescue may share a common mechanism based on the structure of the microtubule as a whole and how it zippers from a sheet into a tube. In a sense, the microtubule itself has a 'conformational change' underlying its unique function – dynamic instability.

3. Nucleation in Bulk: beyond dynamic instability

Well beyond the onset of unbounded growth, dynamic instability gives way to what might be called normal growth. The typical time between catastrophes becomes so long that the slow process of tubulin denaturation becomes a concern. In this regime beyond dynamic instability, microtubules continue to distinguish themselves from conventional materials by their homogeneous nucleation.

Part crystal, part polymer, microtubules spontaneously nucleate in three dimensions but extend in only one. The rate limiting step of curling into a tube establishes the critical size for the nucleating seed. Once nucleated, the microtubule consumes a negligible amount of tubulin without filling space. Observations are limited by the lifetime of tubulin rather than depletion of the supply.

In what follows we present direct observations of the homogeneous nucleation of microtubules at different concentrations and temperatures. This work was done in collaboration with Kim Sneppen. There is a steep power law dependence of the nucleation rate on the tubulin concentration $(r \sim C^{12\pm2})$. This behavior defines the nature of the critical seed and permits an estimate of the lifetime of tubulin in solution ($\sim$7 hours at 18°C). The results compare favorably with indirect observations in the literature (Voter and Erickson, 1984; Fygenson, et al., 1995)

3.1 Power law approach to onset

The procedure for measuring microtubule nucleation is straightforward. Under the microscope, a sample without nucleating sites is cooled to $\sim$ 4°C for $\sim$ 25 minutes to force the disassembly of any microtubules, and then quickly warmed (see section III.3.3.2). For the next 15 minutes to

107

two hours, independent fields of view (separated by at least 90 µm) are monitored by translating the sample. In each field of view, the number of microtubule ends is counted while sweeping the focus through the full depth of the sample. At the end of each sweep, the time is noted.

Since every nucleation event generates two microtubule ends, the number of nucleation events is half of the number of ends. (Microtubules which pass through the field of view without ending are not included in the count.) Great care must be taken to insure proper counting of the ends of microtubules which lie at a steep angle to the plane of focus.

The typical field of view is $\sim 34 \cdot 10^{-12}$ liters, 50 µm deep and 22.5×30 µm^2 wide. Such thick samples minimize the effects of the non-specific absorption of tubulin to glass surfaces (section III.2.1.2.) The maximum thickness is limited to 50 µm by the working distance of the objective. When the nucleation rate was very fast ($\sim 10^6 / \text{cm}^3 \text{sec}$), we reduced the sample thickness to 25 µm so that it would take less time to sweep the focus ($\sim 1 \text{ min} / 50$ µm).

Observation stops when saturation sets in (see section IV.3.2) or visibility is impaired by high densities of microtubules (> 30/field of view). Note that even at such a high density, the amount of tubulin in microtubule form is never more than $\sim 1\%$ of the initial tubulin concentration (≥ 12 µM).

The measurement is repeated for a variety of tubulin concentrations (12µM to 60 µM) and temperatures (20°C to 30°C). Figure 4.18 is a typical plot of the density of microtubule ends versus time. The counts are binned in time, choosing the bin width so that there is, on average, one new end in each. The density increases linearly and then saturates. The slope of the initial rise corresponds to the nucleation rate r (with units of number per volume per time). It ranges from one new end in every field of view every
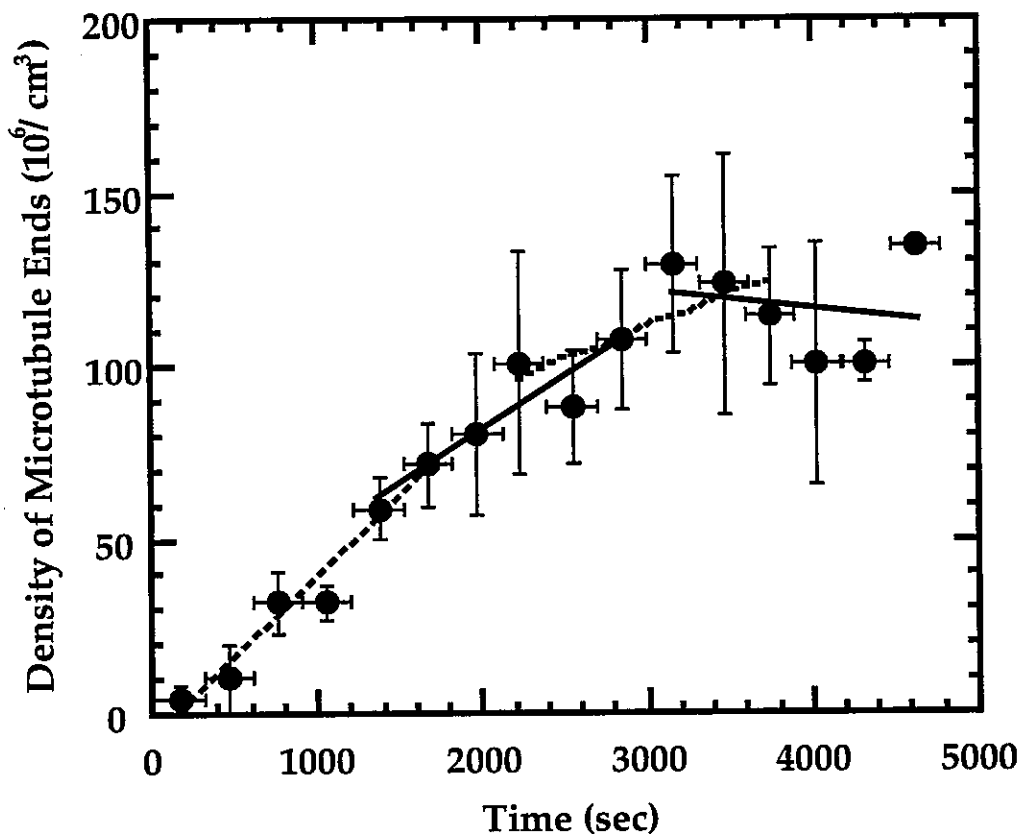
Fig. 4.18. Density of microtubule ends vs. time. The lines are least-squares linear fits to six points each. C = 60 μM, T = 18°C.

109

minute to one new end in _fifty_ fields of view in an hour. For the slowest rates several samples were used until a minimum of 4 microtubule ends was recorded.

Figure 4.19 shows how r varies with concentration for three different temperatures. At each temperature, a power law fits the data well:

$$r \sim C^{12 \pm 2}.$$

As in the case of site nucleation (section IV.1.1), the onset of bulk nucleation is not sharp. A practical onset, defined by an average of one new microtubule end per field of view every five minutes ($r = 10^5 \mathrm{cm}^{-3}\mathrm{sec}^{-1}$), is plotted as the uppermost line on the phase diagram (Figure 4.1). These points were determined by increasing the temperature in steps of $\sim 1°\mathrm{C}$ on a single sample and waiting ~ 15 minutes at each temperature until the nucleation rate approached the onset criterion. In the case of overshoot, a second sample at the same concentration was observed $0.5°\mathrm{C}$ below the last temperature to confirm the location of onset.

3.2 The lifetime of tubulin in solution

The steep power law indicates an extreme sensitivity to concentration and explains the saturation observed in Figure 4.18. Purified tubulin slowly denatures with time, lowering the effective concentration of tubulin dimers. (Denaturation is commonly attributed to the oxidation of amino acid residues and a consequent change in protein conformation.) Microtubule dynamics appear unaffected for ~ 2 hours at modest temperatures ($18°\mathrm{C}$) (section III.1.4). However, dynamics are only weakly concentration dependent ($\sim C$) compared to the C^{12} scaling of the nucleation rate. If the concentration decreases by 10%, assembly slows by 10% (barely detectable) but nucleation falls by >70%. Thus, nucleation rate is sensitive measure of the denaturation of tubulin.
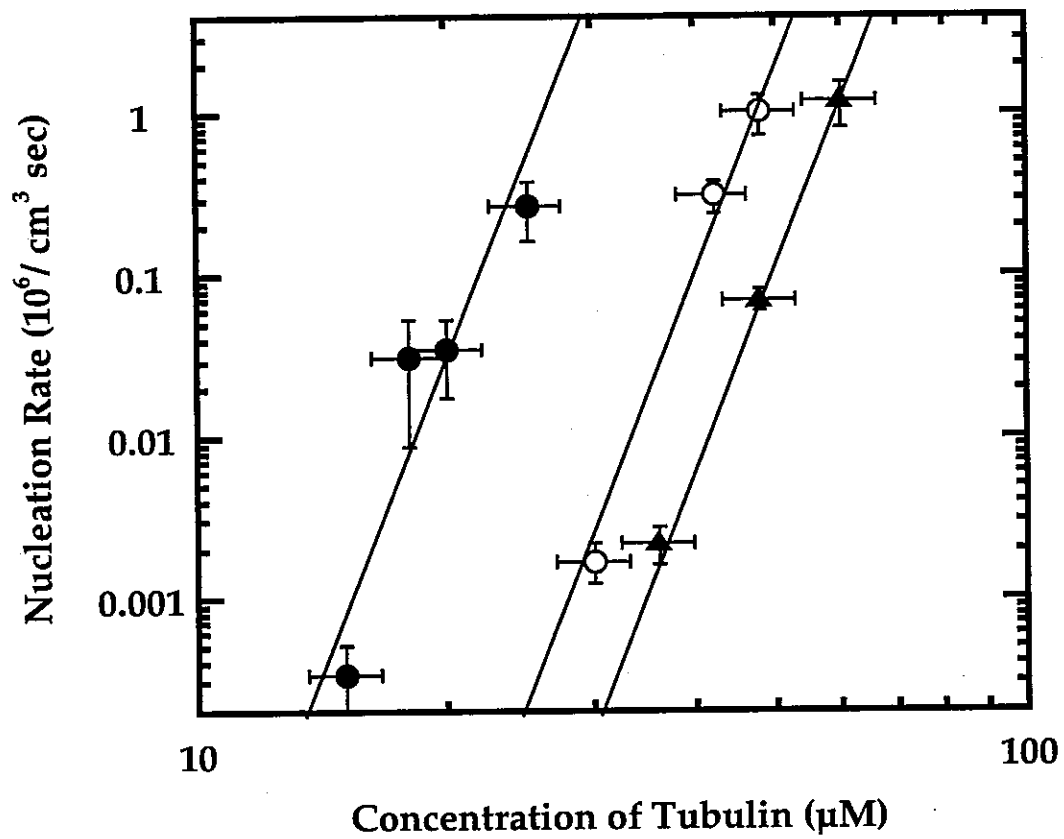
Fig. 4.19. Nucleation rate vs. concentration. Measurements were made at three different temperature: 30°C (black dots); 22°C (open dots); 20°C (black triangle). The lines have slope 12.

Suppose the concentration decays exponentially $C(t) = C_o e^{-t/\tau_{tub}}$. The lifetime of the tubulin τ_{tub} can be calculated from the evolution of the nucleation rate:

$$\frac{\dot{r}(t_1)}{\dot{r}(t_2)} = \frac{r(t_1)}{r(t_2)} = e^{(12\pm2)(t_2-t_1)/\tau_{tub}} \quad \rightarrow \quad \tau_{tub} \approx \frac{(12\pm2)(t_2-t_1)}{\ln(r(t_1)/r(t_2))}.$$

For example, we estimate the nucleation rate from Figure 4.18 using least-squares linear fits to six points at a time,

time (sec)	rate (cm^{-3}sec^{-1})
1000	4.6±0.5
2000	3.0±0.7
3000	1.8±0.9
4000	-0.5±1.3

and deduce $\tau_{tub} \sim (2.6\pm0.4)\times10^4 \, \mathrm{sec} \approx (7\pm1)$ hours. Thus, after half an hour at 18°C, the tubulin concentration has decayed to 93% of its original value. After two hours it lowers to 75%. Evidently, the time constraints we placed on our experiments were appropriate (see section III.1.4). Of course, the lifetime of the tubulin is likely to decrease somewhat at higher temperatures. The details of the temperature dependence remain to be explored.

3.3 Construction of the critical seed

When the rate of a chemical reaction increases with the concentration of a reactant to the power X, it usually means that X molecules of that reactant are involved in the reaction (Levine, 1995). Thus, the power law behavior of the nucleation rate suggests that nucleation relies on the association of approximately 12 tubulin dimers. This is easily understood from a simple model.

Small aggregates of tubulin dimers are constantly forming and dissolving. To a good approximation, an aggregate grows or shrinks one dimer at a time. g, the characteristic rate of growing by one dimer, depends

on the frequency of collisions with dimers, so it is proportional to their concentration C. s, the characteristic rate of losing a dimer, is insensitive to the dimers in solution and is therefore independent of C.

The phenomenon of nucleation implies that aggregates smaller than the critical size N tend to dissolve while aggregates of size N or larger tend to grow. The simplest way to model this is to make g and s depend on x, the size of the aggregate: $g(x) < s(x)$ when $x < N$ and $g(x) > s(x)$ when $x \geq N$.

A constant nucleation rate implies a steady state population of sub-critical aggregates, described by

$$g(x) \cdot c(x) = s(x+1) \cdot c(x+1) \quad \text{for} \quad x < N-1$$

where $c(x)$ is the concentration of aggregates of size x. Starting from $x = 1$ and iterating, we deduce that the nucleation rate per unit volume is

$$r = g(N-1)c(N-1) = g(N-1)\frac{g(N-2)c(N-2)}{s(N-1)} = g(N-1)\left[\prod_{x=1}^{N-2}\frac{g(x)}{s(x+1)}\right]c(1) \propto C^N$$

where $c(1) = C$ is the concentration of tubulin dimers and we have taken $g(x) \propto C$ into account. Thus, as expected, the power law implies that N tubulin dimers are needed to nucleate a microtubule spontaneously in the bulk and the measurements in Figure 4.19 indicate that $N = 12 \pm 2$ dimers.

Though we change the concentration by a factor of 5 in the experiment, there is not a detectable variation in N. N should depend on the concentration since $g(x) \propto C$ and therefore $g(x) - s(x) \propto C$. The lack of such dependence implies that $g'(x)$ and/or $s'(x)$ is large, at least near $x = N$. A sharp size dependence is one indication that geometrical constraints dominate the formation of the nucleating seed.

This observation together with the striking similarity between N and the number of protofilaments in the circumference of a microtubule (see section II.2) strongly suggest that microtubule nucleation depends upon an

aggregate of tubulin dimers wrapping around into a short tube. As we discussed in the previous section, the wrapping or 'zippering' of a tubulin sheet into a tube is a likely step in microtubule growth (Chrétien and Karsenti, 1995), making it even more reasonable to suggest it as a critical step in the assembly of the critical seed.

One implication of this interpretation is that the distribution of protofilament numbers (n_{pf}) should be predictably controlled by the conditions of spontaneous nucleation. Echoing the discussion in section IV.2.3, tubulin dimers may form sheet-like aggregates which fluctuate in curvature with thermal energy. The probability of assembling an aggregate with certain number of protofilaments multiplied by the probability of bending that aggregate into a tube would determine the likely number of protofilaments in a microtubule (see Figure 4.20). For example, a deep quench into the regime of spontaneous nucleation will create aggregates which grow quickly compared to how often they fluctuate in curvature. As a result there should arise a distribution of n_{pf} with a majority of microtubules having a n_{pf} corresponding to the lowest energy bond angle between protofilaments. On the other hand, a shallow quench will generate microtubules with comparatively small n_{pf} since only small aggregates are likely to assemble.

These predictions could be tested under the electron microscope. Electron microscopy has revealed the variability of microtubule n_{pf} (Chrétien and Wade, 1991). One might look for correlated changes in the distribution of the microtubule n_{pf} that correlate with nucleation rate. It has been shown that the distribution of n_{pf} changes with the buffer composition (Ray, et al., 1993). One might also check if this mysterious sensitivity correlates with buffer dependent shifts in the onset of homogeneous nucleation.
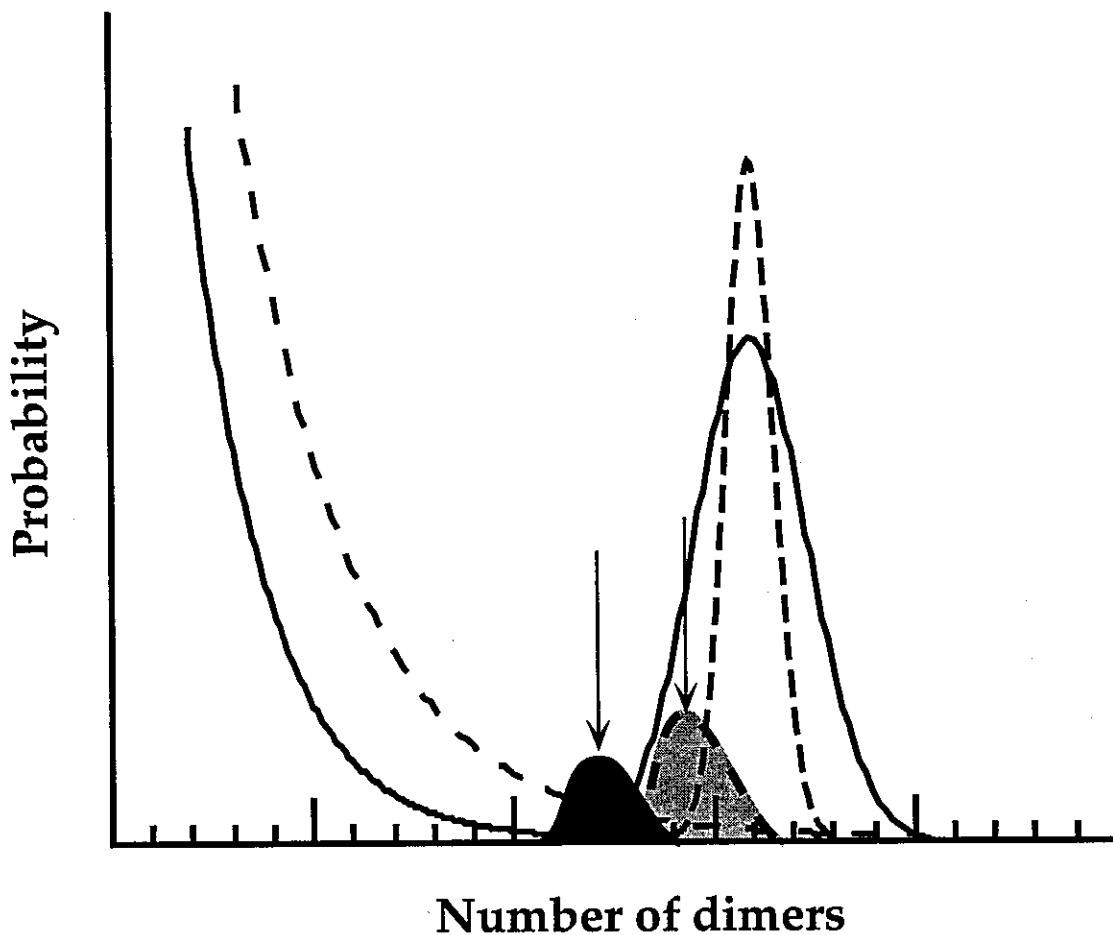
Fig. 4.20. Illustration of different nucleation conditions favor microtubules with different numbers of protofilaments. The decreasing curves represent the probability of formation of an aggregate as a function of the number of dimers in the aggregate. The peaked curves represent the probability of closing a sheet-like aggregate of so many dimers into a tube. The dashed curves represent conditions of high tubulin concentration (larger aggregates) and low temperature (fewer curvature fluctuations). The solid curves represent conditions of low tubulin concentration (smaller aggregates) and high temperature (greater flexibility). The products of the pairs of curves are represented in the shaded regions. The darker region corresponds to the lower concentration/higher temperature and the lighter one to the higher concentration lower temperature. Notice how the typical number of dimers in the most probable aggregate changes.

3.4 Conclusions

As in other instances of homogeneous nucleation (e.g. the condensation of droplets from vapor), the onset of spontaneous nucleation of microtubules can only be defined in terms of a practically observable nucleation rate. Usually, however, concentration (or its analog, vapor pressure) plays a key role in determining the size of the critical nucleus. Once again, microtubules are remarkably different.

Homogeneous nucleation of microtubules is dramatically affected by the unique microtubule structure. A tremendous change in the stability of the tubulin aggregate occurs once a tubular geometry is achieved. This is deduced from the size of the critical aggregate, which resembles the number of protofilaments in the microtubule, and from the rather slow nucleation rates observed. A rough estimate based on the model presented in section IV.3.3 reveals the relative rates of association and dissociation of sub-critical aggregates $g/s \sim 10^{-19}$ (assuming $g(x)/s(x+1)=(g/s)C$ is roughly independent of x for $x<N$ and approximating $g(N-1)$ by the velocity of growth measured in section IV.2.2.) Comparison with the relative rates of assembly and disassembly of the macroscopic microtubule $\left(V_g/V_s \sim 10^{-1}\right)$ emphasizes the importance of the closed geometry.

In the previous section (IV.2.3), we considered the zippering of the microtubule as a mechanism of catastrophe (Chrétien and Karsenti, 1995) . The rate of spontaneous nucleation of microtubules is only significant under conditions in which the rate of catastrophe is negligible, but the importance of the "zippering" is even more evident. We conclude that structure, at least as much as hydrolysis, is an essential factor in the unique behavior of microtubules (see section IV.2.4).

4. Introducing Glycerol – a stabilizing agent

We have until now restricted our experiments to an excruciatingly pure system of only tubulin, water, magnesium salt and GTP. Having characterized microtubule behavior rather thoroughly in this pure system, we are now ready to introduce simple chemical modifiers to the mix and test models of microtubule behavior by trying to explain their effects. In this section, we describe the consequences of introducing glycerol at various concentrations into the buffer.

As noted in Chapter II, the versatility of microtubules in living systems is strongly linked to the activity of associated proteins which affect their dynamics. The detailed manner in which these proteins stabilize or destabilize microtubules is only beginning to be explored (Dreschel, et al., 1992). It is hoped that the experiment described here will illustrate how the phase diagram can provide a meaningful organization for such studies.

Glycerol is commonly used in biological experiments as a protein stabilizer and cryo-protectant (Scopes, 1987). It forms strong hydrogen bonds with water, increasing the viscosity of the solvent and the chemical potential of protein solutes (Gekko and Timasheff, 1981b). Studies suggest that protein molecules in mixed glycerol-water solvents preferentially bind water near their hydrophobic regions and are therefore less amenable to conformational changes in the mixed solvent than in water alone (Gekko and Timasheff, 1981a). Bulk measurements have indicated that glycerol increases the rate, extent and stability of microtubule polymerization (Lee and Timasheff, 1977; O'Brien and Erickson, 1989). Exactly how these effects are manifested in terms of changes in the assembly, disassembly, catastrophe and/or rescue of individual microtubules is not known.

To address this question, samples of 14 μM tubulin with nucleating sites and various concentrations of glycerol (1.5 M < G < 3.5 M) were observed at 18.5°C. Glycerol was introduced by diluting a concentrated buffer solution with varying amounts of water and glycerol (50% by weight in water) so that in the final solution all components (save glycerol) were present in the same concentrations and at the same pH as before (section III.2.2). The concentration of glycerol was determined by averaging four independent measurements of the mass density of the buffer. The error in the measurement was ±0.1 M. During one hour, time-series of the lengths of faster-growing (plus-ended) microtubules were recorded and the proportion of occupied sites was measured. From the time series, the velocity of growth, the velocity of shortening, the mean lifetime of the growing state and the probability of rescue were extracted (see section IV.2.2). In addition, at the same tubulin concentration and the highest glycerol concentration, the temperature was changed to determine the onset of bulk nucleation (section IV.3).

4.1 The effect on dynamic instability: slower disassembly, less catastrophe

Glycerol affects dynamic instability as shown in Figures 4.21 and 4.22. The velocity of growth V_g is unchanged (Figure 4.21a). The velocity of shortening V_s diminishes (Figure 4.21b). The typical time spent growing T_g to increases exponentially (Figure 4.22a) and, finally, the probability of rescue P_r rises sharply to saturation (Figure 4.22b).

The relatively high concentrations of glycerol (between 1 and 4 M) necessary to observe an effect indicate that the activity of glycerol is not due to strong binding with tubulin or the microtubule. Instead, glycerol must have a non-specific or thermodynamic mechanism for interaction.
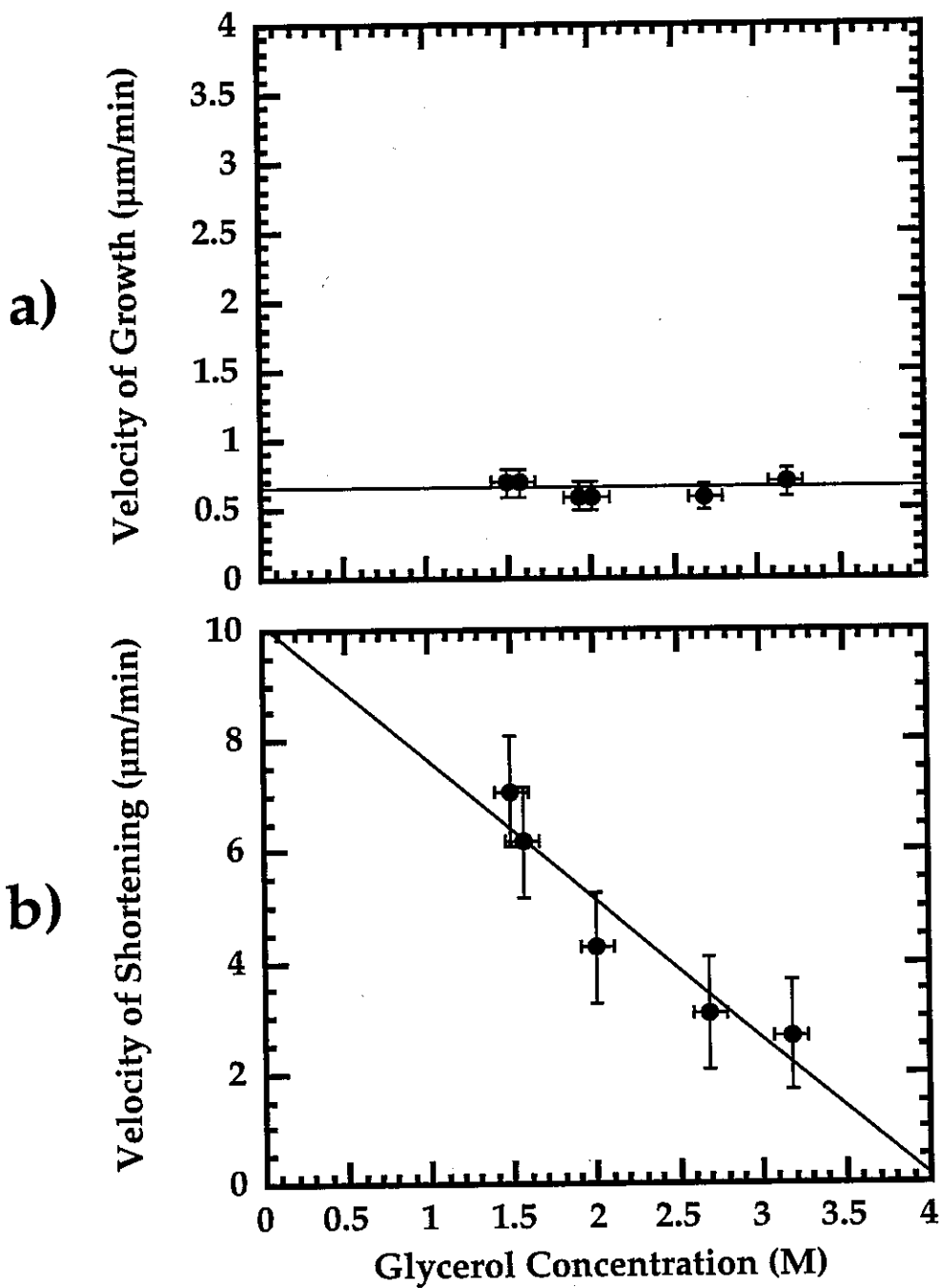
Fig. 4.21. The effect of glycerol on the velocities of growth and shortening. Plus ends only. a) Velocity of growth vs. glycerol concentration. The line represents the expected growth velocity without glycerol (see Figure 4.6). b) Velocity of shortening vs. glycerol concentration. The line is a least squares fit to the data. $C = 14 \mu M$, $T = 18.5°C$.
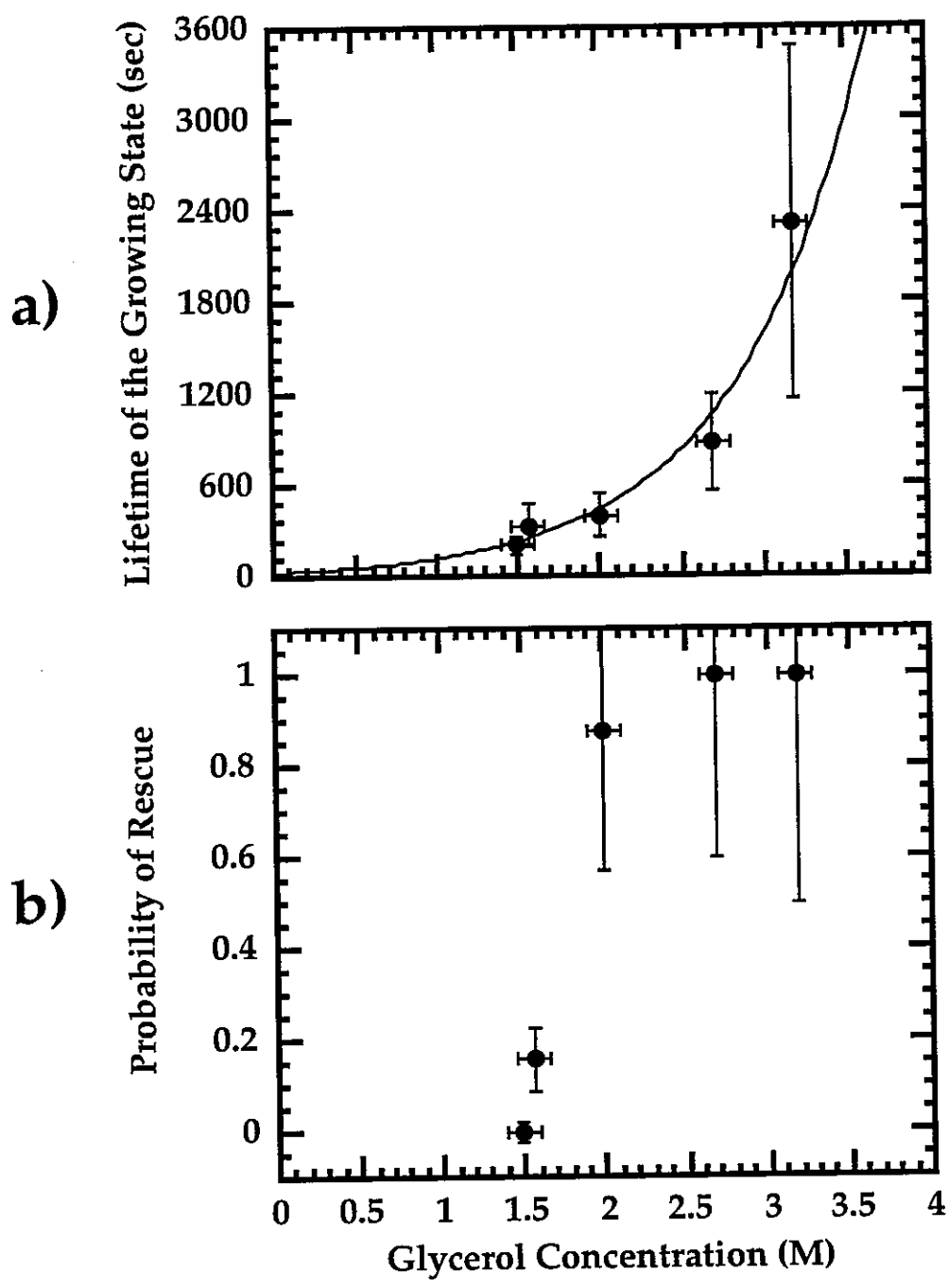
Fig. 4.22. The effect of glycerol on transitions between growth and shortening (and vice versa). a) Lifetime of the growing state vs. glycerol concentration. The line is a least squares fit to an exponential form. b) Probability of rescue vs. glycerol concentration. $C = 14\ \mu M$, $T = 18.5°C$.

One interesting clue comes from the viscosity of the solution, which increases by a factor of two between the highest and lowest glycerol concentrations (see Figure 4.23). It is quite surprising that no effect on the velocity of growth is observed. The diffusion of tubulin dimers must be slowed by higher viscosity ($D \propto 1/\eta$). The fact that V_g does not change means either 1) something other than diffusion is determining the rate at which dimers attempt to bind to the microtubule or 2) the effect of increased viscosity is exactly canceled by another effect which promotes microtubule assembly.

Of the two, the first possibility is less plausible. With or without glycerol, microtubule growth proceeds at the same rate (compare Figures 4.6 and 4.22a). Without glycerol, this rate depends on diffusion, as indicated by its dependence on the tubulin concentration (Walker, et al., 1988). It is unlikely that, because of glycerol but independent of its concentration, microtubule growth will be held constant at its original (glycerol-free) rate. The definitive test would measure V_g versus tubulin concentration in the presence of glycerol. Most likely, V_g increases in proportion to the tubulin concentration in the presence of glycerol, as it did in its absence.

To appreciate the plausibility of the second explanation, consider that the same strong hydrogen bonding property of glycerol which gives it its unusually high viscosity also causes glycerol to be preferentially excluded around hydrophobic regions on the surface of protein molecules (Gekko and Timasheff, 1981a; Gekko and Timasheff, 1981b). Thus, more entropy is gained when protein molecules aggregate and hide their hydrophobic regions in a mixed glycerol-water solvent than in water alone. Microtubule assembly is driven by this entropy gain (see section IV.2.2).

121
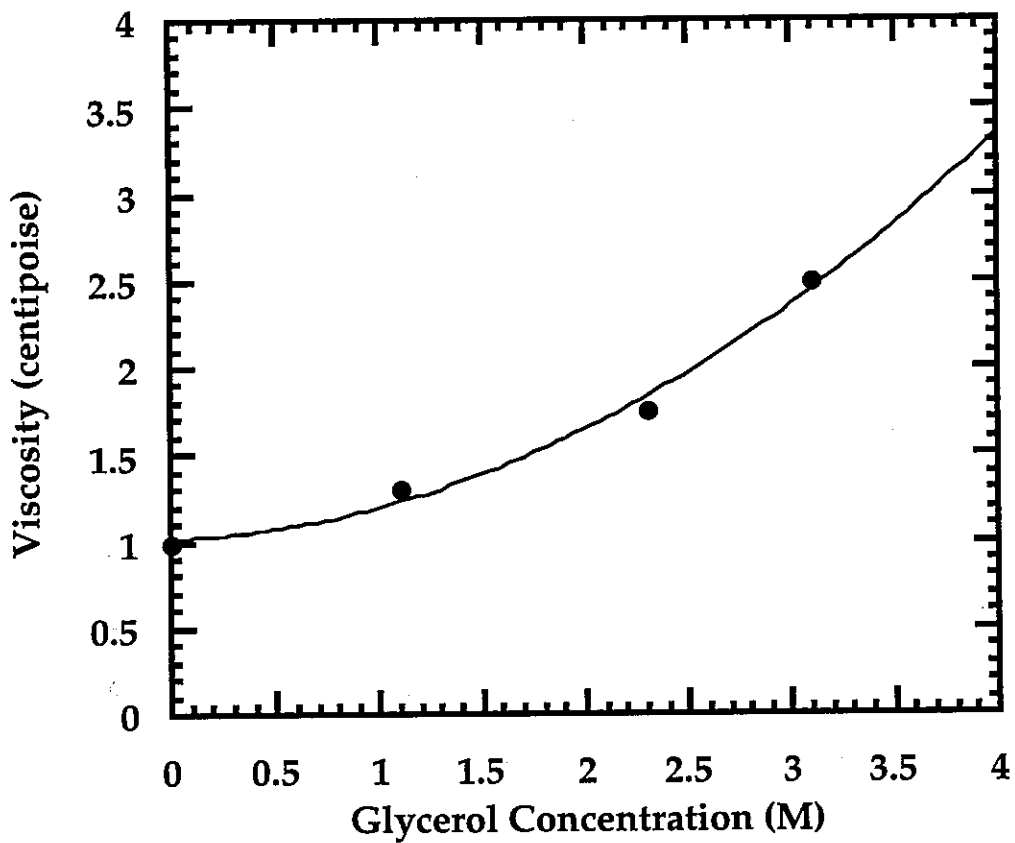
Fig. 4.23. Viscosity vs. glycerol concentration at 20°C. From the "CRC Handbook of Tables for Applied Engineering Science", 2nd ed., R.E. Bolz and G.L. Tuve, Eds., The Chemical Rubber Company., 1973. page 96.

Thus, while glycerol increases viscosity and thereby reduces the flux of dimers to the microtubule end, it also increases the thermodynamic driving force behind microtubule assembly and thereby enhances the probability that an incoming dimer will bind to the microtubule. Since both processes reflect the stronger hydrogen bonding in the mixed solvent, it is likely that they depend on the concentration of glycerol in the same way and their combined effects on microtubule assembly may very well cancel.

The effect can explain the other observations as well. First, consider that disassembly is also driven by reducing the entropy of water molecules surrounding the tubulin dimer (section IV.2.2). This means that GTP-hydrolysis must induce a conformational change in the microtubule-bound tubulin dimers which orders water. The release of water molecules which become "bound" as a result can then drive disassembly. The presence of glycerol, however, opposes such a conformational change. As a result, the hydrolysis may become less effective (i.e. some tubulin dimers may hydrolyze their GTP without undergoing the associated conformational change) or even slow down. By affecting hydrolysis in either way, glycerol would suppress catastrophe and slow disassembly.

Rescue becomes more likely at higher concentrations of glycerol. In fact, the probability of rescue reaches 1 as the mean lifetime of the growing state exceeds $\sim 660\,\mathrm{sec}$ (Figure 4.22), just as it did without glycerol (section IV.2.3). This reinforces our earlier speculation that rescue is actually linked to catastrophe in a way which makes T_g the only relevant parameter (section IV.2.3). In terms of the zippering model, the interpretation would be that glycerol makes zippering the sheet-like portion more difficult. Catastrophe becomes less frequent because the tube cannot close completely as often, and rescue becomes more likely since more gaps are left behind.

123

4.2 The effect on nucleation: slower on sites, faster in bulk

The proportion of occupied sites P_{occ} increases exponentially with the concentration of glycerol (Figure 4.24), as it did with temperature. However, with glycerol the probability of rescue approaches 1 well before the proportion of occupied nucleating sites does the same (compare Figures 4.22b and 4.24). At 2.5 M glycerol, only one in ten nucleating sites have microtubules even though the rate of complete catastrophe $R_{CC} = (1 - P_r)/T_g$ is almost zero (see section IV.1.1). We can not offer a satisfactory explanation for this fact. Perhaps, the rate of nucleation R_N decreases at higher glycerol concentrations so that small, but finite values of R_{CC} dominate the ratio $P_{occ} = R_N/(R_{CC} + R_N)$ (see section IV.1). However, why glycerol should inhibit microtubule nucleation on sites is unclear. It has the opposite effect on nucleation in bulk.

At 3.4 M glycerol and 14μM tubulin the onset of homogeneous nucleation of microtubules occurs at T = 21.5°C. The nucleation rate is essentially the same as was observed at four times the tubulin concentration and a few degrees colder (C = 60 μM, T = 18°C) without glycerol (Figure 4.25). The kinetics of the nucleation process are unchanged: the density of microtubule ends shows a linear increase and eventually saturates. Saturation occurs at later times, indicating that glycerol extends the lifetime of tubulin (see section IV.3.2) despite a 3.5° increase in temperature.

The shift in the onset of spontaneous nucleation to lower temperatures and tubulin concentrations is consistent with the effects of glycerol on individual microtubules (section IV.4.1). In terms of our simple model for spontaneous nucleation (section IV.3.3), the effect of glycerol is to decrease s, the rate of losing a dimer from an aggregate, without changing g, the rate of adding a dimer to an aggregate. Thus, at a given tubulin concentration, the rate of homogeneous nucleation $r \propto (g/s)^{10\pm2} C^{12\pm2}$ increases in the presence of
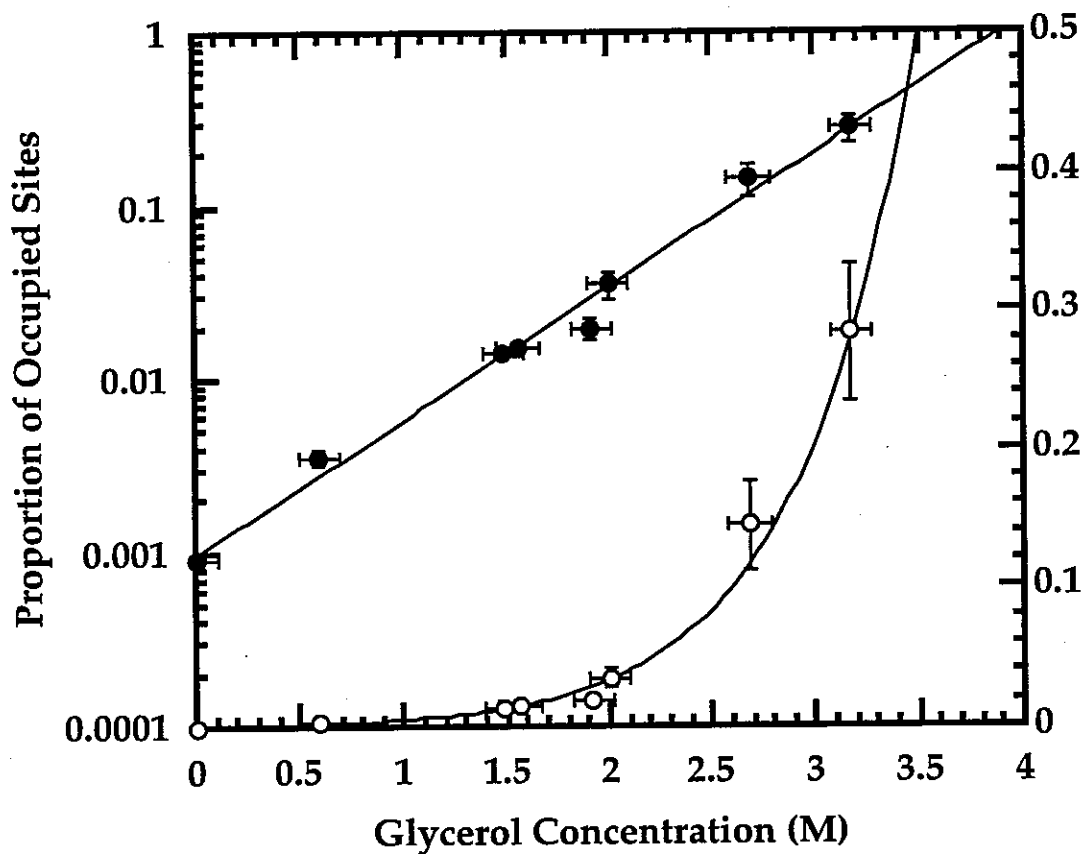
Fig. 4.24. Proportion of occupied sites vs. glycerol concentration. Black dots correspond to the left axis, open circles correspond to the right axis. No distinction was made between plus and minus ended microtubules. The lines are least-squares fits to an exponential form.
$C = 14 \, \mu M$, $T = 18.5°C$.
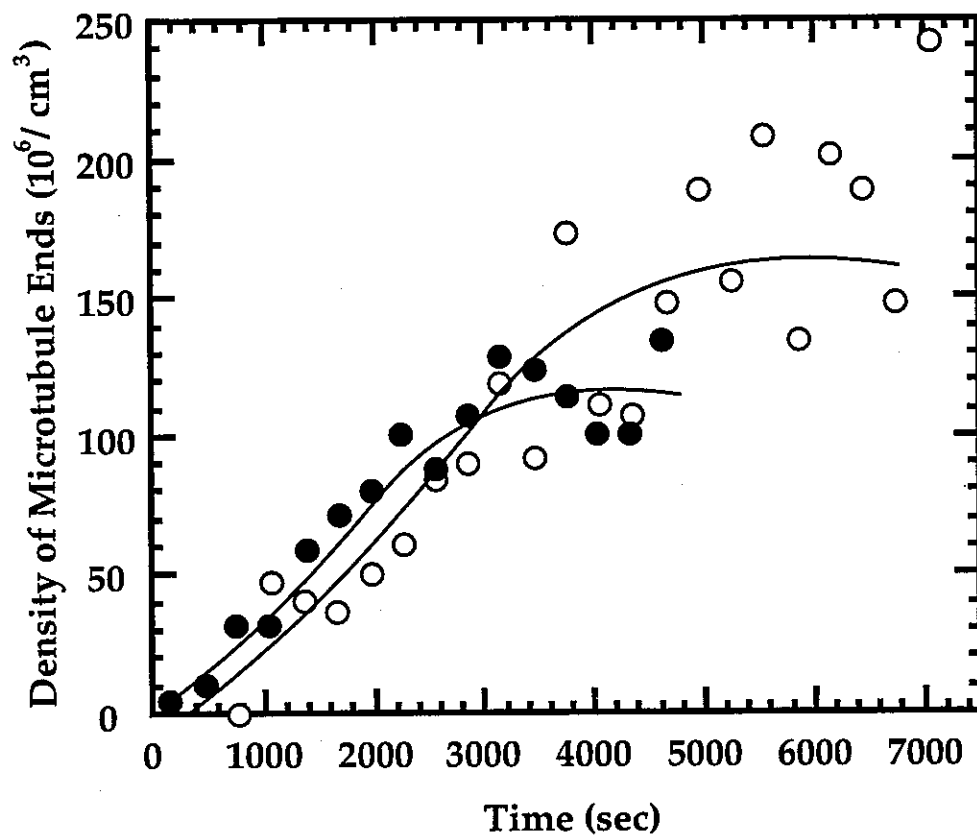
Fig. 4.25. Number of microtubule ends vs. time, with and without glycerol. Black dots: without glycerol, $C = 60\ \mu M$ and $T = 18°C$. Open circles: with 3.4M glycerol, $C = 14\ \mu M$ and $T = 21.5°C$. The lines are drawn by hand to guide the eye and point out the similar initial rate of nucleation which saturates at later times in the presence of glycerol.

glycerol. We estimate that the presence of 3.5M glycerol increases g/s by a factor of 3 or 4. (Compare $r \sim 0.04$ when $C = 14\mu M$, $T = 21.5°C$ and $G = 3.5M$, with an extrapolation to $C = 14\mu M$ of the measurements at $T = 22°C$ and $G = 0M$ shown in Figure 4.18, which indicates a nucleation rate about 5 or 6 orders of magnitude less.)

4.3 Conclusions

In summary, glycerol shifts the features of the phase diagram to lower temperatures and concentrations. It promotes both unbounded growth and spontaneous nucleation of microtubules at temperatures and tubulin concentrations which otherwise do not allow such behavior. The stabilizing nature of glycerol on microtubules is manifested as a reduction in the frequency of catastrophes, a correlated increase in the probability of rescue, and a slower rate of disassembly. The mechanism by which this stabilization occurs is two-fold. First, hydrolysis is inhibited. This makes the disassociation of tubulin less favorable. It is reflected in lower rates of microtubule disassembly and higher rates of bulk nucleation. Experiments using non-hydrolyzable analogs of GTP are consistent with this interpretation (Hyman, et al., 1992). Second, glycerol makes zippering a tubulin sheet into a microtubule more difficult and thereby increases the number of gaps left behind the zippering front. This is reflected in a lower frequency of catastrophe and a higher probability of rescue.

Finally, our reasoning implies that many other chemicals could have the same effect as glycerol. In the literature, this effect is discussed in terms of changes in the chemical activity or osmotic pressure of the water (Colombo, et al., 1992). It would be interesting to test this hypothesis by introducing other non-specifically interacting chemicals (e.g. sucrose, polyethylene glycol).

4.5 Closing Remarks

Our approach to the study of microtubules has been that of the physicist faced with a new material. We have examined the nucleation, assembly and dynamics of microtubules over a wide range of temperatures and concentrations, well beyond the regime of biological relevance (37°C, 15μM). Interestingly, microtubules retain their basic characteristics far from their biological context. A practical consequence of this is that experiments carried out under foreign (perhaps pragmatic) conditions may well be biologically relevant. On a more philosophical level, this robustness inspires hope for general and fundamental rules concerning biological phenomena.

The exercise of mapping the phase diagram of microtubules has revealed how biology can put a new twist on familiar physical phenomena. Nucleation, for example, can be a steady state process. In particular, site nucleation can be prevented from saturating by dynamic instability and bulk nucleation can proceed unchecked because one dimensional microtubules barely perturb the three dimensional bath of tubulin dimers. "Crystallization", for another example, can be enhanced by increasing temperature. Finally, detailed balance, or the microscopic fluctuations we expect between a condensed phase and a diffuse phase in equilibrium, can appear amplified into macroscopic fluctuations far from equilibrium.

From these surprises we extract three themes to guide future inquiry into biological systems. FORM. It tips the balance of reactions. The form (or conformation) of the tubulin dimer determines the intricate structure of the microtubule as well as its underlying stability. RHYTHM. It comes from chemical energy and thermal fluctuations. The energy (or, more precisely, the free energy) of GTP hydrolysis cycles tubulin in the microtubule between

conformations and, perhaps, the thermal fluctuations which curl a tubulin sheet into a microtubule synchronize the effect. WATER. It is ubiquitous, essential and involved. The interaction between tubulin and water distinguishes conformations of tubulin and drives its aggregation as well as its dissolution.

Besides charting the phase diagram, our contribution to the understanding of microtubule has been diverse and detailed. We have measured characteristics of both heterogeneous and homogeneous nucleation. We have demonstrated the existence of the transition between bounded and unbounded growth, and quantified its onset as a function of temperature in terms of the characteristics of dynamic instability. Finally, we have determined how the stabilizing effect of glycerol is manifested in all aspects of microtubule behavior.

Of course, much remains to be organized and understood about microtubules. Variables such as hydrostatic pressure (Salmon, 1975), buffer salts (Simon, et al., 1992; Ray, et al., 1993), Mg++ (Correia, et al., 1987; Gal, et al., 1988), and, of course, MAPs (Matus, 1990; Burns, 1991; Dreschel, et al., 1992) have been explored but remain to be organized in the context of a phase diagram. Other variables, such as osmotic pressure and redox potential, are generally unexplored and potentially insightful (Colombo, et al., 1992; Benezra, 1994). Finally, models with mathematical structure, physical sense, and predictive power have begun to appear (Dogterom and Leibler, 1993; Flyvbjerg, et al., 1994), but are still in short supply.

Nevertheless, the contents of this chapter are sufficient to support the application of microtubules in other studies of general physical interest — which brings us to the next portion of the thesis.

CHAPTER V

MICROTUBULES INSIDE VESICLES

0. Overview

Until now, this thesis has focused on microtubules as an interesting material to be characterized and understood for its own sake. The relevance of this work to biological systems has been rather remote. This chapter is different. Here, we take advantage of the experimental control gained in the previous chapter and use microtubules to build and study a simple, model system that (topologically) resembles a real cell.

The system is a near-spherical vesicle with tubulin inside. The tubulin assembles into microtubules when the temperature is raised. Microtubules which span the diameter of the vesicle cause it to distort through a dramatic sequence of shapes. Eventually, the microtubules can become so long that they are forced to buckle and double over completely.

Microtubules are generally thought of as passive supports (stabilizing cell shapes) or guides (organizing the transport of vesicles and, during cell division, chromosomes). The observations presented in this chapter demonstrate conclusively that *microtubule polymerization alone can generate a significant force* (~1 pN).

Distortions similar to the ones described here have been observed in living cells (Travis and Bowser, 1990; Knops, et al., 1991; Tucker, et al., 1993), so it is likely that a microtubule generated force is relevant in biological systems. However, even if this force is not biologically relevant, the system of microtubules inside vesicles can be an instructive example of a 'thermal ratchet' or 'brownian machine'. Also, it can serve as a reminder that the physics of the cellular world is dominated by the power of thermal noise.

1. Introduction

The membranes we use to confine microtubules are similar to the membranes of real cells. Both are made of double layers of amphiphilic molecules called phospholipids. These molecules have a phosphate-based hydrophilic region (the head group), which is either charged or zwitterionic, and a carbon-based hydrophobic region (the tail), which is made of one or two carbon chains between 4 and 24 atoms long. In solution, amphiphilic molecules spontaneously arrange themselves so as to remove their hydrophobic groups from water. Usually, they form a sort of sandwich, ~40Å thick, in which two sheets of molecules come together with their tails inward and their head groups on the outside. See Figure 5.1. The bilayer sandwich is a 2-D fluid and locally planar, but on large scales it tends to curve into cylinders or spheres to avoid exposing edges to the water.

A phospholipid membrane which encapsulates a finite volume is called a liposome or a vesicle. When several bilayers encapsulate the same volume, the vesicle is said to be multi-lamellar. Otherwise it is called uni-lamellar. The membranes of most cells are unilamellar. We do not know precisely how many lamellae make up the membranes of our artificial cells, however, from their low-contrast and floppy appearance under the microscope, we expect that some are unilamellar, or nearly so (see section V.2).

Vesicles come in a variety of shapes and sizes. Near-spherical vesicles have received most of the scientific attention, both theoretical and experimental, with narrow tubes coming a distant second. The review article by Lipowsky (Lipowsky, 1991) is a good introduction to the field. What follows, by contrast, is an extremely brief and biased one.

131
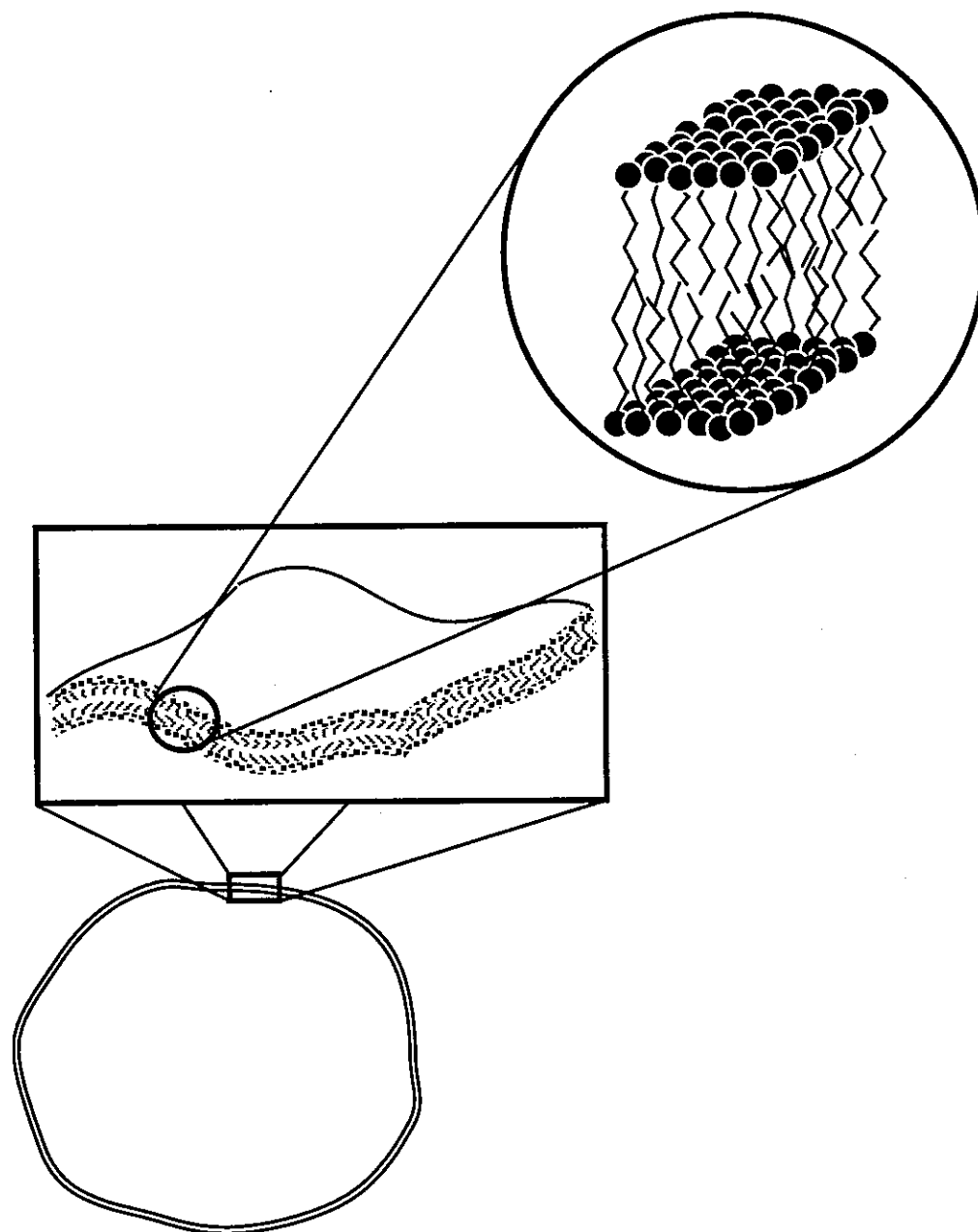
Fig. 5.1. Schematic of the structure of a lipid bilayer membrane. On a scale hundreds or thousands of times larger than its thickness (40Å), the bilayer curves to enclose a finite volume. Within the bilayer itself, the lipid molecules are aligned perpendicular to the plane of the membrane and are disordered (liquid-like) in the plane.

132

Theoretical study of deformations in near-spherical membranes began in 1970 with the work of Canham (Canham, 1970). Classic contributions were made by Helfrich and co-workers (Helfrich, 1973; Deuling and Helfrich, 1976) and, recently, an organization of the various vesicle shapes has emerged (Svetina and Zeks, 1989). Experimentally, the field began with the electron micrographs of Bangham (Bangham and Horne, 1964) and was at first dominated by the study of the bi-concave shape of red blood cells. Dramatic progress was made with the introduction of the micropipette technique to perform direct mechanical measurements on individual vesicles (Kwok and Evans, 1981; Evans and Kwok, 1982). Currently research focuses on vesicle-vesicle interactions (e.g. budding and fusion) (Döbereiner, et al., 1993).

Although relevance to biological systems is perpetually cited as an important motivation for these studies, deformations are traditionally induced by physically convenient stresses: temperature, osmotic pressure, hydrostatic pressure, bilayer asymmetry, even magnetism and laser tweezing (Helfrich, 1973; Evans and Kwok, 1982; Sackmann, et al., 1986; Svetina and Zeks, 1989; Berndl, et al., 1990; Farge and Devaux, 1992; Bar-Ziv and Moses, 1994). With the possible exception of bilayer asymmetry (Devaux, 1991), biologically relevant stresses have been neglected. It is hoped that the present work will demonstrate microtubules inside vesicles as an ideal system for a physical study of more immediate biological relevance.

The rest of this chapter is divided into three parts. The first discusses the materials and methods for preparing vesicles containing tubulin. The second describes our observations: the nucleation of microtubules inside of vesicles, the shapes of vesicles deformed by microtubules and the buckling of those microtubules. The final section presents some of the many open questions and technical challenges that remain.

2. Methods

Microtubules were first encapsulated in vesicles by Hotani and Miyamoto (Hotani and Miyamoto, 1990), who also observed deformations induced by their polymerization. (Similar work has also been done with another component of the cytoskeleton, actin filaments (Cortese, et al., 1989; Miyata and Hotani, 1992).) The present work modifies their methods and extends their observations. The details of the methods and measurements have been described elsewhere (Betterton, 1994), but hey are sufficiently new that they bear repetition.

Encapsulating substances inside vesicles has many industrial applications ranging from cosmetics to drug delivery. Not surprisingly, there exists a wide variety of methods for encapsulation. The choice is governed by the final application (e.g. desired vesicle size, the material to be encapsulated). The different techniques are assessed in terms of 1) how efficiently and homogeneously the material in question is encapsulated and 2) the uniformity of the vesicle population, with regard to both size and lamellarity. Besides these criteria, the main experimental challenge is to avoid damaging the material to be encapsulated. For an introduction to the various methods, the book *Liposomes: A Practical Approach* is a good resource (New, 1990a).

Vesicles containing tubulin are best prepared by the freeze-thaw technique (New, 1990b). This method is based on ice crystals rupturing the membranes of small vesicles as they are frozen rapidly, and then allowing the fragments to coalesce into large vesicles as the solution slowly thaws (Pick, 1981). Despite studies which indicate that high protein concentrations and salty solutions are not efficiently entrapped (Pick, 1981), we have consistently had success with ~60 μM tubulin in the standard buffer (section III.2.2.1).

Freeze-thaw is superior to other methods in many ways. First, it does not require changing the chemical composition of the buffer. Second, it is not harmful to the tubulin, which is anyway stored in the frozen state and can be thawed and re-frozen several times without noticeable degradation. Third, it is quick, the longest step being the thaw, which takes ~20 minutes. Fourth, the process of freezing and thawing mixes the solution thoroughly, so the concentration of tubulin entrapped is relatively homogeneous and controllable. And, finally, the resulting vesicles are a good size for viewing under the light microscope. They range from 0.5μm to 50μm in diameter, with many around 5μm.

We experimented extensively with different lipids and combinations of lipids. This search was done with the help of Adam Simon (then at NEC Research) and Erez Braun (then at Princeton University). Our chief requirement was that the fluid-gel transition of the lipids be below 4°C (Silvius, 1982), so that tubulin would be encapsulated in dimer form. Therefore, we focused on unsaturated lipids (those with at least one double bond in their tails). Mixtures of charged and neutral phospholipids worked best. Neutral lipids worked well in buffer alone, but negatively charged ones were required for success with (negatively charged) tubulin.

We had the best success with a combination of 60% DOPC (1,2-Dioleoyl-sn-Glycero-3-Phosphocholine, M.W. = 786.12 g) and 40% DOPS (1,2-Dioleoyl-sn-Glycero-3-Phospho-L-Serine, M.W. = 810.02 g). Both are synthetic lipids, available with a high degree of purity. Both have two, 18-carbon chains, with a double bond in each chain. DOPS has a negatively charged head group and DOPC is neutral (zwitterionic). Finally, both are commonly used and reasonably well characterized in the literature (Silvius, 1982; Evans and Needham, 1987).

The preparation procedure is illustrated in Figure 5.2. Using gas-tight syringes (series 1700, Hamilton), stock solutions of synthetic DOPC (10 mg/ml, cat. no. 850375, Avanti) and DOPS (5 mg/ml, cat. no. 840035, Avanti) in chloroform are deposited on the bottom of a disposable glass test tube (12x75mm) (cat. no. 14-961-26, Fisher). The volumes are such as to yield the 60/40 ratio at an eventual concentration of about 2.5 mg lipid/ml buffer. For example, 20μl DOPS and 15μl DOPC will yield 100μl of final solution.

The chloroform is left to evaporate in a fume hood and the test tube is stored overnight in a vacuum desiccator to extract the remaining solvent. The film can be stored either in vacuum or under nitrogen for about a week.

The film is resuspended to a concentration of 2.5 mg/ml in room temperature buffer (PM$_2$G$_1$, Appendix B) without tubulin. The buffer is identical to the one used earlier (see section III.2.2.1). Resuspension is not a critical procedure, but it is good practice to perform any violent agitation of the solution (e.g. vortexing) under nitrogen (oxygen in solution rapidly degrades the lipid). In the end, there should be no lipid film left on the bottom of the test tube and the solution should be silvery and opaque. Under the microscope, large clumps of irregular, multi-lamellar liposomes of all sizes (1 - 100μm) can be seen.

The freeze-thaw technique works best on solutions of small (~30 nm), unilammelar vesicles (SUVs). To transform multi-lamellar liposomes into SUVs, the test tube is flushed with nitrogen, sealed with parafilm, and suspended in an ultrasonic water bath (model 1210, Branson) for about 45 minutes. The solution becomes clearer, though occasionally clumps of lipid remain. Under the microscope, it appears much more dilute and, if the imaging is properly tuned, the background seems to be teeming with unresolvable structures. The solution is now primarily SUVs.

136
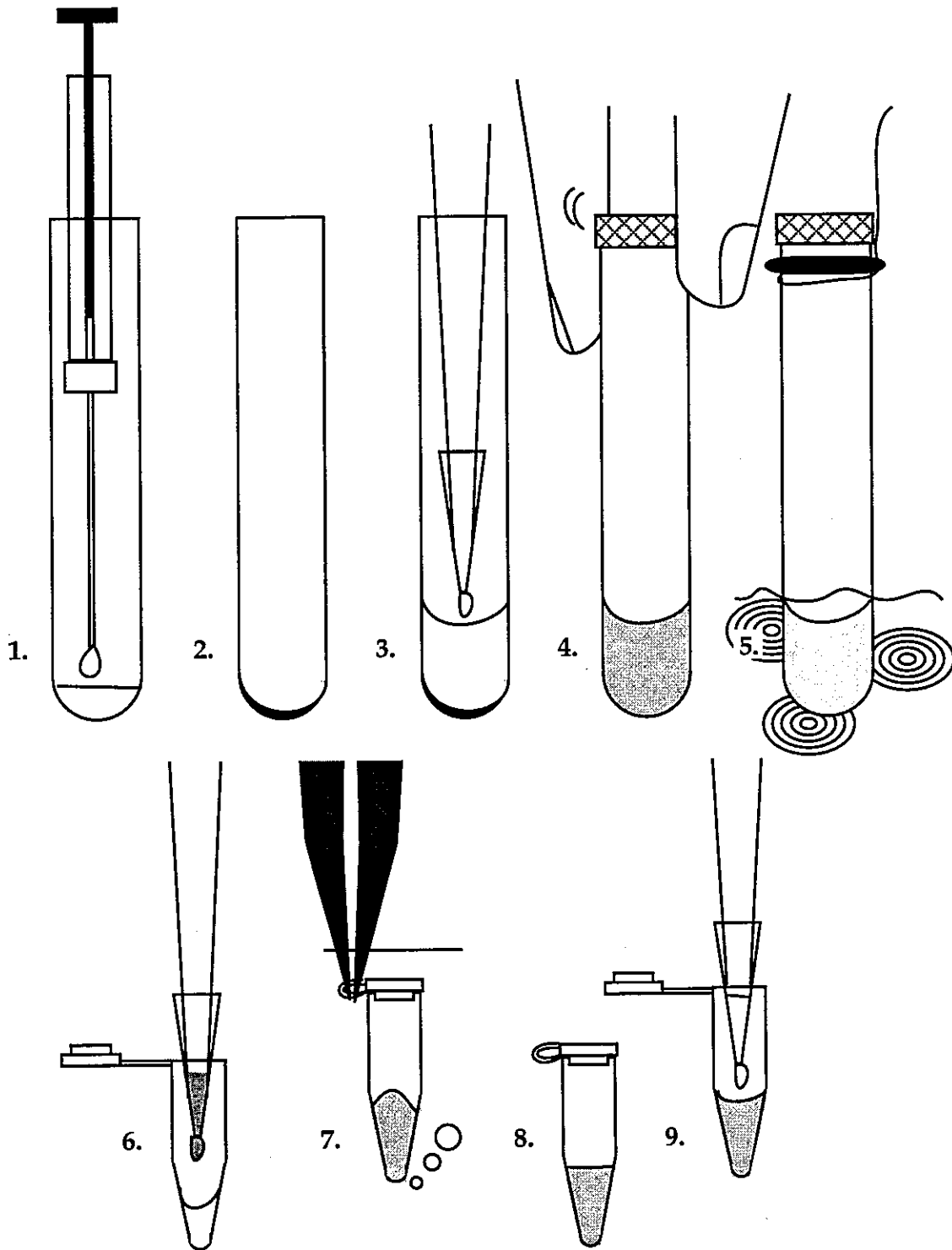
Fig. 5.2. The Freeze/Thaw procedure. 1. Deposit lipid in chloroform. 2. Evaporate chloroform. 3. Add buffer (no tubulin). 4. Resuspend lipid (under nitrogen). 5. Sonicate lipid solution (under nitrogen). 6. Add sonicated lipid to tubulin solution. 7. Flash freeze in liquid nitrogen. 8. Thaw on ice. 9. Dilute with buffer (no tubulin).

The SUVs are mixed 1:1 with cold (depolymerized) tubulin solution, in a microcentrifuge tube. Both the SUVs and the tube are chilled on ice in advance to prevent polymerization of the tubulin. The concentration of tubulin in this mixture is approximately the concentration encapsulated in vesicles after the freeze/thaw, and should be adjusted accordingly. For example, one part of 60 μM tubulin stock mixed with an equal part of SUVs in buffer (2.5 mg/ml), makes a solution of 30 μM tubulin and 1.3 mg/ml lipid. After a freeze-thaw, the vesicles will contain approximately 30 μM tubulin. This is a typical working condition.

Rapid freezing is achieved by immersion in liquid nitrogen. The thaw is done on ice. The thawed solution is cloudy, with the cloudy part sometimes clumped in the middle. (A few gentle swishes homogenize the solution.) It is often desirable to dilute (1:3-1:10) with plain buffer (cold, no tubulin) to lower the density of vesicles and the concentration of tubulin in the surrounding fluid. This both increases the number of isolated vesicles and inhibits the formation of microtubules outside them.

Observations are made under the light microscope using DIC, as before. Temperature is used to control the polymerization of microtubules inside the vesicles (see section III.3). At low temperatures (or without microtubules), the vesicles are regular and round. They tend to cluster over time and some have smaller vesicles or SUVs trapped inside. Some of the vesicles are particularly low in contrast, and we speculate that they are unilamellar. The definitive test of lamellarity requires measuring the mechanical properties of the vesicle (Kwok and Evans, 1981). As this parameter is particularly useful for understanding the system of microtubules in vesicles, we are presently developing the ability to perform such measurements.

3. Results

3.1 Nucleation

When the temperature is raised, microtubules nucleate and grow inside the vesicles. The temperature for onset of spontaneous nucleation depends on the concentration of entrapped tubulin, as expected. Increasing the temperature a few degrees at a time, and waiting ~ 15 minutes at each step, we observed microtubules nucleate in most vesicles at the same temperature. We conclude that the concentration of tubulin in the vesicles is fairly uniform, as expected with the freeze/thaw method. (Typically, at 30°C and an estimated 30 μM tubulin, >75% of the vesicles contain microtubules.)

What is surprising is that microtubules nucleate more readily inside vesicles than outside. This effect was studied in collaboration with Meredith Betterton (Betterton, 1994). It is most apparent in samples that are not diluted after the freeze/thaw. When the temperature is raised abruptly, from 4°C to 30°C, for example, microtubules appear inside vesicles before they appear in the surrounding solution. Presumably, the tubulin concentration inside and outside of the vesicles are equal. If there is a difference, one would expect the entrapped concentration to be lower. Therefore, the interior of the vesicle must somehow promote nucleation.

To quantify the effect, we attempted to measure the rate of nucleation inside vesicles. Cooling (4°C) and heating (30°C) three samples a total of seven times, watching five different vesicles, we noted the number of microtubules inside each vesicle as a function of time. Inside vesicles, individual microtubules are not easy to detect, much less count. Thus, we can only offer a rough estimate of the nucleation rate, $r \sim 0.1 \, \mathrm{min^{-1} \mu m^{-3}} \sim 2 \cdot 10^9 \, \mathrm{cm^{-3} sec^{-1}}$. For example, after about 3 minutes we saw about 5

microtubules inside a vesicle 3μm in diameter. Comparison with measurements made at the same temperature in the absence of vesicles (section IV.3) reveals that this nucleation rate is a factor of 10^4 greater than the rate in bulk solution (Figure 5.3).

What can explain this dramatic enhancement of spontaneous nucleation? The short debye length of the salty buffer (~1 nm) makes coulombic interactions unlikely. A van-der Waals attraction between the bilayer and the protein is however plausible and would cause the tubulin to concentrate near the membrane. The $C^{12\pm2}$ scaling of the rate of spontaneous nucleation (section IV.3.1) means that the effective concentration must be at least double the expected concentration to explain the effect.

While enhanced nucleation is unexpected, suppressed nucleation due to the limited amount of tubulin in the vesicle is expected. Consider a vesicle of 2 μm radius. With a tubulin concentration of 30 μM tubulin, it contains about 6×10^5 tubulin dimers, or about 370 μm worth of microtubule. Six microtubules, each 6μm long would deplete the concentration by about 10%. The nucleation rate, being extremely sensitive to the dimer concentration ($r \sim C^{12\pm2}$, section IV.3), would be noticeably reduced ($0.9^{12} = 0.28$). Of course, the effect is exaggerated in smaller vesicles and insignificant in larger ones. A vesicle 0.2 μm in radius, with the same tubulin concentration inside, does not contain enough tubulin for even one microtubule the length of its diameter. A similarly filled vesicle 10μm in radius could support a total of 2,500μm of microtubule before for its dimer concentration is affected by as little as 5%.

Unfortunately, our attempts to document the effect of vesicle size have not been successful. Since microtubules rarely align with the plane of focus and eventually bundle together, they are difficult to detect and count. Methods for overcoming this difficulty are discussed at the end of the chapter.
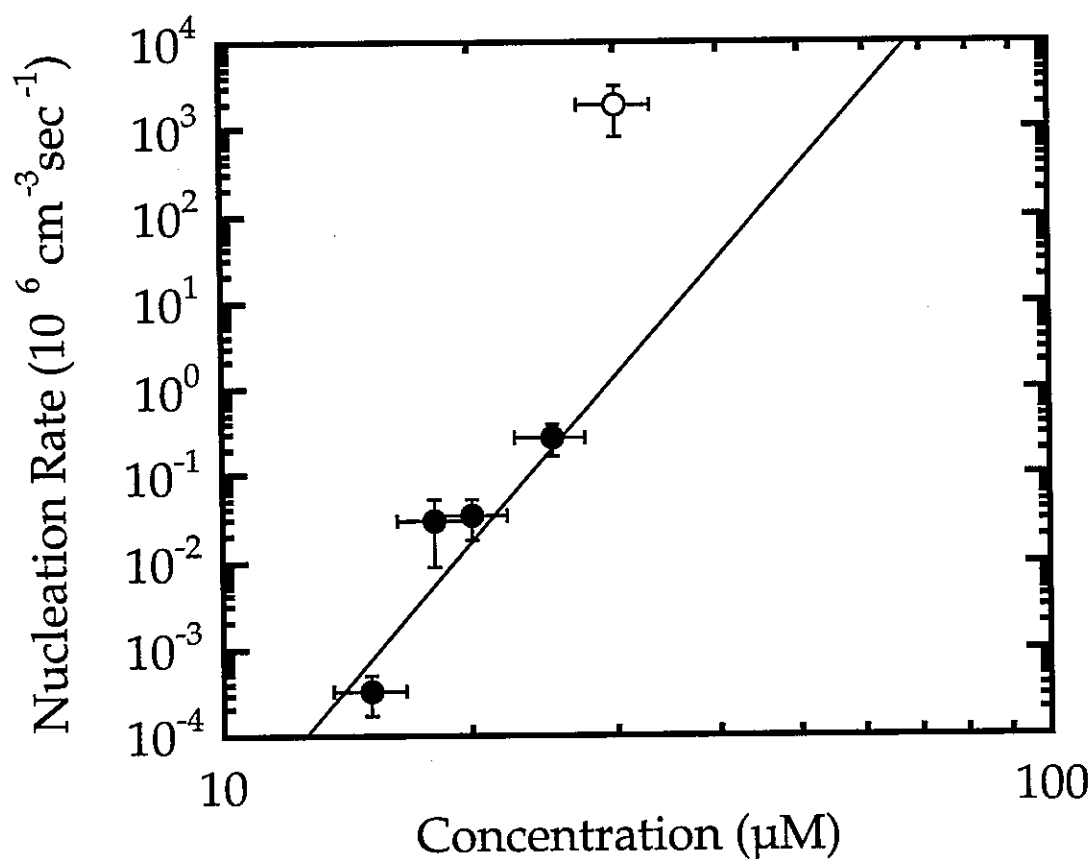
Fig. 5.3. Comparison of the rate of spontaneous nucleation inside and outside vesicles. The black dots are measurements of the nucleation rate in bulk (from section IV.3) and the open dot is the estimated nucleation rate within vesicles. The line represents the power law $r \sim C^{12}$, determined from the bulk measurements (section IV.3). T = 30°C.

3.2 Morphogenesis

3.2.1 Observations

Under the influence of entrapped microtubule(s), a near-spherical vesicle undergoes a specific sequence of shape changes, illustrated in Figures 5.4 - 5.6. As long as the microtubule(s) are shorter than the vesicle diameter, $2R_o$, the spherical shape fluctuates unperturbed (Figure 5.4, top). Once their length exceeds $2R_o$, the vesicle becomes prolate. At first, it is an ellipsoid, but quickly becomes sausage shaped (Figure 5.4, bottom). At this stage, the membrane still fluctuates visibly.

As the microtubule(s) grow, the membrane becomes taut and the sausage turns into a football (Figure 5.5). Despite the apparent contact between the microtubule ends and the membrane, the microtubule(s) continue to grow. The football eventually collapses at the extremities (Figure 5.6), sheathing the ends of the microtubules in cylindrical tubes while the body of the vesicle retracts into a rounder, football shape. We call this a "phi" shape since it resembles the greek letter ϕ.

The symmetry of the shapes is apparent as they diffuse rotationally (Figure 5.7, top row). They are figures of revolution about the axis defined by the microtubule(s). They are also symmetric about the plane that bisects the microtubule axis, with the exception of the phi (ϕ) shape, whose two cylindrical arms are not always equal in length (Figure 5.8).

The sequence of shapes is reversible and reproducible. Vesicles distort and relax through the sequence over and over as microtubules inside grow and shorten in response to changes in the temperature or the natural rhythm of dynamic instability. Occasionally, as the microtubules shorten quickly the membrane relaxation lags behind (Figure 5.7, bottom row).
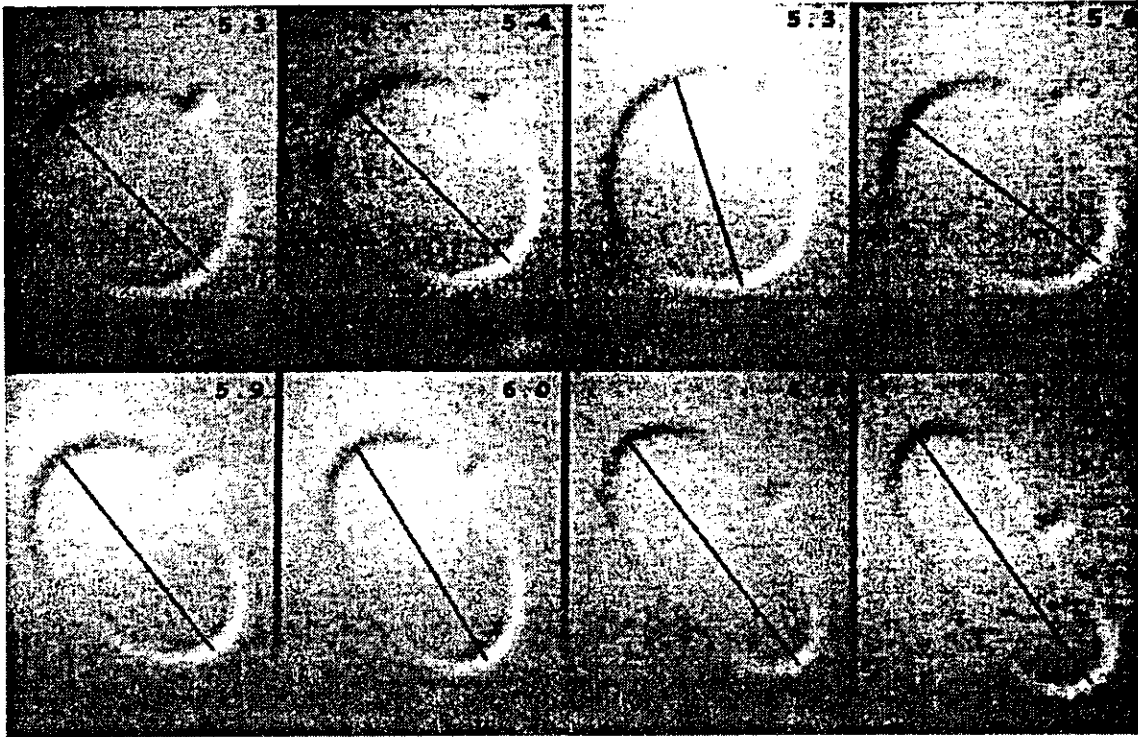
Fig. 5.4. Sequence of vesicle shapes, part I: sphere to sausage. The microtubules are not visible in the images, though they are occasionally glimpsed in the live video. The line in each image is a hand drawn estimate of the length and mean orientation of the microtubule(s) inside. The number in the upper right hand corner is the length of the line in microns.

143
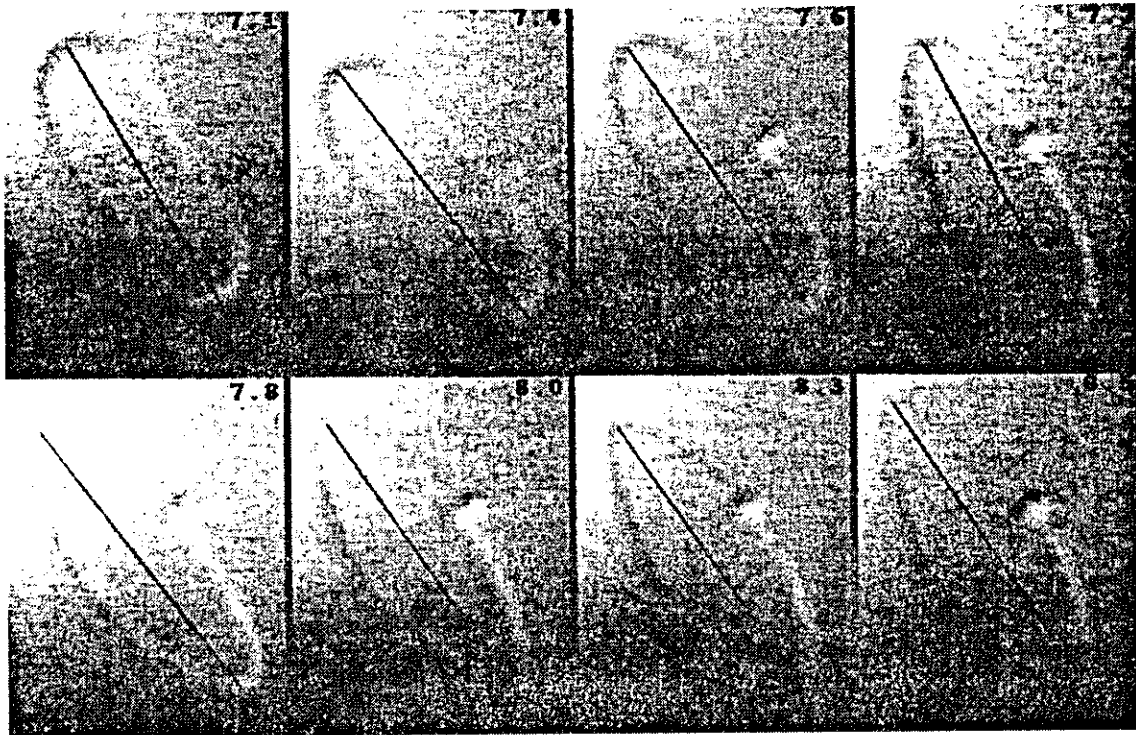
Fig. 5.5. Sequence of vesicle shapes, part II: sausage to football. Same vesicle as in Figure 5.4, a short time later. Again, the numbers represent the length (in microns) of the line that has been drawn by hand onto each image.
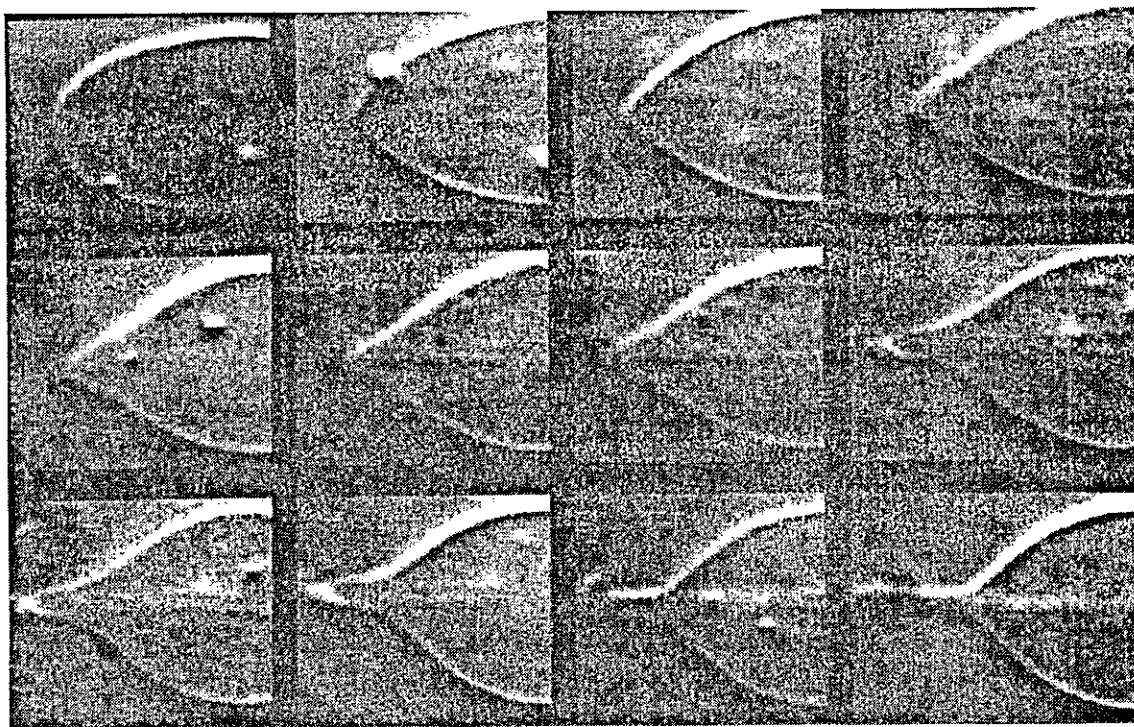
Fig. 5.6. Sequence of vesicle shapes, part III: football to phi (φ) shape. One half of a larger vesicle (not the same as in the two previous figures). The sequence flows from upper left to lower right across the page. Notice the development of negative curvature in the middle and bottom rows.
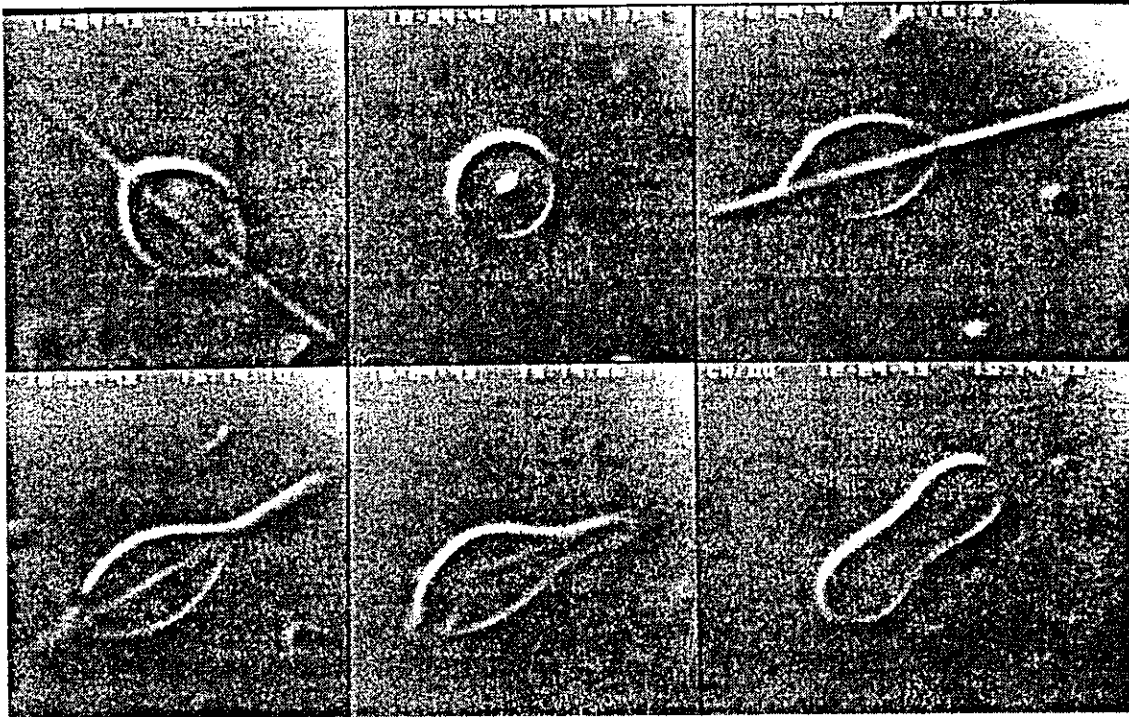
Fig. 5.7. Perspectives of vesicle shapes. A phi (ϕ) shaped vesicle as it diffuses rotationally (center, top row). In the bottom row, the microtubules are shortening and the vesicle is unable to change shape as quickly.

146
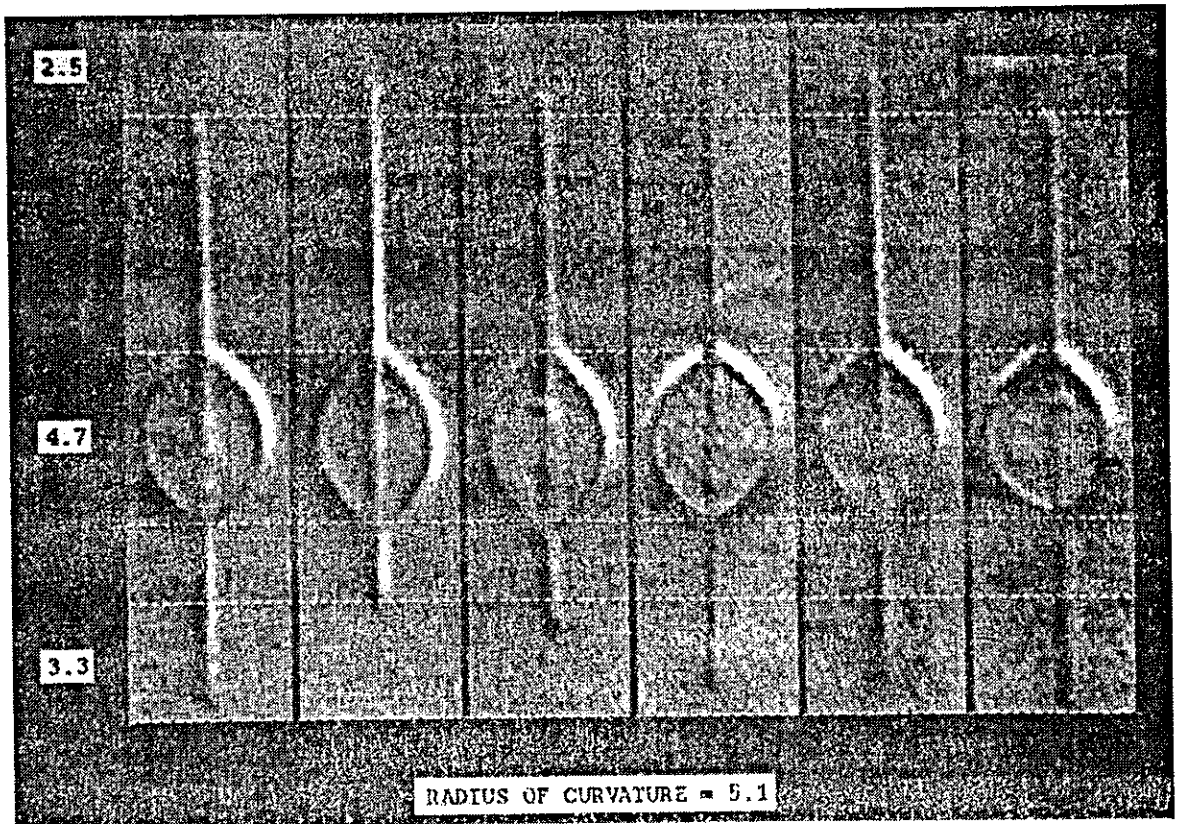
Fig. 5.8. Dynamic instability inside a vesicle. A phi (φ) shaped vesicle of changing length indicating that dynamic instability persists inside the vesicle. Notice that the arms are not constrained to be equal in length. The clearly visible line through in the central, football-like portion of the vesicle indicates that probably more the one microtubule is inside. The numbers represent the length (in μm) between the dotted lines.

147

Even in the extremely restrictive phi (ϕ) geometry, microtubules exhibit dynamic instability (Figure 5.8). Some measurements of vesicle length versus time are plotted in Figure 5.9. However, it is difficult to draw conclusions about the nature of dynamic instability inside of vesicles. First, most vesicles contain several microtubules, so a catastrophe of the longest one will often be "rescued" by a shorter one. Second, even if a vesicle contains only one microtubule, the length dynamics of the two ends of the microtubule will be indistinguishable. Finally, the measurement is complicated by a low sampling rate imposed by the fact that the freely diffusing vesicle only rarely aligns with its entire length in the plane of focus. We plan to develop ways to restrict the microtubules to the plane of focus and hope to measure the influence of membrane tension on the rate of microtubule assembly.

The sequence of shapes outlined above is common among near-spherical vesicles and will be the center of the discussion which follows. Before closing, however, we note the observation of occasional unusual vesicle shapes, including stars, pearls and eyeglasses (ϕ) (Figure 5.10). Upon depolymerization of the microtubules, it becomes clear that such anomalous shapes originate from either grossly non-spherical vesicles or from vesicles with unusually large numbers of microtubules and/or lamellae. This is not to imply that all non-spherical vesicles generate strange shapes, however. Often normal looking phi (ϕ) shaped vesicles relax into non-spherical (usually prolate) vesicles upon depolymerization.
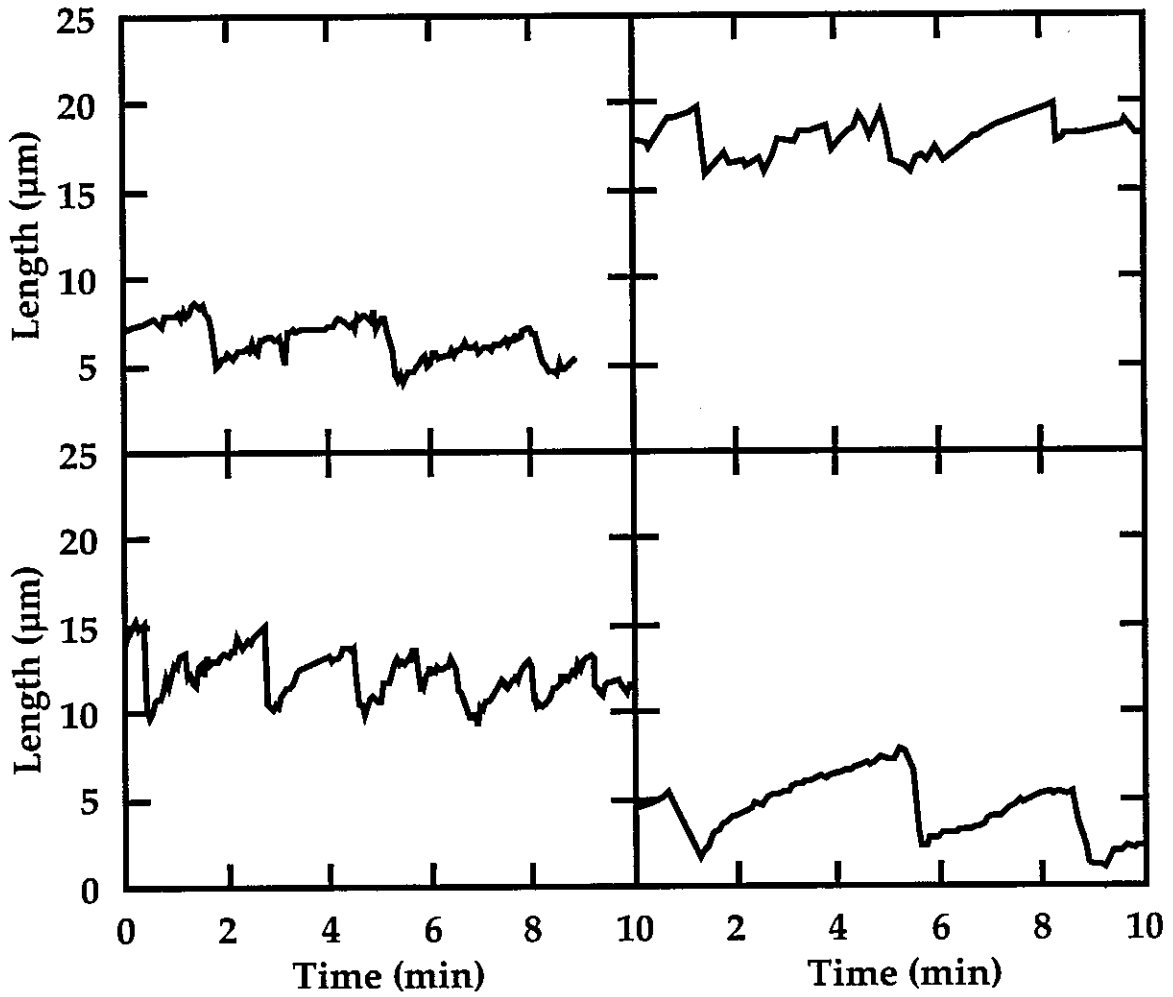
Fig. 5.9. A sampling of time series of the lengths of distorted vesicles.
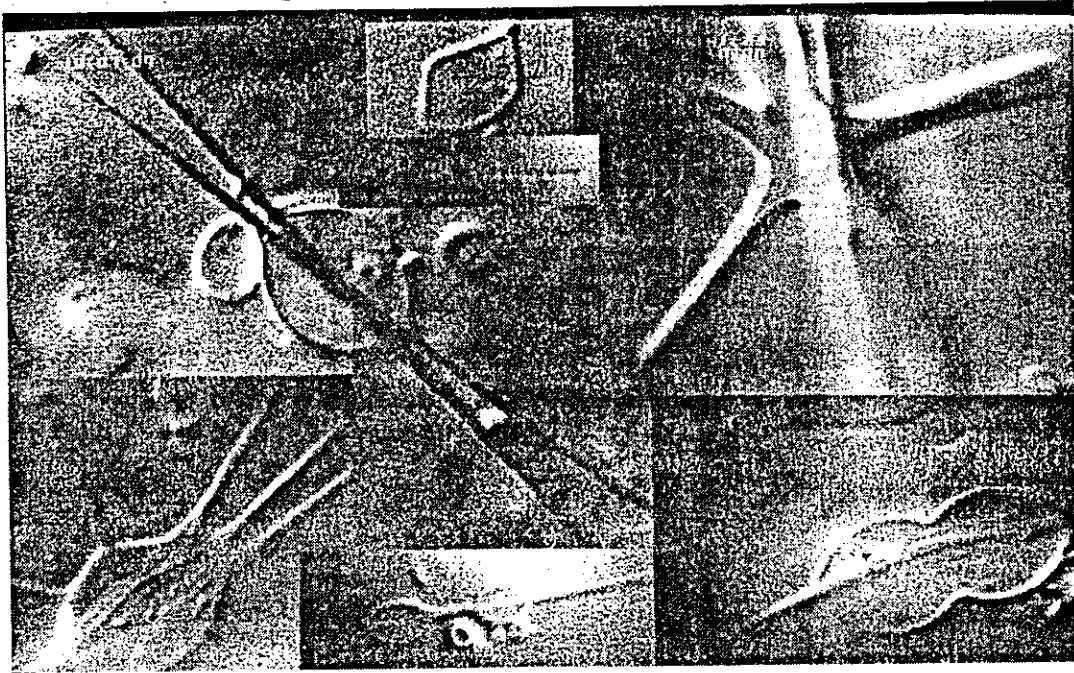
Fig. 5.10. Some unusual vesicle shapes. Vesicles with multiple protrusions are common at high tubulin concentrations and high temperatures. Sometimes the protrusions are gently buckled. Phi (ϕ) shaped vesicles with multiple football portions are also seen. They may be related to normal-looking phi (ϕ) shaped vesicles which relax into a 'string of pearls' upon deploymerization. The squarish vesicle appears to contain two nearly perpendicular microtubules somehow locked in competition.

3.2.2 Modeling

The sequence of vesicle shapes: sphere → sausage → football → phi generates a host of questions: Why do all the microtubules align? Does the membrane ever rupture? How can we understand the unusual progression of shapes? Can a single microtubule in a vesicle cause them, or is it an inherently collective effect? Is there an attractive interaction between microtubules and the membrane that prompts the collapse from the football to the phi (ϕ) shape? Finally, are the microtubules actually pushing on the membrane? If so, how can they continue to add dimers to their ends?

In this subsection we address all but the final two questions with simple arguments and unsophisticated models. A discussion of the force generated is deferred to the next section, in which the observation of microtubules buckling inside of vesicles makes the issue more dramatic and permits a more quantitative approach.

Why do the microtubules align? Since there is no evidence for an attractive interaction between microtubules without vesicles, they must align because of interactions with the vesicle membrane. It is known that a very small pressure difference across the membrane is sufficient to make a near-spherical vesicle become ellipsoidal (Helfrich, 1973). Microtubules tend to grow slowly (~ 1 μm/min) while frequently bumping against the membrane. As they grow longer than the minor axis of the ellipsoid, they must become confined to a solid angle about the major axis. The pressure exerted by their collisions with the membrane is increasingly directed along the long axis of the distorted vesicle, thereby distorting it further. The longer the microtubules grow, the more they are restricted until, eventually, they are completely aligned.

151

While this is the case for most vesicles, some do develop multiple protrusions, as shown in Figure 5.10. We speculate that when microtubules grow quickly ($\sim$5 - 10 μm/min) they can become confined by a small local distortions in the membrane. This is consistent with the fact that such shapes are only seen when the tubulin concentration and/or the temperature are high (C$\sim$50μM, T$\sim$35°C). Hotani and Miyamoto also observed star-shaped vesicles ("multi-polar liposomes") at very high tubulin concentrations (Hotani and Miyamoto, 1990). They suggest that these unusual shapes depend upon the presence of a rigid nucleating site (e.g. a region of the membrane attached to the glass surface of the sample). We have observed star-shaped vesicles which are independent of any anchoring surface and conclude that no such nucleating site is necessary.

Real cells, of course, contain specialized microtubule nucleating sites which presumably constrain the microtubules out of alignment. It would be interesting to encapsulate such nucleating sites (e.g. centrosomes) along with tubulin inside of vesicles and observe the shapes that result upon polymerization.

Does the membrane ever rupture? No, vesicles never rupture as a result of microtubules poking them from the inside. Observations of buckled microtubules presented in the next section will make this absolutely clear. However, the fact that microtubules would depolymerize immediately if exposed to the low concentration of tubulin in the solution outside the vesicles is evidence of the integrity of the membrane.

It is perhaps more interesting to ask whether microtubules can cause an irreversible transformation of any kind in the vesicle membrane. While we never observed a vesicle change shape after a cycle of microtubule polymerization, we suspect that irreversible changes may occur when the

entrapped tubulin concentration is very high. Under such conditions, observations always begin after the microtubules have polymerized at least once (during the filling of the sample cell, see section III.2.3).

Our suspicions are based on the occasional, normal looking phi (ϕ) shape which relaxes into a chain of small spherical vesicles (with a larger one where the center of the phi used to be), rather than a single large one (Figure 5.10). Such chains are not common in our vesicle preparations in the absence of tubulin, so we think it likely that the vesicle began as a single sphere. 'Strings of pearls' are a documented but poorly understood instability of lipid tubes under tension (Bar-Ziv, 1994). Thus we speculate that when entrapped microtubules grow very quickly, the lipid in the region of high curvature near the tip of the protrusion, is under considerable tension. Perhaps this tension induces the redistribution of lipid from the inner to the outer bilayer (sort of squeezes them out). The natural time-scale for flip-flop (exchange between the bilayers) is quite long (several hours) (Kornberg and Connell, 1971), so any bilayer asymmetry developed during an initial growth spurt will persist for the duration of an experiment. Upon depolymerization of the microtubules, residual bilayer asymmetry may drive the formation of pearls. As we have not been able to encapsulate tubulin in single component vesicles, there is also the possibility of lipid demixing across the bilayers.

How can we understand the progression of shapes? Is the phi (ϕ) shape the result of a specific interaction between the microtubules and the membrane? Or are all the shapes simply minimizing the mechanical energy of a membrane forced to accommodate a rod (or set of rods) longer than its spherical diameter? To approach these questions, we consider the curvature and stretching energies of the shapes as a function of their axial extent.

Helfrich demonstrated that the energy stored in a membrane is completely characterized by its area, A, and principle curvatures, C_1 and C_2 (Helfrich, 1973). The elastic stretching energy *per unit area*, E_s, is given by

$$E_s = \frac{k_s}{2}\left(\frac{\Delta A}{A_o}\right)^2; \qquad \Delta A = A - A_o,$$

where k_s is the stretching elastic constant and A_o is the area at zero tension. The elastic bending energy *per unit area*, E_b, is given by

$$E_b = \frac{k_c}{2}(C_1 + C_2 - C_o)^2 + k_c^* C_1 C_2,$$

where C_o is the spontaneous curvature and k_c and k_c^* are the elastic moduli of curvature for cylindrical and saddle bending, respectively. Experiments on unilamellar vesicles find k_s is about 10^{-6} erg/μm^2 (Evans and Needham, 1987). k_c is much smaller by comparison, on the order of 10^{-12} erg (Faucon, et al., 1989). Considering that thermal energies are typically $5 \cdot 10^{-14}$ erg, we can see that temperature alone can cause a micron-sized vesicle to fluctuate gently in curvature but will not change its area by more than 1Å^2.

The symmetry of the observed shapes allows us to use simple geometrical representations, illustrated in Figure 5.11. The sausage shape is a cylinder with two hemispherical endcaps. The length of the cylinder, $2L$, and the radius of the endcaps, R, completely specify the shape. The football shape is, in cross-section, an intersection of two identical circles. It is described by R, the radius, and Θ_{max}, the angular extent, of the arcs. The unphysical discontinuity in the slope at the extremes can be removed by defining an angle, Θ, at which a pair of spherical caps of radius $r^* = R(1 - \cos\Theta_{max}/\cos\Theta)$ and height $h = r^*(1 - \sin\Theta)$ take over. Finally, the phi (ϕ) shape is part football $\{R, \Theta_{max}\}$ and part sausage $\{r, L\}$. And again, the discontinuity where they meet can be removed by an specifying an angle, Θ, at which a circular arc of radius $r^* = \left(R(\cos\Theta - \cos\Theta_{max}) - r\right)/(1 - \cos\Theta)$ joins the two smoothly.
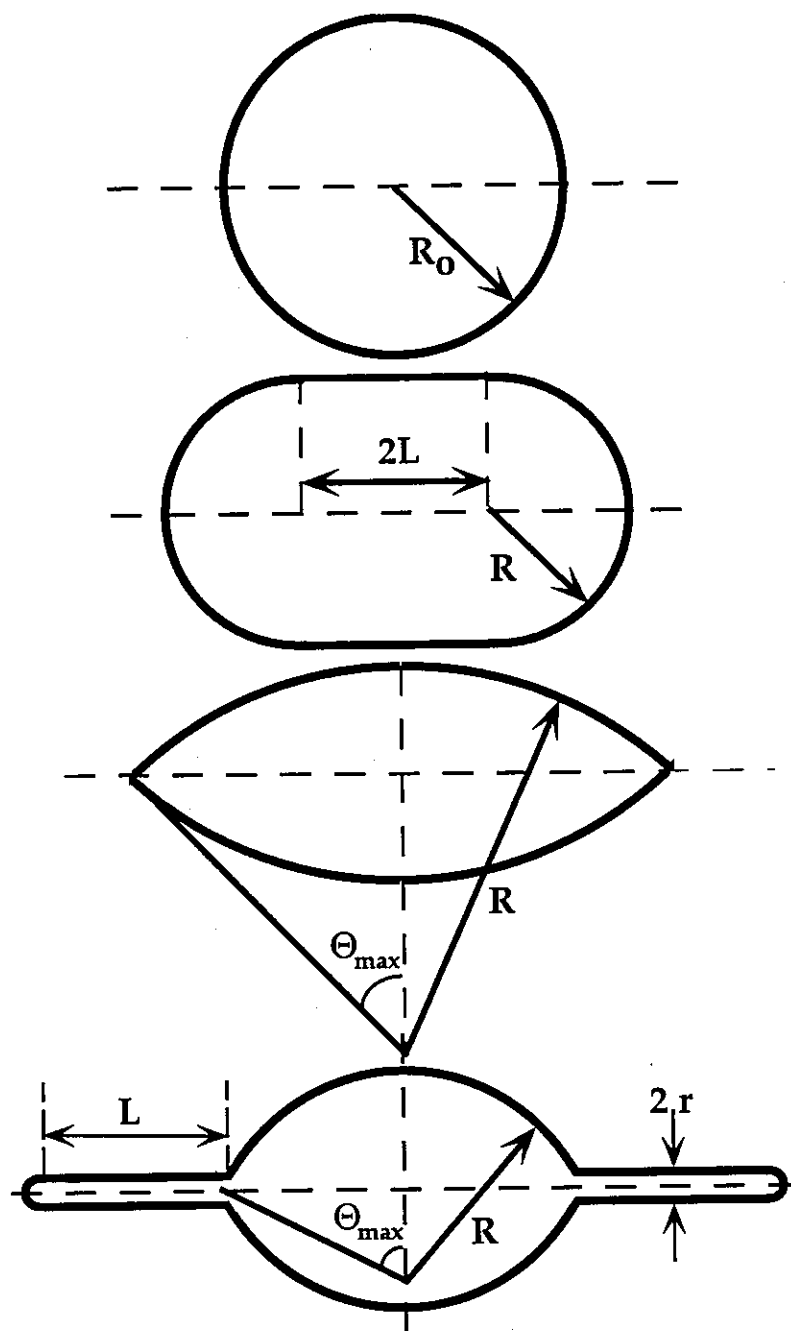
Fig. 5.11. Parameterization of vesicle shapes.

The formulas for axial extension, volume, surface area and curvature energy are given in Appendix C. For simplicity, we assume $C_o = 0$ and normalize all lengths in terms of $R_o \equiv 1$, the radius of the undistorted vesicle, and all energies in terms of $8\pi k_c$, the curvature energy of a spherical vesicle.

Using these formulas, it is an exercise in numerical methods to find the values of the shape parameters that 1) contain a microtubule of a certain length and 2) minimize the energy of the membrane while 3) maintaining a constant volume. (See references (Deuling and Helfrich, 1976) and (Svetina and Zeks, 1989) for examples of such calculations.) The constraint of constant volume is justified by the relative impermeability of the membrane to proteins and ions. While water can flow rather freely through a bilayer (permeability coefficient $k \sim 5 \, \mu m/sec$ (Thompson and Huang, 1966)), a net loss of volume must create an osmotic pressure difference across the membrane. The energetic cost of this can be estimated from $\Pi \Delta V$, where Π is the final osmotic pressure difference and ΔV is the change in volume. When $\Delta V/V \ll 1$, the osmotic pressure difference is related to the volume change as $\Pi = \beta C_o \Delta V/V$, where $\beta \sim 2.5 \cdot 10^7$ dyne-liters/(cm$^2 \cdot$moles) and C_o is the original solute concentration in the vesicle (Evans and Waugh, 1977). In the buffer we use, $C_o \sim 0.1$ M. If $\Delta V/V$ is as little as 0.01, and $V \sim 10 \, \mu m^3$ so $\Delta V \sim 10^{-13}$ cm^3, then the energy cost is about 10^{-9} ergs, or about $10^5 k_B T$.

To test the calculations, one can estimate the surface area and volume of a vesicle in its various shapes, as illustrated in Figure 5.12. There is initially an apparent increase in surface area/volume, which is most likely an indication that the undistorted vesicle was not a perfect sphere. In this case, it was probably slightly squashed along the line of sight.
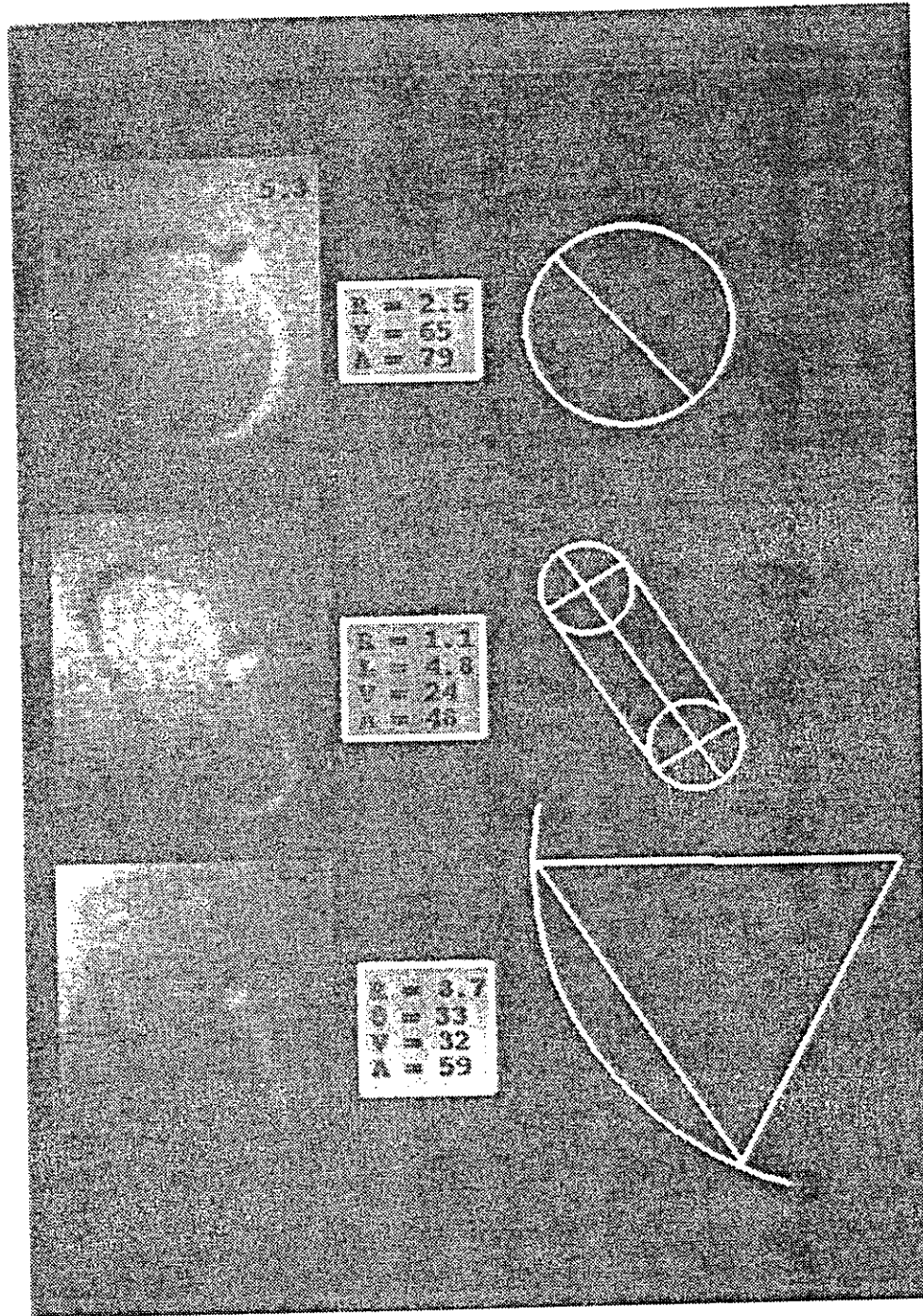
Fig. 5.12. Measured shape parameters of a vesicle. The vesicle is the same as the one shown in Figures 5.4 and 5.5. The numbers in the upper right corner of the images represent the estimated length (in μm) of the microtubule(s) inside. Note that the surface area and volume of the sphere is apparently larger than those of the other two forms, which are not significantly different. Most likely the sphere is actually slightly oblate.

157

A complete theoretical analysis of the shapes is beyond the scope of this thesis. Instead, we foreshadow a deeper analysis by some simple calculations:

It is not hard to calculate the energy of the sausage and football shapes which maintain a volume of $\frac{4}{3}\pi R_o^3$ and minimize curvature energy while accommodating a microtubule of length Z. The curvature energy of such shapes and their surface area are plotted as a function of Z in Figure 5.13. Notice that the football shape is lower in both curvature energy and surface area than the sausage shape for short lengths, $Z < 3.5R_o$. This conflicts with our observation that the sausage shape occurs before (i.e. for smaller Z) than the football shape (see Figures 5.4-5.6) and suggests that something besides the curvature and stretching energies is determining the shape of the vesicle.

Entropy may be the answer. Microtubules can fluctuate through a larger solid angle in the sausage shape than in the football shape. The number of distinguishable orientations available to a microtubule of length L increases by approximately $(L/2)^2 \Delta\Omega / \pi a^2$, where $\Delta\Omega$ is the difference in available solid angle, and πa^2 is the area of a microtubule end. The change in entropy associated with N microtubules in an increased solid angle $\Delta\Omega$ is $Nk_B \ln\big((L/2a)^2(\Delta\Omega/\pi)\big)$, which corresponds to an energetic gain of:

$$T\Delta S = Nk_B T \ln\big((L/2a)^2(\Delta\Omega/\pi)\big), \qquad (V.1)$$

Reasonable numbers ($L^2 \sim 10$ μm^2, $a^2 \sim 10^{-4}$ μm^2 and $\Delta\Omega \sim 1$) suggest that, for each microtubule inside, the sausage shape gains about 10k$_B$T over the football shape. If there are 5 microtubules in a vesicle, for example, the sausage shape may not give way to the football shape until $Z > 2.5R_o$ (see Figure 5.13, bearing in mind that $8\pi k_c \approx 300 k_B T$). Thus, entropy may stabilize the sausage shape at small Z.
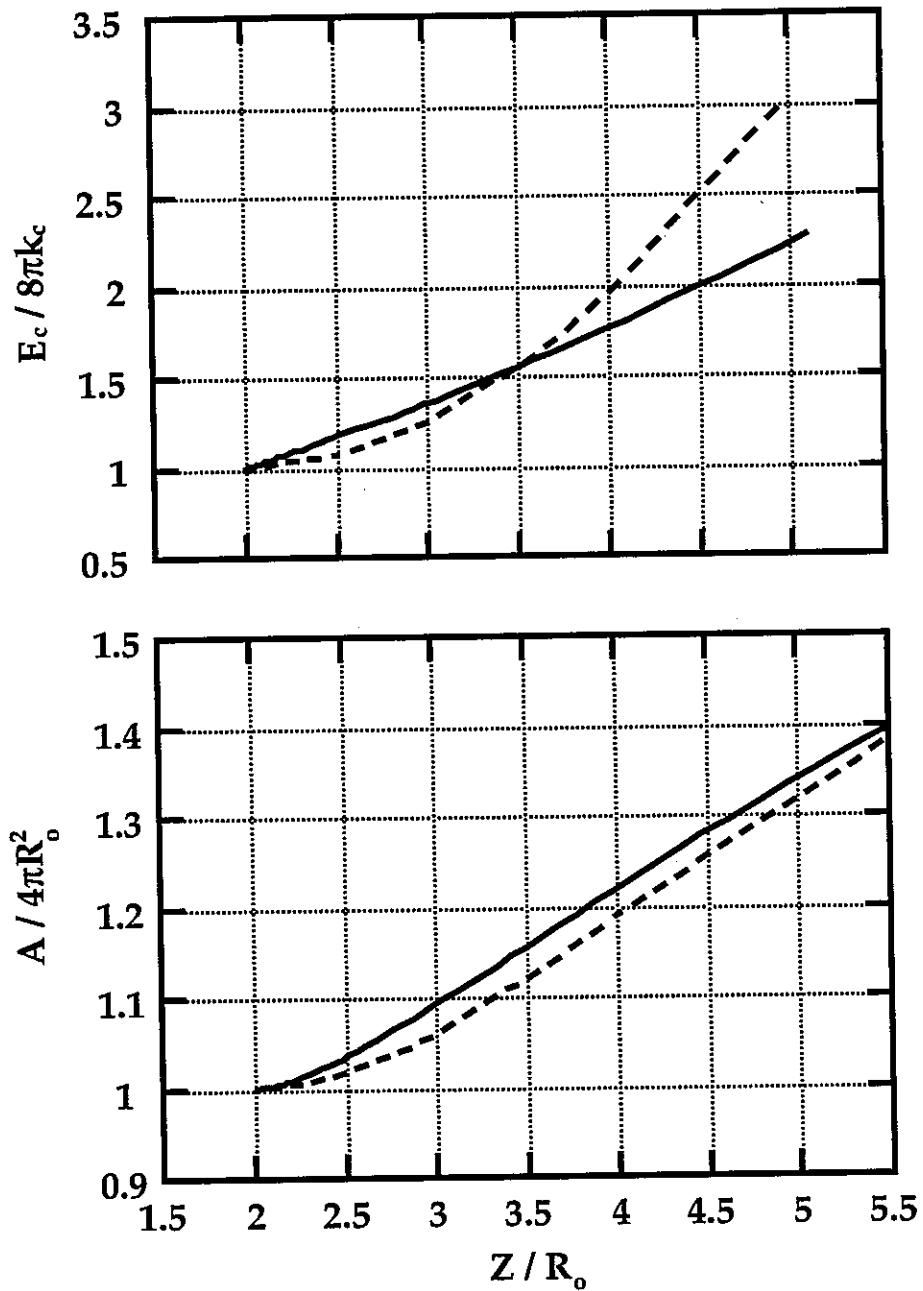
Fig. 5.13. Numerical comparison of the sausage and football shapes. Upper graph: curvature energy of the sausage (solid line) and football (broken line) shapes versus axial length Z, rescaled in terms of the initial spherical vesicle ($E_c = 8\pi k_c ; A = 4\pi R_o^2 ; Z = 2R_o$). Lower graph: surface area of same. The shape parameters were calculated by holding the volume constant at $\frac{4}{3}\pi R_o^3$ and minimizing the curvature energy. The relevant formulas are given in Appendix C.

Although the phi (ϕ) shape involves too many parameters to be addressed by a simple calculation, we expect that it does not depend on a specific interaction between the microtubule and the membrane for its stability. At first it seems that the tightly curved arms of the phi shape would require some specific interaction for their stability. However, the narrow arms of the phi shape allow it to accommodate long microtubules practically without stretching and, since the contribution of the arms to the bending energy is proportional to surface area as well as curvature, the creation of a high curvature region of very small area may be driven by membrane energetics alone. We intend to conduct the numerical minimization of the membrane energy to test this reasoning.

With some simplifications, we can estimate the cross-sectional radius of the arms r, which gives the minimum energy phi (ϕ) shape. We treat the central, football shaped region as spherical. Also, we neglect contributions from the necks and endcaps (see Appendix C). Using the parameters defined in Figure 5.11, the energy of the phi (ϕ) shape is then

$$E = E_c + E_s = \left(8\pi k_c + \pi k_c \frac{L}{r}\right) + \frac{k_s}{2}\frac{\left(4\pi R^2 + 2\pi r L - 4\pi R_o^2\right)^2}{4\pi R_o^2} \qquad \text{(V.2)}$$

and its derivative with respect to the radius of the arms is

$$\frac{dE}{dr} = -\frac{\pi k_c L}{r^2} + k_s\left[\left(\frac{R}{R_o}\right)^2 - 1 + \frac{1}{2}\frac{r}{R_o}\frac{L}{R_o}\right]2\pi L. \qquad \text{(V.3)}$$

The second derivative is always positive, so the zero crossing of the first derivative is a minimum. Setting the first derivative to zero gives

$$\frac{k_c}{k_s} = 2r^2\left[\left(\frac{R}{R_o}\right)^2 - 1 + \frac{1}{2}\frac{r}{R_o}\frac{L}{R_o}\right] \sim \frac{r^3 L}{R_o^2} \qquad \text{(V.4)}$$

since $R/R_o \sim 1$. Solving for r in terms of R_o and using reasonable values,

$$\frac{r}{R_o} \sim \left(\frac{k_c}{k_s L R_o}\right)^{1/3} \sim \left(\frac{10}{10^7 \cdot 10 \cdot 1}\right)^{1/3} \sim 5 \cdot 10^{-3}. \qquad \text{(V.5)}$$

160

Thus, for vesicles about 2 μm in diameter, the phi (φ) shape will have arms about 10 nm in diameter. This is of the order of the microtubule diameter, suggesting that, at least for small vesicles or vesicles with multiple microtubules, the cylindrical arms in the phi shape may come into contact with the encapsulated microtubules.

A better calculation would take the membrane thickness into account since it is actually not very different (~5 nm) from the estimated cylinder diameter. Also, entropic energies, which are not included, may be significant in creating some distance between the membrane and the microtubule. Still, despite its crudeness, the calculation does not lose consistency with the essential feature of the phi shape: that the cylindrical arms are extremely narrow. This reinforces our wonder at the ability of microtubules to polymerize in such a restricted geometry and leads into the next subsection.

In closing, our qualitative understanding of the sequence of vesicle shapes can be summarized as follows: Near-spherical vesicles with microtubules inside begin to deform when the microtubules reach the size of the vesicle diameter. An initial deformation induces the microtubules to align slightly, which reinforces the deformation and promotes further alignment. A sausage shaped vesicle accommodates the microtubules while allowing them some freedom of movement. As the microtubules get longer, the curvature energy of the membrane becomes more important than the entropy of the microtubules and the sausage shape yields to a football shape. As the microtubules continue to grow, the football shape cannot contain them without greatly increasing the surface area. As a result, the membrane collapses into the phi (φ) shape, which accommodates long microtubules by subjecting a very small amount of surface area to very high curvatures.

3.3 Force Generation

Throughout the shape transformations, the energy of the membrane increases as the microtubules grow. This change in energy with changing length satisfies the formal definition of a force. Yet, it appears paradoxical that the microtubule ends should be pushing up against the membrane and at the same time be accessible to tubulin dimers.

A common reaction to the paradox is to question whether the microtubules can really be thought of as pushing against the membrane. The pictures in this section are dramatic evidence of the membrane pushing on the microtubules. They illustrate microtubules actually buckling under the force of the microtubule-membrane interaction. Often, the buckled microtubule ends up completely doubled over! And still it grows.

3.3.1 *Observations*

The sequence of vesicle shapes seems to end with the phi (ϕ) shape. We have observed vesicles with $Z > 10R_0$ in this morphology. In the end, the phi (ϕ) shape is limited not by the energetics of the membrane, but by the strength of the microtubules. Microtubules often reach lengths at which they are unstable to buckling under the "weight" of the vesicle.

Buckling is a completely common occurrence with an unmistakable signature: usually, the microtubule doubles over completely (in a radius that can be as small as 1μm) and the vesicle becomes sort of semi-phi or psi (ϕ) shaped. Psi (ϕ) shapes were observed by Hotani and Miyamoto, but lacking the ability to depolymerize the microtubules under the microscope, they did not recognize these shapes as descendent from the phi (f) shapes (Hotani and Miyamoto, 1990). Microtubules buckling and doubled over inside vesicles are shown in Figures 5.14 and 5.15, respectively.
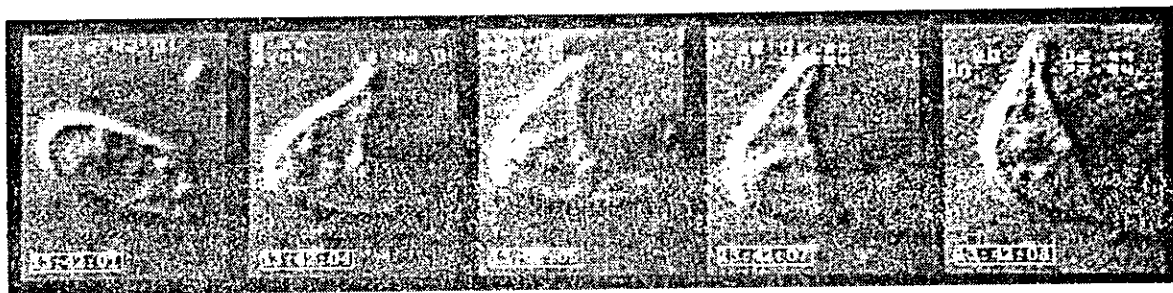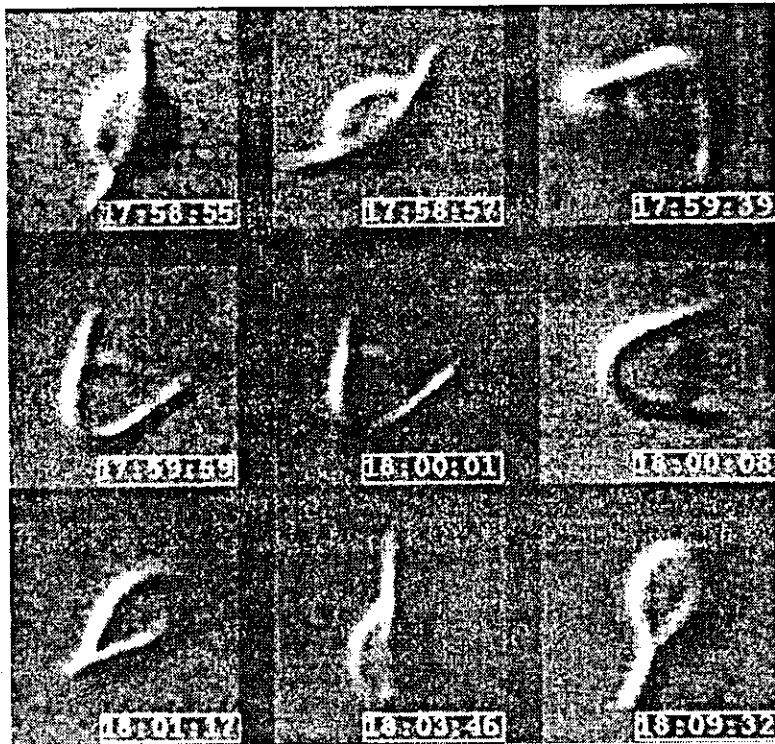
Fig. 5.14. Examples of microtubules buckling inside of vesicles. In the series of nine, the vesicle diffuses rotationally. The 8th and 9th images demonstrate the buckled microtubules in a side and top view, respectively. The central image 7.5 μm x 7.5 μm. In the series of five, each image frame is 12.5 μm top to bottom. The vesicle has many smaller vesicles trapped inside.
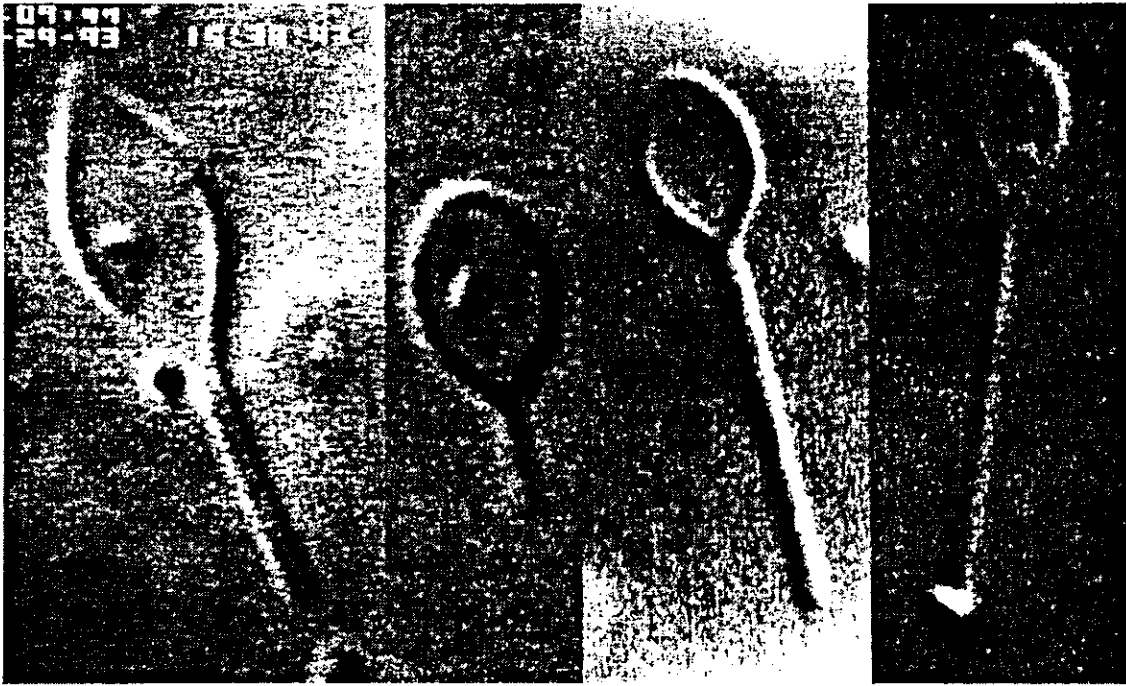
Fig. 5.15. Four different vesicles containing doubled over microtubules (psi (φ) shapes. Images are 20 μm top to bottom.

Buckling is reproducible and reversible. Despite the sharpness of the bend the microtubules do not break. The shape of a membrane around buckled microtubules depends on the length at which buckling occurs. If the microtubule(s) are short enough, the vesicle becomes sausage shaped, but very taut. Longer buckled microtubule(s) give the vesicle the shape of a tear drop. The cusp of the tear drop eventually collapses into a single narrow cylindrical arm as the microtubule(s) continue to grow, generating the psi (φ) shape. Like the phi (ϕ) shape, the psi (φ) is long-lived: microtubules continue to grow with both ends in the same cylindrical arm! If the microtubule is long enough, the vesicle may assume the psi (φ) shape immediately upon buckling. Thus, the progression of shapes is quite analogous to the one outlined in the previous section.

These forms are not rotationally symmetric since the bent microtubules define a plane rather than a line. Instead, they have reflection symmetry across the plane as well as in the plane about the line that bisects the microtubule. The psi (φ) shape, for example, is usually a paddle, thinner than it is wide.

3.3.2 Deductions

The critical length L_c at which buckling occurs is related to the force F applied to the ends of a microtubule by

$$F = 12YI/L_c^2 = 12k_BTL_p/L_c^2 \qquad (V.6)$$

where Y is the Young's modulus ($\sim 1\,GPa$), I is the moment of inertia of the microtubule, ($\sim 10^{-28}\,cm^4$) and $L_p = YI/k_BT$ is its persistence length ($\sim 0.5\,cm$). (A simple derivation is given in appendix D.) Notice that the Young's modulus of the microtubule is not very different from that of actin filaments or polystyrene. The extraordinary stiffness of a microtubule derives from its large moment of inertia (Gittes, et al., 1993).

To compare buckling events in different vesicles, consider how the applied force depends on the characteristics of the vesicle. First, if a vesicle contains more than one microtubule, the force applied by the membrane is distributed over all the microtubules equally. So, vesicles which contain different numbers of microtubules N, but are otherwise identical will have $L_c \sim \sqrt{N}$. Second, if a vesicle has more than one lamella, the applied force or, equivalently, the rate of change in membrane energy with microtubule length, will be greater since the stretching and bending elastic moduli are directly proportional to the number of lamellae (Kwok and Evans, 1981). Finally, the overall size of the vesicle also matters. If the vesicle is too large, individual microtubules may buckle as soon as they encounter the membrane and never completely align. See Figure 5.16.

To summarize, a single microtubule in a multi-lamellar vesicle buckles at a short length. Several microtubules inside a uni-lamellar vesicle may not buckle until they are very long, if at all. Finally, in very large vesicles ($R_o > 10 \, \mu$m), microtubules will buckle individually as soon as they become long enough to span the vesicle diameter.

Although we observed a variety of critical buckling lengths, we were unable to distinguish a binning of the lengths corresponding to multiple microtubules (Betterton, 1994). The trend was probably obscured by variations in the number of lamellae in the vesicles.

Assuming that the typical buckling event, $L_c \sim 10 \, \mu$m, involves a single microtubule, we can estimate the applied force: $F \sim 600 k_b T / \mu$m $\sim 3 \cdot 10^{-12} N$ (see equation V.6). This value is consistent with the calculations given in the previous section. For example, consider the force applied by phi (ϕ) shaped vesicles. Given the relative magnitudes of and it is reasonable to assume the surface area is constant. Then, by equation V.2, the energy of the membrane
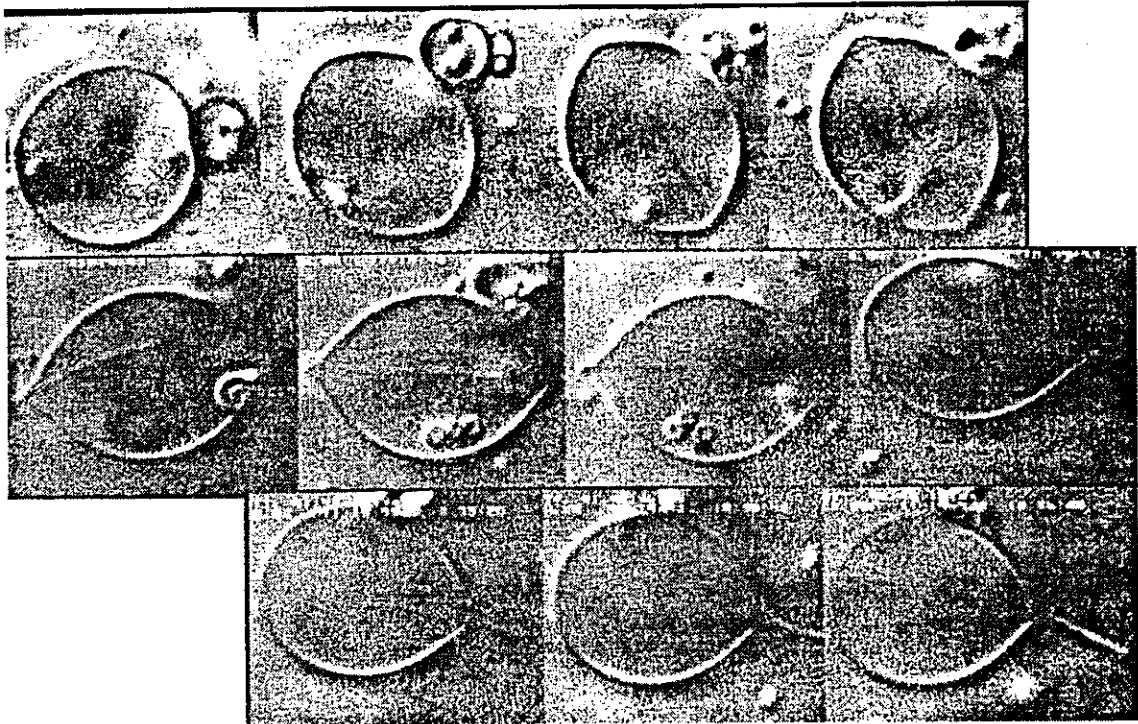
Fig. 5.16. Microtubules buckling inside a very large vesicle. Each image is 17.5 μm top to bottom. The large vesicle has some smaller vesicles trapped inside which diffuse in and out of focus.

is simply proportional to the length of the arms and the applied force is a constant that depends only on their radius r. A rough estimate gives

$$F = \frac{dE}{dL} = \frac{\pi k_c}{r} \sim \frac{3 \cdot 20 k_B T^2}{0.02 \mu m} \sim 3 \cdot 10^3 k_B T / \mu m \sim 2 \cdot 10^{-12} N$$

Thus, the microtubule generated force seems to be an order of magnitude weaker than the forces generated by typical molecular motors (Svoboda, et al., 1993; Finer, et al., 1994; Bourdieu, et al., 1995). Even so, it is capable of gradually storing many thousands of $k_B T$ of energy in the curvature of the membrane because it can be maintained over many microns.

3.3.3 *Modeling*

Although there can be no doubt that a mechanical force is generated between the membrane and the microtubule(s), the question remains, how can the microtubule both push on the membrane and grow from its ends? We propose that the mechanism may be a 'thermal ratchet', and support this conjecture with rough estimates of some relevant parameters.

The notion of a thermal ratchet was first introduced by Feynman as an instructive example of a system which appears to violate the second law of thermodynamics (Feynman, et al., 1966). Briefly, the system consists of a ratchet and paul, and a heat bath. The ratchet is connected to a heat bath, so it jiggles around but, because of the paul, it only actually moves in one direction. At first it appears that directed motion (the equivalent of work) is extracted from the heat bath without any heat loss, in violation of the second law of thermodynamics. The catch is that the paul also has a temperature. If it is at the same temperature as the ratchet, it jiggles just as much and allows the ratchet to move in both directions. The paul can rectify the motion of the ratchet only if it is held at a lower temperature than the ratchet. Thus the system can do work, but only because heat flows from the warmer ratchet to the cooler paul, in keeping with the second law.

Recently, generalized thermal ratchets has received theoretical attention (Ajdari and Prost, 1992; Magnasco, 1994). It has been suggested as a possible model for the generation of mechanical forces on the molecular level, where thermal energies are especially significant. The generalized thermal ratchets are built from an asymmetric, periodic potential (a ratchet) and a diffusing particle. They require an external energy source, usually chemical or electrical, which either modulates the height of the potential at regular intervals (Ajdari and Prost, 1992) or provides a periodic forcing (Magnasco, 1994). The former is more simply explained: When the potential is on, the particle is localized. When the potential is off, it diffuses. In the asymmetric potential, the localized particle is held closer to one of the neighboring wells than the other. This bias means that when it diffuses, the particle enters the territory of one of the neighboring wells sooner than the other. If the potential is pulsed on after a certain time, such that the diffusing particle was more likely to enter the region of the closer well than the farther one, the particle will be localized either in its original well, or in the nearer of the two neighboring wells. After many repetitions, the particle will have moved in the preferred direction. Recently, such a thermal ratchet was demonstrated experimentally using latex beads in an optical trap (Faucheux, 1995).

Thermal ratchet motors operate in concert with thermal noise and without inertia. Therefore they seem well suited as models of the transduction of chemical energy into mechanical energy in biological systems where thermal energies can be significant (Vale and Oosawa, 1990; Simon, et al., 1992; Peskin, et al., 1993; Finer, et al., 1994; Magnasco, 1994). In many instances, however, the energy transduction occurs at the level of a single protein molecule in co-operation with a long protein polymer (e.g. kinesin

and microtubules, myosin and actin). Such "molecular motors" are not ideal systems in which to test the theory of thermal ratchets. The resolution and measurement of the small forces ($\sim 10^{-11}$ N) on minute length scales (~ 10 nm) create formidable challenges for experimentalists. Furthermore, as these challenges begin to be met (Svoboda, et al., 1993; Finer, et al., 1994; Bourdieu, et al., 1995), "power-stroke" models, in which the energy transduction takes place via a change of conformation of the protein, seem better suited to the data (e.g. velocity, efficiency) (Magnasco, 1995).

Thermal ratchet models are perhaps more fruitfully applied to experiments on vesicles containing microtubules. This system is ideal because of its pure and macroscopic nature. It is pure because it involves only one protein, tubulin. It is macroscopic because the force it generates is reflected on a length scale of many microns (i.e. over the entire vesicle).

The system of a microtubule in a vesicle can be considered a thermal ratchet in the following sense. The membrane near the tip of the microtubule fluctuates due to thermal noise. Occasionally fluctuations create a distance large enough for a tubulin dimer to access the tip of the microtubule. If during this fluctuation, a dimer attaches to the end of the microtubule, the membrane will be prevented from relaxing back to its original position. It will be 'ratcheted' forward the length of a tubulin dimer.

To make analogy with the brownian particle in a sawtooth potential, consider the membrane near the microtubule end as trapped in an well defined on one side by the microtubule end and on the other by its own curvature energy. On the side of the microtubule the potential is steep, essentially a hard core repulsion. On the other side, it is rises gently. For the phi (ϕ) shape, it is linear in the distance ($E_c \propto L$), see Figure 5.17. Instead of pulsing on and off, this potential occasionally hops forward a discrete step.
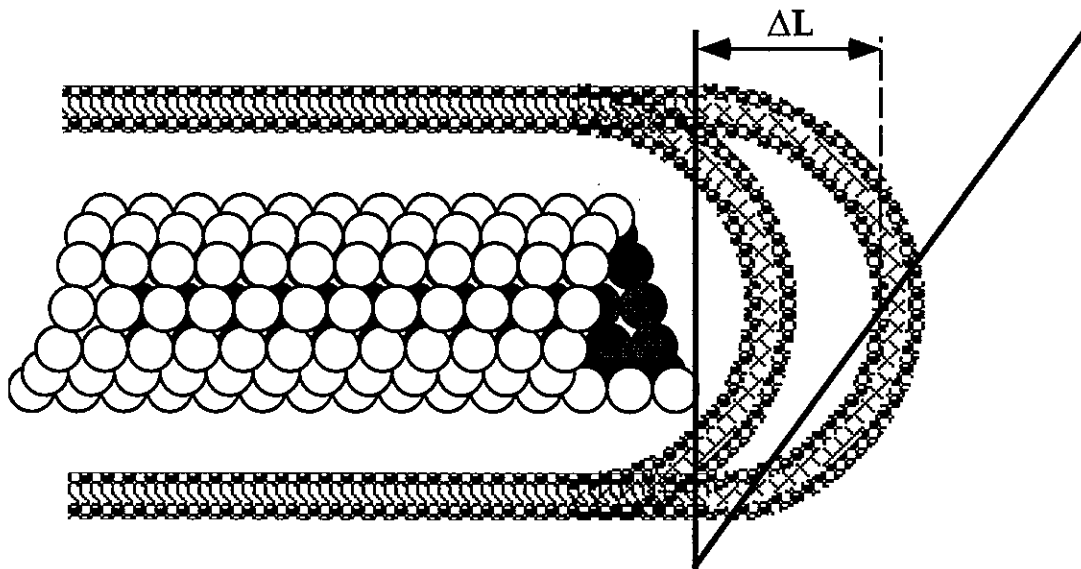
Fig. 5.17. Schematic of a microtubule inside a vesicle as a brownian ratchet.

To determine whether a thermal ratchet model is appropriate for this system, a first check is whether the energy gained by elongating the microtubule is greater than the energy stored in the displacement of the membrane. Following that, an estimate of the frequency of the necessary membrane fluctuations can be compared to the observed rate of microtubule growth. To simplify the calculations, we consider a microtubule in a phi (ϕ) shaped vesicle.

Continuing the earlier approximation of the phi (ϕ) shape as a combination of a sphere and a cylinder (see section V.3.3.2), we have already calculated $\Delta E/\Delta L = \pi k_c/r \sim 10^3 k_B T/\mu m$. So the energy required to elongate the arm by $\Delta L = 10^{-2}$ μm (the length of a dimer) is on the order of $10 k_B T$. The energy gained by binding a dimer to the microtubule end can be estimated from the equilibrium rates of the forward and reverse assembly reaction (*not* disassembly), $k_{on}/k_{off} = e^{-\Delta E/k_B T}$. Measured values for these rates in the literature are not in close agreement, but range from $\sim 2 k_B T - 10 k_B T$, as reflected by the discrepancy in the apparent critical concentration for microtubule growth: <0.05 μM (Dreschel, et al., 1992) versus ~ 5 μM (Walker, et al., 1988). Though the energy balance is borderline, it is not unreasonable. Perhaps several dimers must bind to the end during a membrane fluctuation to make it stick.

The frequency of dimer-sized fluctuations can be estimated from the dispersion relation of the membrane rescaled by the appropriate Boltzmann factor,

$$\omega \sim \frac{k_c}{\eta r}\left(\frac{2\pi}{\Delta L}\right)^2 e^{-\Delta E/kT}$$

where k_c is the curvature elastic constant, η is the viscosity of water, r is the radius of the arm of the vesicle and ΔL is the size of the fluctuation. An

order of magnitude estimate, using $k_c \sim 20k_B T = 10^{-19} J$, $\eta \sim 10^{-3}$ kg m^{-1}s^{-1}, $r \sim 2 \cdot 10^{-8}$ m, and $\Delta L \sim 10^{-8}$ m, gives a frequency of $10^9 Hz$. Multiplying by $e^{-10} = 5 \cdot 10^{-5}$, we find a dimer-sized fluctuation occurs with a frequency of $5 \cdot 10^4 Hz$, or once every 20 *micro*seconds. This is considerably more frequent than the time between the addition of subsequent dimers to the tip of a microtubule ($V_g \sim 2$ µm/min = $3250/60 Hz \approx 60 Hz = 17$ milliseconds).

From these rough estimates of the relevant frequencies and energies, we conclude that the system of a microtubule inside a vesicle may be appropriately modeled as a thermal ratchet. It remains to consider more deeply the consequences of the thermal ratchet model and test it by varying parameters (e.g. membrane tension, temperature) which strongly affect the frequency of fluctuations or the energy of binding.

4. Open Questions

This exploration into the system of microtubules in vesicles has raised more issues that it has resolved. We have addressed several questions in a rough or qualitative manner, but a solid understanding of the system will require a more quantitative study. Of the questions we have not addressed, the most pressing is, perhaps, Is microtubule assembly noticeably slowed by the presence of the membrane? and, If so, how much? One straightforward approach to the answer would be to measure the rate of assembly of a single microtubule end and correlate it with the tension in the vesicle (e.g. the length of the arms of the phi (ϕ) shape). Another approach would be to look at assembly while maintaining constant tension on the membrane.

The limitations, at present, are experimental. We lack a reliable way to control, or even measure, the number of microtubules or the number of lamellae in a vesicle. To remedy the situation, we are investigating several

new techniques. First, to determine the number of lamellae in the vesicle of interest, we are developing the technique of micropipetting (Kwok and Evans, 1981). Concurrently, we are experimenting with ways to produce vesicles which are more uniformly distributed with respect to their size and their number of lamellae (e.g. gel filtration, centrifugation). For better control over the number of microtubules in the vesicles, we plan to encapsulate nucleating sites (pieces of stabilized microtubules) and work at temperatures low enough to suppress bulk nucleation. A natural extension would be to label the sites (e.g. fluorescently) so as to count them *in situ*. A possible flourish would be to block one of the ends (e.g. the minus end) from nucleating and thereby study the growth of only one end. Finally, a basic improvement would be simply to constrain the microtubule(s) inside the vesicles to lie in the plane of focus of the microscope (e.g. restraining them with a micropipette, aligning them in an electric field).

Finally, it would, of course, be extremely useful to have a detailed structural picture of the microtubule ends near the vesicle wall. The apparent zippering of free microtubule ends raises the question of whether the microtubule is actually pushing on the membrane with its sheet-like end. Perhaps, the sheet like end is doubled over and the zipper is actually pushing the membrane forward? We have attempted to visualize microtubules inside of vesicles using cryo-electron microscopy, with little success. The major problem is that the vesicles must be quite small ($\sim 100\,\text{nm}$) to be transparent to the electrons ($\sim 300\text{kV}$), but it is hard to get enough tubulin inside such a small vesicle to support polymerization. Considerable effort, in collaboration with Peggy Bisher and Michael Treacy at NEC Research and Frank Booy and Alastair Stevens at the National Institutes of Health, have yielded a single enigmatic micrograph (Figure 5.18).

174

Fig. 5.18. Electron micrograph of a microtubule inside a vesicle. The system is frozen in a thin sheet of vitrious ice. The microtubule diameter (~25 nm) can be referenced for scale. Arrows indicate regions where a microtubule end seems to come in contact with the membrane.

175

CHAPTER VI

CONCLUSIONS

In this thesis, we have looked at physical properties of microtubule assembly, both alone and interacting with a brownian obstacle. Although microtubule assembly bears geometrical resemblance to both crystallization and polymerization, it is not adequately described in terms of these or any other common physical processes. First, it is driven by entropy. An increase in temperature or a high concentration of glycerol increases the entropic cost of hydrating tubulin dimers, favoring their aggregation. Second, it reaches steady state far from equilibrium. Within the microtubule, tubulin dimers hydrolyze GTP and consequently destabilize their aggregate. This destabilization is also entropically driven via surrounding water molecules. Upon disassembly of the microtubule, tubulin dimers return into solution, freeing nucleation sites, and preventing the assembly reaction from reaching equilibrium. Finally, microtubule assembly proceeds in two structural steps, the first being the formation of a sheet of dimers and the second, the curling and zippering of the sheet into a tube.

We have seen how these three aspects intertwine to generate the distinguishing characteristics of microtubule behavior. The coexistence of assembling and disassembling microtubules means nucleating sites do not saturate at low temperatures. At high temperatures, even though both assembly and disassembly are enhanced, the nucleating sites saturate because assembly lasts longer and disassembly is more likely to be interrupted. At low temperatures, a fluctuating, destabilizing process, associated with GTP-hydrolysis, prompts the transition to disassembly. When high temperatures are combined with low concentrations, those fluctuations can be limited by the assembly rate. There is reason to believe that the destabilizing process

176

involves curling a tubulin sheet at the end of the microtubule into a tube. Such a step is clearly important in the spontaneous nucleation of microtubule.

We have also seen how microtubule assembly in a finite volume, defined by a brownian membrane is sufficient to generate mechanical force and establish a primitive morphogenesis. Simple estimates imply that these are general phenomena (i.e., they do not require a chemically specific interaction between the microtubule and the membrane) and can be modeled by a thermal ratchet mechanism.

The picture that emerges suggests the microtubule as a model system for studying the nature of conformational change as a driving force in biological phenomena. Conformational change is a ubiquitous model for the function of proteins. Dynamic instability can be considered the result of conformational changes of individual tubulin molecules co-ordinated and/or magnified by the "conformational change" (from sheet to tube) of their aggregate. Microtubule-mediated force generation can be contrasted with the conventional model of molecular-sized power-stroke conformational changes. Further studies of microtubule behavior could lead to a more solid understanding of conformational change in general.

In conclusion, microtubule assembly is a powerful reminder that the physics of biological systems is rooted in thermal noise, protein conformations and the unique nature of water. Perhaps one day a man-made material will mimic the unusual properties of microtubules, but until then microtubules themselves are suitable for application in non-biological contexts.

REFERENCES

AJDARI, A. and PROST, J. (1992). *C. R. Academie des Science Paris, II* **315**, 1635.

ALBERTS, B., BRAY, D., LEWIS, J., RAFF, M., ROBERTS, K. and WATSON, J.D. (1994). *Molecular Biology of the Cell.* New York, Garland.

ALLEN, R.D., DAVID, G.B. and NOMARSKI, G. (1969). The Zeiss-Nomarski differential interference equipment for transmitted-light microscopy. *Proceedings of the Royal Microscopical Society* **4**, 193-221.

ALLEN, R.D., ALLEN, N.S. and TRAVIS, J.L. (1981). Video-enhanced contrast, differential interference contrast (AVEC-DIC) microscopy. *Cell Motility and the Cytoskeleton* **1**, 291-302.

AMOS, L.A. and AMOS, W.B. (1991). *Molecules of the Cytoskeleton.* London, MacMillan.

ATKINS, P.W. (1990). *Physical Chemistry.* New York, W. H. Freeman and Company.

BANGHAM, A.D. and HORNE, R.W. (1964). Negative staining of phospholipids and their modification by surface-active agents as observed in the electron microscope. *Journal of Molecular Biology* **8**, 660-668.

BAR-ZIV, R. and MOSES, E. (1994). Instability and 'pearling' states produced in tubular membranes by competition of curvature and tension. *Physical Review Letters* **73**, 1392-1395.

BAYLEY, P.M., SCHILSTRA, M.J. and MARTIN, S.R. (1990). Microtubule dynamic instability: Numerical simulation of microtubule transition properties using a lateral cap model. *Journal of Cell Science* **95**, 33-48.

BENEZRA, R. (1994). An intermolecular disulfide bond stabilizes E2A homodimers and is required for DNA binding at physiological temperatures. *Cell.* **79**, 1057-1067.

BERNDL, K., KÄS, J., LIPOWSKY, R., SACKMANN, E. and SEIFERT, U. (1990). Shape transformations of giant vesicles: extreme sensitivity to bilayer asymmetry. *Europhysics Letters* **13**, 659-664.

BETTERTON, M. (1994). Microtubules and Vesicles. B.A. Thesis, Princeton University.

BOURDIEU, L., DUKE, T., ELOWITZ, M.B., WINKLEMANN, D.A., LEIBLER, S. and LIBCHABER, A. (1995). Spiral defects in motility assays: a measure of motor protein force. *submitted to Science.*

BURNS, R.G. (1991). Assembly of chick brain MAP2-tubulin microtubule protein. *Biochemical Journal* **277**, 231-238.

CANHAM, P.B. (1970). The minimum energy of bending as a possible explanation of the biconcave shape of the human red blood cell. *Journal of Theoretical Biology* **26**, 61-81.

CAPLOW, M. (1992). Microtubule Dynamics. *Current Opinion in Cell Biology* **4**, 58-65.

CAPLOW, M. and SHANKS, J. (1990). Mechanism of the microtubule GTP-ase reaction. *Journal of Biological Chemistry* **265**, 8935-8941.

CARLIER, M.-F. (1988). Role of nucleotide hydrolysis in the polymerization of actin and tubulin. *Cellular Biophysics* **12**, 105-117.

CARLIER, M.-F. (1989). Role of nucleotide hydrolysis in the dynamics of actin filaments and microtubules. *International Review of Cytology* **115**, 139-170.

CARLIER, M.-F., DIDRY, D. and PANTALONI, D. (1987). Microtubule elongation and guanosine 5'-triphosphate hydrolysis: Role of guanine nucleotides in microtubule dynamics. *Biochemistry* **26**, 4428-4437.

CARLIER, M.-F. and PANTALONI, D. (1981). Kinetic analysis of guanosine 5'-triphosphate hydrolysis associated with tubulin polymerization. *Biochemistry* **20**, 1918-1924.

CASSIMERIS, L. (1993). Regulation of microtubule dynamic instability. *Cell Motility and the Cytoskeleton* **26**, 275-281.

CASSIMERIS, L. and SALMON, E.D. (1991). Kinetochore microtubules shorten by loss of subunits at the kinetochores of prometaphase chromosomes. *Journal of Cell Science* **98**, 151-158.

CHRÉTIEN, D. and KARSENTI, E. (1995). Correlation of microtubule dynamics with their end structure. *Preprint*.

CHRÉTIEN, D., KARSENTI, E. and LIBCHABER, A. (1995). Personal Communications.

CHRÉTIEN, D. and WADE, R.H. (1991). New data on the microtubule surface lattice. *Biology of the Cell* **71**, 161-174.

CLARKSON, T.W., SAGER, P.R. and SYVERSEN, T.L.M. (1986). *The Cytoskeleton: A Target for Toxic Agents*. New York, Plenum.

COLOMBO, M.F., RAU, D.C., and PARSEGIAN, V.A. (1992). Protein solvation in allosteric regulation: A water effect on hemoglobin. *Science* **256**, 655-659.

CORREIA, J.J., BATY, L.T. and WILLIAMS, Jr., R.C. (1987). Mg^{2+} dependence of guanine nucleotide binding to tubulin. *Journal of Biological Chemistry* **262**, 17278-17284.

CORTESE, J.D., SCHWAB, III, B., FRIEDEN, C. and ELSON, E.L. (1989). Actin polymerization induces a shape change in actin containing vesicles. *Proceedings of the National Academy of Sciences, USA* **86**, 5773-5777.

COUE, M., LOMBILLO, V.A. and MACINTOSH, J.R. (1991). Microtubule depolymerization promotes particle and chromosome movement in vitro. *Journal of Cell Biology* **112**, 1165-1175.

DAWSON, R.M., ELLIOTT, D.C., ELLIOTT, W.H. and JONES, K.M. (1986). *Data for Biochemical Research*. New York, Oxford University Press.

DEULING, H.J. and HELFRICH, W. (1976). The curvature elasticity of fluid membranes: a catalogue of vesicle shapes. *Journal de Physique* **37**, 1335-1345.

DEVAUX, P. (1991). Static and dynamic lipid asymmetry in cell membranes. *Biochemistry* **30**, 1163-1173.

DÖBEREINER, H.-G., KÄS, J., NOPPL, D., SPRENGER, I. and SACKMANN, E. (1993). Budding and Fission of Vesicles. *Biophysical Journal* **65**, 1396-1403.

DOGTEROM, M. and LEIBLER, S. (1993). Physical aspects of the growth and regulation of microtubule structures. *Physical Review Letters* **70**, 1347-1350.

DRESCHEL, D.N., HYMAN, A.A., COBB, M.H. and KIRSCHNER, M.W. (1992). Modulation of the dynamic instability of tubulin assembly by the microtubule-associated protein tau. *Molecular Biology of the Cell* **3**, 1141-1154.

DUSTIN, P. (1984). *Microtubules*. Berlin, Springer-Verlag.

EIPPER, B.A. (1974). Properties of rat brain tubulin. *Journal of Biological Chemistry* **249**, 1407-1416.

ERICKSON, H.P. and O'BRIEN, E.T. (1992). Microtubule Dynamic Instability and GTP Hydrolysis. *Annual Review of Biophysics and Biomolecular Structure* **21**, 145-166.

EVANS, E. and KWOK, R. (1982). Mechanical calorimetry of large DMPC vesicles in the phase transition region. *Biochemistry* **21**, 4874-4879.

EVANS, E. and NEEDHAM, D. (1987). Physical properties of surfactant bilayer membranes: thermal transitions, elasticity, rigidity, cohesion, and colloidal interactions. *Journal of Physical Chemistry* **91**, 4219-4228.

EVANS, E.A. and WAUGH, R. (1977). Osmotic correction to elastic area compressibility measurements on red cell membrane. *Biophysical Journal* **20**, 307-313.

FARGE, E. and DEVAUX, P.F. (1992). Shape changes of giant liposomes induced by an asymmetric transmembrane distribution of phospholipids. *Biophysical Journal* **61**, 347-357.

FAUCHEUX, L.P. (1995). Forces in the Brownian World. Ph.D. Thesis, Princeton University.

FAUCON, J.F., MITOV, M.D., MÉLÉARD, P., BIVAS, I. and BOTHOREL, P. (1989). Bending elasticity and thermal fluctuations of lipid membranes. Theoretical and experimental requirements. *Journal de Physique* **50**, 2389-2414.

FAWCETT, D.W. (1981). *The Cell*. Philadelphia, W. B. Saunders.

FEYNMAN, R.P., LEIGHTON, R.B. and SANDS, M. (1966). *The Feynman Lectures on Physics*. Reading, MA, Addison-Wesley.

FINER, J.T., SIMMONS, R.M. and SPUDICH, J.A. (1994). Single myosin molecule mechanics: piconewton forces and nanometer steps. *Nature* **368**, 113-119.

FLYVBJERG, H., HOLY, T. and LEIBLER, S. (1994). Stochastic dynamics of microtubules: A model for caps and catastrophes. *Physical Review Letters* **73**, 2372-2375.

FRAUSTO DA SILVA, J.J.R. and WILLIAMS, R.J.P. (1991). *The Biological Chemistry of the Elements* Oxford, Clarendon.

FYGENSON, D.K., BRAUN, E. and LIBCHABER, A. (1994). Phase Diagram of Microtubules. *Physical Review E* **50**, 1579-1588.

FYGENSON, D.K., FLYVBJERG, H., SNEPPEN, K., LIBCHABER, A. and LEIBLER, S. (1995). Bulk Nucleation of Microtubules. *to appear in Physical Review E.*

GAL, V., MARTIN, S. and BAYLEY, P. (1988). Fast disassembly of microtubules induced by Mg^{2+} or Ca^{2+}. *Biochemical and Biophysical Research Communications* **155**, 1464-1470.

GEKKO, K. and TIMASHEFF, S. (1981a). Thermodynamic and kinetic examination of protein stabilization by glycerol. *Biochemistry* **20**, 4677-4686.

GEKKO, K. and TIMASHEFF, S.N. (1981b). Mechanism of Protein Stabilization by Glycerol: Preferential Hydration in Glycerol-Water Mixtures. *Biochemistry* **20**, 4667-4676.

GILDERSLEEVE, R.F., CROSS, A.R., CULLEN, K.E., FAGEN, A.P. and WILLIAMS, Jr., R.C. (1992). Microtubules grow and shorten at intrinsically variable rates. *The Journal of Biological Chemistry* **267**, 7995-8006.

GITTES, F., MICKEY, B., NETTLETON, J. and HOWARD, J. (1993). Flexural rigidity of microtubules and actin filaments measured from thermal fluctuations in shape. *Journal of Cell Biology* **120**, 923-934.

HAMES, B.D. and RICKWOOD, D. (1990). *Gel Electrophoresis of Proteins: A Practical Approach*. Oxford, IRL Press.

HARRIS, E.L.V. and ANGAL, S. (1989). *Protein Purification Methods: A Practical Approach*. Oxford, IRL Press.

HELFRICH, W. (1973). Elastic properties of lipid bilayers: Theory and possible experiments. *Zeitschrift fuor Naturforsch* **28 C**, 693-703.

HIMES, R.H. (1989). Dynamics of antarctic fish microtubules at low temperatures. *Biochemistry* **28**, 5089-5095.

HORIO, T. and HOTANI, H. (1986). Visualization of the dynamic instability of individual microtubules by dark-field microscopy. *Nature* **321**, 605-607.

HOTANI, H. and MIYAMOTO, H. (1990). Dynamic features of microtubules as visualized by dark-field microscopy. *Advances in Biophysics* **26**, 135-156.

HULETT, J.R. (1964). Deviations from the Arrhenius Equation. *Quarterly Reviews of the American Chemical Society* **18**, 227-242.

HYAMS, J.S. and BRINKLEY, B.R. (1989). *Mitosis: Molecules & Mechanisms*. London, Academic Press.

HYMAN, A.A., SALSER, S., DRESCHEL, D.N., UNWIN, N. and MITCHISON, T.J. (1992). Role of GTP hydrolysis in microtubule dynamics: information from a slowly hydrolyzable analogue, GMPCPP. *Molecular Biology of the Cell* **3**, 1155-1167.

INOUÉ, S. (1959). Motility of cilia and the mechanism of mitosis. *Reviews of Modern Physics* **31**, 402-408.

INOUÉ, S.A. (1986). *Video Microscopy*. New York, Plenum.

ISRAELACHVILI, J.N. (1993). *Intermolecular and Surface Forces*. London, Academic Press.

KIRSCHNER, M. and MITCHISON, T. (1986). Beyond self-assembly: From microtubules to morphogenesis. *Cell* **45**, 329-342.

KIRSCHNER, M.W., WILLIAMS, R.C., Jr., WEINGARTEN, M. and GERHART, J.C. (1974). Microtubules from mammalian brain: Some properties of their depolymerization products and a proposed mechanism of assembly and disassembly. *Proceedings of the National Academy of Sciences, USA* **71**, 1159-1163.

KNOPS, J., KOSIK, K.S., LEE, G., PARDEE, J.D., COHEN-GOULD, L. and McCONLOGUE, L. (1991). Overexpression of tau in a non-neuronal cell induces long cellular processes. *Journal of Cell Biology* **114**, 725-733.

KORNBERG, R.D. and CONNELL, H.M. (1971). Inside-outside transitions of phospholipids in vesicle membranes. *Biochemistry* **10**, 1111-1120.

KOWALSKI, R.J. and WILLIAMS, Jr., R.C. (1993). Unambiguous classification of microtubule ends *in vitro*: Dynamic properties of the plus and minus ends. *Cell Motility and the Cytoskeleton* **26**, 282-290.

KRAUHS, E., LITTLE, M., KEMPF, T., HOFER-WARBINEK, R., ADE, W. and POSTINGL, H. (1981). Complete amino acid sequence of β-tubulin from porcine brain. *Proceedings of the National Academy of Sciences, U.S.A.* **78**, 4156-4160.

KWOK, R. and EVANS, E. (1981). Thermoelasticity of large lecithin bilayer vesicles. *Biophysical Journal* **35**, 637-652.

LACEY, A.J. (1989). *Light Microscopy in Biology: A Practical Approach*. Oxford, IRL Press.

LEE, J.C., FRIGON, R.P. and TIMASHEFF, S.N. (1973). The chemical characterization of calf brain microtubule protein subunits. *Journal of Biological Chemistry* **248**, 7253-7262.

LEE, J.C. and TIMASHEFF, S.N. (1977). *In vitro* reconstitution of calf brain microtubules: Effects of solution variables. *Biochemistry* **16**, 1754-1763.

LEHNINGER, A.L. (1970a). *Nucleoside 5'-diphosphates and 5'-triphosphates (NDPs and NTPs)*. Biochemistry . New York, Worth. 246-247.

LEHNINGER, A.L. (1970b). *The standard free energy of hydrolysis of ATP*. Biochemistry . New York, Worth. 298-304.

LEVINE, I.N. (1995). *Physical Chemistry*. New York, McGraw-Hill.

LEIKEN, S., PARSEGIAN, V.A., RAU, D.C., and RAND, R.P. (1993). Hydration Forces. *Annual Reviews of Physical Chemistry* **44**, 369-395.

LIPOWSKY, R. (1991). The conformation of membranes. *Nature* **349**, 475-481.

MacINTOSH, J.R. and HERING, G.E. (1991). Spindle fiber action and chromosome movement. *International Reviews of Cell Biology* **7**, 403-426.

MAGNASCO, M.O. (1994). Molecular Combustion Motors. *Physical Review Letters* **72**, 2656-2659.

MAGNASCO, M.O. (1995). Personal communication.

MANDELKOW, E. and MANDELKOW, E.-M. (1990). Microtubular structure and tubulin polymerization. *Current Opinion in Cell Biology* **2**, 3-9.

MANDELKOW, E.-M., MANDELKOW, E. and MILLIGAN, R.A. (1991). Microtubule dynamics and microtubule caps: A time resolved cryo-electron microscopy study. *The Journal of Cell Biology* **114**, 977-991.

MANDELKOW, E.-M., SCHULTHEISS, R., RAPP, R., MÜLLER, M. and MANDELKOW, E. (1986). On the surface lattice of microtubules: Helix starts, protofilament number, seam, and handedness. *Journal of Cell Biology* **102**, 1067-1073.

MANDELKOW, E., SCHULTHEISS, R. and MANDELKOW, E.-M. (1984). Assembly and three-dimensional image reconstruction of tubulin hoops. *Journal of Molecular Biology* **177**, 507-529.

MARGOLIS, R.L. and WILSON, L. (1978). Opposite end assembly and disassembly of microtubules at steady state *in vitro*. *Cell* **13**, 1-8.

MATUS, A. (1990). Microtubule-Associated Proteins. *Current Opinion in Cell Biology* **2**, 10-14.

MELKI, R., CARLIER, M.-F. and PANTALONI, D. (1990). Direct evidence for GTP and GDP-P$_i$ intermediates in microtubule assembly. *Biochemistry* **29**, 8921-8932.

MELKI, R., CARLIER, M.-F., PANTALONI, D. and TIMASHEFF, S.N. (1989). Cold depolymerization of microtubules to double rings: Geometric stabilization of assemblies. *Biochemistry* **28**, 9143-9152.

MITCHISON, T. and KIRSCHNER, M. (1984a). Dynamic Instability of Microtubule Growth. *Nature* **312**, 237-242.

MITCHISON, T. and KIRSCHNER, M. (1984b). Microtubule assembly nucleated by isolated centrosomes. *Nature* **312**, 232-237.

MITCHISON, T. (1993). Localization of an exchangeable GTP binding site at the plus end of microtubules. *Science* **261**, 1044-1047.

MIYATA, H. and HOTANI, H. (1992). Morphological changes in liposomes caused by polymerization of encapsulated actin and spontaneous formation of actin bundles. *Proceedings of the National Academy of Sciences, U.S.A.* **89**, 11547-11551.

NEW, R.R.C. (1990a). *Liposomes: A Practical Approach.* Oxford, Oxford University Press.

NEW, R.R.C. (1990b). *Preparation of liposomes: the freeze-thaw sonication method.* Liposomes: A Practical Approach Ed. R.R.C. New. New York, Oxford University Press. 58-60.

O'BRIEN, E.T. and ERICKSON, H.P. (1989). Assembly of pure tubulin in the absence of free GTP: Effect of magnesium, glycerol, ATP, and the non-hydrolyzable analogues. *Biochemistry* **28**, 1413-1422.

O'BRIEN, E.T., VOTER, W.A. and ERICKSON, H.P. (1987). GTP hydrolysis during microtubule assembly. *Biochemistry* **26**, 4148-4156.

OOSAWA, F. and ASAKURA, S. (1975). *Thermodynamics of the Polymerization of Protein.* New York, Academic Press.

PEASE, D.C. (1941). Hydrostatic pressure effects upon the spindle figure and chromosome movement. I. Experiments on the first mitotic division of *Urechis* eggs. *Journal of Morphology* **69**, 405-442.

PERLMUTTER-HAYMAN, B. (1976). *The Temperature-Dependence of E_a.* Progress in Inorganic Chemistry Ed. S.J. Lippard. New York, John Wiley & Sons, Inc. 229-297.

PESKIN, C.S., ODELL, G.M. and OSTER, G.F. (1993). Cellular motions and thermal fluctuations: The brownian ratchet. *Biophysical Journal* **65**, 316-324.

PICK, U. (1981). Liposomes with a large trapping capacity prepared by freezing and thawing of sonicated phospholipid mixtures. *Archives of Biochemistry and Biophysics* **212**, 186-194.

PORTER, K.R. (1980). *Some notes on the early characterization of microtubules.* Microtubules and Microtubule Inhibitors Eds. M. DeBrabander and J.D. Mey. Amsterdam, Elsevier/North-Holland. 555-568.

POSTINGL, H., KRAUHS, E., LITTLE, M. and KEMPF, T. (1981). Complete amino acid sequence of α-tubulin from porcine brain. *Proceedings of the National Academy of Sciences, U.S.A.* **78**, 2757-2761.

RAY, S., MEYHÖFER, E., MILLIGAN, R.A. and HOWARD, J. (1993). Kinesin follows the microtubule's protofilament lattice. *Journal of Cell Biology* **121**, 1083-1093.

RICKWOOD, D. (1984). *Centrifugation: A Practical Approach*. Oxford, IRL Press.

SACKMANN, E., DUWE, H.-P. and ENGELHARDT, H. (1986). Membrane bending elasticity and its role for shape fluctuations and shape transformations of cells and vesicles. *Faraday Discussions of the Chemical Society* **81**, 281-290.

SALMON, E.D. (1975). Pressure induced depolymerization of brain microtubules *in vitro*. *Science* **189**, 884-886.

SCHLIWA, M. (1986). *The Cytoskeleton: An Introductory Survey*. New York, Springer-Verlag.

SCHNAPP, B.J. (1986). Viewing single microtubules by video light microscopy. *Methods in Enzymology* **134**, 561-573.

SCOPES, R.K. (1987). *Protein Purification: Principles and Practice*. New York, Springer-Verlag.

SHELANSKI, M.L. and TAYLOR, E.W. (1967). Isolation of a protein subunit from microtubules. *The Journal of Cell Biology* **34**, 549-554.

SILVIUS, J.R. (1982). *Thermotropic phase transitions of pure lipids in model membranes and their modification by membrane proteins*. Lipid-Protein Interactions Eds. P.C. Jost and O.H. Griffith. New York, John Wiley & Sons. 239-281.

SIMON, J.R., PARSONS, S.F. and SALMON, E.D. (1992a). Buffer conditions and non-tubulin factors critically affect the microtubule dynamic instability of sea urchin egg tubulin. *Cell Motility and the Cytoskeleton* **21**, 1-14.

SIMON, S.M., PESKIN, C.S. and OSTER, G.F. (1992b). What drives the translocation of proteins? *Proceedings of the National Academy of Sciences, U.S.A.* **89**, 3770-3774.

SLAUTTERBACK, D.B. (1963). Cytoplasmic microtubules. I. Hydra. *Journal of Cell Biology* **18**, 367-388.

SLOBODA, R.D., RUDOLPH, S.A., ROSENBAUM, J.L. and GREEGARD, P. (1975). Cyclic-AMP dependent endogenous phosphorylation of a microtubule-associated protein. *Proceedings of the National Academy of Sciences, U.S.A.* **72**, 177-181.

STEWART, R.J., FARRELL, K.W. and WILSON, L. (1990). Role of GTP hydrolysis in microtubule polymerization: Evidence for a coupled hydrolysis mechanism. *Biochemistry* **29**, 6489-6498.

SVETINA, S. and ZEKS, B. (1989). Membrane bending energy and shape determination of phospholipid vesicles and red blood cells. *European Biophysics Journal* **17**, 101-111.

SVOBODA, K., SCHMIDT, C.F., SCHNAPP, B.J. and BLOCK, S.M. (1993). Direct observation of kinesin stepping by optical trapping interferometry. *Nature* **365**, 721-727.

TAYLOR, E.W. (1965). The mechanism of colchicine inhibition of mitosis. I. Kinectics of inhibition and the binding of H^3-colchicine. *Journal of Cell Biology* **25**, 145-160.

THOMPSON, T.E. and HUANG, C. (1966). The water permeability of lipid bilayer membranes. *Annals of the New York Academy of Sciences* **137**, 740-744.

TRAVIS, J.L. and BOWSER, S.S. (1990). Microtubule-membrane interactions *in vivo*: direct observation of plasma membrane deformation mediated by actively bending cytoplasmic microtubules. *Protoplasma* **154**, 184-189.

TUCKER, J.B., PATON, C.C., HENDERSON, C.G. and MOGENSEN, M.M. (1993). Microtubule rearrangement and bending during assembly of large curved microtubule bundles in mouse cochlear epithelial cells. *Cell Motility and the Cytoskeleton* **25**, 49-58.

VALE, R.D. (1990). Microtubule-based motor proteins. *Current Opinion in Cell Biology* **2**, 15-22.

VALE, R.D. and OOSAWA, F. (1990). Protein motors and Maxwell's demons: Does mechanochemical transduction involve a thermal ratchet? *Advances in Biophysics* **26**, 97-134.

VERDE, F., DOGTEROM, M., STELZER, E., KARSENTI, E. and LEIBLER, S. (1992). Control of microtubule dynamics and length by cyclin A- and cyclin B-dependent kinases in *Xenopus* egg extracts. *Journal of Cell Biology* **118**, 1097-1108.

VOTER, W.A. and ERICKSON, H.P. (1984). Kinetics of microtubule assembly: Evidence for a two-stage nucleation mechanism. *Journal of Biological Chemistry* **259**, 10430-10438.

VOTER, W.A., O'BRIEN, E.T. and ERICKSON, H.P. (1991). Dilution-induced disassembly of microtubules: Relation to dynamic instability and the GTP cap. *Cell Motility and the Cytoskeleton* **18**, 55-62.

WALKER, R.A., O'BRIEN, E.T., PRYER, N.K., SOBOEIRO, M.F., VOTER, W.A., ERICKSON, H.P. and SALMON, E.D. (1988). Dynamic instability of individual microtubules analyzed by video light microscopy: Rate constants and transition frequencies. *Journal of Cell Biology* **107**, 1437-1448.

WALKER, R.A., INOUE, S. and SALMON, E.D. (1989). Asymmetric behavior of severed microtubule ends after ultraviolet-microbeam irradiation of individual microtubules *in vitro*. *Journal of Cell Biology* **108**, 931-937.

WALKER, R.A., PRYER, N.K. and SALMON, E.D. (1991). Dilution of microtubules observed in real time *in vitro*: Evidence that cap size is small and independent of elongation rate. *Journal of Cell Biology* **114**, 73-81.

WARNER, F.D. and MACINTOSH, J.R., Eds. (1989). Cell Movement: Kinesin, Dynein, and Microtubule Dynamics. New York, Alan R. Liss.

WEBER, K. and OSBORN, M. (1981). *Microtubule and intermediate filament networks in cells viewed by immunofluorescence microscopy.* Cytoskeletal Elements and Plasma Membrane Organization Eds. G. Poste and G.L. Nicolson. Amsterdam, North-Holland. 1-53.

WEINGARTEN, M.D., LOCKWOOD, A.H., HUO, S.-Y. and KIRSCHNER, M.W. (1975). A protein factor essential for microtubule assembly. *Proceedings of the National Academy of Sciences, U.S.A.* **72**, 1858-1862.

WEISENBERG, R.C., DEERY, W.J. and DICKINSON, P.J. (1976). Tubulin-nucleotide interactions during the polymerization and depolymerization of microtubules. *Biochemistry* **15**, 4248-4254.

WILLIAMS, R.C., Jr. and LEE, J.C. (1982). Preparation of tubulin from brain. *Methods in Enzymology* **85**, 376-385.

APPENDIX A
HOW TO PURIFY TUBULIN

I. Check Stocks and Supplies

A. Chemicals: GTP (cat. no. G8877 [Sigma, #3]),
ATP (cat. no 519979, [Mannheim, #45]),
PMSF (cat. no. P7626, [Sigma, #3]),
EGTA (cat. no. E4378, [Sigma, #3]),
Pipes (cat. no. P6757, [Sigma, #3]),
Phosphocellulose (type P11, [Whatman, #30]),
NaOH, HCl, $MgSO_4$, Glycerol,
Glutamic Acid, Sucrose, Tris,
Bio-Rad Bradford dye

B. Disposables: Gloves, Pipette tips, 0.5 ml MicroCentrifuge Tubes, Weigh Boats, Kimwipes, Filter Ware, Plastic Pipettes, Aluminum Foil, Pasteur Pipettes, Cuvettes

C. General: Pure Water, Ice, Scissors, Column Tubing, Pump Tubing, Column filters

II. Clean
A. Glassware
1. *graduated cylinders: 25ml, 50ml, 100ml, 2000ml*
2. *beakers: 2 x 150ml, 4 x 2000ml, 4000ml*
3. *flasks: 2 x 2000ml vacuum, 1000ml, 500ml*
4. *dounces and pestles: 30ml, 2 x 50ml*
5. *funnels: small, large, 600ml glass fritted*
B. Stirrers — teflon rods and bars, lucite sticks
C. Centrifuge Ware — 36 tubes, seals and caps
D. Column
E. Electrophoresis equipment

III. Prepare Buffers
A. PEM — 1000 ml
B. Brain Buffer (BB) — 200 ml
C. GTP stock — 10 ml
D. ATP stock — 5 ml
E. Column Buffer (CB) — 3000 ml

IV. Prepare PhosphoCellulose

A. Set up
1. *connect a vacuum pump to the fitting on a small flask*
2. *seal the small flask with a pipe in a rubber stopper*
3. *connect the pipe to the fitting on a 2 liter flask*
4. *seal the large flask with a 600ml coarse glass fritted filter funnel*
5. *fill a large container with pure water, cover with foil*
6. *connect an aspirator pump to the faucet*

B. Weigh PC — about 90g   weight: _____g
1. *Whatman® Fibrous Cation Exchanger P11 (stored dry at 4°C)*
2. *WEAR GLOVES (to protect the PC)*
3. *Use large weigh dish, clean metal spatula and open air balance*

C. Wash in NaOH
1. *make 0.1 M NaOH*
   a. in a 4 liter beaker put 8 g NaOH and 2 liters H_2O
   b. stir until dissolved
2. *gently pour PC into the 2 liters of 0.1 M NaOH*
3. *stir slowly by hand with a teflon rod until well mixed*
4. *measure pH with paper (powder sticks to electrodes)*
   a. if pH ≥12, skip to IV.E.5
   b. if pH < 12, continue
5. *let PC settle (about 15 minutes)*
6. *meanwhile, repeat IV.C.1.*
7. *after PC has settled, remove the supernatant*
   a. use the aspirator pump and a Pasteur pipette
   b. take the very fine PC, too (it clogs the filter)

D. Filter PC
1. *pour the settled PC into the funnel*
2. *turn on the vacuum pump*
3. *DO NOT LET THE PC DRY OUT!*
   a. turn off the vacuum leaving a few mm of fluid
   b. top off with the pure water if necessary

E. Final wash in NaOH
1. *rinse the 4 liter beaker and fill with NaOH from IV.C.6*
2. *gently pour PC into the 2 liters of 0.1 M NaOH*
3. *stir slowly by hand with a teflon rod until well mixed*
4. *measure pH with paper (powder sticks to electrodes)*
   a. if pH < 12, return to step IV.C.5 and repeat
   b. if pH ≥12, continue
5. *let PC sit at pH ≥12 for 20 min., stirring occasionally*
6. *meanwhile, make 0.1 M HCl*
   a. in a beaker put 20ml 37% HCl and 2 liters H_2O
   b. cover and set aside
7. *after PC has settled, remove the supernatant*

F. Rinse PC
   1. *have 4 liters of pure water at hand*
   2. *pour the settled PC into the funnel*
   3. *turn on the vacuum pump*
   4. *pass all 4 liters of water through the PC*
      a. the large flask will get full
      b. have another empty one handy
   5. *DO NOT LET THE PC DRY OUT!*
G. Wash in HCl
   1. *rinse the 4 liter beaker and fill with HCl from IV.E.6*
   1. *gently pour PC into the 2 liters of 0.1 M HCl*
   2. *stir slowly by hand with a teflon rod until well mixed*
   3. *measure. pH with paper (powder sticks to electrodes)*
      a. if pH ≤ 3, skip to
      b. if pH > 3, continue
   5. *let PC settle (about 15 minutes)*
   6. *meanwhile, repeat IV.E.6.*
   7. *after PC has settled, remove the supernatant*
H. Filter PC
I. Final wash in HCl
   1. *rinse the 4 liter beaker and fill with HCl from IV.G.6*
   2. *gently pour PC into the 2 liters of 0.1 M HCl*
   3. *stir slowly by hand with a teflon rod until well mixed*
   4. *measure the pH*
      a. if pH > 3, return to step IV.G.5 and repeat
      b. if pH ≤ 3, continue
   5. *let PC sit at pH ≤ 3 for 20 min., stirring occasionally*
   6. *meanwhile, make 0.1 M MgSO4*
      a. in a beaker, put 49.3 g•7H$_2$O and 2 liters H$_2$0
      b. stir until dissolved
   7. *after PC has settled, remove the supernatant*
J. Rinse PC
K. Wash in MgSO$_4$
   1. *rinse 4 liter beaker and fill with MgSO4 from IV.I.6*
   2. *gently pour PC into the 2 liters of 0.1 M MgSO4*
   3. *stir slowly by hand with a teflon rod until well mixed*
   4. *let PC sit for 20 minutes, stirring occasionally*
   5. *after PC has settled, remove the supernatant*
L. Filter PC
M. Wash in Column Buffer (CB)
   1. *rinse 4 liter beaker and fill with 2 liters CB*
   2. *gently pour PC into the 2 liters of CB*
   3. *stir slowly by hand with a teflon rod until well mixed*
   4. *check pH with meter (all the fine PC is gone)*
      a. if pH ≠ 6.7, adjust pH with conc. NaOH or HCl, return to IV.L and repeat
      b. if pH = 6.7, continue

191

N. Store PC
 1. *in a glass bottle, with a little excess buffer on top*
 2. *in the fridge at 4 °C*
 3. *for less than 1 month (if > 1 week, add Azide)*

V. Prepare Column
A. Assemble
 Mark on the side of the glass tube 22cm and 18cm from the bottom
B. Fill
 1. *position the column in the cold, adjust to vertical*
 2. *pour PC:*
   Remove the plunger; tilt the column about 20°; swish the jar of PC around; pour the PC down the side of the column; fill to the 22 cm mark; **do not over fill**; right the column; quickly repeat if necessary; rinse PC down the sides with CB from a pipette; cover the column opening with foil; wait 30 min; check the height of the settled PC
   i) <u>if it is << 18 cm:</u> seal the column top with parafilm; unclamp the column invert it, resuspending the PC, reclamp the column; allow to resettle and the check again
   ii) <u>if it is >> 18 cm:</u> unclamp the column; pour out some of the PC; seal the column top with parafilm; invert it, resuspending the PC; reclamp the column, allow the PC to resettle and then check again
 3. *let excess CB drain out the bottom tubing, leave 2mm covering PC*
 4. *close the column*
   insert the plunger: the bottom filter should wet the CB completely, but not disrupt the surface of the PC; secure the plunger in position
C. Equilibrate
 1. *make tubing connections*
  a. to the peristaltic pump use 1.52 mm i.d. tubing
  b. to the fraction collector use teflon tubing that comes with column
 2. *release trapped air*
  a. hold the plunger by hand and loosen its o-ring
  b. open the bottom tubing so it drains into a beaker
  c. turn the pump to low speed (10 rpm=1.6ml/min)
  d. when the air has gone, secure the plunger
 3. *flow CB through the column*
  a. turn the pump speed up to 30 rpm (5 ml/min)
  b. let at least 250 ml of CB flow through
  c. PC will settle a little more under the flow
  d. lower the pump speed to 12 rpm (1.8ml/min)
  e. stop the pump
D. Prepare Fraction Collector
 1. *Load with 5ml test tubes*
 2. *Make sure drops fall squarely into tubes*

VI. Get Brain
A. The day before
1. call slaughterhouse for permission, time, etc.
mention that we have a permit on file

Trenton Packing (Joe)
610 Roebling Ave.
Trenton, NJ 08611
(609) 394-3369

2. prepare the lab
Chill overnight in the fridge: 12 centrifuge tubes, a 600 ml beaker, blender, rotor and homogenizers. Equilibrate the water bath at 34°C. Reserve the centrifuge for the next two days. Prepare a wastebasket (a beaker lined with a plastic bag).

3. prepare to leave early next morning, from home
Have crushed ice in a cooler & gloves in car. In the ice, have a **thin** plastic bag w/BB

B. At the slaughterhouse
1. note the time of the kill   *approx: ___ : ___ a.m.*
2. put brain in BB in bag, bury in ice (wear gloves)
3. make sure it gets COLD quickly
4. note the time when it got on ice   *approx: ___ : ___ a.m.*

VII. Prepare Brain
A. Organize
1. fill 2 ice buckets and the ice tray with ice from fridge
2. put the 600 ml beaker in one and the tubes in the other
4. make a well in the ice in the tray and line it with foil
5. put the brain in the foil-lined well of ice

B. Clean — wear gloves always
1. try to keep the brain cold (on ice) as much as possible
2. dry outside and tare the beaker, keeping it chilled
3. use kimwipes to grip the meninges and peel them off
4. discard cerebellum (white) and meninges (bloody membrane)
5. rinse the brain with cold PEM if necessary

C. Chop — use scissors
D. Weigh — use a 600ml beaker   weight: _____ g
E. Add
1. PEM: 0.5ml for every gram of brain
calculate:

2. PMSF to 1mM (protease inhibitor, dry, doesn't dissolve well)
calculate:

3. ATP to 1mM (releases motors, fuels regeneration of GTP)
calculate

4. Glycerol: 1ml for every 10ml PEM
calculate:

F. Blend — in the cold: low - 15 sec, medium - 15 sec, high - 45 sec.

G. Balance in <u>chilled</u> centrifuge tubes
    1. use a funnel
    2. pour the "brain shake", filling tubes to 3/4 full
    3. fill one of the tubes completely
      Use a Pasteur pipette; break the pipette to widen its opening (stick the point of one
      pipette in the barrel of another and bend to snap, then smooth the broken end in a
      flame); seal the centrifuge tube; dry the outside; tare it in a beaker on the balance
    4. bring another tube to the same weight
      Dry the outside of another tube; put it in the beaker on the balance AND put its seal
      and cap on the balance; fill (with the Pasteur pipette) until its weight equals that
      of the previous tube; seal and cap
H. Load Rotor — balanced tubes opposite one another

VIII. 1st Cold Spin
    A. Speed — 100,000g (29,000 rpm for Ti50.2)
    B. Time — 60 minutes   started at: _____:_____.
    C. Temperature — 4°C
    D. Meanwhile
      Chill a 100 ml graduated cylinder. Warm 6 sealed centrifuge tubes in the water bath
    E. Afterwards — set the centrifuge to 34°C

IX. Prepare Supernatant
    A. Measure — volume of supernatant: _____ <u>ml</u>
    1. pour supernatants into the chilled 100ml graduated cylinder
    2. mushy pellets down (firm pellets up) when pouring
    B. Save — sample **C1S**
    1. transfer 100µl of the supernatant to a microcentrifuge tube
    2. store at -20°C (in freezer)
    C. Add
    1. ATP — bring to 1mM ATP
calculate:

    2. GTP — bring to 0.2mM GTP
calculate:

    3. Glycerol — 3ml glycerol for every 10ml supernatant
      Add last for best mixing. Use a disposable plastic pipette
calculate:

    D. Mix — do not make bubbles!
    E. Balance — in <u>warm</u> centrifuge tubes
    F. Incubate — 34°C for 45 minutes started at: _____:_____.
      Meanwhile: dump pellets into zip-loc bag and remove to outside dumpster soak tubes
                 in bleach+water until there is time for proper cleaning. Warm rotor
                 under running tap (hot water), dry well, store in an oven at 34°C
    G. Load Rotor

X. 1st Hot Spin
   A. Speed — 100,000g (29,000 rpm for Ti50.2)
   B. Time — 75 minutes   started at: _____ : _____.
   C. Temperature — 34°C
   D. Meanwhile
   > Put four clean centrifuge tubes on ice. Put two 50ml dounces on ice. Set up teflon pestle in drill head in the cold
   E. Afterwards — set the centrifuge to 4°C

XI. Prepare Pellets
   A. Measure
   1. *volume of supernatant*   _____ ml
   > Pour the supernatants into a graduated cylinder, pellets up. Keep the pellets on ice
   2. *volume of pellets:*   _____ ml
   > Determine how much water in an empty tube make a drop the size of a pellet, multiply by the number of pellets
   B. Suspend Pellets — with twice their volume of PEM
   > Add some PEM to one of the tubes, use a lucite rod to scrape the pellet off the sides of the tubes, pour the slurry into a chilled 50ml dounce, repeat for each pellet. If the expected final volume exceeds the volume of a dounce, use two dounces. Use the leftover PEM to rinse the tubes and then pour it into the dounce(s).
   C. Add — GTP to 0.2mM
calculate:

   D. Homogenize
   1. Set Up: work in the cold; load teflon pestle into drill head; slide dounce onto pestle until teflon is submerged; turn the drill head at about 5 rpm
   2. Run: take care to keep the dounce cold (friction with the pestle creates heat); don't hold your hand around part with liquid, keep ice around as much as possible, try to keep the pestle turning smoothly; slowly push the dounce **up** the pestle making sure pestle continues to rotate; stop just before teflon hits bottom; slowly pull the dounce **down** the pestle making sure pestle continues to rotate; stop before pestle breaks surface of liquid; **repeat** at least three times
   3. End: stop the drill head; slowly slide the dounce off the pestle, being careful not to create many bubbles; cover the mouth of the dounce with Aluminum foil
   E. Incubate — at 4°C for 30 min. started at: _____ : _____.
   > Meanwhile: Chill rotor: fill and surround with crushed ice; dry well (use bunches of kimwipes to dry holes); store in fridge. Save sample of supernatant for gel–**H1S**
   F. Save — sample **H1P**
   G. Balance — in <u>chilled</u> centrifuge tubes
   H. Load Rotor

XII. 2nd Cold Spin
   A. Speed — 100,000g (29,000 rpm for Ti50.2)
   B. Time — 55 minutes   started at: _____ : _____.
   C. Temperature — 4°C
   D. Meanwhile
   > Chill a 50 ml graduated cylinder. Warm a couple centrifuge tubes in the water bath
   E. Afterwards — set the centrifuge to 34°C

XIII. Prepare Supernatant
A. Measure — volume of supernatant: _____ ml
B. Save — sample **C2S**
C. Add
1. *GTP — bring to 0.8mM GTP*
calculate:

2 *Glycerol — 3.5ml glycerol for every 10ml supernatant*
calculate:

D. Mix — avoid bubbles!
E. Balance in <u>warmed</u> centrifuge tubes
F. Incubate — 34°C for 30 minutes   started at: ____:_____
    Meanwhile: Resuspend a pellet in 1ml PEM and save sample *C2P*. Warm rotor.
G. Load Rotor

XIV. 2nd Hot Spin
A. Speed — 100,000g (29,000 rpm for Ti50.2)
B. Time — 135 minutes   started at: ____:_____
C. Temperature — 34°C
D. Meanwhile
    Put a clean centrifuge tube on ice. Put the 30ml dounce on ice. Set up the teflon pestle
    in drill head in the cold
E. Afterwards — set the centrifuge to 4°C

XV. Prepare Pellets
A. Measure
1. *volume of supernatant*   _____ ml
    Pour the supernatants into a graduated cylinder, pellets up. Keep the pellets on ice.
2. *Save sample of supernatant – **H2S***
3. *volume of pellets:*   _____ ml

Break
Cover each pellet with 1ml PEM; Flash freeze in liquid N_2 in centrifuge tubes
Store @ -80°C overnight; Turn of centrifuge; Chill rotor, dounce, etc. in fridge overnight
SLEEP
Turn on centrifuge, set to 4°C. Thaw the pellets quickly (in water bath) and put on ice

XV. Prepare Pellets continued
B. Suspend Pellets — in three times their volume of PEM
    Take volume in which they were frozen into account
C. Add — GTP to 0.2mM
D. Homogenize
E. Incubate — at 4°C for 30 min. started at: ____:_____
    Meanwhile: Chill rotor. Chill a pair of tubes. Make sure centrifuge is set to 4°C.
F. Save — sample **H2P**
G. Balance — in <u>chilled</u> centrifuge tubes
H. Load Rotor

196

XVII. 3rd Cold Spin
A. Speed — 100,000g (29,000 rpm for Ti50.2)
B. Time — 55 minutes   started at: _____ : _____ .
C. Temperature — 4°C
D. Meanwhile
     Chill a 50 ml graduated cylinder. Warm a pair of clean centrifuge tubes in the bath
E. Afterwards — set the centrifuge to 34°C

XVIII. Prepare Supernatant
A. Measure — volume of supernatant: _____ ml
B. Save — sample **C3S**
C. Add
     1. *GTP — bring to 0.8mM GTP*
     2 *Glycerol — 3.5ml glycerol for every 10ml supernatant*
D. Mix — avoid bubbles!
E. Balance in <u>warmed</u> centrifuge tubes
F. Incubate — 34°C for 30 minutes   started at: _____ : _____ .
G. Meanwhile
     Resuspend a pellet in 1ml PEM, save sample *C3P*. Warm rotor
H. Load Rotor

XIX. 3rd Hot Spin
A. Speed — 150,000g (35,000 rpm for Ti50.2)
B. Time — 85 minutes   started at: _____ : _____ .
C. Temperature — 34°C
D. Meanwhile
     Put a clean centrifuge tube on ice. Put the 30ml dounce on ice. Set up teflon pestle in
     drill head in the cold
E. Afterwards — set the centrifuge to 4°C

XX. Prepare Pellet
A. Measure
     1. *volume of supernatant*   _____ ml
     2. *volume of pellets:*   _____ ml
B. Suspend Pellets — in three times their volume of CB
C. Add — GTP to 0.2mM
D. Homogenize
E. Incubate — at 4°C for 30 min. started at: _____ : _____ .
     Meanwhile: Chill rotor. Chill a pair of tubes. Make sure centrifuge is set to 4°C.
     Save sample of supernatant for gel–**H3S**. Begin XXII.A. if there is time
F. Save — sample **H3P**
G. Balance — in <u>chilled</u> centrifuge tubes
H. Load Rotor

XXI. 4th Cold Spin
A. Speed — 150,000g (35,000 rpm for Ti50.2)
B. Time — 15 minutes   started at: _____:_____.
C. Temperature — 4°C
D. Meanwhile
     Warm up the spectrophotometer. Check up on the column
E. Afterwards — set the centrifuge to 34°C

XXII. Run Column
A. Equilibrate with CB+GTP   started at: _____:_____.
     1. *pump 100ml of CB with 1mM GTP through at 12 rpm (fast)*
     2. *drain into a beaker*
     3. *DON'T LET IT RUN DRY*
B. Flow Tubulin — rpm = ml/min
C. Monitor Concentration

XXIII. Concentrate Tubulin
A. Add 0.186g glutamic acid per ml of tubulin
     1. *stir slowly at room temperature*
     2. *wait until fully dissolved*
B. Balance in <u>warmed</u> centrifuge tubes
C. Incubate — 34°C for 25 minutes   started at: _____:_____.
D. Load Rotor
E. Final Hot Spin
     1. *Speed — 75,000g (22,000 rpm for Ti50.2)*
     2. *Time — 20 minutes*   *started at: _____:_____.*
     3. *Temperature — 34°C*
     4. *Meanwhile - Do a real Bradford to know concentration*
     5. *Afterwards — set the centrifuge to 4°C*
F. Resuspend Pellets in PM$_2$
     1. *determine volume from concentration measurement*
     2. *recommended stock concentration ~100μM*
G. Incubate — at 4°C for 30 min.   started at: _____:_____.
H. Final Cold Spin
     1. *Speed — 150,000g (35,000 rpm for Ti50.2)*
     2. *Time — 25 minutes*   *started at: _____:_____.*
     3. *Temperature — 4°C*
I. Put Supernatant on Ice

XXIV. Store
A. Aliquot
     1. *choose volume to fill cryo-tube and minimize number of thaws*
     2. *500μl of 100mM in 750μl cryo-vials tubulin works well*
     3. *Label unambiguously*
B. Flash Freeze — in liquid N$_2$
C. Store — in liquid N$_2$ for up to 1.5 years

Column Buffer (CB)

25 mM Pipes	(mw: 302.4 g/mole)	pH 6.7
1 mM EGTA	(mw: 380.4 g/mole)	
0.5 mM MgSO$_4 \cdot$7H$_2$0	(mw: 246.5 g/mole)	

Sterile filter   Store at 4°C for less than 3 months.

Brain Buffer (BB)

320mM Sucrose	(mw: 342.3 g/mole)	pH 7.4
25mM Tris	(mw: 121.1 g/mole)	

Sterile filter   Store at 4°C for less than 3 weeks.

PEM

100mM Pipes	(mw: 302.4 g/mole)	pH 6.9
2mM EGTA	(mw: 380.4 g/mole)	
1mM MgSO$_4 \cdot$7H$_2$0	(mw: 246.5 g/mole)	

Sterile filter   Store at 4°C for less than 3 months.

100mM ATP stock

200 mg ATP in 3.64 ml PEM
Store on ice during prep, or at -20°C for extended periods (< 2 weeks)

50mM GTP stock

100 mg GTP in 3.53 ml PEM (for purification) or PM$_2$ (for experiments)
Store on ice during prep, or as aliquots of ~15µl @ -20°C (< 2 weeks)

PM$_2$

100mM Pipes	(mw: 302.4 g/mole)	pH 6.9
2mM EGTA	(mw: 380.4 g/mole)	
2mM MgSO$_4 \cdot$7H$_2$0	(mw: 246.5 g/mole)	

Sterile filter   Store at 4°C for less than 3 months

PM$_2$G$_1$

20µl 50mM GTP stock in 980 µl PM$_2$ Do not store, make as needed

APPENDIX C

MEMBRANE ENERGY CALCULATIONS

This appendix gives the formula for several quantities associated with the vesicle shapes described in the text. The shape parameters are defined as in Figure 5.11, with the additional parameter θ, which represents the angle at which a new radius of curvature is introduced to over come singularities in the slope in the football (endpoints) and the phi (joints) shapes. The stretching energy is simply derived from the computed surface area, and therefore not presented below.

Z = axial extent; V = volume; A = surface area; E_c = curvature energy

THE SPHERE:

$$Z = 2R_o$$
$$V = \tfrac{4}{3}\pi R_o^3$$
$$A = 4\pi R_o^2$$
$$E_c = \tfrac{1}{2}k_c \int dA \left(\tfrac{1}{R_1} + \tfrac{1}{R_2}\right)^2 = 8\pi k_c$$

THE SAUSAGE:

$$Z = 2(R + L)$$
$$V = \tfrac{4}{3}\pi R^3 + 2\pi R^2 L = \tfrac{4}{3}\pi R^3 \left(\frac{3Z}{4R} - \frac{1}{2}\right)$$
$$A = 4\pi R^2 + 4\pi RL = 2\pi RZ$$
$$E_c = 8\pi k_c + 2\pi k_c \frac{L}{R} = 8\pi k_c \left(\frac{Z}{8R} + \frac{3}{4}\right)$$

THE FOOTBALL:

$$Z = 2R\left(1 - \cos\theta_{max}(\sec\theta - \tan\theta)\right)$$
$$V = 2\pi R^3 \left\{ \tfrac{1}{3}(1 - (\cos\theta_{max}/\cos\theta))(2 - 3\sin\theta + \sin^3\theta) - \theta\cos\theta_{max} \right.$$
$$\left. + \tfrac{1}{4}\sin\theta(5 + 2\cos(2\theta_{max}) - \tfrac{1}{2}\sin(2\theta)\cos\theta_{max} + \tfrac{1}{12}\sin(3\theta)) \right\}$$
$$A = 4\pi R^2 \left\{ (1 - (\cos\theta_{max}/\cos\theta))^2 (1 - \sin\theta) + \sin\theta - \theta\cos\theta_{max} \right\}$$
$$E_c = 8\pi k_c \left\{ 1 + \tfrac{1}{4}\cos\theta_{max}\cot\theta_{max}\left[\ln\left(\sin\frac{\theta_{max} + \theta}{2}\right) - \ln\left(\sin\frac{\theta_{max} - \theta}{2}\right) \right] \right\}$$
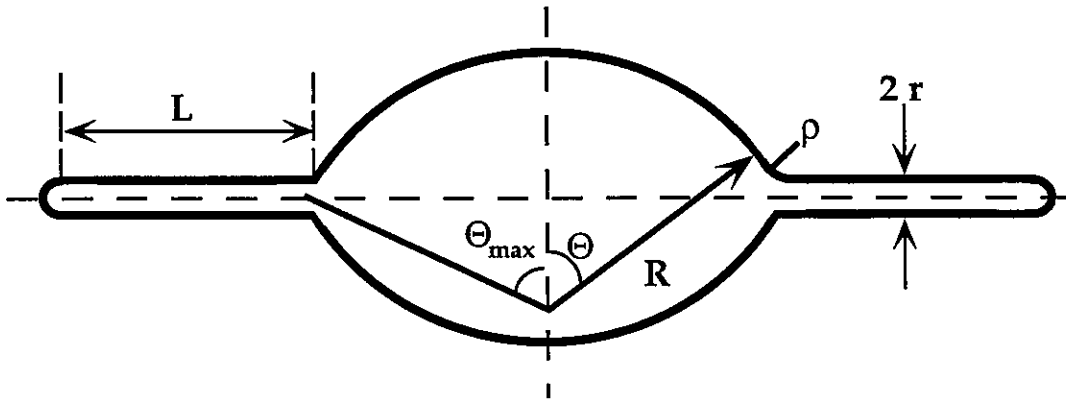
THE PHI: Define an additional parameter $\rho \equiv \dfrac{R(\cos\theta - \cos\theta_{max}) - r}{1 - \cos\theta}$, which

describes the radius of curvature of the neck-like region that joins the football

portion to the two sausage-like arms of the phi (ϕ) shape.

$$Z = 2(R\sin\theta + \rho\sin\theta + L + r)$$

$$V = 2\pi R^3\left\{-\theta\cos\theta_{max} + \tfrac{1}{4}\sin\theta\left(5 + 2\cos(2\theta_{max})\right) - \tfrac{1}{2}\sin 2\theta\cos\theta_{max} + \tfrac{1}{12}\sin 3\theta\right\}$$
$$+ \tfrac{4}{3}\pi r^3\left(\frac{3}{2}\frac{L+r}{r} - \frac{1}{2}\right)$$
$$+ 2\pi r^3\left\{\theta\left(1 + \frac{r}{\rho}\right) + \left(7 + 8\frac{r}{\rho} + 4\frac{r^2}{\rho^2}\right)\frac{\sin\theta}{4} + \left(1 + \frac{r}{\rho}\right)\frac{\sin 2\theta}{2} + \frac{\sin 3\theta}{12}\right\}$$

$$A = 4\pi R^2\left(\sin\theta - \theta\cos\theta_{max}\right)$$
$$+ 4\pi r(r + L)$$
$$+ 4\pi\left\{r^2(\theta + \sin\theta) + r\rho\theta\right\}$$

$$E_c = 8\pi k_c\left\{\sin\theta + \tfrac{1}{4}\cos\theta_{max}\cot\theta_{max}\left[\ln\left(\sin\frac{\theta_{max}+\theta}{2}\right) - \ln\left(\sin\frac{\theta_{max}-\theta}{2}\right)\right]\right\}$$
$$+ 8\pi k_c\left\{\frac{r+L}{4r} + \frac{3}{4}\right\}$$
$$+ 8\pi k_c\left\{\frac{(1+r/\rho)^2\tan^{-1}\sqrt{\tan^2\theta/2(2+r/\rho)/r/\rho}}{2\sqrt{r/\rho(2+r/\rho)}} - \sin\theta\right\}$$

201

APPENDIX D

DERIVATION OF THE BUCKLING FORCE

To figure out how the force F_b needed to buckle a rod depends on its length L it is enough to know the displacement ΔL at which the energy stored in compressing the rod equals the energy stored in bending it. For simplicity, we neglect the details of the shape of the rod and consider its cross-sectional size r. To first order in ΔL, the energy of stretching/compressing is

$$E_s = \frac{1}{2} k_s \left(\frac{\Delta L}{L}\right)^2$$

where $k_s \propto Y(r^2 L)$, the elastic stretching constant of the rod, is proportional to Y the Young's modulus of the material times the volume of the rod. The energy of bending to a curvature $C = 1/R^2$, is
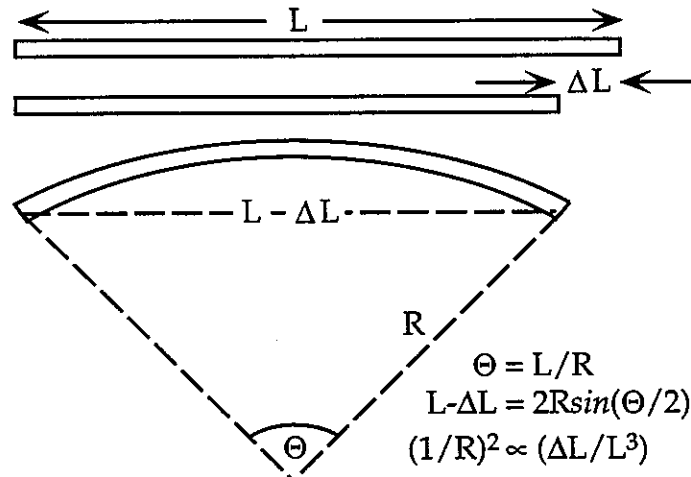
$$E_b = \frac{1}{2}\int k_b C^2 d\ell = \frac{1}{2}\frac{k_b L}{R^2}$$

where $k_b = YI \propto Yr^4$, the elastic bending constant of the rod, is proportional to Y times $I \propto r^4$ the moment of inertia of the rod about the bending axis.

Setting the two equal to one another, yields

$$\frac{\Delta L^2}{L^2} = \frac{r^2}{R^2}.$$

Since R and ΔL are related as shown in the figure below, we find $\Delta L/L = r^2/L^2$ and therefore, the force is $F_b = k_b(\Delta L/L) = Yr^4/L^2 \propto YI/L^2$.

$$\Theta = L/R$$
$$L-\Delta L = 2R sin(\Theta/2)$$
$$(1/R)^2 \propto (\Delta L/L^3)$$

COMPANIES

Amicon, Beverly, MA 01915. *(800)343-1397.*

Apple Computer, Cupertino, CA 95014. *(408)996-1010.*

Avanti Polar Lipids, A.P., Alabaster, AL 35007. *(800)227-0651.*

Beckman Instruments, Palo Alto, CA 94304. *(800)742-2345.*

Bio-Rad, Hercules, CA 94547. *(800)424-6723.*

Branson, Danbury, CT 06813. *(203)796-0400.*

California Fine Wire, Grover City, CA 93433. *(805)489-5144.*

Carolina Biological Supply, Burlington, NC 27215. *(919)584-0381.*

Colorado Video, Boulder, CO

Corning Glass Works, Corning, NY 14830. *(see Fisher,Thomas or VWR).*

Devcon, Danvers, MA

Fluoroware, Chaska, MN 55318. *(612)448-3131.*

Fisher Scientific, Springfield, NJ 07081. *(800)766-7000.*

Hamamatsu, Bridgewater, NJ 08807. *(908)231-1116.*

Hamilton, Reno, NV 89520. *(800)648-5950.*

Hydro, Research Triangle Park, NC 27709. *(800)950-7426.*

Imagen, Trenton, NJ 08549. *(609)393-9686.*

International Products, Burlington, NJ 08016. *(609)386-8770.*

Keithley Instruments, Cleveland, OH 44139. *(216)248-0400.*

Kimberly-Clark, Atlanta, GA 30076. *(800)241-2739.*

NEC, Mountain View, CA 94043. *(415)960-6000.*

Omega, Stamford, CT 06906. *(800)622-2378.*

Osram, Montgomery, NY 12549. *(800)431-9980.*

Perceptics, Knotsville, TN 37932. *(615)966-9200.*

Rainin, Woburn, MA 01801. *(800)472-4646.*

Simco, Hatfield, PA 19440. *(215)822-6401.*

Taylor-Wharton Cryogenics, Theodore, AL 36590. *(800)428-3304.*

Technical Video, Woods Hole, MA 02543. *(508)563-6377.*

Thomas Scientific, Swedesboro, NJ 08085. *(800)345-2100.*

Trenton Packing, Trenton, NJ 08611. *(609)394-3369.*

VWR, Piscataway, NJ 08855. *(800)932-5000.*

Whatman, Hillsboro, OR 97123. *(800)942-8626.*

Yokogawa, Newnan, GA 30265. *(404)253-7000.*

Zeiss, Thornwood, NY 10594. *(914)747-1800.*